ADAPTIVE KRIGING MODEL FOR RARE EVENTS ESTIMATION AND RLSTM-ASSISTED DYNAMIC RELIABILITY ANALYSIS

ZHANG YU

PhD

The Hong Kong Polytechnic University

2025

The Hong Kong Polytechnic University

Department of Civil and Environmental Engineering

Adaptive Kriging Model for Rare Events Estimation and rLSTM-assisted Dynamic Reliability Analysis

ZHANG Yu

A thesis submitted in partial fulfilment of the requirements for the degree of Doctor of Philosophy

Nov 2024

CERTIFICATE OF ORIGINALITY

I hereby declare that this thesis is my own work and that, to the best of my knowledge and belief, it reproduces no material previously published or written, nor material that has been accepted for the award of any other degree or diploma, except where due acknowledgement has been made in the text.

____ ___ (Signed)

ZHANG Yu (Name of student)

ABSTRACT

Uncertainties in structural materials and environmental conditions are widely recognized for their significant impact on structural performance. For instance, concrete strength is statistically determined from a limited number of specimens, and similar variability is observed in the modulus and yield strength of steel, both of which should be treated as random variables. In addition, natural variability is present in environmental conditions, such as wind velocity. As a result, structural responses are inherently uncertain due to the propagation of these uncertainties from both structural parameters and external loads. Therefore, it is essential to thoroughly investigate the uncertainty propagation process.

Structural reliability analysis plays a crucial role in assessing structural safety and guiding the design process. However, efficiently and accurately estimating failure probabilities remains a significant challenge. Over the past few decades, various approaches have been developed to address this issue. Among them, Monte Carlo simulation (MCS) is the most straightforward method, but it demands substantial computational resources, particularly when dealing with time-intensive performance functions. Although the first- and second-order reliability methods are computationally efficient, they often lack accuracy when applied to nonlinear structures. Recently, surrogate model-based methods have garnered increasing attention. A surrogate model serves as an efficient alternative to the original costly physical model. Commonly used surrogate models include the Kriging model, polynomial chaos expansion, support vector regression, and neural networks.

The adaptive Kriging model has gained popularity in recent years due to its ability to be refined iteratively using active learning strategies. However, improvements in its efficiency for estimating failure probabilities are still needed. Structural failures are typically rare events, and applying adaptive Kriging with MCS is inefficient for estimating small failure probabilities, as training the Kriging model with a large number of candidate samples is time-consuming. To address this challenge, a distance-based subdomain approach is developed to focus on candidate samples near the limit state surface. During training, the Kriging model is refined iteratively within these subdomains, rather than across the entire Monte Carlo population. To further reduce the computational cost of performance function evaluations, a new stopping criterion is proposed. This criterion accounts for the accuracy of failure probability estimation, allowing the active learning process to terminate at an appropriate stage. Furthermore, for estimating very rare events, such as failure probabilities smaller than 10^{-6}, an adaptive Kriging model with spherical decomposition-based Monte Carlo simulation can be employed. However, conventional stopping criteria are inadequate for halting the active training process at an appropriate stage, especially for practical engineering structures. Therefore, a new stopping criterion tailored to the adaptive Kriging model with spherical decomposition-based Monte Carlo simulation is proposed, based on the relative error of failure probability.

In addition, the reliability analysis of stochastic dynamic systems, such as engineering structures subjected to stochastic seismic excitation or wind loads, remains challenging. Existing studies primarily focus on extreme value theory and the moments method. The first passage failure probability can be estimated from the

extreme value distribution of the responses of interest. However, constructing surrogate models for stochastic dynamic systems is difficult due to the high dimensionality that arises when simulating stochastic excitations. For example, the spectral representation method requires thousands of random phases to simulate the stochastic excitation. Even when only the extreme response is of concern, the Kriging model is unsuitable for metamodeling due to the curse of dimensionality. To enable the adaptive Kriging model for the reliability analysis of stochastic dynamic systems, a novel long short-term memory network (rLSTM) is proposed. This network considers both time-series stochastic excitation and random structural parameters to predict time history responses. The rLSTM is integrated with an autoencoder to identify low-dimensional latent variables for representing the approximate extreme value space created by the rLSTM, which are then used to construct the Kriging model. An active learning strategy is subsequently employed to facilitate the reliability analysis of stochastic dynamic systems. To improve the accuracy and training stability of rLSTM network, a physics-informed rLSTM is constructed by incorporating the uncertain governing equations of dynamics. Additionally, conventional adaptive Kriging model continuously require information from the performance function, making parallel computing infeasible. This limitation significantly impedes the application of the adaptive Kriging model to computationally expensive models. To tackle this problem, a prediction error-based offline learning strategy is introduced. This approach allows the adaptive Kriging model to be refined in a single step, significantly reducing the computational burden of reliability analysis for stochastic dynamic systems.

Overall, this research put emphasis on adaptive Kriging model for rare events estimation and reliability analysis of stochastic dynamic systems. The sampling scheme and stopping criteria are improved for small failure probabilities estimation. With the aid of long short-term memory networks, latent variables for constructing Kriging model of extreme responses are identified, making the adaptive Kriging model available for reliability analysis of stochastic dynamic systems.

LIST OF PUBLICATIONS

Journal articles

Zhang, Y., Dong, Y., & Beer, M. (2024). rLSTM-AE for dimension reduction and its application to active learning-based dynamic reliability analysis. *Mechanical Systems and Signal Processing*, 215, 111426.

Zhang, Y., Dong, Y., & Frangopol, D. M. (2024). An error-based stopping criterion for spherical decomposition-based adaptive Kriging model and rare event estimation. *Reliability Engineering & System Safety*, 241, 109610.

Zhang, Y., Dong, Y., & Xu, J. (2023). An accelerated active learning Kriging model with the distance-based subdomain and a new stopping criterion for reliability analysis. *Reliability Engineering & System Safety*, 231, 109034.

Zhang, Y., Dong, Y., & Feng, R. (2023). Bayes-informed mixture distribution for the EVD estimation and dynamic reliability analysis. *Mechanical Systems and Signal Processing*, 197, 110352.

Zhang, Y., Li, Y., & Dong, Y. (2022). Probabilistic analysis of long-term loss incorporating maximum entropy method and analytical higher-order moments. *Journal of Infrastructure Preservation and Resilience*, 3(1), 7.

Jia, L., **Zhang, Y.**, Zhu, D., & Dong, Y. (2022). 3D numerical modeling and quantification of oblique wave forces on coastal bridge superstructures. *Journal of Marine Science and Engineering*, 10(7), 860.

ACKNOWLEDGMENTS

First, I would like to express my deepest gratitude to my chief supervisor, Dr. You Dong, for his patience and excellent guidance throughout my PhD studies at the Hong Kong Polytechnic University. Dr. Dong has always been supportive and helpful, enabling me to successfully conduct my research. Additionally, I would like to extend my sincere thanks to my co-supervisor, Prof. Songye Zhu, for his encouragement and support during my PhD journey. I am also immensely grateful to Prof. Michael Beer for his invaluable support during my attachment program in Germany. Finally, I would like to thank all the professors who shared their insights and provided constructive feedback during my PhD studies. I sincerely appreciate Dr. Siu Kai Lai as the Chairman of BoE, Prof. Limin Zhang from The Hong Kong University of Science and Technology and Dr. Alice Alipour from Iowa State University as the examiners of my thesis. Secondly, I gratefully acknowledge the support from the following sponsors: the National Natural Science Foundation of China (Grant No. 52078448), the Research Grants Council of the Hong Kong Special Administrative Region, China (No. PolyU 15219819, PolyU 15221521 and PolyU 15225722) and the Environment and Conservation Fund of the Hong Kong Special Administrative Region, China (No. ECF 42/2022). Finally, and most importantly, I am deeply grateful to my parents for their immense and unwavering love and support. They have raised me and taught me to be an independent thinker. This work would not have been possible without their support.

CONTENTS

LIST OF FIGURES

LIST OF TABLES

CHAPTER 1 INTRODUCTION

1.1 Research background

Over the past few decades, uncertainties in engineering problems have become widely recognized for their significant impact on structural response and structural safety assessment. These inherent and unavoidable uncertainties are prevalent in both material parameters and applied loads. For instance, experimental data show considerable variations in the strengths of concrete and steel, and these material uncertainties critically affect structural resistance (Alpsten, 1972; Celik & Ellingwood, 2010). Uncertainties are also apparent in natural loads, such as wind load, where the maximum wind speed follows an Extreme Value Type I distribution (Harris, 1996; Simiu et al., 1978). Additionally, live loads exhibit probabilistic properties, as noted in Culver's survey (Culver, 1976). Uncertainties in engineering problems are commonly classified into two categories: aleatory uncertainties and epistemic uncertainties. Aleatory uncertainties refer to the inherent randomness in data and are irreducible; they are typically represented by precise probabilistic distributions. In contrast, epistemic uncertainties arise from a lack of knowledge and can be reduced by gathering more data or information. Several approaches have been developed to model epistemic uncertainty, including the theory of evidence and fuzzy set theory. Probability boxes have been further developed to model both aleatory and epistemic uncertainties (Schöbi & Sudret, 2017). In this research, the propagation of the aleatory uncertainty is of concern.

The structural responses must satisfy the predefined requirements such as structural safety against collapse, limitations on damage and adhering to other criteria (Melchers & Beck, 2018). Each requirement could be a limit state and these limit states are of vital importance for structural safety assessment. Denote the limit state as a performance function $G(\mathbf{X})$, where $\mathbf{X}$ is a vector of random variables that describes uncertainties arising from external loads and materials. The failure probability can be defined as the probability of the failure event $G(\mathbf{X}) \leq 0$. Reliability is the probability that a system or component can perform its intended functions under specified operating conditions (Barlow & Proschan, 1996). Structural reliability analysis seeks to assess the failure probability or reliability of engineering structures using analytical or numerical methods. Estimating reliability is crucial for probabilistic design and for preventing potential structural failures (Afshari et al., 2022).

Various approaches have been developed for efficient structural reliability analysis, which can be divided into four categories as illustrated in Figure 1-1. 1) The first/second order reliability methods are two elementary approaches for reliability analysis (Hasofer & Lind, 1974; Rackwitz, 2001), while they may be not applicable to a strongly nonlinear engineering system; 2) Sampling techniques such as the crude Monte Carlo simulation (MCS) are not restricted by the distribution types of input variables or system complexity. Despite its versatility, the crude Monte Carlo simulation is time-consuming for practical engineering problems. To address this issue, various improved versions have been proposed (Au & Beck, 2001; Engelund & Rackwitz, 1993); 3) surrogate model-based approaches aim to replace the original time-consuming complex computational models with some easy-to-run mathematical

models, thus avoiding the need to propagate uncertainties through the original complex systems. Commonly used surrogate models include the Kriging model (Kaymaz, 2005), polynomial chaos expansion (Sudret, 2008b), neural networks (Afshari et al., 2022) and so on; 4) the last category is the so-called moments-based methods, which employs the statistical moments of responses of engineering structures to fit an unknown probability density function (PDF) of interest (Zhang & Pandey, 2013; Zhao & Ono, 2001). Commonly used methods include the maximum entropy method (MEM) (Zhang & Pandey, 2013), Pearson system (Xu, Zhang, et al., 2020), the shifted generalized lognormal distribution (SGLD) (Low, 2013) and so on. Then, the failure probability can be readily obtained from the fitted PDF.

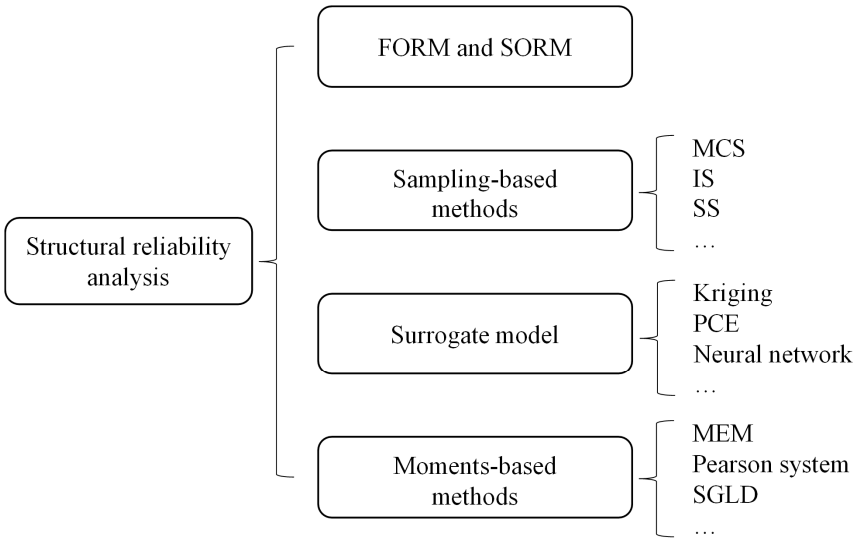

Figure 1-1 Approaches for structural reliability analysis

With the growing complexity of computational models, uncertainty propagation process is becoming more time-consuming, necessitating the development of more advanced reliability analysis techniques for efficient analysis. Recently, surrogate models such as Kriging, polynomial chaos expansion (PCE),

support vector regression, and neural networks have gained attention for their ability to replace costly computational models and provide predictions more efficiently. However, achieving high accuracy in reliability analysis requires a precise metamodel, and a large design of experiments (DoE) to train these models remains time-consuming. The Kriging model offers notable stochastic properties, such as local uncertainty in predictions, which can be leveraged for active learning approaches to develop an adaptive Kriging model. Active learning involves iteratively updating the Kriging model by adding new points to the DoE. These new points are strategically selected to significantly enhance the model's accuracy. An active learning reliability method combining Kriging and Monte Carlo simulation, known as AK-MCS, has demonstrated its advantages in failure probability estimation (Echard et al., 2011). However, iteratively updating the Kriging model with a large number of candidate samples is time-consuming and inefficient for estimating rare failure probabilities. To address this, advanced sampling techniques such as importance sampling and subset sampling have been integrated with the adaptive Kriging model for rare event estimation (Echard et al., 2013; Huang et al., 2016). Additionally, the choice of learning functions for selecting the next best point to improve the Kriging model impacts its efficiency. Stopping criteria are crucial for the accuracy of the trained adaptive Kriging model. However, determining when to halt the active learning process can be challenging, as many stopping criteria focus on the accuracy of the Kriging model while neglecting its impact on failure probability estimation.

Moreover, while many improved adaptive Kriging models have proven effective for reliability analysis of static engineering systems, their application to stochastic dynamic engineering systems is less explored. For example, the reliability

analysis of nonlinear structures subjected to stochastic seismic excitation is a relatively under-investigated area (Dang et al., 2021). This limited focus may stem from two primary reasons. First, capturing the complex dynamics of engineering structures with a Kriging model is challenging. Second, simulating stochastic excitation often requires a large number of random variables. For example, the spectrum representation method (SRM) (Shinozuka & Deodatis, 1991) requires thousands of random phases uniformly distributed on $[0, 2\pi]$. Treating these random variables as input features for stochastic dynamic systems results in high-dimensional systems. However, Kriging models and polynomial chaos expansion face the "curse-of-dimensionality" and are not well-suited for such high-dimensional problems. Alternatively, methods like the stochastic harmonic function representation can simulate stochastic excitation with only a few dozen random phases (Chen et al., 2017). Nevertheless, these random phases are mainly used for simulating stochastic excitation and do not serve as relevant input features for stochastic dynamic systems, as they have little impact on structural responses. Recently, machine learning techniques, such as long short-term memory (LSTM) and physics-informed LSTM, have been adopted for predicting time history responses of dynamic systems (R. Zhang et al., 2019; R. Zhang et al., 2020b). However, the accuracy of deep neural networks can be limited due to insufficient observations for reliability analysis. Consequently, the adaptive Kriging model remains a viable choice for dynamic reliability analysis. Identifying relevant input features for stochastic dynamic systems is crucial for constructing an effective adaptive Kriging model. Machine learning-based techniques, such as autoencoders for latent space identification, offer promising solutions for this challenge.

In addition, the adaptive Kriging model is updated iteratively, with the initial (DoE) typically enriched by adding one point at a time. This approach impedes parallel computing and significantly increases the computational burden. Although strategies for selecting multiple samples to allow parallelization have been proposed (Lelièvre et al., 2018; Schöbi et al., 2017), the refinement of the Kriging model remains challenging to complete in a single step and continues to require information from the actual computational model. Consequently, the conventional adaptive Kriging model can be considered an online adaptive Kriging model. Online learning strategies may face two major issues when applied to reliability analysis of complex computational models, such as those built with commercial finite element software. First, there is the challenge of implementing parallel computing, and second, the potential convergence problems of complex finite element models, which can lead to failures in both the models' convergence and the overall active learning process.

Overall, adaptive Kriging model has received increasing attention over the last few years. However, it still encounters several drawbacks.

1) Adaptive Kriging model has the difficulty in assessing rare failure probabilities.

2) most of the stopping criteria of learning process cannot reflect the accuracy of failure probability estimation.

3) applying adaptive Kriging model to dynamic reliability analysis of stochastic engineering systems remains difficult.

4) the updating process continuously requires information from real computational models and the refinement of Kriging model cannot be completed in a single step.

Addressing these issues is of significance for the application of the adaptive Kriging model to reliability analysis of practical engineering structures and probabilistic design.

1.2 Research Objectives

The proposed research aims to develop a more advanced adaptive Kriging model for rare events estimation and to enhance the application of conventional adaptive Kriging models for reliability analysis of engineering structures under stochastic excitation. The research objectives are as follows:

1) To develop an improved sampling scheme that identifies candidate samples near failure domains, enabling the Kriging model to be trained with these selected samples instead of the entire Monte Carlo population.

2) To propose an error-based stopping criterion that can reflect the relative error of failure probability estimation by the Kriging model, which can stop the active training process at an appropriate stage and thereby reduce the computational burden.

3) To develop an LSTM network capable of simultaneously considering time-variant stochastic excitation and time-invariant random structural parameters. A physic-informed LSTM network that can model uncertain governing equations of dynamics is further investigated for time history responses prediction.

4) To make the conventional adaptive Kriging model available for reliability analysis of stochastic dynamic systems, the LSTM network and autoencoder techniques are adopted to identify the latent space of stochastic dynamic systems for the construction of Kriging model.

5) To investigate an offline learning strategy for refining the Kriging model in a single step, eliminating the need for iterative updates. This approach benefits the dynamic reliability analysis of practical engineering structures.

1.3 Outline

This thesis consists of eight chapters and the framework is described in Figure 1-2. The organization of the thesis is summarized as follows:

Chapter 1 introduces the research background, outlining the research challenges and summarizing the objectives.

Chapter 2 presents a literature review of approaches for structural reliability analysis, with a focus on surrogate models, particularly adaptive Kriging models. It reviews adaptive Kriging models for estimating rare failure probabilities and conducting dynamic reliability analysis.

Chapter 3 presents an improved sampling scheme for the crude Monte Carlo simulation, allowing for the selection of candidate samples near the limit state surface. The Kriging model can be refined using these selected samples, eliminating the need for the entire Monte Carlo population. Additionally, an error-based stopping criterion is formulated to terminate the enrichment of the DoE.

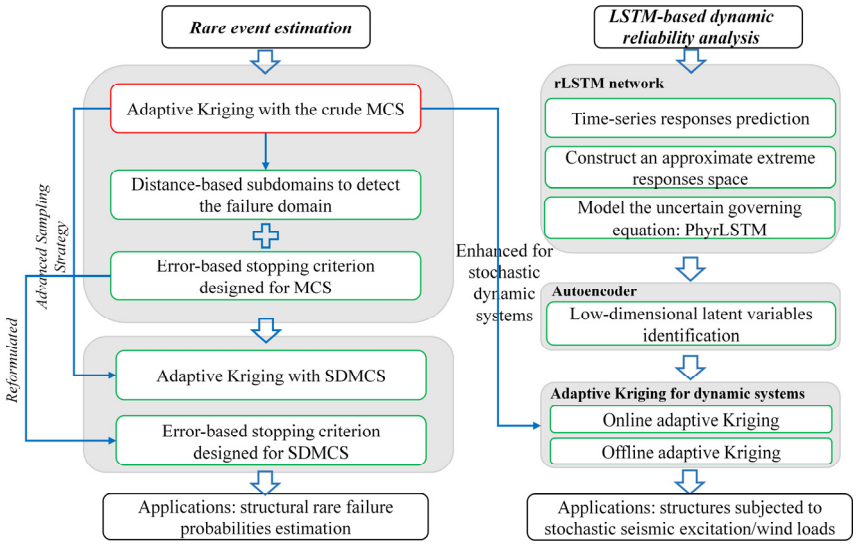

Figure 1-2 Framework of the proposed research

Chapter 4 adopts the spherical decomposition-based MCS (SDMCS) to reduce the number of candidate samples and the error-based stopping criterion developed in Chapter 3 is further reformulated for adaptive Kriging model incorporated with SDMCS.

Chapter 5 introduces an rLSTM network for stochastic dynamic systems, capable of simultaneously considering stochastic excitation and random structural parameters. The rLSTM, combined with an autoencoder, identifies latent variables for stochastic systems from the approximate extreme responses space. These identified latent variables are then utilized with the adaptive Kriging model for dynamic reliability analysis.

Chapter 6 shows a physics-informed rLSTM neural work (PhyrLSTM) for metamodeling of a highway bridge subjected to the stochastic seismic excitation, which can integrate the uncertain governing equation of dynamics. PhyrLSTM is then

combined with the autoencoder to construct an adaptive Kriging model for dynamic reliability analysis of the highway bridge under the stochastic seismic excitation.

Chapter 7 develops an error-based offline learning strategy designed to refine the Kriging model in a single step. It introduces the offline adaptive Kriging model (OAK) for dynamic reliability analysis, incorporating rLSTM and autoencoder techniques. This chapter investigates the dynamic reliability analysis of a highway bridge subjected to stochastic seismic excitation and a transmission tower exposed to stochastic wind loads.

Chapter 8 draws conclusions and provides possible future research.

CHAPTER 2 LITERATURE REVIEW

2.1 Introduction

Over the past few years, uncertainties have been widely acknowledged, significantly affecting structural responses, safety, and design. Researchers have developed various approaches for uncertainty propagation and reliability analysis to examine how these inherent uncertainties influence engineering structural behavior. Commonly used methods include gradient-based techniques (FORM and SORM), simulation-based methods, surrogate models, and moments-based methods. Recently, surrogate modeling or metamodeling techniques such as Kriging, PCE, and deep learning tools have gained increasing popularity since they can replace time-consuming computational models with easy-to-run surrogate models. The computational burden primarily stems from calls to costly computational models so the application of surrogate models can significantly reduce computational efforts. The accuracy of surrogate models is remarkably affected by design of experiments. However, limited observations often fail to train a surrogate model with sufficient accuracy for structural reliability analysis. To address this, an adaptive Kriging model incorporated with MCS is designed for structural reliability analysis, leveraging the advantages of the Kriging model. The DoE of the Kriging model is iteratively enriched using learning functions, and the training process terminates based on a predefined stopping criterion. Various adaptive Kriging models have been proposed to improve sampling approaches, learning functions, and stopping criteria. Most research focuses on the

reliability analysis of static engineering problems, while adaptive Kriging models for stochastic dynamic systems are seldom investigated.

2.2 The formulation of reliability analysis

For a typical reliability analysis problem, a performance function can be defined as:

$$Y = G(\mathbf{X}) \tag{2-1}$$

Where $\mathbf{X} = [X_1, X_2, ..., X_d]^{\mathrm{T}}$ is a *d*-dimensional vector collecting independent random variables with a joint probability density function $f_{\mathbf{X}}(\mathbf{x})$ and $G(\mathbf{X})$ is a performance function. Then, the probability of failure gives:

$$P_f = \Pr[G(\mathbf{X}) \le 0] \tag{2-2}$$

where Pr denotes probability, Eq. (2-2) can be calculated by the following integral:

$$P_f = \int_{\Omega_F} f_{\mathbf{X}}(\mathbf{x}) \mathrm{d}\mathbf{x} \tag{2-3}$$

where Ω_F denotes the failure domain.

The analytical solution of Eq. (2-3) is usually intractable due to the implicit and complex failure domain. Monte Carlo simulation can be employed to circumvent this limitation. Generate a MC population with N_{MC} candidate points (CPs) and the failure probability can be estimated by:

$$P_f \approx \frac{1}{N_{\mathrm{MC}}} \sum_{i=1}^{N_{\mathrm{MC}}} I\left(G\left(\mathbf{x}^{(i)}\right)\right) \tag{2-4}$$

in which $I(\cdot)$ is an indicator function such that $I = 1$ for $G(\mathbf{x}) \le 0$ and $I = 0$ otherwise. The coefficient of variation (CoV) gives:

$$\mathrm{CoV}(P_f) = \sqrt{\frac{1-P_f}{N_{\mathrm{MC}} \times P_f}} \tag{2-5}$$

2.3 Categories of structural reliability analysis methods

Various approaches have been developed for efficient reliability analysis of engineering structures. Gradient-based methods, such as the first- and second-order reliability methods (FORM and SORM), are two fundamental approaches for reliability analysis (Hasofer & Lind, 1974; Rackwitz, 2001). However, FORM and SORM are based on the most probable point (MPP) and consider the limit state surface as a linear or quadratic function. Consequently, they may not be applicable to many practical cases and are prone to significant errors when the limit state surface is strongly nonlinear. The remaining three categories of reliability analysis methods are sampling-based simulation methods, moments-based methods, and surrogate model-based methods, each of which is briefly reviewed in the following section.

2.3.1 Sampling-based method

Crude Monte Carlo simulation is the most direct method for uncertainty propagation and reliability analysis. However, its application to practical engineering structures is hindered by repeated evaluations of costly computational models. In engineering contexts with high reliability targets, the failure probability typically ranges from $10^{-6} \sim 10^{-3}$. The size of MC population is inversely proportional to the order of failure probability and $10^5 \sim 10^8$ samples are required to achieve a reliable estimation

(Schöbi et al., 2017), which is impractical for real-world engineering. Therefore, MCS is usually regarded as the reference method since it is not limited by forms of performance functions and types of distributions.

Some advanced sampling techniques are developed to tackle challenges that MCS encounters. Importance sampling (IS) based on the variance reduction technique is developed (Au & Beck, 1999; Melchers, 1989), while the performance of IS relies on the prudent choice of the auxiliary distribution or the so-called IS density, the failure probability by IS can be calculated as:

$$P_f \approx \frac{1}{N_{\mathrm{IS}}} \sum_{i=1}^{N_{\mathrm{IS}}} I\left(\mathbf{x}^i\right) \frac{f_{\mathbf{X}}\left(\mathbf{x}^i\right)}{q_{\mathrm{IS}}\left(\mathbf{x}^i\right)} \tag{2-6}$$

where $q_{\mathrm{IS}}(\mathbf{x})$ is the importance sampling density. Instead of sampling from the MC density, IS uses samples from the auxiliary distribution $q_{\mathrm{IS}}(\mathbf{x})$ to reduce the estimator's variance (Tabandeh et al., 2022). Although the optimal IS density is not realizable, a near-optimal density function may be adopted. Ang et al. (1992) found an IS density by minimizing the mean square error between kernel density and the optimal solution. Then, Au and Beck (1999) enhanced importance sampling by employing a more efficient sampling scheme, namely Markov Chain Monte Carlo simulation. More recently, a cross-entropy-based IS was proposed by minimizing the relative entropy between the optimal solution and Gaussian mixtures (Kurtz & Song, 2013).

Subset sampling (SS) transforms a rare failure event into a series of intermediate conditional events with higher failure probabilities. This approach

significantly reduces the computational effort required by Monte Carlo simulation, as fewer samples are needed to estimate a relatively large failure probability. (Au & Beck, 2001). Suppose a sequence of failure events with increasing thresholds or structural capacities:

$$F_1 \supset F_2 \supset \cdots \supset F_m = F, b_1 < b_2 < \cdots b_m = b \tag{2-7}$$

The failure probability P_f can be estimated as:

$$\begin{aligned} P_f &= P(F_m) = P\left(\bigcap_{i=1}^{m} F_m\right) \\ &= P(F_1)\prod_{i=1}^{m-1} P(F_i \mid F_{i-1}) \end{aligned} \tag{2-8}$$

Therefore, the failure probability estimation depends on $P(F_1)$ and conditional failure probabilities $P(F_i \mid F_{i-1})$, which can be calculated by MCS and Markov Chain Monte Carlo simulation, respectively. In addition, line sampling technique (Koutsourelakis, 2004; Koutsourelakis et al., 2004; Song et al., 2020) has also been adopted for reliability analysis. Although these advanced sampling techniques can significantly reduce computational efforts compared to crude MCS, a considerable number of model evaluations are still required. Consequently, these techniques are often used in conjunction with surrogate models.

2.3.2 Moments-based method

The core idea of the moments-based method is to construct the underlying distribution of interest using the statistical moments of structural responses, such as mean, standard deviation, skewness, and kurtosis (Zhao & Ono, 2001). The moments-based

method requires neither iteration nor computation of derivatives so it can be readily applied to structural reliability analysis. However, the accuracy of the moments-based method depends on two main factors: the estimation of statistical moments and the selection of an appropriate distribution model for fitting.

Univariate dimension reduction method (UDRM) and bivariate dimension reduction method (BDRM) are two popular approaches for statistical moments estimation (Rahman & Xu, 2004; Xu & Rahman, 2004). Both methods rely on Taylor series expansion to decompose a multi-dimensional integration for statistical moments estimation into a summation of several lower-dimensional integrations. However, UDRM may lack accuracy for nonlinear systems, and the number of integration points required by BDRM increases dramatically with the number of random variables. Recently, cubature formulae and their improvements have been also proposed for reliability analysis (Xu & Kong, 2018; Xu, Zhang, et al., 2020; D. Zhang et al., 2022). Sampling techniques such as Latin hypercube sampling, Sobol sequences, and Latinized Partially Stratified Sampling (LPSS) are commonly used for estimating statistical moments of engineering structures subjected to stochastic excitation (Dang et al., 2021; Dang & Xu, 2020; Shields & Zhang, 2016; Zhang, Dong, & Feng, 2023). Besides the estimation of statistical moments, the selection of distribution model for covering the PDF of interest is also of importance. Various distribution models have been developed such as the Johnson system (Johnson et al., 1995), Pearson system (Xu, Zhang, et al., 2020) and Hermite model (Win t′ erstein, 1988). The maximum entropy method is considered to be the most unbiased estimation of the underlying PDF given statistical moments as constrains (Jaynes, 1957; Li & Zhang, 2011; Zhang & Pandey, 2013). Additionally, Low (2013)

developed a shifted generalized lognormal distribution (SGLD) for reliability analysis. Recently, a distribution model by mixing an inverse Gaussian distribution and a lognormal distribution was proposed for seismic reliability of nonlinear structures (Dang & Xu, 2020). Although the moments-based method is relatively straightforward to implement, its accuracy is significantly influenced by the estimation of statistical moments and the choice of distribution models.

2.3.3 Surrogate model

With growing complexity of computational models or simulation codes, reliability analysis of engineering structures is becoming more challenging. Surrogate models offer a faster alternative to the original computational models, reducing the need for extensive evaluations. Consequently, surrogate models have garnered significant attention in recent years. Commonly used surrogate models include Polynomial Chaos Expansion, Kriging, support vector regression, and neural networks.

Polynomial chaos expansion can explicitly represent a random output in a suitable space spanned by polynomial basis, which has been widely used in uncertainty analysis. PCE originates from Wiener's study (Wiener, 1938) and was initially designed for Gaussian distributions. It was later extended to a generalized PCE (Lucor & Karniadakis, 2004; Xiu & Karniadakis, 2002) considering to accommodate non-Gaussian distributions. Characterizing the PDF of the structural response of interest is equivalent to determining the unknown coefficients of PC expansions. Projection method (Le Maıtre et al., 2002) or regression approach (Berveiller et al., 2006; Choi et al., 2004) can be utilized to obtain coefficients of PC basis. It is known that the number of unknown coefficients increases dramatically

with the dimension of input random variables. To address this issue, the sparse PCE was proposed to mitigate the computational burden. A stepwise regression method was developed for stochastic finite element analysis and sensitivity analysis (Blatman & Sudret, 2010a, 2010b), which retains a small number of significant basis functions to construct the PCE. Blatman and Sudret (2011) proposed an adaptive algorithm based on least angle regression to detect important terms of PC expansion. To further reduce the number of unknown coefficients, Zhang and Xu (2021) used a dimension-reduction model based on contribution-degree analysis and stepwise regression method to build a sparse PCE. PCE still encounters the "curse-of-dimensionality", and efforts have been made to address high-dimensional problems (He et al., 2020; Papaioannou et al., 2019; Yue et al., 2021). PCE plays a crucial role in structural reliability analysis, and its performance has been extensively validated (Bhattacharyya, 2021; Hu & Youn, 2011; Lim & Manuel, 2021; J. Zhang et al., 2022).

The Kriging model, also known as the Gaussian process model, has drawn increasing attention for its ability to provide not only predicted values but also estimates of the local variance of predictions. Initially investigated in geostatistics and later by Matheron (1973). Kriging is also applied to optimization problems due to its stochastic properties. For instance, the efficient global optimization (EGO) method utilizes an active learning strategy to enhance optimization (Jones et al., 1998). Active learning means that Kriging model is updated by adding a new point to the DoE and this point is considered to have a significant improvement on the current Kriging model. Jones et al. (1998) compared the performance of Kriging model and PCE for uncertainty propagation. Subsequently, Kaymaz (2005) developed a MATLAB toolbox termed DACE for constructing Kriging model and compared its

performance with the response surface method in structural reliability analysis. It appears that the Kriging model does not consistently outperform the response surface method unless its parameters are carefully selected (Echard et al., 2011). On the basis of active learning strategy, researchers have increasingly focused on constructing adaptive Kriging models for reliability analysis, as these models can deliver satisfactory results with fewer function evaluations. A summary of adaptive Kriging models is presented in the following section.

The machine learning technique such as support vector machine (SVM) is also employed for reliability analysis. Originally designed for classification tasks, SVM has been extended to address regression problems, known as support vector regression (SVR) (Roy & Chakraborty, 2023). In structural reliability analysis, SVM has been employed to frame the problem as a classification issue (Alibrandi et al., 2015; Bourinet et al., 2011; Pan & Dias, 2017; Zhao et al., 2017). SVR-based reliability analysis approaches have also been investigated (Bourinet, 2016; Dai et al., 2015; das Chagas Moura et al., 2011; Richard et al., 2012). Additionally, artificial neural networks (ANNs) are versatile machine learning tools capable of modeling highly nonlinear systems across the entire domain (Cardoso et al., 2008). ANNs are commonly used as regression tools to model limit state functions. A well-trained ANN can then be integrated with Monte Carlo simulation (MCS) for structural reliability analysis (Kingston et al., 2011; Papadrakakis et al., 1996). Furthermore, FORM and SORM can be combined with ANNs for enhanced reliability analysis (Goh & Kulhawy, 2003). Papadopoulos et al. (2012) proposed a method that combines subset sampling with neural networks for reliability estimation. More recently, an active learning approach has been developed that integrates deep neural

networks with weighted sampling, allowing the neural network to be iteratively updated by adding new samples (Xiang et al., 2020). However, the accuracy and generalization ability of neural networks are highly dependent on their structure and the quantity of training samples, necessitating further investigation into the network design and selection of observed data.

2.4 Adaptive Kriging model for reliability analysis

Adaptive Kriging models based on active learning strategies have gained significant popularity in recent years. These models are refined adaptively by adding new samples to the design of experiments, with each new sample selected to significantly enhance the current Kriging model. This approach ensures high accuracy of the Kriging model within the domain of interest, such as the limit state surface, without needing to ensure accuracy across the entire domain. Bichon et al. (2008) proposed an efficient global reliability analysis method that leverages Kriging predictions and local variance within an active learning strategy. Subsequently, Echard et al. (2011) developed an active learning reliability analysis method combining Kriging and Monte Carlo simulation, known as AK-MCS. The framework for adaptive Kriging models was established, and many improved versions of AK-MCS have since been developed. Most studies focus on enhancing sampling schemes for generating candidate samples, refining learning functions for selecting the best samples, and optimizing stopping criteria for terminating the active learning process. The framework of adaptive Kriging model is shown in Figure 2-1. An adaptive Kriging model facilitates the construction of an accurate surrogate model within the domain of

interest, and the final refined Kriging model can then be utilized for reliability analysis.

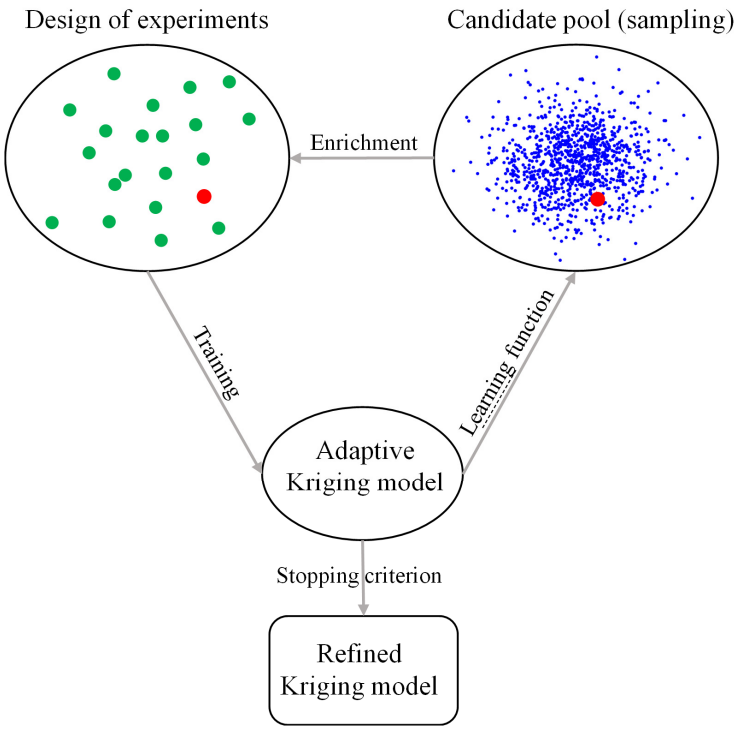

Figure 2-1 Framework of adaptive Kriging model

2.4.1 Learning functions and stopping criteria

Learning function aims to select points that can remarkably enhance the accuracy of the current Kriging model. A learning function termed the expected feasibility function (EFF) was proposed for efficient global reliability analysis (Bichon et al., 2008), which can select points are expected to be close to the limit state surface. The calculation of EFF is based on the Kriging prediction $\mu_K(\mathbf{x})$ and its corresponding local variance $\sigma_K^2(\mathbf{x})$:

$$\mathrm{EFF}(\mathbf{x}) = \left(\mu_K(\mathbf{x}) - a\right)\alpha_1 - \sigma_K(\mathbf{x})\alpha_2 + \left[\Phi\left(\frac{(a+\kappa)-\mu_K(\mathbf{x})}{\sigma_K(\mathbf{x})}\right) - \Phi\left(\frac{(a-\kappa)-\mu_K(\mathbf{x})}{\sigma_K(\mathbf{x})}\right)\right] \tag{2-9}$$

where $\alpha_1 = \left[2\Phi\left(\frac{a-\mu_K(\mathbf{x})}{\sigma_K(\mathbf{x})}\right) - \Phi\left(\frac{(a-\kappa)-\mu_K(\mathbf{x})}{\sigma_K(\mathbf{x})}\right) - \Phi\left(\frac{(a+\kappa)-\mu_K(\mathbf{x})}{\sigma_K(\mathbf{x})}\right)\right]$ and Φ is the standard normal cumulative distribution function, $\alpha_2 = \left[2\phi\left(\frac{a-\mu_K(\mathbf{x})}{\sigma_K(\mathbf{x})}\right) - \phi\left(\frac{(a-\kappa)-\mu_K(\mathbf{x})}{\sigma_K(\mathbf{x})}\right) - \phi\left(\frac{(a+\kappa)-\mu_K(\mathbf{x})}{\sigma_K(\mathbf{x})}\right)\right]$ and ϕ is the standard normal density function. EFF provides an index of how well the true value at point $\mathbf{x}$ is expected to satisfy the constraint $G(\mathbf{x}) = a$ over the domain $a \pm \kappa$. Obviously, a is set as 0 for reliability analysis and κ is suggested as $2\sigma_K^2(\mathbf{x})$. The next best point is the point with the maximum EFF value. The next best point is identified as the one with the highest EFF value. However, this approach may select points that have little impact on the results because the EFF considers the entire space, including regions that contribute little to the failure probability. This can lead to inefficient use of computational resources.

Echard et al. (2011) proposed a so-called U learning function, which can reflect the probability of wrong classification on the sign of a point $\mathbf{x}$:

$$\mathrm{U}(\mathbf{x}) = \frac{\left|\mu_K(\mathbf{x})\right|}{\sigma_K(\mathbf{x})} \tag{2-10}$$

U learning function is widely used due to its simplicity (Echard et al., 2013; Huang et al., 2016). A smaller U value indicates a higher probability of misclassification.

Therefore, the U learning function selects the point from the candidate pool with the smallest U value, as this point is considered to have the highest risk of crossing the limit state surface.

Various learning functions have been developed from different perspectives. An information entropy-based learning function was developed by Lv's work (Lv et al., 2015). Sun et al. (2017) proposed the least improvement function by combining the information provided by Kriging model and joint probability function of random variables. X. Zhang et al. (2019) developed a reliability-based improvement function called REIF. Feng et al. (2023) introduced a novel Kriging-based learning function designed for system reliability analysis, particularly considering correlated failure modes. Besides learning functions designed for the adaptive Kriging, a general failure-pursuing learning strategy was proposed for surrogate models (Jiang et al., 2019). Recently, Bayesian active learning approaches have been developed for reliability analysis (Dang, Valdebenito, Faes, et al., 2023; Dang et al., 2022). Moreover, to enhance the one-by-one enrichment of DoE, parallel computing strategies have been investigated in conjunction with adaptive Kriging models (Lelièvre et al., 2018; Schöbi et al., 2017; Xiao et al., 2022; Xiong & Sampath, 2021).

With regard to stopping criteria, most of them are based on a prescribed threshold for the learning function value. For instance, Bichon et al. (2008) employed a threshold of 0.001 for the maximum EFF value as a stopping criterion. Echard et al. (2011) adopted $\min\left(U\left(\mathbf{x}\right)\right) \geq 2$ as the convergence condition for the active learning process. Although the U stopping criterion is widely used, it has been shown to be overly conservative for failure probability estimation (Schöbi et al., 2017). This can

lead to unnecessary evaluations of the costly performance function when using adaptive Kriging with the U stopping criterion. (Fauriat & Gayton, 2014) pointed out that the Kriging model was sufficiently accurate if 2% of the candidate samples satisfied the U stopping criterion. Another group of stopping criteria are constructed on the basis of the stabilization of a specific value during the active learning process. For instance, Gaspar et al. (2017) proposed a stopping criterion based on the stability of the estimated failure probability. Similarly, stability in the bounds of the estimated failure probability or the reliability index has been used as a convergence condition (Moustapha et al., 2022; Schöbi et al., 2017). However, these criteria also rely on a predefined threshold, which is typically chosen based on researchers' experience. The impact of this selected threshold on the accuracy of failure probability estimation remains unclear. Recently, stopping criteria based on the relative error of the failure probability have been developed. Wang and Shafieezadeh (2019) proposed an error-based stopping criterion (ESC) considering probabilities of wrong classification of all Monte Carlo samples. However, the accuracy of the failure probability may have been in stabilization before ESC is met for some cases (J. Wang et al., 2022). Zhang et al. (2021) developed an approach to estimate the maximum error of the posterior failure probability given a confidence level.

2.4.2 Rare event estimation

In the context of practical engineering and a high-reliability targets, failure probabilities of practical cases are typically small (10^{-6}~10^{-3}) and sometimes very rare ($<10^{-6}$) (Schöbi et al., 2017). AK-MCS requires an iterative process with Monte Carlo (MC) sampling to refine the Kriging model, which can be time-consuming,

especially with large populations. To address this, advanced sampling techniques are often integrated with adaptive Kriging models to improve efficiency in estimating rare events.

Adaptive Kriging model has been combined with importance sampling for small failure probabilities estimation (Guo et al., 2020; Jia & Wu, 2024; Xiao et al., 2020). Echard et al. (2013) combined the importance sampling with the adaptive Kriging (AK-IS) for rare events estimation. However, traditional importance sampling, which relies on the most probable failure point, may not be accurate for reliability problems involving multiple failure regions. To address this, an improved AK-IS was proposed for handling multiple failure regions (Cadini et al., 2014). A method termed Meta-IS-AK was developed by combing adaptive Kriging based IS and IS based adaptive Kriging model to efficiently estimate failure probabilities in cases with multiple failure regions (Zhu et al., 2020). X. Zhang et al. (2020) introduced an adaptive Kriging-oriented importance sampling method for structural system reliability analysis, enhancing the sampling center through an active learning strategy. To further reduce the number of model evaluations, Yun et al. (2018) improved adaptive Kriging with a modified importance sampling by using a contributive weight function. Chen et al. (2019) developed a hybrid strategy by combining MCS and IS for small failure probabilities estimation. Additionally, Yun et al. (2020) proposed an improved AKMCS by using the radial-based importance sampling for reliability analysis.

Subset sampling technique is also employed to generate the candidate pool for active learning process. Huang et al. (2016) proposed AK-SS by combining adaptive

Kriging model with subset sampling while the candidate pool for training is still generated by MCS. An active learning reliability method combining Kriging constructed with exploration and exploitation of failure region and subset simulation (AKEE-SS) is proposed (J. Zhang et al., 2019). Ling et al. (2019) proposed a coupled subset simulation and adaptive Kriging model for rare events estimation, where the adaptive Kriging model was updated for each intermediate failure event. Zhang and Quek (2022) also updated Kriging model at each simulation level and Kriging model was utilized to determine the threshold for each level. Recently, the spherical decomposition-based MCS was adopted to replace the crude MCS for adaptive Kriging (Su et al., 2020), significantly reducing the number of candidate samples. Additionally, line sampling has been integrated with active learning strategies for structural reliability analysis (Dang, Valdebenito, Song, et al., 2023; Wang et al., 2023)

2.4.3 Dynamic reliability analysis

Compared to static reliability analysis problems, dynamic reliability analysis is more complex and time-consuming due to highly nonlinear and time-dependent structural behaviors. Various theories are devoted to efficiently evaluating the first passage failure probability of a dynamic system (Dang et al., 2021; Hu & Du, 2013; Roberts & Spanos, 1986; Sudret, 2008a). The out-crossing rate method is one of the most widely used approaches for dynamic reliability analysis, however, the joint probability density function of the response and its velocity required by the Rice formula (Rice, 2013) for estimating the mean out-crossing rate is usually intractable.

Evaluating the first passage failure probability of dynamic systems remains challenging due to uncertainties arising from both structural properties and time-variant excitations. Alternatively, this evaluation can be transformed into estimating the extreme value distribution (EVD) of a dynamic system's response (Chen & Li, 2007; Lutes & Sarkani, 2004). From the EVD perspective, the complex time-dependent dynamic reliability analysis can be simplified to a time-invariant counterpart, as only the extreme response within a given time interval is of interest. Consequently, advanced approaches for static reliability analysis, such as MCS and SS, can be employed to derive the EVD of the dynamic system. However, these methods require numerous dynamic analyses to achieve accurate results, particularly for rare failure events estimation. With the development of the extreme value theory, it is possible to use the Gumbel distribution (Næss & Gaidai, 2009; Naess & Gaidai, 2008) and the generalized extreme value distribution (Grigoriu & Samorodnitsky, 2014) to cover the unknown EVD of interest. Additionally, various parametric distributions have been developed to provide flexible approximations of the underlying PDF, such as the shifted generalized lognormal distribution (Low, 2013; Xu, Wang, et al., 2020), the recently developed fractional moments based mixture distribution (Dang & Xu, 2020) and the moment-generating function based mixture distribution (Dang et al., 2021). The maximum entropy method, using either integer moments (Li & Zhang, 2011) or fractional moments (Xu & Dang, 2019; Zhang & Pandey, 2013) can also be employed for evaluating the EVD. However, these moments-based methods require further investigation regarding the accuracy of moments estimation and the flexibility of the distribution model in fitting the EVD. The probability density evolution method (PDEM) has been investigated for EVD

estimation and is applicable to strongly nonlinear dynamic systems (Chen & Li, 2007; Chen & Li, 2005), however, it may be not suitable for problems with high-dimensional random variables and small failure probabilities (Dang et al., 2021).

Surrogate models can be employed when extreme responses are of interest (Lu et al., 2018; Wang & Wang, 2015). However, surrogate models for dynamic reliability analysis of engineering structures subjected to stochastic excitation (e.g., earthquakes and wind) are rarely found. This is due to the complex dynamics and the simulation of stochastic excitation. For instance, seismic motions are typically modeled as non-stationary stochastic processes, and the spectral representation method (Liu et al., 2016; Shinozuka & Deodatis, 1991) can be employed. Typically, 500-1000 or more random phases are required to characterize non-stationary seismic motions. If these random phases are considered input features, it results in a high-dimensional dynamic reliability analysis problem. Hence, the surrogate model-based methods may be not a rational choice for dynamic reliability analysis due to the "curse-of-dimensionality". One can extract the peak excitation and structural parameters as input features while ignoring time-dependent dynamics may lead a significant error. Zhou and Peng (2022) investigated the reliability analysis of a 110-dimensional stochastic dynamic system by combining an autoencoder with an adaptive Gaussian process model, they employed the stochastic harmonic function representation method for simulating stochastic excitations (Chen et al., 2017). However, only extreme responses were considered when constructing the surrogate model and time series responses were ignored.

Therefore, dynamic systems subjected to the stochastic excitation have not been well studied in terms of metamodel construction and reliability analysis. The spectrum representation method results in a high-dimensional dynamic system, primarily due to the thousands of random phases required to simulate the stochastic excitations. These random phases are not the pertinent input features; instead, the generated time-variant stochastic excitations are. Conventional surrogate models, such as Kriging and PCE, cannot be directly constructed for stochastic dynamic systems, even if only extreme responses are of interest. Although alternative approaches for simulating stochastic excitation, which require fewer random variables, exist (Chen et al., 2017; Liu et al., 2016), constructing conventional surrogate models remains challenging since the pertinent input features are implicit for time-dependent stochastic dynamic systems. Recently, a powerful deep learning tool called the long short-term memory has been employed to deal with the sequence-to-sequence data, allowing for the circumvention of high-dimensional random phases. LSTM has been investigated for metamodeling of nonlinear structures (R. Zhang et al., 2019; R. Zhang et al., 2020b) using only the time-variant excitation as the input feature. However, the uncertainties of structural parameters and seismic ground motions have not been considered in the metamodel construction.

Overall, adaptive Kriging model has shown its advantages in the field of static reliability analysis. However, Kriging model for extreme responses prediction of stochastic dynamic systems is challenging due to implicit input features. Therefore, identifying the input features of a stochastic dynamic system is necessary before constructing a Kriging model. Once identified, the active learning strategy can be employed for the dynamic reliability analysis of stochastic engineering structures.

2.5 Summary

This chapter reviews several commonly used methods for structural reliability analysis, including sampling-based simulation, moments-based methods, and surrogate models. Among these, Kriging model has gained significant attention in recent years, particularly due to advancements in active learning strategy. This strategy allows for the development of adaptive Kriging models by iteratively adding samples to DoE. However, adaptive Kriging models still face several challenges, such as inefficiency in rare event estimation, limitations in reliability analysis of stochastic dynamic systems, and difficulties with parallel computing. Rare failure probabilities and structures subjected to dynamic loads are prevalent in practical engineering problems. Therefore, it is crucial to further explore the efficiency of adaptive Kriging models for rare failure estimation. In addition, developing adaptive Kriging models for stochastic dynamic systems and investigating parallel computing strategies are essential for improving reliability analysis in practical engineering applications.

CHAPTER 3 ADAPTIVE KRIGING MODEL WITH A NEW STOPPING CRITERION AND DISTANCE-BASED SUBDOMAINS FOR RELIABILITY ANALYSIS

3.1 Introduction

Reliability analysis for computationally expensive models poses significant challenges. Monte Carlo simulation is commonly employed in conjunction with the active learning assisted Kriging model (AKMCS), which can significantly reduce the number of model evaluations. However, updating a Kriging model with numerous samples is time-consuming, especially for the small failure probability estimation. To alleviate the computational effort induced by the active learning process, a distance-based subdomain is first developed to select the candidate points in the vicinity of the limit state surface. Accordingly, a Kriging model is trained within distance-based subdomains and Kriging predictions on the whole population can be avoided. Additionally, to further mitigate the computational effort caused by time-demanding model evaluations, a new stopping criterion is formulated based on the expected upper bound of the relative error of failure probability. A reasonable target threshold for the new stopping criterion is suggested, grounded in the quantification of the selected threshold's impact on the relative error of the failure probability. One analytical performance function and three numerical models including a 61-bar truss, a reinforced concrete planar frame and a bolted steel beam-column joint are investigated to demonstrate the efficiency and accuracy of the proposed approach.

3.2 Active learning method incorporating Kriging model and MCS

3.2.1 Kriging model

Although MCS is a straightforward way for estimating failure probabilities, it can be computationally expensive, especially when dealing with time-consuming models. To address this issue, surrogate models are often used to reduce the computational cost. In this thesis, the Kriging model is adopted due to its sophisticated stochastic properties.

For a performance function $Y = G(\mathbf{X})$, Kriging model is based on the idea that $G(\mathbf{X})$ is a realization of Gaussian process $\mathcal{G}(\mathbf{X})$ (Echard et al., 2011; Matheron, 1973):

$$\mathcal{G}(\mathbf{X}) = \mathbf{f}(\mathbf{X})^{\mathrm{T}} \boldsymbol{\beta} + z(\mathbf{X}) \tag{3-1}$$

$\mathbf{f}(\mathbf{X})^{\mathrm{T}} \boldsymbol{\beta}$ is a deterministic term providing the trend of Kriging model, where $\mathbf{f}(\mathbf{X})^{\mathrm{T}} = \left[f_1(\mathbf{X}), f_2(\mathbf{X}), ..., f_k(\mathbf{X}) \right]$ are basis functions and $\boldsymbol{\beta}^{\mathrm{T}} = \left[\beta_1, \beta_2, ..., \beta_k \right]$ is a vector of regression coefficients. Note that the ordinary Kriging is usually adopted, i.e., $\mathbf{f}(\mathbf{X})^{\mathrm{T}} \boldsymbol{\beta} = \beta$. z(**X**) is a stationary Gaussian process with zero mean and covariance:

$$\operatorname{cov}\left(z\left(\mathbf{x}^{(i)}\right), z\left(\mathbf{x}^{(j)}\right) \right) = \sigma_z^2 R_{\mathbf{0}}\left(\mathbf{x}^{(i)}, \mathbf{x}^{(j)}\right) \tag{3-2}$$

in which σ_z^2 is the variance of process and $R_{\boldsymbol{\theta}}(\cdot)$ is a correlation function with respect to parameters $\boldsymbol{\theta}$. The anisotropic squared-exponential function is employed as the correlation function:

$$R_{\boldsymbol{\theta}}\left(\mathbf{x}^{(i)},\mathbf{x}^{(j)}\right)=\prod_{k=1}^{d}\exp\left[-\theta_k\left(x_k^{(i)}-x_k^{(j)}\right)^2\right] \tag{3-3}$$

Given a design of experiment with N training points (TPs), i.e., $\boldsymbol{\mathcal{X}}=\left[\mathbf{x}^{(1)},\mathbf{x}^{(2)},...,\mathbf{x}^{(N)}\right]^{\mathrm{T}}$ with $\mathbf{x}^{(i)}\in\mathbb{R}^d$ and $\boldsymbol{\mathcal{Y}}=\left[y_1,y_2,...,y_N\right]^{\mathrm{T}}$ with $y_i=G\left(\mathbf{x}^{(i)}\right)\in\mathbb{R}^1$, then the scalar β and process variance σ_z^2 can be estimated by:

$$\hat{\beta}=\left(\mathbf{1}^{\mathrm{T}}\mathbf{K}^{-1}\mathbf{1}\right)^{-1}\mathbf{1}^{\mathrm{T}}\mathbf{K}^{-1}\boldsymbol{\mathcal{Y}} \tag{3-4}$$

and

$$\hat{\sigma}_z^2=\frac{1}{N}\left(\boldsymbol{\mathcal{Y}}-\beta\mathbf{1}\right)^{\mathrm{T}}\mathbf{K}^{-1}\left(\boldsymbol{\mathcal{Y}}-\beta\mathbf{1}\right) \tag{3-5}$$

where $\mathbf{1}$ is a unit vector with the size $N\times 1$ and $\mathbf{K}_{ij}=R_{\boldsymbol{\theta}}\left(\mathbf{x}^{(i)},\mathbf{x}^{(j)}\right)$. Note that scalar parameters $\boldsymbol{\theta}$ of correlation function can be calculated via the maximum likelihood estimation. Then, the Kriging mean at a new point $\mathbf{x}$ can be computed as (Matheron, 1973):

$$\mu_K\left(\mathbf{x}\right)=\beta+\mathbf{k}\left(\mathbf{x}\right)^{\mathrm{T}}\mathbf{K}^{-1}\left(\boldsymbol{\mathcal{Y}}-\beta\mathbf{1}\right) \tag{3-6}$$

where $\mathbf{k}\left(\mathbf{x}\right)=\left[R_{\boldsymbol{\theta}}\left(\mathbf{x},\mathbf{x}^{(1)}\right),R_{\boldsymbol{\theta}}\left(\mathbf{x},\mathbf{x}^{(2)}\right),...,R_{\boldsymbol{\theta}}\left(\mathbf{x},\mathbf{x}^{(N)}\right)\right]^{\mathrm{T}}$, and the Kriging variance can be analytically expressed as:

$$\sigma_K^2(\mathbf{x}) = \sigma_z^2\left[1 + c(\mathbf{x})^{\mathrm{T}}\left(\mathbf{1}^{\mathrm{T}}\mathbf{K}^{-1}\mathbf{1}\right)^{-1} c(\mathbf{x}) - \mathbf{k}(\mathbf{x})^{\mathrm{T}}\mathbf{K}^{-1}\mathbf{k}(\mathbf{x})\right] \tag{3-7}$$

in which $c(\mathbf{x}) = \mathbf{1}^{\mathrm{T}}\mathbf{K}^{-1}\mathbf{k}(\mathbf{x}) - 1$.

Kriging is an exact interpolation method, which means $\mu_K\left(\mathbf{x}^{(i)}\right) = G\left(\mathbf{x}^{(i)}\right)$ at observed points with a null Kriging variance. For unexplored points, the uncertainty of predictions can be estimated and $G\left(\mathbf{x}^{(i)}\right)$ follows a normal distribution with mean $\mu_K\left(\mathbf{x}^{(i)}\right)$ and the standard deviation $\sigma_K\left(\mathbf{x}^{(i)}\right)$.

3.2.2 Adaptive Kriging model with MCS

On the basis of local variance provided by Kriging model, an active learning method, incorporating Kriging model and Monte Carlo simulation termed AKMCS, is proposed (Echard et al., 2011). The main procedure is summarized as follows.

(1) Generate a MC population with N_{MC} candidate points (CPs).

(2) Generate an initial DoE with N_0 training points (TPs) and construct an initial Kriging model.

(3) Enrich the DoE by selecting the next best point via a learning function.

(4) Use the enriched DoE to train Kriging model until meeting the condition of convergence.

(5) Estimate P_f by using Kriging predictions on CPs via the refined Kriging model:

$$P_f = \frac{1}{N_{MC}} \sum_{i=1}^{N_{MC}} I\left(\mu_K\left(\mathbf{x}^{(i)}\right)\right) \tag{3-8}$$

Various learning functions are developed for the enrichment of DoE, among which the U learning function is widely used due to its simplicity:

$$U(\mathbf{x}) = \frac{\left|\mu_K(\mathbf{x})\right|}{\sigma_K(\mathbf{x})} \tag{3-9}$$

The probability of the wrong classification at point **x** can be calculated as:

$$P_{\mathrm{w}}(\mathbf{x}) = \Phi\left(-\frac{\left|\mu_K(\mathbf{x})\right|}{\sigma_K(\mathbf{x})}\right) \tag{3-10}$$

where $\Phi(\cdot)$ represents the cumulative distribution function of the standard normal distribution. The smaller the U value, the higher the probability of incorrect classification. Therefore, the next best training point is selected by finding the minimum value of the U function. The enrichment of the DoE continues until the minimum U value exceeds 2, ensuring that the probability of incorrect classification is less than 0.0228 (Echard et al., 2011).

3.3 Proposed adaptive Kriging model with distance-based subdomains

Although AKMCS can significantly reduce the number of model evaluations for reliability analysis, sometimes the computational effort of the active learning strategy itself is expensive. This is due to the need for Kriging predictions across the entire MC population, especially when assessing small failure probabilities (Echard et al.,

2013). In practice, only the failure points and the candidate points in the vicinity of limit state surface are of interest for reliability analysis. Therefore, the Kriging predictions over the entire domain are not necessary. To this end, a distance-based subdomain is proposed to identify candidate points around the limit state surface. The failure domain can be covered by several distance-based subdomains. Only the points within these subdomains are used to update the Kriging model. This strategy, termed AKDS in this thesis, focuses the training of the Kriging model within distance-based subdomains. Furthermore, a new stopping criterion is theoretically derived from the expected upper bound of the relative error of failure probability. This criterion further reduces the computational effort associated with time-consuming performance function evaluations.

3.3.1 Distance-based subdomain

It is known that a candidate point with a minimum value of U learning function has a high potential risk crossing the limit state surface (Echard et al., 2011), indicating that this point is close to both the LSS and the failure domain. Therefore, candidate points near this point contain crucial information about the failure domain and the LSS of interest. Based on this idea, candidate points around the point with the minimum U value are first identified using a distance-based strategy. In this thesis, the point with the minimum U value is referred to as a location point (LP), as it serves to locate a distance-based subdomain, as illustrated in Figure 3-1.

Given a location point $\mathbf{x}_{\mathrm{LP}}$ and points belong to a MC candidate pool S, e.g., $\left[\mathbf{x}^{(1)}, \mathbf{x}^{(2)}, ..., \mathbf{x}^{(N_{\mathrm{MC}})}\right]^{\mathrm{T}}$, the Euclidean distance can be calculated as:

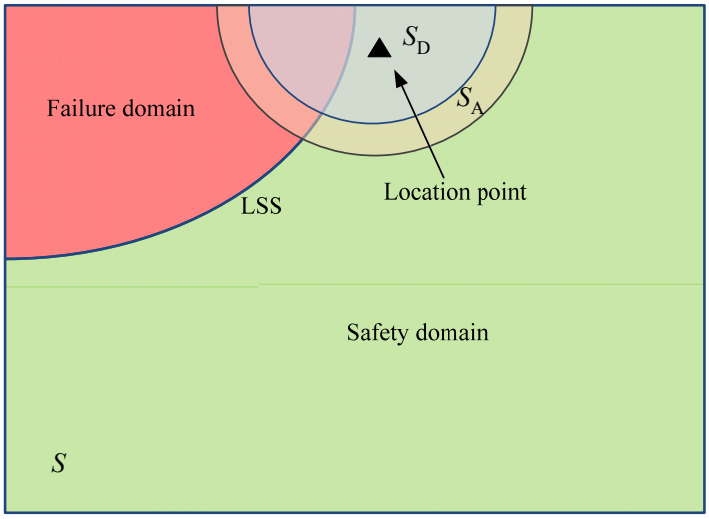

Figure 3-1 Concepts of a distance-based subdomain and an adjacent distance-based subdomain

$$r_i = \left\| \mathbf{x}^{(i)} - \mathbf{x}_{\mathrm{LP}} \right\|^2, i = 1, 2, .., N_{\mathrm{MC}} \tag{3-11}$$

Therefore, varying the number of candidate points around $\mathbf{x}_{\mathrm{LP}}$ can be determined by setting different thresholds for Euclidean distance. The distance-based subdomain S_{D} can be given as:

$$S_{\mathrm{D}} = \left\{ \mathbf{x} \in S \mid \mathbf{r} \le \bar{r} \right\} \tag{3-12}$$

where $\mathbf{r}$ is a vector collecting the Euclidean distance obtained by Eq. (3-11) and $\bar{r}$ is the threshold of Euclidean distance.

In this thesis, only the selected candidate points (SCPs) in a distance-based subdomain S_{D} are employed for updating a Kriging model. Hence, the number of candidate points in the distance-based subdomain should be limited and it is denoted as N_{D}. To this end, an algorithm similar to the bisection method, as shown in Table 3-1, is proposed to limit the number of candidate points within a distance-based

subdomain. This algorithm adaptively finds an appropriate threshold r_{m} to ensure that the number of candidate points remains at an expected level $\bar{N}_{\mathrm{D}}$. Note that the final number of selected candidate points may not exactly match $\bar{N}_{\mathrm{D}}$ due to the implementation of an allowable error κ to facilitate the algorithm. A fluctuation of up to 10% is considered acceptable.

Table 3-1 Algorithm 1 for determining subdomains

Algorithm 1: Determine the distance-based subdomain S_{D}
Input: A location point $\mathbf{x}_{\mathrm{LP}}$; Candidate points **X** in *S*; An expected number of points in S_{D} denoted as $\bar{N}_{\mathrm{D}}$.
Output: Distance-based subdomain S_{D} with N_{D} selected candidate points
1. Calculate Euclidean distance $r_i \leftarrow \left\|\mathbf{x}^{(i)}-\mathbf{x}_{\mathrm{LP}}\right\|^2$, $\mathbf{r}=\left[r_1,r_2,....,r_{N_{MC}}\right]^{\mathrm{T}}$
2. Determine the maximum Euclidean distance $r_{\max} \leftarrow \max(\mathbf{r})$
3. Determine the minimum Euclidean distance $r_{\min} \leftarrow \min(\mathbf{r})$
4. Initiate the upper bound of distance $r_{\mathrm{u}} \leftarrow r_{\max}$
5. Initiate the lower bound of distance $r_{\mathrm{L}} \leftarrow r_{\min}$
6. Initiate an allowable error of the number of candidate points in S_{D} $\kappa \leftarrow 1$
7. While $\kappa > 0.1$ or $\kappa < -0.1$
8. Calculate the medium distance $r_{\mathrm{m}} \leftarrow (r_{\mathrm{u}}+r_{\mathrm{L}})/2$
9. Obtain $S_{\mathrm{D}}=\{\mathbf{x}\in S \mid \mathbf{r}\le r_{\mathrm{m}}\}$ with N_{D} selected candidate points
10. Calculate the allowable error of the number of selected points $\kappa=(N_D-\bar{N}_D)/\bar{N}_D$
11. if $\kappa > 0.1$ then
12. Update the upper bound $r_{\mathrm{u}} \leftarrow r_{\mathrm{m}}$
13. else
14. Update the lower bound $r_{\mathrm{L}} \leftarrow r_{\mathrm{m}}$
15. end if
16.End While

3.3.2 Training a Kriging model within distance-based subdomains

Given an initial DoE and a random subdomain S_{R} ($S_{\mathrm{R}} \subset S$) with N_{R} candidate points scattered in the whole candidate pool *S*, a Kriging model can be constructed

based on the initial DoE, the first location point can be easily found by using the Kriging predictions on candidate points within S_{R} :

$$\mathbf{x}_{\mathrm{LP}}^{(1)} = \arg\min_{\mathbf{x}\in S_{\mathrm{R}}} U\left(\mathbf{x}\right) \tag{3-13}$$

Note that in this step, the Kriging model does not require refinement through the active learning strategy, as it is used solely to identify the first location point. This random subdomain is employed to avoid performing a large number of Kriging predictions across the entire candidate pool. Hence, the number of candidate points in S_{R} can be set to $N_{\mathrm{R}} \le 10^6$ to guarantee the efficiency. The effect of this parameter is investigated in example 1. Once the first location point is obtained, the first distance-based subdomain $S_{\mathrm{D}}^{(1)}$ containing $N_{\mathrm{D}}^{(1)}$ SCPs can be accordingly found via the proposed algorithm. Seen from Figure 3-1, the distance-based subdomain S_{D} covers a piece of the whole LSS.

The whole LSS can be divided into pieces by several distance-based subdomains. Accordingly, Kriging model for LSS is updated piece-by-piece. For each segment, only selected candidate points within each S_{D} are used for the active learning strategy so that the efficiency of the training process can be significantly improved. In this thesis, a Kriging model trained within a distance-based subdomain $S_{\mathrm{D}}^{(j)}$ is referred to as a local Kriging model $\hat{G}_j$, for the sake of simplicity in describing the proposed procedure.

The next key step is to identify the subsequent LP to determine the next distance-based subdomain. Due to the first local Kriging model $\hat{G}_1$ is refined within $S_{\mathrm{D}}^{(1)}$ through the active learning strategy, it may also provide insights into the LSS near $S_{\mathrm{D}}^{(1)}$. Herein, a distance-based subdomain adjacent to S_{D}, denoted as S_{A}, is introduced. This adjacent distance-based subdomain S_{A} can also be identified using the algorithm outlined in Table 3-1. It is important to note that the location point used for this subdomain is the same as the one used for locating S_{D}. The selected candidate points within S_{D} should be removed from the candidate pool *S* so that only candidate points around S_{D} are selected. The adjacent distance-based subdomain is defined as:

$$S_{\mathrm{A}} = \left\{ \mathbf{x} \in S \mid \mathbf{r} \le r_{\mathrm{m}} \right\}, S \leftarrow S_{-\mathrm{D}} \tag{3-14}$$

in which $S_{-\mathrm{D}}$ means a new candidate pool obtained by removing S_{D} from *S*. The adjacent distance-based subdomain is represented by the light-yellow region shown in Figure 3-1. Then, the next LP $\mathbf{x}_{\mathrm{LP}}^{(j+1)}$ can be found by the previously trained local Kriging model and candidate points within $S_{\mathrm{A}}^{(j)}$:

$$\mathbf{x}_{\mathrm{LP}}^{(j+1)} = \arg\min_{\mathbf{x} \in S_{\mathrm{A}}^{(j)}} U\left(\mathbf{x}\right), j = 1, 2, \ldots \tag{3-15}$$

Another important issue is to determine the number of distance-based subdomains used for detecting the whole failure domain and LSS. When getting a

well-trained local Kriging model for a distance-based subdomain $S_{\mathrm{D}}^{(j)}$, the failure domain belongs to $S_{\mathrm{D}}^{(j)}$ can be obtained as follows:

$$\Omega_F^j = \left\{ \mathbf{x} \in S_{\mathrm{D}}^{(j)} \mid \hat{G}_j\left(\mathbf{x}\right) \le 0 \right\}, j = 1, 2, \cdots \tag{3-16}$$

The number of failure points within $S_{\mathrm{D}}^{(j)}$ is recorded as $\hat{N}_f^{(j)}$ and can be estimated as:

$$\hat{N}_f{}^{(j)} = \sum_{k=1}^{N_{\mathrm{D}}^{(j)}} I\left(\mu_{\hat{G}_j}\left(\mathbf{x}^{(k)}\right)\right) \tag{3-17}$$

when $\hat{N}_f{}^{(j)} = 0$, it can be assumed that the previous $S_{\mathrm{D}}^{(j)}$s have covered the whole failure domain and the LSS. Consequently, the number of $S_{\mathrm{D}}^{(j)}$s can be determined.

Then, the failure probability can be estimated as:

$$\hat{P}_f = \frac{\hat{N}_f}{N_{\mathrm{MC}}} \tag{3-18}$$

where N_f represents the number of failure points in the whole population *S*, and N_f can be estimated as:

$$\hat{N}_f = \sum_{j=1}^{n} \hat{N}_f^{(j)} \tag{3-19}$$

where *n* is the number of distance-based subdomain S_{D} used for covering the entire failure domain and LSS.

An alternative way to approximate $\hat{N}_f$ is using the final refined Kriging model $\hat{G}_n$ and MC population, which can be calculated as:

$$\hat{N}_f = \sum_{i=1}^{N_{\mathrm{MC}}} I\left(\mu_{\hat{G}_n}\left(\mathbf{x}^{(i)}\right)\right) \tag{3-20}$$

the accuracy and efficiency of failure probability obtained by Eqs. (3-19) and (3-20) are discussed in the following illustrative examples. The training process of a local Kriging model for each piece of LSS within S_{D} follows the same procedure as the conventional AKMCS, a new best training point within each S_{D} is defined as:

$$\mathbf{x}^* = \arg\min_{\mathbf{x}\in S_{\mathrm{D}}^{(j)}} U\left(\mathbf{x}\right) \tag{3-21}$$

and $N_0 = \max\left\{12, 2d\right\}$ initial TPs produced by Latin hypercube sampling (LHS) is employed for training.

3.3.3 Proposed ε stopping criterion for training a Kriging model

The training process for a Kriging model stops when the following condition is met (Echard et al., 2011):

$$\min_{\mathbf{x}\in S} U\left(\mathbf{x}\right) \geq 2 \tag{3-22}$$

However, the stopping condition for updating Kriging model expressed by Eq. (3-22) is overly conservative for estimating the failure probability since it solely draws attention to the accuracy of Kriging model for the LSS. In addition to considering the accuracy of the metamodel, it is also important to account for the

accuracy of the failure probability estimation. Therefore, the impact of points with high probabilities of incorrect classification on the accuracy of failure probability estimation should be investigated first.

Suppose that the number of candidate points corresponding to $\left\{\mathbf{x}\in S\,|\,U\left(\mathbf{x}\right)<2\right\}$ (also termed as the dangerous points) is N_U. Let Z denote the event that k points within the domain $\left\{\mathbf{x}\in S\,|\,U\left(\mathbf{x}\right)<2\right\}$ are in wrong classification, the probability of Z can be formulated as:

$$\Pr\left\{Z=k\right\}=\sum_{i=1}^{C_{N_U}^{k}}\left[\prod_{j=1}^{k}p_{i,j}\prod_{m=k+1}^{N_U}\left(1-p_{i,m}\right)\right] \tag{3-23}$$

in which $C_{N_U}^{k}=\dfrac{N_U!}{k!\left(N_U-k\right)!}$, $p_{i,j}$ and $p_{i,m}$ are probabilities of the wrong classification. On the basis of Eq. (3-10) and $0\le U\left(\mathbf{x}\right)<2$, $p_{i,j}$ and $p_{i,m}$ satisfy:

$$0.023=\Phi\left(-2\right)<p_{i,j},p_{i,m}\le\Phi\left(0\right)=0.5 \tag{3-24}$$

For the sake of simplicity, we assume that $p_{i,j}=p_{i,m}=p$, and then Z follows the binomial distribution $Z\sim B\left(N_U,p\right)$. Thus, the probability of $\left\{Z=k\right\}$ gives:

$$\Pr\left\{Z=k\right\}=C_{N_U}^{k}p^{k}\left(1-p\right)^{N_U-k} \tag{3-25}$$

The mean and variance of Z gives:

$$\mathbb{E}\left[Z\right]=N_U p,\ \mathrm{Var}\left[Z\right]=N_U p\left(1-p\right) \tag{3-26}$$

If $Z = k$ points are in wrong classification, the range of estimated failure probability $\hat{P}_f$ can be calculated as:

$$P_f - \frac{Z}{N_{\mathrm{MC}}} \le \hat{P}_f \le P_f + \frac{Z}{N_{\mathrm{MC}}} \tag{3-27}$$

The left-hand side represents the scenario where all *k* points are actually negative but are identified as positive. Conversely, the right-hand side represents the case where all *k* points are actually positive but are identified as negative. The relative error of failure probability can be estimated as:

$$R = \left| \frac{\hat{P}_f - P_f}{P_f} \right| \times 100\% \le \frac{Z}{N_{\mathrm{MC}} P_f} \times 100\% \tag{3-28}$$

Denote the upper bound of the relative error of P_f as R_U $(R_U \ge 0)$:

$$R_U = \frac{Z}{N_{\mathrm{MC}} P_f} \tag{3-29}$$

The expected upper bound of the relative error of P_f can be calculated as:

$$\mathbb{E}\left[R_U\right] = \frac{1}{N_{\mathrm{MC}} P_f} \mathbb{E}\left[Z\right] = \frac{N_U p}{N_{\mathrm{MC}} P_f} \times 100\% \tag{3-30}$$

where $\mathbb{E}$ is the expectation operator. Since $N_f = N_{\mathrm{MC}} P_f$, and Eq. (3-30) can be reformulated as:

$$\mathbb{E}\left[R_U\right] = \frac{N_U p}{N_f} \times 100\% = \varepsilon p \times 100\% \tag{3-31}$$

where ε is the ratio of the number of the dangerous points to the number of points within the failure domain:

$$\varepsilon = \frac{N_U}{N_f}, \varepsilon \geq 0 \tag{3-32}$$

The variance of the upper bound of the relative error of P_f can be calculated as:

$$\mathrm{Var}\left[R_U\right] = \frac{1}{N_f^2}\mathrm{Var}\left[Z\right] = \frac{1}{N_f^2} N_U p\left(1-p\right) = \frac{\varepsilon p\left(1-p\right)}{N_f} \tag{3-33}$$

Moreover, the confidence interval of R_U can be estimated by:

$$R_U \in \left[\max\left(R_U^- = \varepsilon p - \delta\sqrt{\frac{\varepsilon p\left(1-p\right)}{N_f}}, 0 \right), R_U^+ = \varepsilon p + \delta\sqrt{\frac{\varepsilon p\left(1-p\right)}{N_f}} \right] \tag{3-34}$$

in which δ is the quantile of a standard normal distribution corresponding to a confidence level. For instance, if the confidence level is 95%, then δ=1.96 .

Seen from Eq. (3-34), the confidence interval of R_U is related to ε , p and N_f . To further estimate the confidence interval of R_U , assume that $N_f = a \times 10^b$, where $a \in \mathbb{R}^+, 1 \leq a < 10$ and $b \in \mathbb{N}$. Therefore, the lower and upper bounds of R_U gives:

$$R_U^- \geq \max\left(\varepsilon p - \delta\sqrt{\frac{\varepsilon p\left(1-p\right)}{10^b}}, 0 \right), \quad R_U^+ \leq \varepsilon p + \delta\sqrt{\frac{\varepsilon p\left(1-p\right)}{10^b}} \tag{3-35}$$

where the equal sign in Eq. (3-35) works when a = 1. Subsequently, the confidence interval shown in Eq. (3-34) can be reformulated as:

$$R_U \in \left[\max\left(\varepsilon p - \delta\sqrt{\frac{\varepsilon p(1-p)}{10^b}}, 0 \right), \varepsilon p + \delta\sqrt{\frac{\varepsilon p(1-p)}{10^b}} \right] \tag{3-36}$$

Herein, we first consider the worst condition for P_f estimation, where all dangerous points have the maximum probability of misclassification, i.e., $p_{i,j} = p_{i,m} = p = 0.5$. Then the maximum expected R_U, i.e., $\mathbb{E}\left[R_U\right]_{\max}$, and the estimated confidence interval with a 95% confidence level are presented in Table 3-2. As seen from the Table 3-2, for a fixed ratio ε, the variation of R_U increases as b decreases, which results from the lack of enough MC candidate samples for the failure probability estimation. It is well known that to ensure a low variation of failure probability, the required number of MC samples increases with a descending failure probability. For instance, to achieve $\mathrm{CoV}\left(P_f\right) \le 0.1$ given $P_f = 10^{-t}$ and $t \in \mathbb{N}^+$, the following number of MC samples is required based on Eq. (2-5) (Schöbi et al., 2017):

$$N_{\mathrm{MC}} \ge \frac{1}{\left[\mathrm{CoV}\left(P_f\right)\right]^2 P_f} = 10^{t+2} \tag{3-37}$$

which means that $N_f = N_{\mathrm{MC}} P_f \ge 10^2$, i.e., $b \ge 2$. Thus, the length of the confidence interval is significantly smaller when the number of Monte Carlo samples is sufficiently large. This conclusion is also evident from Eq. (3-36). When b is sufficiently large, meaning the number of Monte Carlo samples is adequate to ensure

a low CoV of P_f, and then the bounds of the relative error of failure probability are given by:

$$R_U^- \approx R_U^+ \approx \varepsilon p = \mathbb{E}\left[R_U\right] \tag{3-38}$$

Furthermore, $\mathbb{E}\left[R_U\right]$ with respect to p is shown in Table 3-3. Given $\varepsilon = 0.1$ and $p = \Phi(-1)$, if N_f is equal to 10^3, then $N_U = \varepsilon N_f = 100$ points fall into the domain corresponding to $\left\{\mathbf{x} \in S \,|\, U(\mathbf{x}) < 2\right\}$. These 100 points do not satisfy the U stopping criterion, i.e., $\min_{\mathbf{x}\in S} U(\mathbf{x}) \geq 2$. But the expected upper bound of the relative error of failure probability is as small as 1.6%, indicating that even if $\varepsilon N_f = 100$ points are exempt from the conventional U stopping criterion, the accuracy of the P_f estimation remains reliable. Thus, the conventional U stopping criterion is conservative for some cases. Accordingly, the following ε stopping criterion is proposed to exempt εN_f dangerous points from the U stopping criterion:

$$\varepsilon \leq \overline{\varepsilon} \tag{3-39}$$

Note that the maximum expected upper bound of the relative error of P_f is 5% when $\varepsilon = 0.1$, i.e., $\mathbb{E}\left[R_U\right]_{\max} = 5\%$. Due to the expected value and all the bounds of R_U are derived by considering the extreme conditions, we can infer from Eq. (3-38) that the relative error of failure probability satisfies the following equation given $\varepsilon = 0.1$:

$$R \leq R_U \approx \mathbb{E}\left[R_U\right] \leq \mathbb{E}\left[R_U\right]_{\max} = 5\% \tag{3-40}$$

Therefore, in this thesis, a threshold of $\overline{\varepsilon} = 0.1$ is suggested, ensuring that the expected upper bound of the relative error of failure probability remains below 5%. To evaluate the stopping criterion, the estimated number of failure points can be employed, as it will approach the true one with continued training, and at the early stage of training, the number of dangerous points is very large. Furthermore, the results in Table 3-3 can also provide a guideline for choosing different thresholds of the proposed stopping criterion to achieve varying levels of accuracy.

Table 3-2 Mean and confidence interval of the upper bound of the relative error against ε and b given $p = 0.5$

Parameters	ε=0.05	ε=0.1	ε=0.2	ε=0.3
b=0	[0%, 24.4%]	[0%, 36.0%]	[0%, 53.8%]	[0%, 68.7%]
b=1	[0%, 9.4%]	[0%, 14.8%]	[0%, 23.9%]	[0%, 32.0%]
b=2	[0.3%, 4.7%]	[1.9%, 8.1%]	[5.6%, 14.4%]	[9.6%, 20.4%]
b=3	[1.8%, 3.2%]	[4.0%, 6.0%]	[8.6%, 11.4%]	[13.3%,16.7%]
b=4	[2.3%, 2.7%]	[4.7%, 5.3%]	[9.6%, 10.4%]	[14.5%,15.5%]
$\mathbb{E}[R_U]_{\max}$	2.5%	5.0%	10.0%	15.0%

Table 3-3 The expected upper bound against ε and p

Parameters	$\varepsilon = 0.05$	$\varepsilon = 0.1$	$\varepsilon = 0.2$	$\varepsilon = 0.3$
$p = \Phi(0)$	2.5%	5.0%	10.0%	15.0%
$p = \Phi(-0.5)$	1.5%	3.1%	6.2%	9.3%
$p = \Phi(-1)$	0.8%	1.6%	3.2%	4.8%
$p = \Phi(-1.5)$	0.3%	0.7%	1.3%	2.0%
$p = \Phi(-2)$	0.1%	0.2%	0.5%	0.7%

3.3.4 Computational procedure

Figure 2 shows the flowchart of the proposed method and the procedure is described in detail as follows:

(1) Initiate j=1, q=0 and generate a candidate sample pool S_{MC} with N_{MC} candidate points.

(2) Select N_0 training points via LHS as an initial training set $\boldsymbol{\mathcal{X}} = \boldsymbol{\mathcal{X}}_0 = \left[\mathbf{x}_1, \mathbf{x}_2, .., \mathbf{x}_{N_0}\right]^{\mathrm{T}}$ and compute the corresponding performance function values $\boldsymbol{\mathcal{Y}} = \boldsymbol{\mathcal{Y}}_0 = \left[y_1, y_2, ..., y_{N_0}\right]^{\mathrm{T}}$.

(3) Let $S = S_{\mathrm{MC}}$ and select a random subdomain S_{R} with N_{R} scattered candidate points within S.

(4) Obtain a Kriging model $\hat{G}_0$ by using $\{\boldsymbol{\mathcal{X}}_0, \boldsymbol{\mathcal{Y}}_0\}$.

(5) Find the first location point $\mathbf{x}_{\mathrm{LP}}^{(1)}$ via $\hat{G}_0$ and candidate points inside S_{R}.

(6) Determine a distance-based subdomain $S_{\mathrm{D}}^{(j)}$ by using algorithm 1.

(7) Train a local Kriging model $\hat{G}_j$ by using $\{\boldsymbol{\mathcal{X}}, \boldsymbol{\mathcal{Y}}\}$.

(8) Compute U learning function values of the selected candidate points within $S_{\mathrm{D}}^{(j)}$ and enrich $\{\boldsymbol{\mathcal{X}}, \boldsymbol{\mathcal{Y}}\}$ with the next best training point and the corresponding performance function value until meeting the proposed stopping condition $\varepsilon \le \overline{\varepsilon}$.

(9) Record the number of points in the failure domain of $S_{\mathrm{D}}^{(j)}$ by using Eq. (3-17), i.e., $N_f^{(j)}$.

(10) Update the candidate sample pool S by removing selected candidate points inside $S_{\mathrm{D}}^{(j)}$.

(11) Judge the stopping condition $N_f^{(j)}=0$. If the condition is met, proceed to step (13). Otherwise, determine an adjacent distance-based subdomain $S_{\mathrm{A}}^{(j)}$ using algorithm 1 and let $j=j+1$.

(12) Obtain the next location point $\mathbf{x}_{\mathrm{LP}}^{(j)}$ via $\hat{G}_{j-1}$ and the candidate points within $S_{\mathrm{A}}^{(j-1)}$, and then move to step (6).

(13) Estimate N_f by Eq. (3-19) or Eq. (3-20), and $\hat{P}_f$ can be obtained by using Eq. (3-18).

(14) Check the coefficient of variation of $\hat{P}_f$. If $\mathrm{CoV}\left(\hat{P}_f\right)<5\%$, the proposed method stops, otherwise, the MC candidate pool S_{MC} is enlarged by Eq. (3-41). Let $q=q+1$, AKDS goes back to step (3).

In this research, to efficiently determine the final MC candidate pool S_{MC}, the initial N_{MC} is employed as 10^6. Assume that the $\hat{P}_f$ estimated by the current S_{MC} is $r\times10^{-t}$, where $r\in\mathbb{R}^+$, $1\le r<10$ and $t\in\mathbb{N}^+$. According to Eq. (3-37), S_{MC} can be enlarged as :

$$N_{\mathrm{MC}}=10^{t+2}\left(1+0.5q\right) \tag{3-41}$$

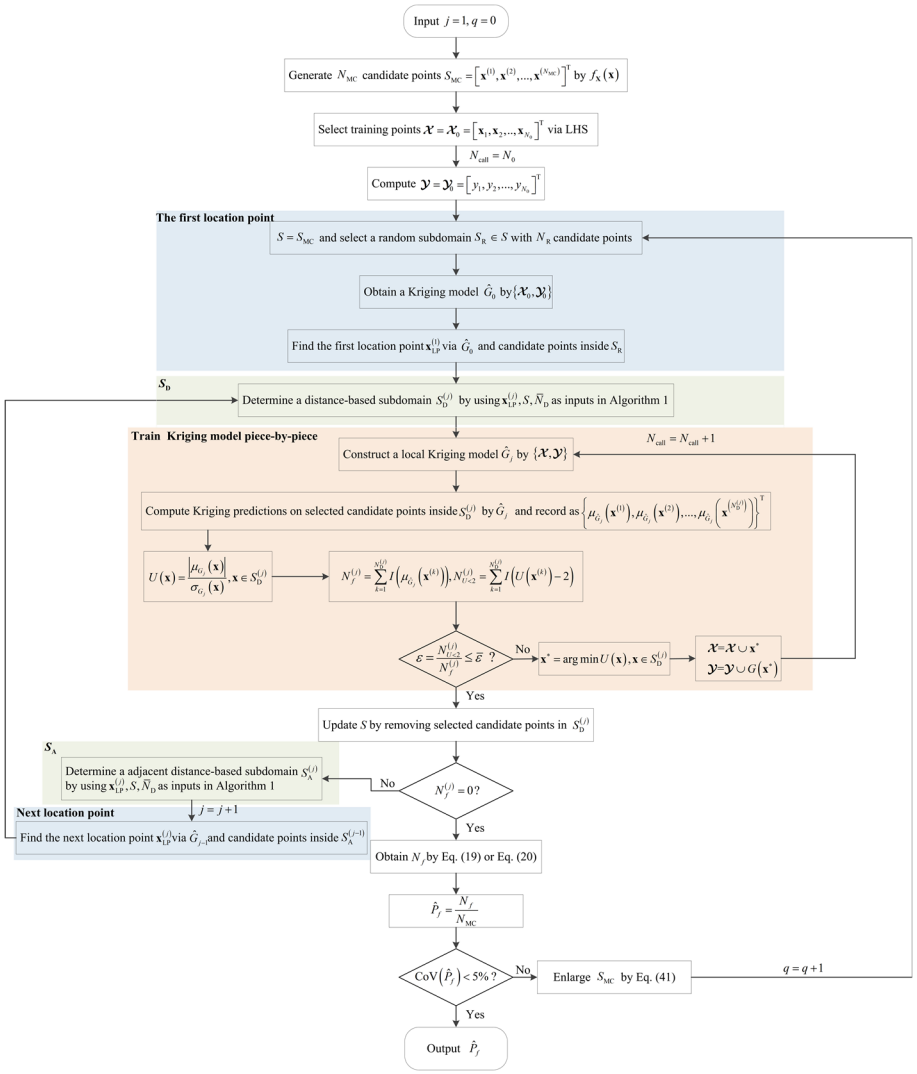

Figure 3-2 Flowchart of the proposed AKDS

3.4 Discussion on the proposed method

Active learning-based Kriging models are often combined with various sampling approaches, which significantly impact the efficiency and accuracy of the AK-based methods. Herein, the approach for selecting candidate samples used in the proposed method is compared with MCS, subset sampling and a spherical decomposition-based MCS (SDMCS) (Su et al., 2020). To demonstrate the application of different simulation methods, a simple 2-D problem is investigated (Echard et al., 2013):

$$G(X_1, X_2) = 0.5(X_1 - 2)^2 - 1.5(X_2 - 5) - 1 \tag{3-42}$$

where X_1 and X_2 are independent standard Gaussian random variables. The numbers of candidate points in each subdomain for SS, SDMCS and the proposed method are all set to 10^5 for comparisons. Note that the procedure for generating the candidate pool in the proposed method requires location points, which is different from the other approaches. Herein, the location points are obtained by Kriging model and U learning function. The failure probabilities obtained by different methods are listed in Table 3-4 and the candidate pools for active learning generated by different strategies are depicted in Figure 3-3.

Table 3-4 Comparisons of different simulation methods

Method	N_{call}	P_f	CoV (%)	R.E. (%)
MCS	1.5×10^8	2.749×10^{-6}	4.92	-
SS	517620	2.907×10^{-6}	3.95	5.75
SDMCS	501879	2.875×10^{-6}	4.95	4.58
Proposed	289058	2.787×10^{-6}	4.89	1.38

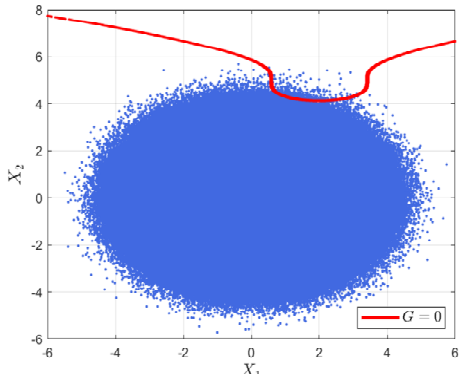

(a) MCS

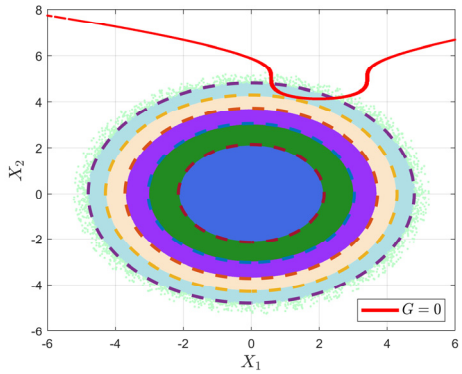

(b) SDMCS

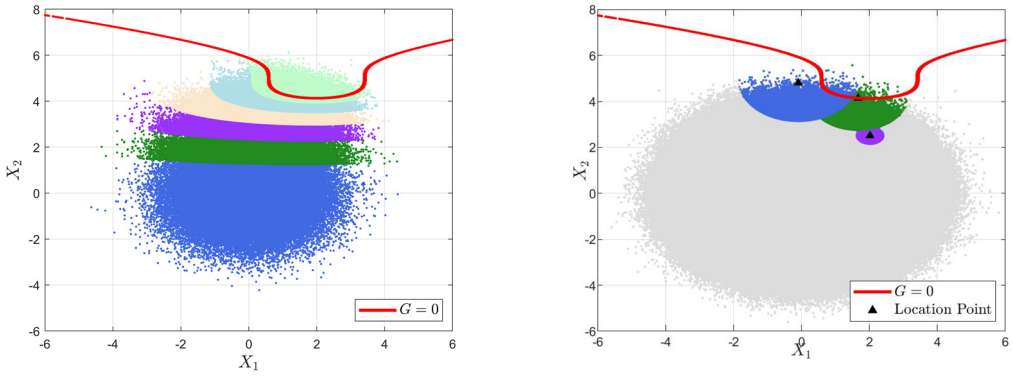

(c) SS (d) Proposed

Figure 3-3 Strategies for generating the candidate pool

As seen from Table 3-4 and Figure 3-3, it can be found that: (1) MCS requires considerable computational costs to estimate such a small failure probability due to a large number of function calls to the performance function. (2) SS transforms the rare event into six intermediate events with relatively larger failure probabilities, significantly reducing the number of required candidate samples to 517620. (3) SDMCS decomposes the whole space into six subdomains based on the spherical radius, also significantly reducing the required number of candidate points to 501879. (4) The proposed strategy only focuses on the region close to the LSS since candidate samples far away from the LSS, i.e., points in the grey region shown in Figure 3-3 (d), have no contribution to the failure domain and LSS. Two distance-based subdomains are sufficient to cover LSS and the failure domain of interest. Thus, the number of candidate samples for active learning using the proposed strategy, i.e., 289058, is further reduced compared to SS and SDMCS. Therefore, the proposed method requires fewer candidate points for active learning since it fully utilizes the location information of the LSS and the failure domain provided by the Kriging mean and variance predictions, whereas other approaches do not account for this aspect.

The computational effort of the Kriging metamodel arises from three main components: the training of Kriging model, Kriging mean and variance predictions. These can be approximated respectively for each subdomain $S_{\mathrm{D}}^{(j)}$ as follows (Su et al., 2020):

$$T_{1,j} \approx t_1 \sum_{i=N_{\mathrm{call},j-1}+1}^{N_{\mathrm{call},j}} i^3 \tag{3-43}$$

$$T_{2,j} \approx t_2 N_{\mathrm{D}} \sum_{i=N_{\mathrm{call},j-1}+1}^{N_{\mathrm{call},j}} i \tag{3-44}$$

$$T_{3,j} \approx t_3 N_{\mathrm{D}} \sum_{i=N_{\mathrm{call},j-1}+1}^{N_{\mathrm{call},j}} i^2 \tag{3-45}$$

where t_1 , t_2 , t_3 are computational time for a single run of the training, mean and variance predictions, respectively. N_{call} means the number of function calls to the performance function and $N_{\mathrm{call},j}$ is the number of function calls in each subdomain. Note that $N_{\mathrm{call},0} = N_0$ is the size of the initial DoE. Consider all subdomains, the computational time for training Kriging model can be estimated as:

$$\begin{aligned} T_1 &\approx \sum_{j=1}^{n} t_1 \sum_{i=N_{\mathrm{call},j-1}+1}^{N_{\mathrm{call},j}} i^3 + t_1 N_{\mathrm{call},0}^3 \\ &= t_1 \sum_{i=N_0}^{N_{\mathrm{call}}} i^3 < t_1 \sum_{i=1}^{N_{\mathrm{call}}} i^3 \\ &= \frac{t_1 N_{\mathrm{call}}^2 \left(N_{\mathrm{call}}+1\right)^2}{4} \approx 0.30 t_1 N_{\mathrm{call}}^4 \end{aligned} \tag{3-46}$$

Similarly, we have:

$$T_2 \approx 0.55 t_2 N_{\mathrm{D}} N_{\mathrm{call}}^2 \tag{3-47}$$

and

$$T_3 \approx 0.39 t_3 N_{\mathrm{D}} N_{\mathrm{call}}^3 \tag{3-48}$$

The total computational time can be estimated as:

$$\begin{aligned} T &= T_1 + T_2 + T_3 \\ &\approx 0.30 t_1 N_{\mathrm{call}}^4 + 0.39 t_2 N_{\mathrm{D}} N_{\mathrm{call}}^3 + 0.55 t_3 N_{\mathrm{D}} N_{\mathrm{call}}^2 \end{aligned} \tag{3-49}$$

Similarly, the computational time for AKMCS can be estimated as:

$$T \approx 0.30 t_1 \bar{N}_{\mathrm{call}}^4 + 0.39 t_2 N_{\mathrm{MC}} \bar{N}_{\mathrm{call}}^3 + 0.55 t_3 N_{\mathrm{MC}} \bar{N}_{\mathrm{call}}^2 \tag{3-50}$$

where $\bar{N}_{\mathrm{call}}$ refers to the number of true simulations by AKMCS. Therefore, the computational time of the AK-based method mainly depends on the number of candidate samples for active learning process and the number of calls to the time-demanding performance function. For the proposed method, Kriging model is trained within each subdomain and the entire LSS is refined piece-by-piece. Thus, the computational time of the proposed method depends on the number of points in each subdomain, i.e., N_{D}, rather than the total number of candidate points for the active learning. Clearly, N_{D} is much smaller than N_{MC} and the computational effort of AKMCS can be significantly reduced. Apart from the candidate pool for active learning, the stopping criterion also plays an important part in the AK-based approaches. As illustrated in the previous section, the proposed stopping criterion can further reduce the number of calls to the performance function.

3.5 Illustrative examples

In this section, four applications, including both analytical and numerical performance functions, are examined to demonstrate the effectiveness of the proposed method. The first example is a 2-D application that illustrates how AKDS refines the entire LSS piece-by-piece, and a parametric study is conducted in this example. The performance of the proposed method is also tested on FEM related to a 61-bar truss, a three-bay six-story reinforced concrete planar frame, and a bolted steel beam-column joint. In addition to the computational cost associated with performance function calls, the CPU time is also considered to account for the computational effort required by active learning process itself in all examples.

3.5.1 Example 1: a series system with four branches

The first benchmark example is a series system with four branches, the performance function gives (Echard et al., 2011; Schueremans & Van Gemert, 2005):

$$G\left(X_1, X_2\right) = \min \begin{Bmatrix} 3 + 0.1\left(X_1 - X_2\right)^2 - \dfrac{X_1 + X_2}{\sqrt{2}} \\ 3 + 0.1\left(X_1 - X_2\right)^2 + \dfrac{X_1 + X_2}{\sqrt{2}} \\ \left(X_1 - X_2\right) + \dfrac{7}{\sqrt{2}} \\ \left(X_2 - X_1\right) + \dfrac{7}{\sqrt{2}} \end{Bmatrix} \tag{3-51}$$

where X_1 and X_2 are standard normal distributed random variables. The procedure for the proposed AKDS is detailed in this example. The proposed procedure is initiated with N_0 Latin hypercube samples and a MC population with N_{MC} candidate

points. Then, an initial Kriging model can be constructed based on the initial DoE. The first location point can be identified by the minimum value of the U learning function predicted on N_R CPs. Subsequently, the first distance-based subdomain $S_D^{(1)}$ can be determined by the algorithm shown in Table 3-1 with an expected number of candidate points $\bar{N}_D$, as shown in Figure 3-4 (a). Next, a local Kriging model is trained within the first subdomain as depicted in Figure 3-4 (b). Then, an adjacent subdomain can be found according to the first LP, and the next location point is determined using the previously trained local Kriging model and the adjacent candidate points, which is shown in Figure 3-4 (c). Finally, the next distance-based subdomain can be readily determined as illustrated in Figure 3-4 (d).

The effects of parameters in the proposed approach on the accuracy of failure probability are first discussed, specifically the number of CPs inside a random subdomain (N_R) and the expected number of CPs within a distance-based subdomain ($\bar{N}_D$). Note that all results are the average values obtained by 10 independent runs of the proposed method and the failure probability is estimated by Eq. (3-20). Average results with respect to different N_R and $\bar{N}_D$ are listed in Table 3-5, with a threshold of $\bar{\varepsilon} = 0.1$. The results in Table 3-5 indicate that the parameter $\bar{N}_D$ plays a more important role in the accuracy of failure probability than N_R. As $\bar{N}_D$ increases, the accuracy of the results improves. However, the computational cost significantly increases with an increasing $\bar{N}_D$. To balance the accuracy and efficiency of the training process, the expected number is adopted as $\bar{N}_D = 10^5$ in this thesis. Furthermore, N_R appears to have little effect on the failure probability since it is only

used for finding the first LP. Therefore, N_R is the same with the number of initial MC population in this thesis, i.e.,10^6.

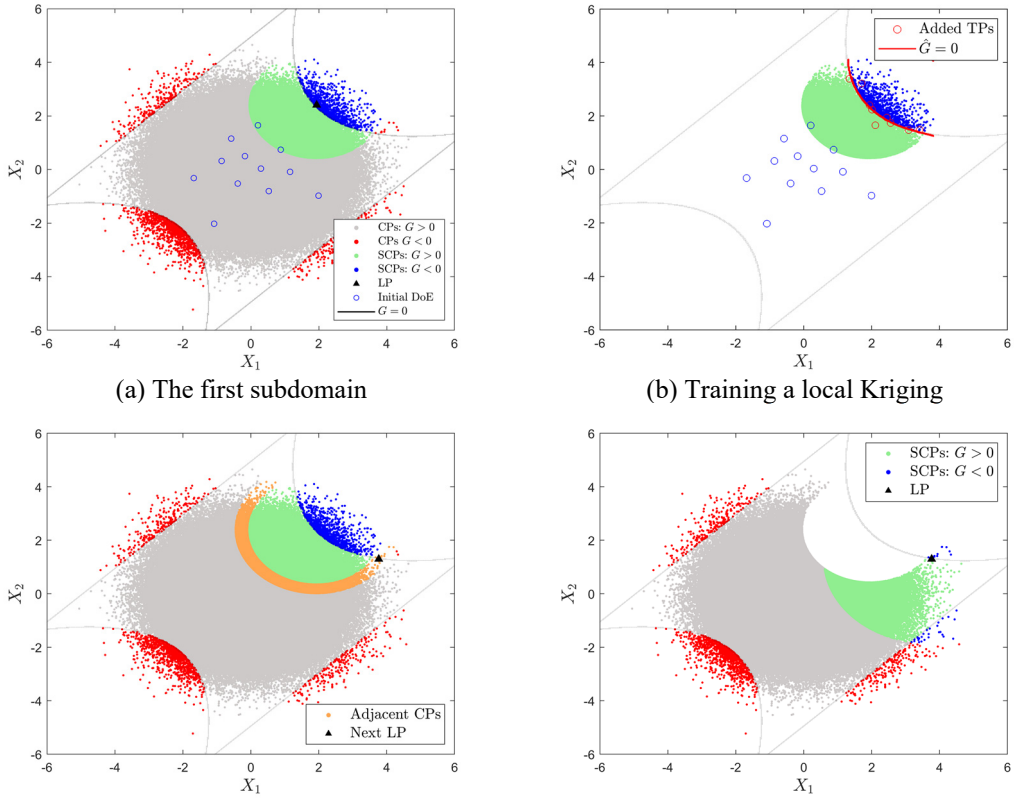

(a) The first subdomain

(b) Training a local Kriging

(c) Adjacent CPs and the next LP

(d) Determine the next subdomain

Figure 3-4 The procedure for the proposed AKDS

Table 3-5 Parametric analysis

Parameter		N_{call}	P_f	R.E.(%)
MCS	-	10^6	2.220×10^{-3}	-
Selected	$N_R=10^6, \bar{N}_D=10^5$	68.6	2.215×10^{-3}	0.24
$N_R\,(\bar{N}_D=10^5)$	5×10^5	67.8	2.212×10^{-3}	0.38
	1×10^5	67.4	2.210×10^{-3}	0.44
	1×10^4	69.5	2.213×10^{-3}	0.32
$\bar{N}_D\,(N_R=10^6)$	5×10^4	67.4	2.213×10^{-3}	0.32
	2×10^4	64.7	2.170×10^{-3}	2.24
	1×10^4	63.8	2.104×10^{-3}	5.24

The evolution of distance-based subdomains is shown in Figure 3-5 given $N_{\mathrm{R}}=10^6, \bar{N}_{\mathrm{D}}=10^5$ and ε stopping criterion. The first-seven distance-based subdomains cover all failure points, dividing the entire LSS into seven pieces. Each piece of LSS can be estimated by a local Kriging model, trained within a distance-based subdomain $S_{\mathrm{D}}^{(j)}$ rather than the whole population. Hence, the whole LSS is estimated piece-by-piece, which significantly reduces the computational effort induced by the active learning process itself. Moreover, the number of added points for training the Kriging model in each distance-based subdomain with U stopping criterion and the proposed ε stopping criterion are shown in Figure 3-6. The proposed ε stopping criterion requires fewer training points for refining each local Kriging model than U stopping criterion, which means that the proposed ε stopping criterion can mitigate the computational effort induced by the performance function calls. The numbers of failure points in each $S_{\mathrm{D}}^{(j)}$, estimated by the Kriging model with U stopping criterion and ε stopping criterion, are shown in Figure 3-7, which are all in good accordance with the true ones. The results in Figure 3-7 reveal that the number of failure points in each subdomain can be accurately estimated by the proposed method.

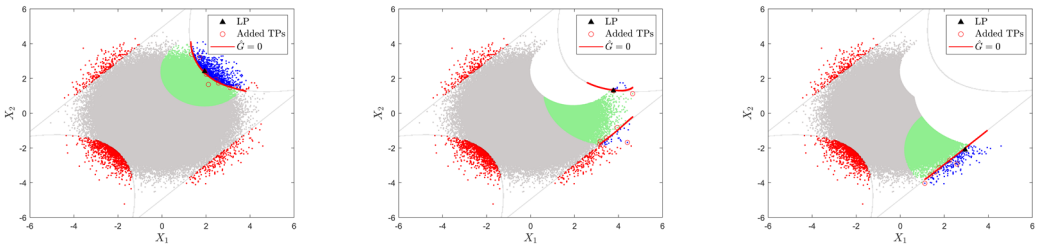

(a) (b) (c)

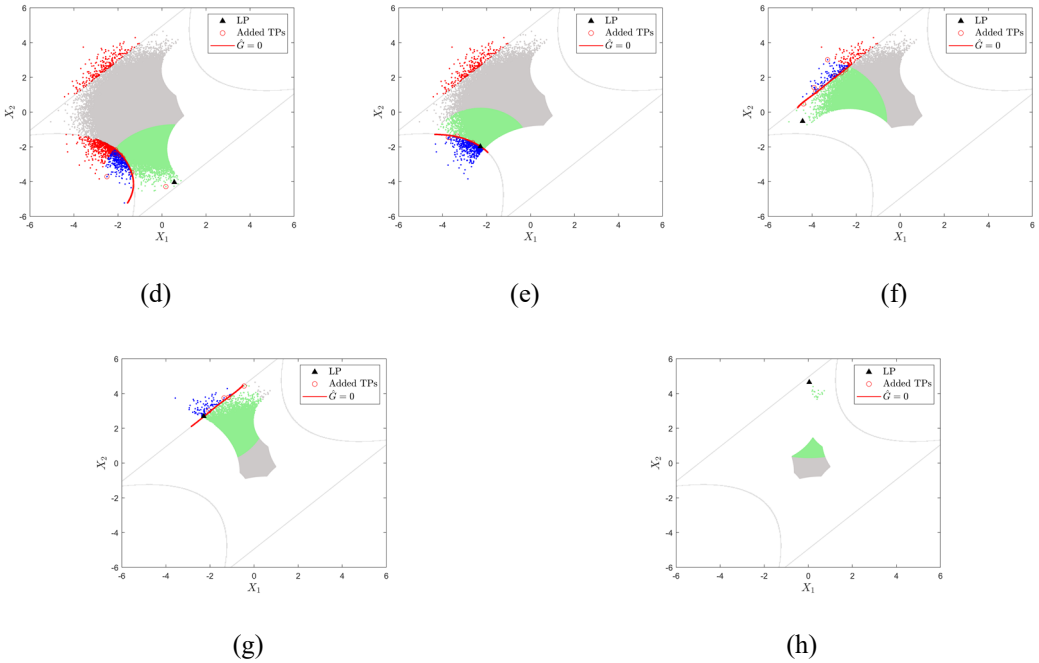

(d) (e) (f)

(g) (h)

Figure 3-5 The evolution of distance-based subdomains

Furthermore, the failure probabilities obtained by different methods are provided in Table 3-6. The number of performance function calls and the CPU time of the active learning process are of interest. All algorithms are performed on a computer with Intel (R) Core (TM) i9-11900K CPU processor at 3.5GHz with 32 GB RAM. Note that the original AK-MCS-U, AK-SS (Huang et al., 2016) and the proposed method are each replicated 10 times with different initial DoEs to provide the average results, respectively. AK-MCS-U and the proposed AKDS are both initiated with a MC population of $N_{\mathrm{MC}}=10^6$ CPs. AKDS- U^1 means that the U stopping criterion is used for training Kriging model and the superscript 1 denotes that Eq. (3-19) is employed for estimating N_f. Similarly, AKDS- U^2 represents that Eq. (3-20) is adopted for the failure probability estimation. Seen from the results, IS and SS require too many function calls and IS cannot produce an accurate result since it is only suitable for problems with a single MPP. By using the same U stopping criterion, the

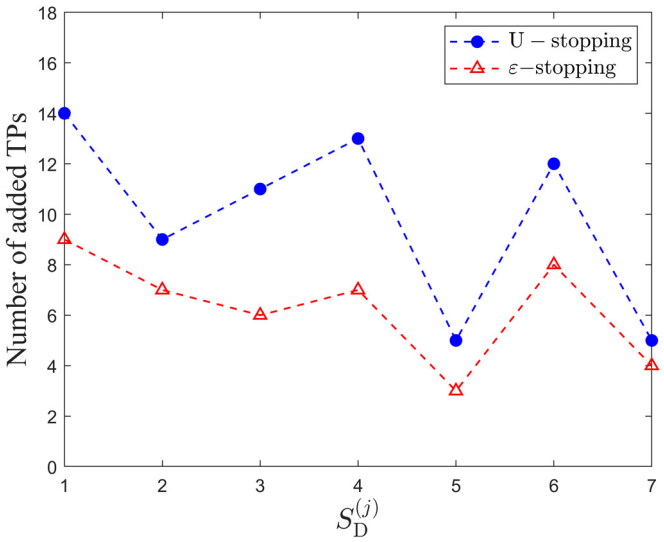

Figure 3-6 The number of added training points in each subdomain by U and ε stopping criterion

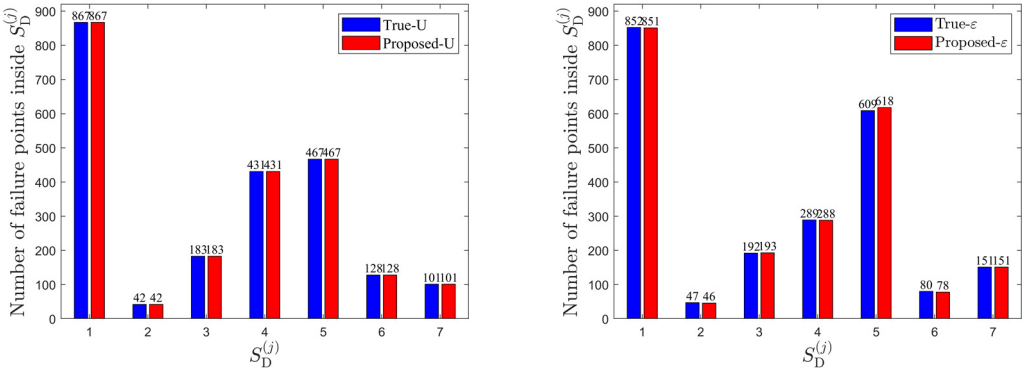

(a) U stopping criterion (b) proposed stopping criterion

Figure 3-7 The number of failure points in each subdomain

proposed AKDS-U consumes 82.9 calls to the performance function while AK-MCS-U requires 86.8 calls, which reveals that the proposed domain decomposition can reduce the number of calls to the performance function. Moreover, AKDS-ε requires fewer function calls by adopting the proposed stopping criterion, i.e., 68.6, which states that the proposed ε stopping criterion can further mitigate the computational burden induced by the performance function calls. Simultaneously, the maximum relative error of failure probability estimated by AKDS is as small as 0.68%. AK-SS results in a lager relative error of failure probability compared to AKDS-ε, despite

consuming a similar computational cost. In this example, the CPU time is primarily caused by the active learning process itself, which involves evaluating numerous candidate samples, while the time spent on running an analytical performance function is negligible. The results show that the proposed domain decomposition strategy accelerates the training process by 85% at least compared to AK-MCS-U as the number of CPs used in the active learning process for the proposed method remains relatively small. Additionally, it is evident that the failure probability estimated using Eq. (3-20) is more accurate than that obtained by Eq. (3-19). However, Eq. (3-20) needs more CPU time than Eq. (3-19) because it involves using Kriging predictions on the entire MC population for the final failure probability estimation.

Table 3-6 Results obtained by different methods for the series system

Method	N_{call}	CPU time (s)	P_f	CoV(%)	R.E.(%)
MCS	10^6	-	2.220×10^{-3}	2.12	-
IS	3.6×10^4	-	2.510×10^{-3}	2.66	13.06
SS	2660	-	2.120×10^{-3}	23.93	4.50
AK-SS	68.3	8	2.180×10^{-3}	2.14	1.79
AK-MCS-U	86.8	48	2.220×10^{-3}	2.12	0.00
AKDS-U[1]	82.9	7	2.217×10^{-3}	2.12	0.13
AKDS-U[2]	82.9	8	2.220×10^{-3}	2.12	0.01
AKDS-ε^1	68.6	4	2.205×10^{-3}	2.13	0.68
AKDS-ε^2	68.6	5	2.215×10^{-3}	2.12	0.24

3.5.2 Example 2: a 61-bar truss

To illustrate the efficiency of the proposed method for finite element models, a 61-bar truss shown in Figure 3-8 is first investigated. The performance function can be given by (Ding & Xu, 2021):

$$G\left(E,F_{1\sim13}\right)=D_{\text{lim}}-D\left(E,F_{1\sim13}\right) \tag{3-52}$$

where $D\left(E, F_{1\sim13}\right)$ denotes the vertical displacement at the mid-point of the truss structure and D_{lim} represents a threshold of 795 mm. The circular cross section is used and the area is 1.229×10^{-3} m^2. The elastic modulus E is a lognormally distributed random variable with a mean of 210 GPa and a CoV of 0.10. The vertical loads F_1 to F_{13} are all lognormally distributed variables, each with a mean of 15 kN and a CoV of 0.15. P_f obtained by different approaches are summarized in Table 3-7, where AK-MCS-U and AKDS are both initiated with $N_{\text{MC}}=10^6$. According to Table 3-7, the relative errors produced by the proposed AKDS across all four cases, as well as by AK-MCS-U, are all less than 1%. The average number of FEM calls required by AKDS-ε is 45.4, which is smaller than 60.8 calls required by AK-MCS-U. Although IS and SS obtain fair good results, they require a significantly higher number of function calls. Besides, AK-SS requires 49.3 function calls, which is larger than 45.4 simulations required by the proposed method. In terms of CPU time, AKDS reduces computational effort by nearly 90% compared to the conventional AK-MCS-U.

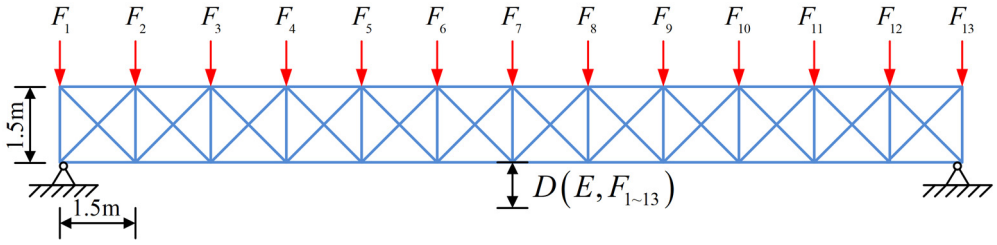

Figure 3-8 A 61-bar truss structure

Table 3-7 Results obtained by different methods for the truss structure

Method	N_{call}	CPU time (s)	P_f	CoV(%)	R.E.(%)
MCS	10^7	-	4.820×10^{-5}	4.55	-
IS	5144	-	4.958×10^{-5}	2.98	2.86
SS	23000	-	4.964×10^{-5}	14.33	2.99

Table 3-7 (continued) Results obtained by different methods for the truss structure

Method	N_{call}	CPU time (s)	P_f	CoV(%)	R.E.(%)
AK-SS	49.7	119	4.921×10^{-5}	3.20	2.10
AK-MCS-U	60.8	534	4.820×10^{-5}	4.55	0.00
AKDS-U[1]	60.6	20	4.814×10^{-5}	4.56	0.12
AKDS-U[2]	60.6	54	4.820×10^{-5}	4.55	0.00
AKDS-ε^1	45.4	13	4.856×10^{-5}	4.54	0.74
AKDS-ε^2	45.4	40	4.857×10^{-5}	4.54	0.77

3.5.3 Example 3: a planar concrete frame structure

This example presents a three-bay six-storey planar reinforced concrete frame with non-linear constitutive laws, as shown in Figure 3-9. The finite element model is constructed by OpenSees, incorporating the Concrete01 and Steel01 constitutive laws. It involves 24 random variables accounting for uncertainties related to structural parameters and external loads, with statistical information provided in Table 3-8. The horizontal displacement of the top floor can be obtained through the finite element analysis, and the implicit performance function can be constructed as (Zhang & Xu, 2021):

$$G(\mathbf{X}) = \Delta_{\text{limit}} - \Delta(\mathbf{X}) \tag{3-53}$$

where $\mathbf{X}$ represents the involved 24 input random variables and the threshold $\Delta_{\text{limit}} = 0.07\text{m}$.

The results obtained by different approaches are shown in Table 3-9. AK-MCS-U and AKDS achieve a comparable accuracy. By using the same U stopping criterion, AK-MCS-U requires 271.4 calls to the FEM whereas AKDS-U only consumes 219.9 FEM evaluations, which demonstrates that the proposed distance-based domain decomposition can reduce the number of calls to the FEM. Furthermore,

AKDS-ε reduces almost 34% of the computational cost induced by FEM evaluations while obtaining a failure probability similar to that of AK-MCS-U. IS and SS require more function calls and do not achieve the same level of accuracy as AK-MCS-U and AKDS. Additionally, the average CPU time for AK-MCS-U is 2953 seconds, compared to only 237 seconds for AKDS-ε^1. Therefore, the total computational burden of the proposed method, encompassing both FEM evaluations and active learning process itself, is reduced by 92% compared to AK-MCS-U. Hence, the process of reliability analysis is significantly accelerated by the proposed strategy. Again, the number of function calls consumed by AK-SS, i.e., 195.2, is larger than 179.5 simulations required by AKDS-ε.

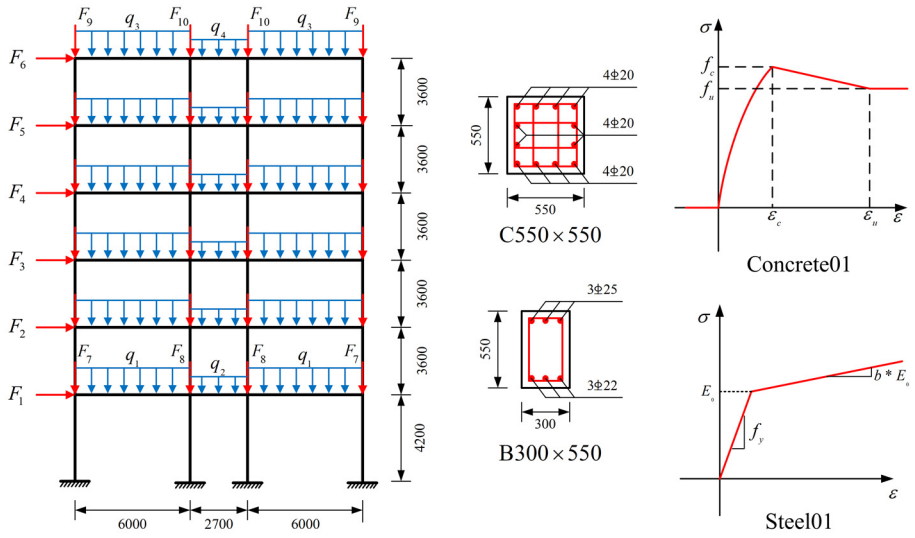

Figure 3-9 A three-bay six-storey planar reinforced concrete frame

Moreover, two stopping criteria, i.e., ESC (Wang & Shafieezadeh, 2019) and the proposed ε stopping criterion, are compared in this example. AK-MCS-ESC with a threshold of 5% terminates the training process slightly earlier, resulting in a relative error of 6.28%. In contrast, using a 1% threshold necessitates additional FEM

evaluations compared to AK-MCS-ε to achieve comparable accuracy. Furthermore, it can be observed that AKDS-ε needs fewer calls than AK-MCS-ε, reinforcing the effectiveness of the proposed domain decomposition in reducing the number of performance function evaluations.

Table 3-8 Random variables for the reinforced concrete frame

Variable	Description	Distribution	Mean	CoV
f_{cc}	Confined concrete compressive strength	Normal	35 MPa	0.1
ε_{cc}	Confined concrete strain at maximum strength	Normal	0.005	0.05
f_{cu}	Confined concrete crushing strength	Normal	25 MPa	0.1
ε_{cu}	Confined concrete strain at crushing strength	Normal	0.02	0.05
f_c	Unconfined concrete compressive strength	Normal	27 MPa	0.1
f_u	Unconfined concrete crushing strength	Normal	0 MPa	-
ε_c	Unconfined concrete strain at maximum strength	Deterministic	0.002	0.05
ε_u	Unconfined concrete strain at crushing strength	Lognormal	0.006	0.05
f_y	Yield strength of rebar	Lognormal	400 MPa	0.1
E_0	Initial elastic modulus of rebar	Lognormal	200 GPa	0.1
b	Strain-hardening ratio of rebar	Lognormal	0.007	0.05
q_1	Uniform load	Lognormal	21.41 kN/m	0.25
q_2	Uniform load	Lognormal	11.48 kN/m	0.25
q_3	Uniform load	Lognormal	22.68 kN/m	0.25
q_4	Uniform load	Lognormal	12.18 kN/m	0.25
F_1	External force	Lognormal	10 kN	0.25
F_2	External force	Lognormal	20 kN	0.25
F_3	External force	Lognormal	30 kN	0.25
F_4	External force	Lognormal	40 kN	0.25
F_5	External force	Lognormal	50 kN	0.25
F_6	External force	Lognormal	60 kN	0.25
F_7	External force	Lognormal	42.43 kN	0.25
F_8	External force	Lognormal	68.25 kN	0.25
F_9	External force	Lognormal	44.03 kN	0.25
F_{10}	External force	Lognormal	71.35 kN	0.25

Table 3-9 Results obtained by different methods for the reinforced concrete frame

Method	N_{call}	CPU time (s)	P_f	CoV(%)	R.E.(%)
MCS	10^6	79786	5.130×10^{-4}	4.41	-
IS	3423	-	4.844×10^{-4}	4.91	5.58
SS	4600	-	4.895×10^{-4}	21.21	4.57
AK-SS	195.2	849	4.883×10^{-4}	2.65	4.82
AK-MCS-U	271.4	2953	5.126×10^{-4}	4.42	0.08
AK-MCS-ESC (5%)	60.7	73	4.808×10^{-4}	4.56	6.28
AK-MCS-ESC (1%)	218.4	1827	5.123×10^{-4}	4.42	0.14
AK-MCS-ε	197.5	1505	5.107×10^{-4}	4.42	0.45
AKDS-U[1]	219.9	367	5.094×10^{-4}	4.43	0.70
AKDS-U[2]	219.9	381	5.117×10^{-4}	4.42	0.25
AKDS-ε[1]	179.5	237	5.102×10^{-4}	4.43	0.55
AKDS-ε[2]	179.5	248	5.138×10^{-4}	4.41	0.16

3.5.4 Example 4: a bolted steel beam-column joint

To further illustrate the performance of the proposed distance-based domain decomposition and the ε stopping criterion for practical time-demanding engineering problems, a bolted steel beam-column joint shown in Figure 3-10 is investigated. The finite element model is constructed using ABAQUS. The dimensions of the beam, column and end plate are $\text{H}400\times180\times10\times20$, $\text{H}600\times350\times20\times20$ and $600\times200\times20$, respectively, with Q235 steel. The diameter of the bolt is 22 mm and the grade is 10.9. The random parameters involved are shown in Table 3-10. The maximum Mises stress of eight bolts is of interest and the performance function gives:

$$G\left(E_{1\sim2}, v_{1\sim2}, F\right) = \sigma_{\text{limit}} - \max_{1\le i\le 8}\left(\sigma^i_{\text{Mises}}\right) \tag{3-54}$$

where the threshold σ_{limit} is specified as 1060 MPa.

The failure probabilities by different methods are listed in Table 3-11. MCS is not feasible for this structural reliability analysis due to the excessive time required,

i.e., over 4.5 years. With the same U stopping criterion, the proposed AKDS-U requires an average of 100.3 calls to the finite element model, compared to 147.0 calls for AK-MCS-U, which illustrates that the proposed domain decomposition can mitigate the computational burden induced by time-demanding FEM evaluations.

Table 3-10 Random variables for the bolted steel beam-column joint

Variable	Description	Distribution	Mean	CoV
E_1	The Young's modulus of the beam, column and end plate	Lognormal	2.06×10^5	0.10
E_2	The Young's modulus of the bolt	Lognormal	2.10×10^5	0.10
v_1	The Poisson's ratio of the beam, column and end plate	Lognormal	0.3	0.05
v_2	The Poisson's ratio of the bolt	Lognormal	0.3	0.05
F	Displacement-controlled load	Lognormal	10 mm	0.20

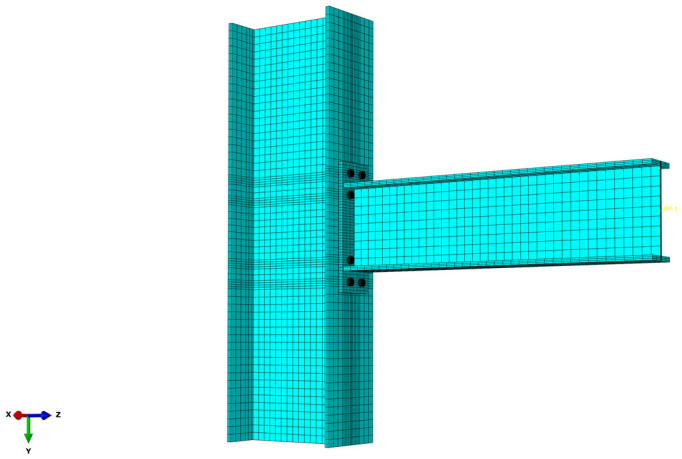

Figure 3-10 FEM of the bolted steel beam-column joint

Furthermore, using the proposed ε stopping criterion significantly decreases the number of FEM calls to just 37.6 evaluations, reducing CPU time by 76% compared to AK-MCS-U, with only 6.4 hours required. Again, AK-SS consumes more finite element analyses than AKDS-ε to evaluate the failure probability.

Table 3-11 Results of reliability analysis for the bolted steel beam-column joint

Method	N_{call}	CPU time	P_f	CoV(%)
MCS	10^6	>4.5 years	–	–
AK-MCS-U	147.0	26.6 hours	1.713×10^{-3}	2.41
AK-SS	65	11.1 hours	1.729×10^{-3}	2.40
AKDS-U[1]	100.3	17.6 hours	1.717×10^{-3}	2.41
AKDS-U[2]	100.3	17.6 hours	1.714×10^{-3}	2.41
AKDS-ε^1	37.6	6.4 hours	1.735×10^{-3}	2.40
AKDS-ε^2	37.6	6.4 hours	1.720×10^{-3}	2.41

3.6 Summary

To mitigate the computational cost of AK-MCS, an accelerated active learning Kriging model with distance-based subdomains termed AKDS is developed in this chapter. The proposed approach aims to alleviate the computational burden of the AK-based methods from two aspects, i.e., the computational effort induced by active learning on a large population and the calls to the time-consuming performance functions. First, a distance-based subdomain is employed to select candidate points in the vicinity of LSS. The Kriging model is trained within distance-based subdomains and Kriging predictions on numerous candidate samples can be avoided, significantly reducing the time for training process itself. Second, the impact of candidate points with high probabilities of wrong classification on the relative error of failure probability is investigated. A new stopping criterion is derived from the expected upper bound of this relative error. Additionally, a threshold $\overline{\varepsilon} = 0.1$ is suggested to exempt εN_f points from the U stopping criterion, ensuring that the accuracy of the failure probability estimation is maintained with the expected upper bound of the relative error remaining below 5%. Consequently, the computational cost results from the time-demanding model evaluations can be further alleviated.

The performance of the proposed AKDS is validated by both analytical and numerical performance functions. Comparisons across four illustrative examples demonstrate that the proposed approach effectively accelerates the active learning process and reduces the number of calls to time-consuming performance functions. Additionally, the accuracy of the failure probability estimation is maintained using this method.

CHAPTER 4 AN ERROR-BASED STOPPING CRITERION FOR SPHERICAL DECOMPOSITION-BASED ADAPTIVE KRIGING MODEL AND RARE EVENT ESTIMATION

4.1 Introduction

The surrogate model-based reliability analysis method, particularly the adaptive Kriging model, has garnered significant attention due to its high accuracy and efficiency in reliability analysis. In practical engineering, where high reliability is a design target, adaptive Kriging is combined with more efficient sampling techniques, such as the spherical decomposition-based Monte Carlo simulation (SDMCS). In this chapter, a new stopping criterion tailored for the adaptive Kriging model with SDMCS (AKSDMCS) is introduced. First, the relative error of the failure probability obtained by AKSDMCS is derived. Then, the impact of samples with high probabilities of misclassification on the relative error of the failure probability is quantified. In each sub-region of SDMCS, it can be found that the number of misclassified points follows a binomial distribution. Subsequently, the expected upper bound of the relative error of the failure probability is formulated. A new stopping criterion for AKSDMCS is then developed. The performance of this proposed stopping criterion is validated through three applications, demonstrating that adaptive Kriging with the proposed stopping criterion effectively halts the active training

process at an appropriate stage and significantly reduces the computational effort required for rare event estimation.

4.2 An error-based stopping criterion for AKSDMCS

Although AKMCS can significantly reduce the computational effort required by time-consuming simulations, its performance in estimating small failure probabilities is limited. In the context of high-reliability design targets, the failure probability of an engineering structure is usually small (Echard et al., 2013; Schöbi et al., 2017). To estimate such a small failure probability, importance sampling or subset sampling may be preferred, as updating the Kriging model with numerous samples generated by MCS is also computationally expensive. Besides IS and SS, a modified MCS named spherical decomposition-based MCS can also be an efficient way to generate candidate pool for training Kriging model and the so-called AKSDMCS was proposed (Su et al., 2020). In this section, a new stopping criterion, which based on the effect of the dangerous points on the accuracy of failure probability, is tailored for the adaptive Kriging with the spherical decomposition-based sampling approach to stop the active training process at an appropriate stage.

4.2.1 Adaptive Kriging with spherical decomposition-based MCS

The spherical decomposition-based MCS is a modified MCS by decomposing the sampling space into a series of subdomains so that the number of candidate samples can be remarkably reduced (Su et al., 2020). Assume that the original sampling space $\Omega \in \mathbb{R}^d$ can be decomposed into n non-overlapping subdomains $\Omega_i, i = 1, 2, ..., n$:

$$\Omega=\bigcup_{i=1}^{n}\Omega_i \tag{4-1}$$

and

$$\Omega_i \cap \Omega_j = \varnothing, i \neq j \tag{4-2}$$

where $\Omega_i = \left\{\mathbf{x} \mid R_{i-1} \leq \left\|\mathbf{x}\right\| < R_i, \mathbf{x} \in \Omega\right\}$ is a spherical ring defined by inner radius R_{i-1} and outer radius R_i . The descending radius sequence $R_0 < R_1 < \cdots < R_n$ is appropriately selected with $R_0 = 0$ and $R_n = +\infty$. Then, the failure probability can be computed as (Su et al., 2020):

$$P_f = \int_{\bigcup_{i=1}^{n}\Omega_i} I\left(\mathbf{x}\right) f_{\mathbf{X}}\left(\mathbf{x}\right) \mathrm{d}\mathbf{x} = \sum_{i=1}^{n} \int_{\Omega_i} I\left(\mathbf{x}\right) f_{\mathbf{X}}\left(\mathbf{x}\right) \mathrm{d}\mathbf{x} \tag{4-3}$$

Consider a truncated PDF $f_{\mathbf{X}}^{i}\left(\mathbf{x}\right)$ corresponding to the *i*-th subdomain Ω_i and $f_{\mathbf{X}}^{i}\left(\mathbf{x}\right) = f_{\mathbf{X}}\left(\mathbf{x}\right) / \delta_i$, where $\delta_i = \int_{\Omega_i} f_{\mathbf{X}}\left(\mathbf{x}\right) \mathrm{d}\mathbf{x}$. Accordingly, Eq. (4-3) can be reformulated as:

$$P_f = \sum_{i=1}^{n} \delta_i \int_{\Omega_i} I\left(\mathbf{x}\right) f_{\mathbf{X}}^{i}\left(\mathbf{x}\right) \mathrm{d}\mathbf{x} = \sum_{i=1}^{n} \delta_i P_i = \sum_{i=1}^{n} P_f^i \tag{4-4}$$

where $P_i = \int_{\Omega_i} I\left(\mathbf{x}\right) f_{\mathbf{X}}^{i}\left(\mathbf{x}\right) \mathrm{d}\mathbf{x} = \Pr\left(\Omega_F \cap \Omega_i \mid \Omega_i\right)$ is a conditional failure probability associated with subdomain Ω_i . P_f^i can be seen as the sub-failure probability contributed by Ω_i . The conditional failure probability can be estimated by the crude MCS:

$$P_i \approx \hat{P}_i = \sum_{j=1}^{N_{\mathrm{MC}}^i} \frac{I\left(\mathbf{x}_i^{(j)}\right)}{N_{\mathrm{MC}}^i} \tag{4-5}$$

where the samples $\left\{\mathbf{x}_i^{(j)}, j = 1, 2, .., N_{\mathrm{MC}}^i\right\}$ are drawn from $f_{\mathbf{X}}^i\left(\mathbf{x}\right)$. Therefore, the estimated failure probability by SDMCS can be calculated by (Su et al., 2020):

$$\hat{P}_f = \sum_{i=1}^{n} \delta_i \hat{P}_i = \sum_{i=1}^{n} \hat{P}_f^i \tag{4-6}$$

Accordingly, the associated variance of failure probability can be derived by (Su et al., 2020):

$$\mathrm{var}\left(\hat{P}_f\right) = \mathrm{var}\left(\sum_{i=1}^{n} \delta_i \hat{P}_i\right) = \sum_{i=1}^{n} \frac{\delta_i^2 \hat{P}_i\left(1 - \hat{P}_i\right)}{N_{\mathrm{MC}}^i} = \sum_{i}^{n} \mathrm{var}\left(\hat{P}_f^i\right) \tag{4-7}$$

and the coefficient of variation of $\hat{P}_f$ can be given by:

$$\mathrm{CoV}\left(\hat{P}_f\right) = \sqrt{\sum_{i=1}^{n} \frac{\delta_i^2 \hat{P}_i\left(1 - \hat{P}_i\right)}{N_{\mathrm{MC}}^i \hat{P}_f^2}} \tag{4-8}$$

The CoV is employed to determine the number of samples over the entire domain, ensuring a small variation of estimated failure probability.

SDMCS is combined with the Kriging model in an adaptive manner, where the required number of subdomains (n) is determined adaptively. The sampling space is first divided into 2 spherical rings and the outmost ring is further decomposed into 2 rings until the required number of samples in the outmost ring is smaller than a predefined value ΔN. The sampling space is decomposed in the radius direction on

the basis of orders of magnitude of probability. The radius R_j is determined by the probability $\Pr\left\{\|\mathbf{x}\| \le R_j, \mathbf{x} \in \Omega\right\} = 1-10^{-j}$ or its equivalent form $\Pr\left\{\|\mathbf{x}\| > R_j, \mathbf{x} \in \Omega\right\} = 10^{-j}$. Note that in the standard normal space, the square of the distance between a point **U** (samples corresponding to **X** in the standard normal space) and the origin point obeys the chi-square distribution $\chi_d^2\left(|\mathbf{U}|^2\right)$ with d degrees of freedom. Thus, the radius can be calculated by $R_j^2 = \tilde{\chi}_d^{-1}\left(1-10^{-j}\right)$, where $\tilde{\chi}_d^{-1}(\cdot)$ is the inverse cumulative distribution of chi-square distribution. The major steps are summarized as follows (Su et al., 2020):

Step 1: Specify the initial sample size ΔN in each subdomain and the target CoV of the estimated failure probability $\mathrm{CoV}_{\mathrm{tol}}$. The radius sequence is $R_0 = 0 < R_1 < \cdots < R_n = +\infty$, where $R_j^2 = \tilde{\chi}_d^{-1}\left(1-10^{-j}\right)$, $j = 1, 2, ..., n-1$. n is initialized as 1.

Step 2: Decompose the outmost ring into 2 rings and let n=n+1. Generate ΔN samples in Ω_{n-1} following the distribution $f_{\mathbf{X}}^{n-1}(\mathbf{x})$. The sampling process is presented as follows. First, draw a random sample following a uniform distribution with support on $[p_1, p_2]$, where $p_1 = 1-10^{-(j-1)}$ and $p_2 = 1-10^{-j}$. Then, calculate the distance $R^2 = \tilde{\chi}_d^{-1}(p)$. Third, calculate the vector $\mathbf{V} = \mathbf{d}/\|\mathbf{d}\|$, where **d** is a standard normal variable. Finally, the required sample in Ω_j can be obtained by $\mathbf{x} = T^{-1}(\mathbf{u})$, where $\mathbf{u} = R\mathbf{V}$ and T is isoprobabilistic transformation.

Step 3: Train Kriging model with a learning function and a stopping criterion. Then, calculate the current failure probability $\hat{P}_f$ on the basis of Eq. (4-5) and Eq. (4-6). Note that in this step, the estimated failure probability contributed by the first-$(n-1)$ subdomains are of concern.

Step 4: Compute the expected number of points N_{MC}^n in Ω_n by:

$$N_{\mathrm{MC}}^n = \delta_n N_{\mathrm{MC}}, N_{\mathrm{MC}} = \frac{1-\hat{P}_f}{\hat{P}_f \mathrm{CoV}_{\mathrm{tol}}^2} \tag{4-9}$$

if $N_{\mathrm{MC}}^n \le \Delta N$, it means that N_{MC}^n samples are sufficient to represent the outmost region, otherwise, go back to step 2.

Step 5: Generate N_{MC}^n samples drawn from PDF $f_{\mathbf{X}}^n(\mathbf{x})$ in Ω_n.

Step 6: Train Kriging model again and calculate the current failure probability with its CoV based on Eq. (4-6) and Eq. (4-8), respectively.

Step 7: If $\mathrm{CoV}\left(\hat{P}_f\right) \le \mathrm{CoV}_{\mathrm{tol}}$, output the estimated failure probability. Otherwise, enrich candidate samples in the spherical ring with the largest sub-variance:

$$i^* = \arg\max_i \left[\mathrm{var}\left(P_f^i\right)\right], i = 1, 2, ..., n \tag{4-10}$$

In this chapter, if $i^* < n$, another ΔN samples are generated in Ω_{i^*}, if $i^* = n$, another N_{MC}^n samples are generated in Ω_{i^*}. Then, return to step 6.

4.2.2 Proposed stopping criterion for AKSDMCS

Although the SDMCS-based adaptive Kriging model significantly reduces the number of candidate samples required for training and conserves computational resources in small failure probability estimation, the stopping criteria used by Su et al. (2020) overlook the accuracy of failure probability estimates. For example, the U stopping criterion is often deemed too conservative for reliability analysis because it only considers the accuracy of the Kriging model for the limit state surface, ignoring the accuracy of the failure probability estimation. Additionally, there is no stopping criterion specifically designed for the adaptive Kriging model that incorporates the spherical decomposition-based sampling technique. In this section, a new stopping criterion based on quantifying the impact of dangerous points on the relative error of the failure probability is developed.

The number of dangerous points, i.e., points with a high probability of wrong classification ($\left\{\mathbf{x}\in\Omega\,|\,U\left(\mathbf{x}\right)<2\right\}$), significantly affects the accuracy of Kriging model and failure probability estimation. Suppose that $Z=k$ samples (Z is a random variable) in the domain $\left\{\mathbf{x}\in\Omega\,|\,U\left(\mathbf{x}\right)<2\right\}$ are in wrong classification, then the range of the estimated failure probability can be calculated as:

$$P_f-\frac{Z}{N_{\mathrm{MC}}}\le\hat{P}_f\le P_f+\frac{Z}{N_{\mathrm{MC}}} \tag{4-11}$$

the left-hand side is true when k points are actually negative but classified as positive, and the right-hand side holds when k points are positive but identified as negative. The relative error of the failure probability can be calculated as:

$$\varepsilon = \left| \frac{\hat{P}_f - P_f}{P_f} \right| \leq \frac{Z}{N_{\mathrm{MC}} P_f} \tag{4-12}$$

and the upper bound of the relative error can be denoted as ε_{u}:

$$\varepsilon_{\mathrm{u}} = \frac{Z}{N_{\mathrm{MC}} P_f} \tag{4-13}$$

then the expected upper bound of the relative error of P_f reads:

$$\mathbb{E}\left[\varepsilon_{\mathrm{u}}\right] = \frac{1}{N_{\mathrm{MC}} P_f} \mathbb{E}\left[Z\right] = \frac{1}{N_f} \mathbb{E}\left[Z\right] \tag{4-14}$$

where $\mathbb{E}$ represents the expectation operator and $N_f = N_{\mathrm{MC}} P_f$ denotes the number of points in the failure domain.

On the basis of spherical decomposition and Eq. (4-6), Eq. (4-12) can be reformulated as:

$$\varepsilon = \left| \frac{\hat{P}_f - P_f}{P_f} \right| = \left| \frac{\sum_{i=1}^{n} \delta_i \hat{P}_i - \sum_{i=1}^{n} \delta_i P_i}{\sum_{i=1}^{n} \delta_i P_i} \right| \tag{4-15}$$

Note that for each ring generated by SDMCS, on the basis of Eq. (4-11), we have:

$$P_i - \frac{Z_i}{N_{\mathrm{MC}}^i} \leq \hat{P}_i \leq P_i + \frac{Z_i}{N_{\mathrm{MC}}^i} \tag{4-16}$$

where $Z_i = k_i$ denotes that k_i points in the domain $\left\{\mathbf{x} \in \Omega_i \,|\, U\left(\mathbf{x}\right) < 2\right\}$ are in wrong classification. Thus, the relative error of P_f satisfies:

$$\varepsilon = \left| \frac{\sum_{i=1}^{n} \delta_i \hat{P}_i - \sum_{i=1}^{n} \delta_i P_i}{\sum_{i=1}^{n} \delta_i P_i} \right| \le \frac{\sum_{i=1}^{n} \delta_i \frac{Z_i}{N_{\mathrm{MC}}^i}}{\sum_{i=1}^{n} \delta_i \frac{N_f^i}{N_{\mathrm{MC}}^i}} \tag{4-17}$$

where N_f^i represents the number of points in the failure domain belonging to the *i*-th ring. Similarly, the upper bound of the relative error of P_f is

$$\varepsilon_{\mathrm{u}} = \frac{\sum_{i=1}^{n} \delta_i \frac{Z_i}{N_{\mathrm{MC}}^i}}{\sum_{i=1}^{n} \delta_i \frac{N_f^i}{N_{\mathrm{MC}}^i}} \tag{4-18}$$

and its expected value can be given as:

$$\mathbb{E}\left[\varepsilon_{\mathrm{u}}\right] = \mathbb{E}\left[\frac{\sum_{i=1}^{n} \delta_i \frac{Z_i}{N_{\mathrm{MC}}^i}}{\sum_{i=1}^{n} \delta_i \frac{N_f^i}{N_{\mathrm{MC}}^i}} \right] = \frac{\sum_{i=1}^{n} \delta_i \frac{\mathbb{E}\left[Z_i\right]}{N_{\mathrm{MC}}^i}}{\sum_{i=1}^{n} \delta_i \frac{N_f^i}{N_{\mathrm{MC}}^i}} \tag{4-19}$$

Z_i is a random variable and its mean value is of interest. To this end, suppose that the number of dangerous points in *i*-th ring ($\left\{\mathbf{x} \in \Omega_i \,|\, U\left(\mathbf{x}\right) < 2\right\}$) is N_U^i. Let Z_i be the event that k_i points in the domain $\left\{\mathbf{x} \in \Omega_i \,|\, U\left(\mathbf{x}\right) < 2\right\}$ are in wrong classification, the probability of the event $\left\{Z_i = k_i\right\}$ can be derived as:

$$\Pr\left(Z_i = k_i\right) = \sum_{c=1}^{C_{N_U^i}^{k_i}} \left[\prod_{a=1}^{k_i} p_{c,a} \prod_{b=k_i+1}^{N_U^i} \left(1 - p_{c,b}\right) \right] \tag{4-20}$$

where $C_{N_U^i}^{k_i} = \dfrac{N_U^i !}{k_i ! \left(N_U^i - k_i\right)!}$. $p_{c,a}$ and $p_{c,b}$ are probabilities of wrong classification. On the basis of Eq. (3-9), $p_{c,a}$ and $p_{c,b}$ satisfy:

$$0.023 = \Phi\left(-2\right) < p_{c,a}, p_{c,b} \le \Phi\left(0\right) = 0.5 \tag{4-21}$$

Consider the worst condition for the failure probability estimation, that is, all points in the domain $\left\{\mathbf{x} \in \Omega \,|\, U\left(\mathbf{x}\right) < 2\right\}$ have the largest probability of wrong classification, i.e., $p_{c,a} = p_{c,b} = p = 0.5$. Thus Z_i follows the binomial distribution $Z_i \sim B\left(N_U^i, p\right)$. The probability of the event $\left\{Z_i = k_i\right\}$ is:

$$\Pr\left(Z_i = k_i\right) = C_{N_U^i}^{k_i} p^{k_i} \left(1 - p\right)^{N_U^i - k_i} \tag{4-22}$$

Obviously, the mean value of Z_i gives:

$$\mathbb{E}\left[Z_i\right] = N_U^i p \tag{4-23}$$

Substituting Eq. (4-23) into Eq. (4-19), results in:

$$\begin{aligned} \mathbb{E}\left[\varepsilon_{\mathrm{u}}\right] &= \frac{\sum_{i=1}^{n} \delta_i \dfrac{N_U^i p}{N_{\mathrm{MC}}^i}}{\sum_{i=1}^{n} \delta_i \dfrac{N_f^i}{N_{\mathrm{MC}}^i}} = \frac{\sum_{i=1}^{n} \delta_i \dfrac{N_U^i}{N_{\mathrm{MC}}^i}}{\sum_{i=1}^{n} \delta_i \dfrac{N_f^i}{N_{\mathrm{MC}}^i}} \times p \\ &= \eta \times p \end{aligned} \tag{4-24}$$

Therefore:

$$\eta=\frac{\sum_{i=1}^{n}\delta_i\frac{N_U^i}{N_{\mathrm{MC}}^i}}{\sum_{i=1}^{n}\delta_i\frac{N_f^i}{N_{\mathrm{MC}}^i}} \tag{4-25}$$

It can be observed that the expected upper bound of the relative error of failure probability is dominated by the indicator η and the probability of wrong classification *p*. If the conventional U stopping criterion is used for adaptive Kriging training, i.e., $\min\left(U\left(\mathbf{x}\right)\right)\geq 2,\forall\mathbf{x}\in\Omega$, there will be no dangerous points in the whole sampling domain, resulting in $N_U^i=0, i=1,2,...,n$ and $\mathbb{E}\left[\varepsilon_{\mathrm{u}}\right]=0$. Hence, the traditional U stopping criterion can significantly ensure the accuracy of the adaptive Kriging model for limit state surface. However, it is usually considered too conservative for failure probabilities estimation as all dangerous points in sampling domain are required to be identified, thereby ignoring the accuracy of the failure probability.

As aforementioned, the worst condition for estimating failure probabilities is considered, i.e., p = 0.5. Thus, it can be observed that the expected upper bound of the relative error of the failure probability is smaller than 5% given $\eta\leq 0.1$ and p=0.5, which is acceptable for the failure probability estimation. Hence, we have:

$$\left\{\mathbb{E}\left[\varepsilon_{\mathrm{u}}\right]\leq 5\%\,|\,\eta\leq 0.1, p=0.5\right\} \tag{4-26}$$

Therefore, the indicator $\eta \le 0.1$ can be a new stopping criterion designed for the adaptive Kriging with SDMCS. To evaluate η, the estimated number of failure points $\hat{N}_f^i$ in each ring can be employed:

$$\hat{\eta}=\frac{\sum_{i=1}^{n}\delta_i\frac{N_U^i}{N_{\mathrm{MC}}^i}}{\sum_{i=1}^{n}\delta_i\frac{\hat{N}_f^i}{N_{\mathrm{MC}}^i}} \tag{4-27}$$

The pseudo code is indicated in Algorithm 2.

Table 4-1 Algorithm 2 for the proposed AKSDMCS

Algorithm 2: Adaptive Kriging model with SDMCS and a new stopping criterion η for rare event estimation

Input: Information of input random variables and performance function $G(\mathbf{X})$

Output: Failure probability P_f

1. Initiate the sample size ΔN in each ring, the target CoV of failure probability $\mathrm{CoV}_{\mathrm{tol}}$ and n=1
2. Select an initial DoE $\{\boldsymbol{\mathcal{X}},\boldsymbol{\mathcal{Y}}\}$ with size $\max\{12,2d\}$ via Latin hypercube sampling
3. While $N_{\mathrm{MC}}^n > \Delta N$ do
4. n=n+1
5. Draw ΔN samples from $f_{\mathbf{X}}^{(n-1)}(\mathbf{x})$ and denote all samples in candidate pool Ω as $\mathbf{X}$
6. While $\eta > 0.1$ do
7. Build Kriging model via DoE $\{\boldsymbol{\mathcal{X}},\boldsymbol{\mathcal{Y}}\}$ and evaluate $\mathbf{X}$ on Kriging model
8. Calculate η by Eq. (4-27)
9. Enrich DoE $\{\boldsymbol{\mathcal{X}},\boldsymbol{\mathcal{Y}}\}$ by U learning function with the point corresponding to $\mathbf{x}^* = \min_{\mathbf{x}\in\Omega} U(\mathbf{x})$
10. End While
11. Calculate the current P_f contributed by the first $1\sim(n-1)$ rings by Eq. (4-6).
12. Calculate the number of samples N_{MC}^n required by the outmost (n-th) ring through Eq. (4-9)
13. End While
14. Generate N_{MC}^n samples from $f_{\mathbf{X}}^n(\mathbf{x})$ in the outmost ring and put them into candidate pool Ω
15. While $\mathrm{CoV}(P_f) > \mathrm{CoV}_{\mathrm{tol}}$ do
16. While $\eta > 0.1$ do
17. Build Kriging model via DoE $\{\boldsymbol{\mathcal{X}},\boldsymbol{\mathcal{Y}}\}$ and evaluate $\mathbf{X}$ on Kriging model
18. Calculate η by Eq. (4-27)
19. Enrich DoE $\{\boldsymbol{\mathcal{X}},\boldsymbol{\mathcal{Y}}\}$ by U learning function with the point corresponding to $\mathbf{x}^* = \min_{\mathbf{x}\in\Omega} U(\mathbf{x})$
20. End While
21. Calculate the current P_f contributed by all rings through Eq. (4-6) and $\mathrm{CoV}(P_f)$ by Eq. (4-8)

Table 4-1 (continued) Algorithm 2 for the proposed AKSDMCS

Algorithm 2: Adaptive Kriging model with SDMCS and a new stopping criterion η for rare event estimation
22. Identify the ring with the largest sub-variance by $i^* = \arg\max_i \left[\mathrm{var}\left(P_f^i\right)\right], i = 1,2,...,n$
23. Enrich i^*-th ring with ΔN samples drawn from $f_{\mathbf{X}}^{i^*}(\mathbf{x})$ if $i^* < n$, otherwise, enrich i^*-th ring with N_{MC}^n samples.
24. End While
25. Output the failure probability P_f

It is known that the adaptive Kriging model with the crude MCS is not suitable for rare events estimation due to the involvement of numerous candidate points. SDMCS, requiring a much smaller candidate pool, can be combined with adaptive Kriging for estimating small failure probabilities. However, SDMCS may significantly increase the number of dangerous points, necessitating more training points when the active training process stops. Here, a 2-D performance function is employed to illustrate the importance of the proposed stopping criterion tailored for adaptive Kriging with SDMCS. The 2-D performance function reads (Echard et al., 2013):

$$G\left(X_1, X_2\right) = 0.5\left(X_1 - 2\right)^2 - 1.5\left(X_2 - 5\right)^3 - 1 \tag{4-28}$$

in which X_1 and X_2 follow the standard normal distribution. Figure 4-1 (a) and (b) show the candidate pool and points in the domain $\left\{\mathbf{x} \in \Omega \,|\, U\left(\mathbf{x}\right) < 2\right\}$ generated by the crude MCS and SDMCS (ΔN=10^5), receptively. Table 4-2 lists the number of candidate points and dangerous points. Note that the number of dangerous points is predicted by Kriging model with an initial DoE. As shown in Table 4-2, to achieve a comparable level of CoV of failure probability (CoV smaller than 5%), the crude MCS requires a much larger candidate pool (1.5×10^8 candidate samples are required)

than SDMCS (only 501879 candidate samples are needed). Thus, MCS remarkably impedes the process of the active training for Kriging model. SDMCS is suitable for rare events estimation combined with adaptive Kriging model, which can save the computational resources caused by the active training process itself. However, as listed in Table 4-2, the number of dangerous points generated by SDMCS is seriously increased (almost 7 times that by the crude MCS), which means that more calls to the real performance function may be required to identify these dangerous points. This issue significantly increases the computational effort for reliability analysis, especially when the real performance function is computationally expensive such as finite element models. To address this issue, the proposed stopping criterion tailored for SDMCS aims to reduce the number of calls to the real performance function.

Table 4-2 Comparisons of the crude MCS and SDMCS

Method	Candidate points	Dangerous points	P_f	CoV
MCS	1.5×10^{8}	717	2.787×10^{-6}	4.89%
SDMCS	501879	4772	2.875×10^{-6}	4.95%

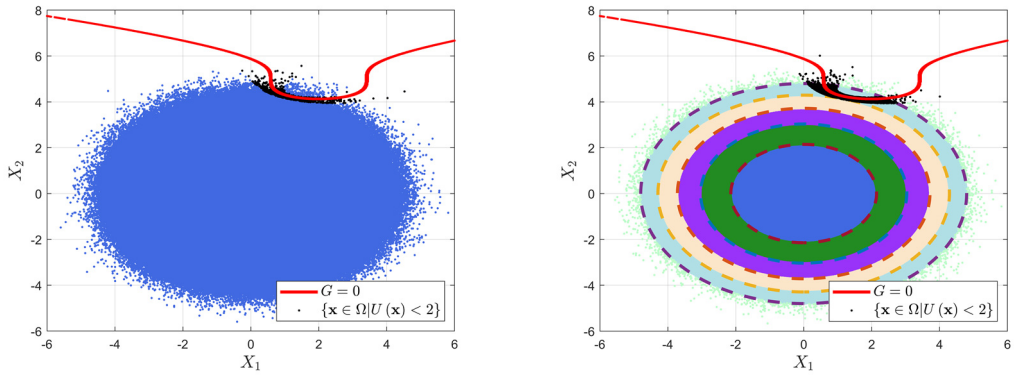

(a) MCS (b) SDMCS

Figure 4-1 Comparison between MCS and SDMCS

4.3 Illustrative examples

In this section, three applications including analytical and numerical performance functions are investigated to showcase the performance of the proposed stopping criterion. The first example investigates a benchmark analytical example considering different levels of failure probabilities estimation. To validate the proposed stopping criterion for small failure probabilities estimation of practical engineering structures, a 61-bar truss and a frame-shear wall structure are studied. The uncertainties associated with both structural parameters and external loads are of concern.

4.3.1 Example 1: a nonlinear oscillator

The first example investigates a nonlinear oscillator shown in Figure 4-2. The performance function is defined as (Echard et al., 2011; Echard et al., 2013):

$$G(\mathbf{X}) = 3r - \left| \frac{2F_1}{m\omega_0^2} \sin\left(\frac{\omega_0 t_1}{2} \right) \right| \tag{4-29}$$

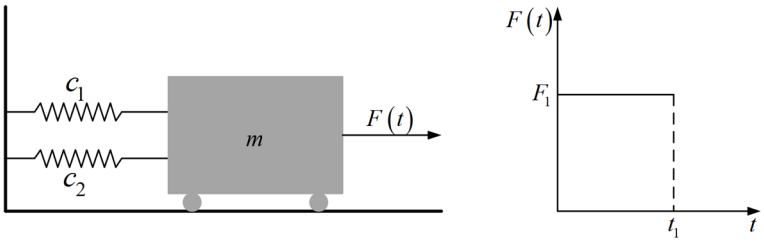

Figure 4-2 a nonlinear oscillator

where $\omega_0 = \sqrt{(c_1 + c_2)/m}$. The mean and CoV of the random variables are listed in Table 4-3. This explicit performance function is a benchmark example and widely investigated to validate AK-based algorithms for reliability analysis. Echard et al. (2011) studied the performance function for AKMCS and it was later extended for

small probabilities estimation (Echard et al., 2013) by revising the mean and CoV of the random variable F_1. Three cases are studied in this example, case 1 refers to $\mu_{F_1} = 0.6$ with a CoV of 0.2, case 2 represents $\mu_{F_1} = 1$ with a CoV of 1/6 and case 3 is $\mu_{F_1} = 0.45$ with a CoV of 1/6.

Table 4-3 Random variables for the nonlinear oscillator

Variable	Distribution	Mean	CoV
m	Normal	1	0.05
c_1	Normal	1	0.1
c_2	Normal	0.1	0.1
r	Normal	0.5	0.1
F_1	Normal	1,0.6,0.45	0.2,1/6,1/6
t_1	Normal	1	0.2

The results by different methods (AK-IS (Echard et al., 2013), AK-SS (Ling et al., 2019), AK-MCS-IS (Chen et al., 2019), AKSDMCS-U (Su et al., 2020) and the proposed method) for reliability analysis are compared in Table 4-4, where N_{call} is the number of performance function calls and $\hat{\beta}$ is the reliability index. Note that the average results over 20 independent runs are provided. Case 1 studies a relatively large failure probability of 2.86×10^{-2}, predicted by 1×10^{5} MCS. AK-MCS-IS, AKSDMCS-U and AKSDMCS with the proposed η stopping criterion all produce satisfactory reliability index compared with the benchmark result provided by MCS. Regarding the number of performance function calls, AKSDMCS with the proposed η stopping criterion reduces the computational effort by at least 58% compared to the other AK-based approaches. The average N_{call} is as small as 22 while AK-MCS-IS takes the most, i.e., 74.

Table 4-4 Results obtained by different methods for the nonlinear oscillator

Method		MCS	AK-IS	AK-SS	AK-MCS-IS	AKSDMCS-U	AKSDMCS-η
Case 1	N_{call}	1×10^{5}	-	-	74	53	22
	$\hat{P}_f$	2.86×10^{-2}	-	-	2.85×10^{-2}	2.78×10^{-2}	2.79×10^{-2}
	$\hat{\beta}$	1.90	-	-	1.90	1.91	1.91
	CoV	1.84	-	-	2.20	0.93	0.94
Case 2	N_{call}	1.8×10^{8}	67	146	95	58	30
	$\hat{P}_f$	9.09×10^{-6}	9.13×10^{-6}	9.65×10^{-6}	9.13×10^{-6}	8.96×10^{-6}	9.05×10^{-6}
	$\hat{\beta}$	5.54	4.29	4.27	4.29	4.29	4.29
	CoV	2.68	2.29	3.65	2.46	1.09	1.85
Case 3	N_{call}	9×10^{10}	667	162	110	68	36
	$\hat{P}_f$	1.55×10^{-8}	1.53×10^{-8}	1.53×10^{-8}	1.56×10^{-8}	1.50×10^{-8}	1.47×10^{-8}
	$\hat{\beta}$	5.54	5.54	5.54	5.53	5.54	5.55
	CoV	2.68	2.70	2.83	2.67	0.64	2.37

Case 2 and case 3 investigate the estimation of extremely small failure probability, with reference results provided by the crude MCS. The crude MCS requires 1.8×10^{8} and 9×10^{10} candidate samples for cases 2 and 3, respectively. Consequently, it is impractical to use the conventional AKMCS for reliability analysis, as the active training on such a large number of samples is time-consuming and the computational capacity is also limited. AKSDMCS with both U and η stopping criterion achieve comparable accuracy, while the proposed η stopping criterion requires fewer performance function calls and mitigates computational costs by almost 50% compared to U stopping criterion for small failure probabilities estimation. AK-IS, AK-SS and AK-MCS-IS all show fair good performance, while they require more function calls than AKSDMCS with the proposed stopping criterion. Additionally, the CoV of the failure probability by AKSDMCS-η is the smallest among AK-IS, AK-SS and AK-MCS-IS, indicating that the proposed method can obtain a more stable result.

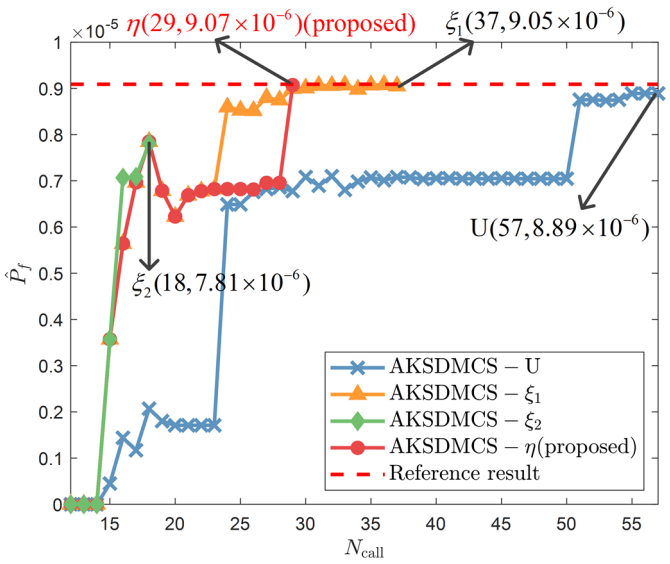

Figure 4-3 Comparisons of four different stopping criteria

To further show the efficiency of the proposed η stopping criterion, different stopping criteria are compared in Figure 4-3, where the stopping criteria ξ_1 and ξ_2 were developed on the basis of the stabilization of the failure regions (Su et al., 2020). ξ_1 and ξ_2 are expressed as follows:

$$\xi_1 = \frac{\left| N_f^{(k-1)} - N_f^{(k)} \right|}{N_f^{(k-1)}} < e_1 \tag{4-30}$$

$$\xi_2 = \sum_{i=1}^{N_C} \frac{\text{card}\left(\hat{G}^{k-1}\left(\mathbf{x}_i\right) \times \hat{G}^{k}\left(\mathbf{x}_i\right) \right)}{N_C} < e_2 \tag{4-31}$$

where $N_f^{(k)}$ represents the number of failure points at k-th iteration of the active learning process. N_C is the total number of candidate points and $\hat{G}^k$ refers to the Kriging model at the k-th iteration. The notation $\times$ denotes "exclusive OR" operation,

which returns true only when the signs of $\hat{G}^{k-1}(\mathbf{x}_i)$ and $\hat{G}^{k}(\mathbf{x}_i)$ differ. The thresholds e_1 and e_2 are suggested to be 0.001 (Su et al., 2020).

As shown in Figure 4-3, U stopping criterion consumes the largest number of function calls. Thus, it is the most conservative stopping criterion. In comparison, the ξ_1 stopping criterion demands additional training points than the proposed stopping criterion when the estimated failure probability approaches the reference value. AKSDMCS with ξ_2 stopping criterion terminates too early, resulting in the inaccuracy of the failure probability estimation. Conversely, the proposed stopping criterion does not require extra training points once the accuracy of the failure probability is achieved. This is because the proposed stopping criterion is derived based on the relative error of the failure probability. For stabilization-based stopping criteria ξ_1 and ξ_2, the thresholds e_1 and e_2 are selected based on the researchers' experience, and the impact of these thresholds on the accuracy of the failure probability is not quantified. U stopping criterion focuses solely on the accuracy of Kriging model while disregarding the failure probability, making it the most conservative option.

According to Eq. (4-20), Z_i follows a Poisson binomial distribution. By using the Poisson binomial distribution, the expected upper bound of the relative error of the failure probability can be reformulated as:

$$\mathbb{E}\left[\varepsilon_{\mathrm{u}}\right]=\frac{\sum_{i=1}^{n}\delta_i\frac{\sum_{a=1}^{N_U^i}p_a}{N_{\mathrm{MC}}^i}}{\sum_{i=1}^{n}\delta_i\frac{N_f^i}{N_{\mathrm{MC}}^i}} \tag{4-32}$$

Table 4-5 Results obtained by using Poisson binomial distribution and binomial distribution

Distribution		Case 1	Case 2	Case 3
Binomial	N_{call}	22	50	36
	$\hat{P}_f$	2.79×10^{-2}	9.05×10^{-6}	1.47×10^{-8}
	CoV	0.94	1.85	2.37
Poisson Binomial	N_{call}	15	23	28
	$\hat{P}_f$	2.83×10^{-2}	8.48×10^{-6}	1.46×10^{-8}
	CoV	9.31	5.59	7.87

Compared to Eq. (4-32), the proposed stopping criterion is clearer and is directly related to the number of dangerous points and the number of failure points. The average results by 20 independent runs of reliability analysis for three cases in this example are listed in Table 4-5. The expected upper bound of the relative error expressed by Eq. (4-32) is adopted as 5%. Although the stopping criterion derived from Poisson binomial distribution is slightly more efficient than that from the binomial distribution, the variation of the failure probability by Eq. (4-32) is much larger than that by the proposed one. For instance, the CoV by the proposed stopping criterion is as small as 0.94% for case 1, whereas that by Eq. (4-32) is 9.31%. This is because the proposed stopping criterion takes into account the worst-case scenario for failure probability estimation and employs the maximum probability of misclassification.

4.3.2 Example 2: A 61-bar truss structure

The second example investigates a 61-bar truss structure, as shown in Figure 4-4, focusing on the vertical displacement at the midpoint of the truss. The 61-bar truss is simulated by a finite element model and the performance function can be given as (Ding & Xu, 2021):

$$G\left(E,F_{1\sim13}\right)=V_{\lim}-V\left(E,F_{1\sim13}\right) \tag{4-33}$$

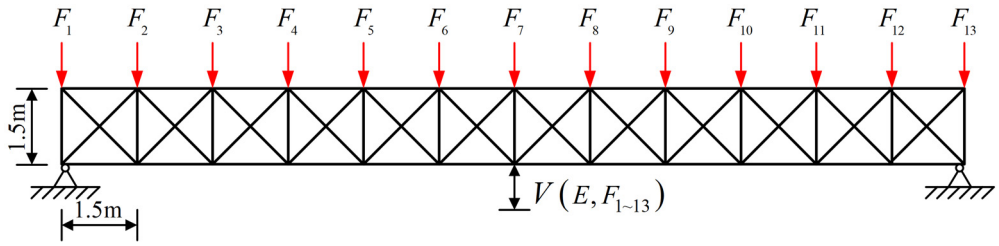

Figure 4-4 A 61-bar truss structure

where $V_{\lim}$ denotes the threshold of the displacement at the midpoint. The elastic modulus E follows the lognormal distribution with a mean of 210 GPa and a CoV of 0.10. The vertical loads F_1 to F_{13} are all lognormally distributed, and each with a mean of 15 (kN) and a CoV of 0.15 (Zhang, Dong, & Xu, 2023). In this example, two different thresholds (0.07 m and 0.09 m) corresponding to two levels of failure probability are studied and the results obtained by different methods are listed in Table 4-6. Note that AK-SS here refers to Ref. Huang et al. (2016).

First, a relatively large failure probability is of concern given $V_{\lim}=0.07$. AKMCS-U requires almost three times as many finite element analyses as AKSDMCS with the proposed η stopping criterion. AKSDMCS with the

conventional stopping criterion demands more computational effort (57) than the proposed one (37), while they achieve comparable accuracy in failure probability estimation. AK-SS also produces satisfactory results but it is not as efficient as the proposed method. Additionally, the CoV by AK-SS (3.13%) is larger than that by AKSDMCS-η (1.59%).

Table 4-6 Results obtained by different methods for the truss structure in chapter 4

Method		MCS	AK-SS	AKMCS-U	AKSDMCS-U	AKSDMCS-η
Case 1	N_{call}	2×10^{5}	48	94	57	37
	$\hat{P}_f$	2.96×10^{-3}	2.97×10^{-3}	3.04×10^{-3}	2.93×10^{-3}	2.98×10^{-3}
	$\hat{\beta}$	2.75	2.75	2.74	2.76	2.75
	CoV	4.11	3.12	3.38	0.28	1.59
Case 2	N_{call}	64000(1)	78	–(2)	87	52
	$\hat{P}_f$	2.05×10^{-7}	2.55×10^{-7}	–	2.08×10^{-7}	2.12×10^{-7}
	$\hat{\beta}$	5.06	5.02	–	5.06	5.06
	CoV	13.1	6.32	–	0.43	1.72

(1) The result is provided by subset sampling due to the crude MCS is time-consuming.
(2) The result is absent due to excessively computational effort of the AKMCS.

Considering the extremely small failure probability with a level of 10^{-7}, MCS would require 10^{9} finite element analyses and it is impossible. Thus, subset sampling is employed to provide a reference result, consuming 64000 runs of the finite element model, with the estimated failure probability being as small as 2.05×10^{-7}. Again, AKMCS is not available for the rare event estimation. AK-SS fails to produce a stable result, as the CoV of the failure probability from 20 independent runs is as large as 6.32%, which is much larger than 1.72% obtained by AKSDMCS-η. AKSDMCS-U and -η produce similar results while AKSDMCS-U requires 35 more calls to the finite element model than AKSDMCS with the proposed stopping criterion.

4.3.3 Example 3: Application to a frame-shear wall structure

To further validate the proposed method for small failure probabilities estimation of practical engineering structures, a 13-storey frame-shear wall structure, considering non-linear constitutive laws, is investigated in the last example. The height of each storey is 3 m, the wall thickness is 300 mm and the floor thickness is 100 mm. The beam section is 300×500 mm and the column section is 500×500 mm, utilizing C35 concrete and HRB400 reinforcement. The geometric configuration and reinforcement details are shown in Figure 4-5.

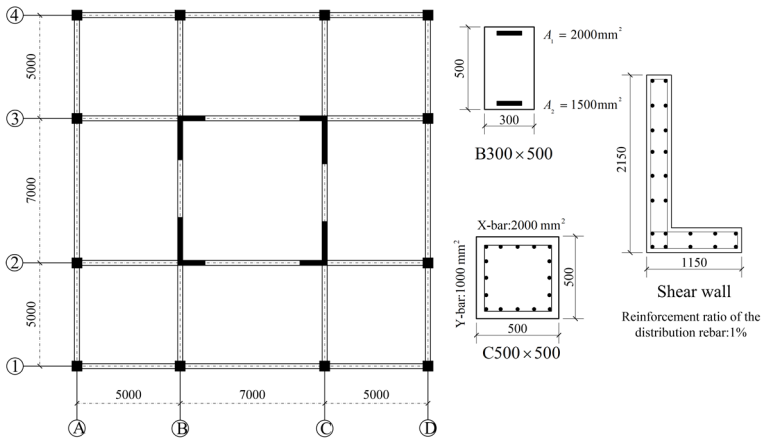

Figure 4-5 The geometric configuration and reinforcement information of a 13-storey frame-shear wall structure

The finite element model can be constructed by OpenSees, employing the constitutive laws Concrete01 and Steel01. The finite element model is depicted in Figure 4-6. Uncertainties existing in both structural parameters and external loads are of concern. The external forces F_1 to F_{13} are applied in the X direction at nodes (0, 0), (0, 5000), (0, 12000) and (0, 17000) of storeys 1 to 13, respectively. The statistical information is listed in Table 4-7.

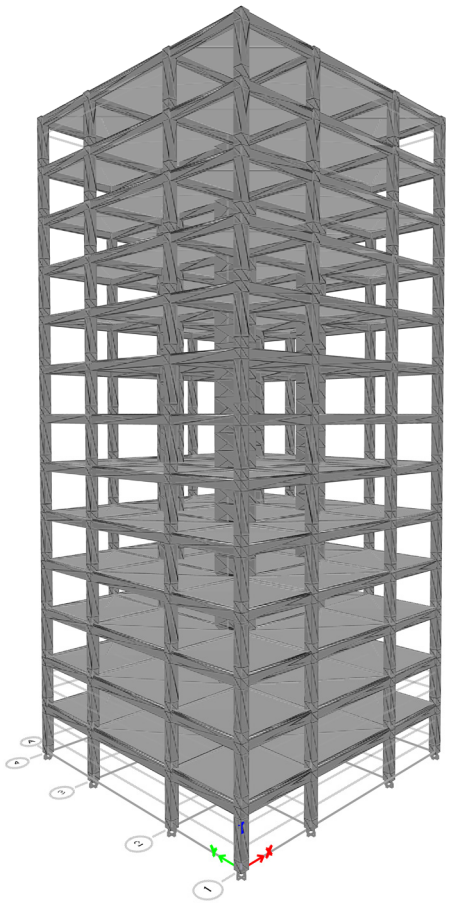

Figure 4-6 The finite element model of the frame-shear wall structure

The maximum inter-storey drift of the frame-shear wall structure is of interest and the performance function reads:

$$G(\mathbf{X}) = \Delta_{\text{lim}} - \max_{1 \le i \le 13} \Delta_i(\mathbf{X}) \tag{4-34}$$

where $\Delta_i(\mathbf{X})$ denotes the maximum drift of the i-th storey and the notation Δ_{lim} represents the threshold.

Table 4-7 Random variables for the frame-shear wall structure

Variable	Description	Distribution	Mean	CoV
f_c	Concrete compressive strength	Normal	23.4 MPa	0.10
ε_c	Concrete strain at maximum strength	Normal	0.0015	0.05
f_u	Concrete crushing strength	Normal	10 MPa	0.10
ε_u	Concrete strain at crushing strength	Normal	0.006	0.05

Table 4-7 (continued) Random variables for the frame-shear wall structure

Variable	Description	Distribution	Mean	CoV
f_y	Yield strength of rebar	Normal	400 MPa	0.10
E_0	Initial elastic modulus of rebar	Normal	200 GPa	0.10
b	Strain-hardening ratio of rebar	Normal	0.01	0.05
F_1	External force	Lognormal	5004 N	0.10
F_2	External force	Lognormal	12324 N	0.10
F_3	External force	Lognormal	20880 N	0.10
F_4	External force	Lognormal	30348 N	0.10
F_5	External force	Lognormal	40560 N	0.10
F_6	External force	Lognormal	51408 N	0.10
F_7	External force	Lognormal	62820 N	0.10
F_8	External force	Lognormal	74724 N	0.10
F_9	External force	Lognormal	87804 N	0.10
F_{10}	External force	Lognormal	99876 N	0.10
F_{11}	External force	Lognormal	113040 N	0.10
F_{12}	External force	Lognormal	126588 N	0.10
F_{13}	External force	Lognormal	140460 N	0.10

Table 4-8 Results obtained by different methods for the frame-shear wall structure

Method		MCS	SS	AKMCS-U	AKSDMCS-U	AKSDMCS-η
Δ_{lim} =30 mm	N_{call}	3×10^{6}	4600	331	399	280
	$\hat{P}_f$	1.41×10^{-4}	1.42×10^{-4}	1.28×10^{-4}	1.41×10^{-4}	1.39×10^{-4}
	$\hat{\beta}$	3.63	3.63	3.66	3.63	3.63
	CoV	4.87	23.34	3.51	3.73	3.80
Δ_{lim} = 34 mm	N_{call}	–[(1)]	6400	–[(2)]	373	289
	$\hat{P}_f$	–	3.94×10^{-6}	–	4.08×10^{-6}	4.07×10^{-6}
	$\hat{\beta}$	–	4.47	–	4.46	4.46
	CoV	–	28.01	–	1.17	1.45

[(1)]The result is absent due to excessively computational effort of the MCS.
[(2)]The result is absent due to excessively computational effort of the AKMCS.

The results obtained by different approaches are shown in Table 4-8. Given a threshold of the maximum inter-storey drift of 30 mm, the reference failure probability obtained by 3×10^{6} MCS is 1.41×10^{-4}. SS is more efficient than MCS but it still requires 4600 finite element analyses to obtain the failure probability. AKMCS-U, AKSDMCS-U and AKSDMCS-η achieve comparable accuracy, however, AKMCS-U and AKSDMCS-U incur higher computational costs than AKSDMCS

with the proposed stopping criterion η. AKSDMCS-η saves more than 100 structural model evaluations compared to U stopping criterion. Moreover, it can be found that AKSDMCS-U requires more function calls than AKMCS-U to achieve a comparable CoV of the failure probability, indicating that SDMCS generates more dangerous points than MCS. Thus, the proposed stopping criterion tailored for SDMCS is of great importance for improving the efficiency of adaptive Kriging with SDMCS.

Given a threshold of 34 mm, the failure probabilities obtained by AKSDMCS with U and η stopping criterion are 4.08×10^{-6} and 4.07×10^{-6}, respectively. Note that the target CoV in a single run is assigned as 7% for this case, as AKSDMCS with U stopping criterion struggles to converge when the target CoV is 5%. MCS is not feasible for evaluating such an extremely small failure probability since more than 10^8 times of finite element analyses would be required. SS requires 6400 calls to the finite element model to estimate the small failure probability while the CoV is excessively large (28.01%). AKMCS is unsuitable for the rare event estimation due to the impracticality of active training with numerous candidate samples. AKSDMCS-U consumes 373 finite element analyses while the proposed method only takes 289 analyses to produce comparable results. Furthermore, the CoV of results by 20 independent runs of AKSDMCS-η is as low as 1.45%, which states that the proposed method is more stable than SS.

4.4 Summary

To mitigate the computational effort required by adaptive Kriging model in rare events estimation, an error-based stopping criterion is tailored for adaptive Kriging with SDMCS. First, the relative error of the failure probability obtained by the spherical decomposition-based Monte Carlo simulation is derived. Incorporated with the Kriging model, the upper bound of this relative error is formulated, and its expected upper bound is derived by accounting for the impact of points with high probabilities of misclassification. In each sub-region generated by SDMCS, the number of samples in wrong classification follows a binomial distribution. This insight is then employed to determine the expected upper bound of the relative error of the failure probability, quantifying the effect of dangerous points on the accuracy of the failure probability estimation. Finally, a new error-based stopping criterion tailored for adaptive Kriging with SDMCS is proposed and the accuracy of failure probabilities estimation is taken into consideration. Three numerical examples are investigated to demonstrate the performance of the newly developed stopping criterion for AKSDMCS. The results validate that the proposed stopping criterion effectively halts the active training process at an appropriate stage, thereby reducing the computational burden associated with unnecessary, time-consuming function calls. It is important to note that this error-based stopping criterion is designed specifically for SDMCS and is not generalized for all sampling techniques. For other sampling approaches, the stopping criterion should be re-derived using the proposed computational process.

CHAPTER 5 RLSTM FOR METAMODELING OF STOCHASTIC DYNAMIC SYSTEMS AND ITS APPLICATION TO RELIABILITY ANALYSIS

5.1 Introduction

A novel method, termed rLSTM-AE, is developed for low-dimensional latent space identification in stochastic dynamic systems with more than 1000 input random variables and active learning-based dynamic reliability analysis. First, a novel long short-term memory network (rLSTM) is developed to consider both time-variant stochastic excitation and time-invariant random variables. This network adopts the time-series excitation as a pertinent input feature, facilitating the metamodeling of high-dimensional stochastic dynamic systems. To address the issue of insufficient accuracy in deep neural networks for reliability analysis due to limited observations, an autoencoder (AE) is incorporated with the rLSTM, forming the rLSTM-AE. This combination is utilized to decompose the approximate extreme value space identified by the rLSTM into a low-dimensional latent space. The dimension of the latent space is adaptively determined by Kriging reconstruction error, which enables Kriging achieve the similar accuracy as rLSTM in extreme responses prediction. The proposed rLSTM-AE extracts low-dimensional features from the perspective of the output space decomposition and considers the time-dependent property of dynamic systems. Finally, the detected latent variables can be combined with the adaptive Kriging for high-dimensional dynamic reliability analysis. A single-degree-of-freedom system

and a reinforced concrete frame structure subjected to the stochastic excitation are investigated to validate the performance of the proposed method.

5.2 rLSTM for modeling of stochastic dynamic systems

5.2.1 A typical stochastic dynamic system: structures subjected to the stochastic seismic excitation

The governing equation for a multi-degree-of-freedom system subjected to the stochastic seismic excitation can be given by:

$$\mathbf{M}\left(\mathbf{X}_S\right)\ddot{\mathbf{u}}+\mathbf{C}\left(\mathbf{X}_S\right)\dot{\mathbf{u}}+\mathbf{K}\left(\mathbf{X}_S\right)\mathbf{u}+\mathbf{F}=-\mathbf{M}\left(\mathbf{X}_S\right)\mathbf{I}a\left(\mathbf{X}_E,t\right) \tag{5-1}$$

where **M**, **C** and **K** are the mass, damping and stiffness matrices, respectively; $\ddot{\mathbf{u}}$, $\dot{\mathbf{u}}$ and $\mathbf{u}$ are acceleration, velocity and displacement vectors, respectively; **F** denotes the restoring force vector; **I** is the force distribution factor; $a\left(\mathbf{X}_E,t\right)$ represents the non-stationary stochastic seismic ground motions. $\mathbf{X}_E=\left(X_{E1},X_{E2},...,X_{Ed_1}\right)$ includes d_1 random variables accounting for uncertainties in seismic ground motions. $\mathbf{X}_S=\left(X_{S1},X_{S2},...,X_{Sd_2}\right)$ is a random vector containing d_2 random variables related to structural parameters.

Various approaches have been developed for simulating the stochastic seismic excitation (Liu et al., 2016; Phoon et al., 2005; Shinozuka & Deodatis, 1991). Herein, the spectral representation method is adopted (Liu et al., 2016):

$$a\left(t\right)=\sqrt{2}\sum_{k=0}^{d_1-1}\sqrt{2S_a\left(w_k,t\right)\Delta w}\left[w_k t+\phi_k\right] \tag{5-2}$$

where $S_a(w,t)$ is the double-sided evolutionary power spectral density function of the frequency *w* and time *t*:

$$S_a(w,t) = |f(w,t)|^2 S(w) \tag{5-3}$$

in which $f(w,t)$ is the amplitude envelope function:

$$f(w,t) = \left[\frac{t}{5}\exp\left(1-\frac{t}{5}\right)\right]^2 \tag{5-4}$$

and $S(w)$ is the one-sided power spectral density function defined by Clough-Penzien spectrum (Dang & Xu, 2020):

$$S(w) = \frac{w_g^4 + 4\zeta_g^2 w_g^2 w^2}{\left(w^2 - w_g^2\right)^2 + 4\zeta_g^2 w_g^2 w^2} \cdot \frac{w^4}{\left(w^2 - w_f^2\right)^2 + 4\zeta_f^2 w_f^2 w^2} S_0 \tag{5-5}$$

in which S_0 is the spectral intensity of seismic acceleration processes; w_g and ζ_g are the dominant frequency and damping ratio of the site soil, respectively; w_f and ζ_f are parameters of the second filter mainly hindering the low-frequency component of seismic acceleration. The discrete frequency w_i gives:

$$w_k = k\Delta w,\ k = 0,1,...,d_1 - 1 \tag{5-6}$$

where Δw is the frequency interval. These parameters are specified as: $w_g = 5\pi$ rad/s, $w_f = 0.1 w_g$ rad/s, $\zeta_g = \zeta_f = 0.60$, $S_0 = 48.9332$ cm^2/s^3, $\Delta w = 0.1$ rad/s, $d_1 = 1001$ and *t* is a time sequence ranging from 0 to 20s with an interval of 0.02s. Thus, the

phase angles ϕ_k s are 1001 independent uniformly distributed random variables over $[0, 2\pi]$, leading to a high-dimensional stochastic dynamic system. Constructing metamodel and conducting reliability analysis for the high-dimensional stochastic dynamic system are challenging due to the "curse-of-dimensionality" and complex dynamics.

5.2.2 Long short-term memory considering both time-variant and time-invariant features: rLSTM

The primary reason for the high-dimensional problem in stochastic dynamic systems investigated here is the inclusion of a large number of random variables for simulating the stochastic excitation. Treating these random variables as input features for the system makes metamodeling and reliability analysis challenging. However, these random variables have little effect on the response of interest, as the dominant feature is the excitation generated by them. Therefore, by directly employing the time-series excitation as the input feature when building the metamodel, the high-dimensional problem can be circumvented.

Long short-term memory network is a powerful deep learning tool to deal with the sequence-to-sequence data and has demonstrated its advantages in capturing time-series input-output relationships (R. Zhang et al., 2019; R. Zhang et al., 2020a). A common LSTM unit consists of a cell *c*, a forget gate *f*, an input gate *i* and an output gate *o*, as shown in Figure 5-1 (a). The cell memorizes the state at the previous time step to capture the long-term dependency and three gates control the information into and out of the cell. The forget gate decides what information can be discarded, the input gate determines what new information to store in the current state and the output

gate decides what information to output according to the previous and current states. At time step t, the equations for the forward process of a LSTM cell can be given by:

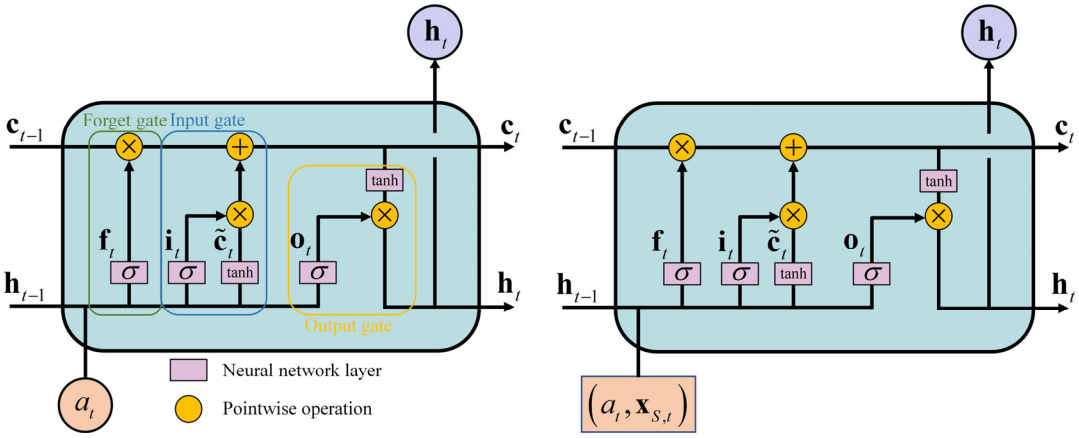

(a) LSTM cell (b) rLSTM cell

Figure 5-1 LSTM and rLSTM cells

$$
\begin{aligned}
\mathbf{f}_t &= \sigma\left(\mathbf{W}_{af} a_t + \mathbf{W}_{hf}\mathbf{h}_{t-1} + \mathbf{b}_f\right) \\
\mathbf{i}_t &= \sigma\left(\mathbf{W}_{ai} a_t + \mathbf{W}_{hi}\mathbf{h}_{t-1} + \mathbf{b}_i\right) \\
\tilde{\mathbf{c}}_t &= \tanh\left(\mathbf{W}_{ac} a_t + \mathbf{W}_{hc}\mathbf{h}_{t-1} + \mathbf{b}_c\right) \\
\mathbf{o}_t &= \sigma\left(\mathbf{W}_{ao} a_t + \mathbf{W}_{ho}\mathbf{h}_{t-1} + \mathbf{b}_o\right) \\
\mathbf{c}_t &= \mathbf{f}_t \odot \mathbf{c}_{t-1} + \mathbf{i}_t \odot \tilde{\mathbf{c}}_t \\
\mathbf{h}_t &= \mathbf{o}_t \odot \tanh\left(\mathbf{c}_t\right)
\end{aligned}
\tag{5-7}
$$

where $\mathbf{W}$ and $\mathbf{b}$ are weight matrices and bias vectors, respectively, $\mathbf{h}$ represents the hidden state and a_t denotes the input feature (seismic ground motions) at time step t. The notation $\odot$ represents Hadamard product (element-wise product). σ and "tanh" represent the sigmoid and hyperbolic tangent activation function, respectively.

The LSTM is typically used to handle sequence-to-sequence data. However, in addition to the time-series ground motions, the input features also include time-invariant random structural parameters. To address this, we first expand the time-

invariant random structural parameters into a time-series sequence. At each time step *t*, the random structural parameters are the same:

$$\mathbf{x}_S(t) = \left(\mathbf{x}_{S,0}, ..., \mathbf{x}_{S,t}, ..., \mathbf{x}_{S,T}\right) \tag{5-8}$$

where $\mathbf{x}_{S,0} = \mathbf{x}_{S,t} = \mathbf{x}_{S,T}$. The sequence of random structural parameters is then concatenated with the time-series input feature, resulting in a combined input $\left(a_t, \mathbf{x}_{S,t}\right)$. To clarify, we denote the LSTM that incorporates both time-variant excitation and time-invariant random parameters as rLSTM, where the letter "r" represents the time-invariant random variables. The diagram is shown in Figure 5-1 (b).

The concatenation of the random structural parameters sequence with time-series ground motions results in input features with vastly different scales. Therefore, dataset normalization is necessary to ensure a stable and efficient training process. Consider a dataset $\mathcal{D} = \left\{a(t), \mathbf{x}_S(t), y(t)\right\}$, where $y(t)$ is the output time history responses of interest. the following normalization process is applied to scale both the input features and output responses:

$$\begin{aligned} \tilde{a}(t) &= a(t) / a_{\mathcal{D},\max} \\ \tilde{y}(t) &= y(t) / y_{\mathcal{D},\max} \\ \tilde{\mathbf{x}}_S(t) &= \left(\mathbf{x}_S(t) - \boldsymbol{\mu}_S\right) / \boldsymbol{\sigma}_S \end{aligned} \tag{5-9}$$

where $a_{\mathcal{D},\max}$ and $y_{\mathcal{D},\max}$ denotes the maximum absolute ground motion and response in Dataset $\mathcal{D}$, respectively. $\boldsymbol{\mu}_S$ and $\boldsymbol{\sigma}_S$ are mean and standard deviation vector of

random structural parameters $\mathbf{X}_S$, respectively. After preprocessing, the dataset is then suitable for training the rLSTM.

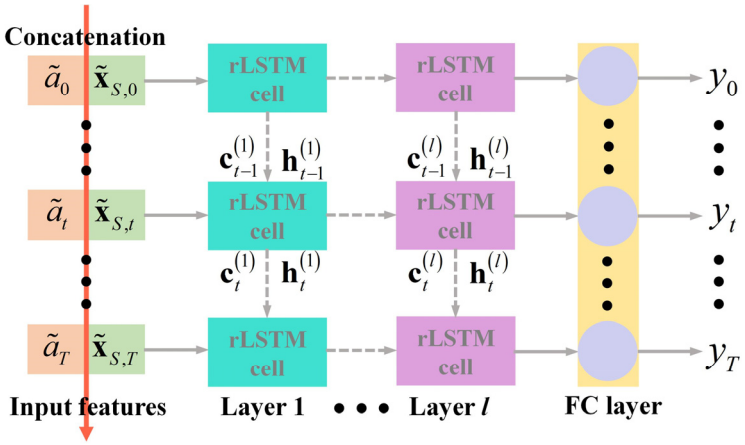

Figure 5-2 rLSTM network

The rLSTM network is depicted in Figure 5-2, where the notation "FC" refers to the fully connected neural network layers. The input feature is a concatenation of time-variant and time-invariant features. The network comprises l rLSTM layers and one fully connected layer. By utilizing the excitation as the pertinent input feature, rLSTM network can bypass the high-dimensional random variables for simulating the seismic excitation (phase angles ϕ_k s). As a result, the rLSTM network is capable of constructing a metamodel for high-dimensional stochastic dynamic systems. Moreover, regardless of the approach used to simulate the stochastic excitation (e.g., spectral representation method and random function-based spectral representation (Liu et al., 2016)), the proposed rLSTM can effectively construct the metamodel, as the ground motions serve as the relevant input features.

5.3 Low-dimensional latent space identification for stochastic dynamic systems by rLSTM-AE

Unlike conventional surrogate models such as Kriging, polynomial chaos expansion, and others, the proposed rLSTM network is capable of constructing surrogates for high-dimensional stochastic dynamic systems. However, performing reliability analysis using metamodels remains a challenging task. A high-accuracy metamodel across the entire space is necessary to accurately assess failure probability. Deep learning tools, including rLSTM, may require a substantial number of observations to achieve this level of accuracy across the whole domain. This challenge is also encountered by Kriging model and polynomial chaos expansion. To address this issue, the adaptive Kriging model is commonly used to transform the regression problem across the entire space into a classification problem that focuses on the limit state surface. Unfortunately, this active learning-based reliability analysis is limited to low-dimensional problems due to the constraints of Kriging model. Therefore, extracting low-dimensional features from high-dimensional stochastic dynamic systems is crucial. In this section, we present a paradigm for detecting low-dimensional latent spaces, using the rLSTM with an autoencoder, termed rLSTM-AE, and demonstrate its application to active learning-based reliability analysis for high-dimensional stochastic dynamic systems.

5.3.1 Active learning strategy for reliability analysis

Accurate estimation often demands a large number of samples, which can be impractical for complex systems. To address this challenge, surrogate models are commonly used to replace the time-consuming performance functions. Despite this,

constructing an accurate surrogate model across the entire space remains difficult. Fortunately, the development of active learning strategies allows the metamodel to concentrate on accurately representing the limit state surface.

AKMCS focuses on accurately constructing the limit state surface using the Kriging model. The training dataset is adaptively expanded by adding samples near the limit state surface through a learning function. As a result, AKMCS emphasizes improving the accuracy of the metamodel specifically for the limit state surface, rather than for the entire space. For points far from the limit state surface, it is not necessary for the metamodel to predict exact values accurately, as long as their signs are correctly identified. The active learning strategy utilizes the stochastic properties of the Gaussian process: Kriging not only provides the mean prediction at a point $\mathbf{x}$ but also quantifies the uncertainty associated with this prediction. The posterior distribution of the prediction at point $\mathbf{x}$, i.e., $\hat{G}(\mathbf{x})$, follows a normal distribution:

$$\hat{G}(\mathbf{x}) \sim \mathcal{N}\left(\mu_K(\mathbf{x}), \sigma_K^2(\mathbf{x})\right) \tag{5-10}$$

where $\mu_K(\mathbf{x})$ and $\sigma_K^2(\mathbf{x})$ are mean prediction and variance by Kriging, respectively. The notation $\mathcal{N}$ denotes the normal distribution. This property has promoted the proposal of various learning functions. The learning function aims to select a best next point that can significantly improve the accuracy of the current Kriging model. U learning function is widely used due to its simplicity:

$$U(\mathbf{x}) = \frac{\left|\mu_K(\mathbf{x})\right|}{\sigma_K(\mathbf{x})} \tag{5-11}$$

The value of U function reflects the probability of wrong classification in predicting the sign of $\mathbf{x}$, i.e., $\Phi\left(-U\left(\mathbf{x}\right)\right)$. A minimum value of U refers to the maximum risk of misclassification in predicting the sign of $\mathbf{x}$. Consequently, such points should be selected and evaluated using the true performance function. The training dataset for Kriging can then be enriched by incorporating these points along with their true values. Define a performance function $W = G(\mathbf{X})$ in this chapter, the procedure of the adaptive Kriging can be summarized as the follows:

Step 1: Generate a MC candidate pool Ω with N_{MC} samples.

Step 2: Randomly select N_0 samples and evaluate them on the real performance function $G(\mathbf{X})$ as an initial training dataset $\left\{\mathbf{x}_{\mathrm{train}}, w_{\mathrm{train}}\right\}$, $w_{\mathrm{train}} = G\left(\mathbf{x}_{\mathrm{train}}\right)$.

Step 3: Train Kriging with the current training dataset.

Step 4: Identify the best next point via the learning function and enrich the training dataset with $\left\{\mathbf{x}^*, w^*\right\}$:

$$\mathbf{x}^* = \arg\min_{\mathbf{x}\in\Omega} U\left(\mathbf{x}\right), w^* = G\left(\mathbf{x}^*\right) \tag{5-12}$$

Step 5: Stop the active learning process when the following condition is met, else go back to step 3:

$$\min\left(U\left(\mathbf{x}\right)\right) \geq 2, \forall \mathbf{x} \in \Omega \tag{5-13}$$

This convergence condition represents that the maximum probability of misclassification on signs of all candidate samples is smaller than $\Phi(-2) = 2.3\%$, which can ensure the accuracy of the surrogate for the limit state surface.

Step 6: The updated Kriging is utilized to predict values of samples in Ω and then the failure probability can be estimated by Eq. (2-4).

This active learning strategy significantly improves the accuracy and efficiency of Kriging for reliability analysis. Commonly, Kriging is not available for mapping sequence-to-sequence data. Here, the extreme value of time history responses is of concern:

$$Y(t) = H\left(a(t), \mathbf{X}_S\right), Y_{\text{ev}} = \max\left(\text{abs}\left(Y(t)\right)\right) \tag{5-14}$$

where $Y(t)$ represents the time history responses of interest, H denotes a high-dimensional stochastic system and Y_{ev} is the extreme response. Given a threshold b, the performance function gives:

$$W = b - Y_{\text{ev}} = G(\mathbf{X}) \tag{5-15}$$

However, Kriging is still not capable of constructing metamodel for high-dimensional systems even if the extreme responses are of interest. This limitation is especially pronounced for the stochastic dynamic systems investigated in this chapter, which involve more than 1000 random variables. Consequently, the adaptive Kriging is also not accessible to reliability analysis of high-dimensional stochastic dynamic systems.

5.3.2 rLSTM with autoencoder for the low-dimensional latent space identification

To enable adaptive Kriging for high-dimensional problems, a fundamental idea is to use the dimension-reduction techniques. Additionally, the number of latent variables resulting from the dimension-reduction should be within several to dozens to ensure the availability and efficiency of Kriging. However, this is extremely challenging for stochastic dynamic systems with more than 1000 features. To deal with thousands of input features, neural network-based feature extraction techniques offer a promising solution. An autoencoder is a type of neural network used for feature extraction from unlabeled data and serves as an unsupervised learning tool (Hinton & Salakhutdinov, 2006). It includes an encoding function and a decoding function. The diagram of the autoencoder is depicted in Figure 5-3.

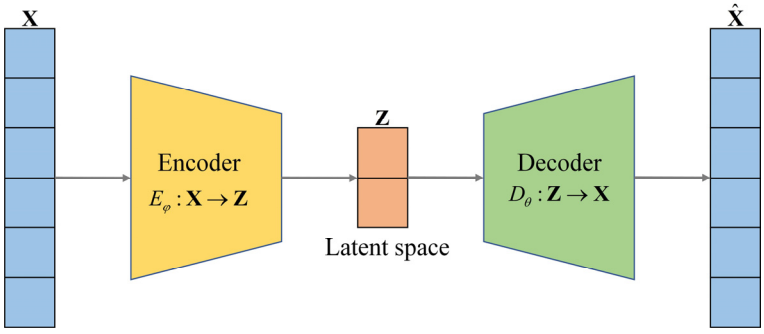

Figure 5-3 The diagram of autoencoder

The encoding function aims to find efficient codes or latent variables of unlabeled data, i.e., $E_{\boldsymbol{\varphi}} : \mathbf{X} \to \mathbf{Z}$ characterized by $\boldsymbol{\varphi}$. The decoding function recreates the input data via the latent variables, i.e., $D_{\boldsymbol{\theta}} : \mathbf{Z} \to \mathbf{X}$ characterized by $\boldsymbol{\theta}$. In theory, this kind of unsupervised learning-based neural network is available for low-dimensional latent variables detection from high-dimensional inputs. However,

regarding the stochastic dynamic systems, we cannot use the input feature $\mathbf{X}=\left(\mathbf{X}_E,\mathbf{X}_S\right)$ directly for dimension-reduction due to the following three reasons:

Reason 1: random phases in vector $\mathbf{X}_E$ for generating the stochastic excitation are not pertinent features for a stochastic system and have little effect on the response of interest.

Reason 2: random phases in vector $\mathbf{X}_E$ contribute equally to the system since they all follow the same uniform distribution. Therefore, it is challenging to detect a few latent variables that can represent such a high-dimensional space with over 1000 similar features.

Reason 3: even though the input features $\mathbf{X}=\left(\mathbf{X}_E,\mathbf{X}_S\right)$ could be directly represented by the low-dimensional latent variables **Z**, the time dependent property of the sequence-to-sequence data (time-dependent complex dynamics) would be ignored using detected latent variables to construct a metamodel.

To tackle these issues, we propose a two-step low-dimensional latent variable detection strategy, termed rLSTM-AE, for feature extraction in high-dimensional stochastic dynamic systems. Typically, the extreme value of the time-series response, i.e., $Y_{\text{ev}}=\max\left\{\text{abs}\left(Y\left(t\right)\right)\right\}$, is of concern. The diagram of the proposed rLSTM-AE approach is depicted in Figure 5-4.

As mentioned earlier, the proposed rLSTM network can handle both stochastic excitation and random structural parameters simultaneously, effectively avoiding the high-dimensional issue induced by random phases. Therefore, the first step of the

proposed rLSTM-AE is to identify an approximate extreme value space using rLSTM. The dimension flow of this step is illustrated as follows:

$$\mathbf{X} \in \mathbb{R}^{d_1+d_2} \xrightarrow{\text{rLSTM}} Y_{\text{ev}}^{\text{rLSTM}} \in \mathbb{R}^1 \tag{5-16}$$

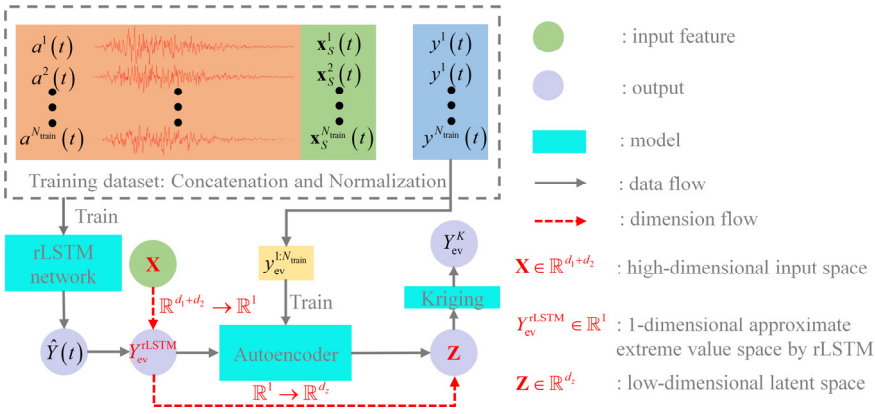

Figure 5-4 rLSTM-AE network

where $Y_{\text{ev}}^{\text{rLSTM}} = \max\left\{\text{abs}\left(\hat{Y}(t)\right)\right\}$ and $\hat{Y}(t)$ is the time-series responses predicted by rLSTM. In this step, rLSTM is used to build a metamodel for stochastic systems and construct an approximate extreme value space, i.e., $Y_{\text{ev}}^{\text{rLSTM}}$. It is important to note that the accuracy of this approximate extreme value space is not sufficient for reliability analysis due to the limited observations available for training the rLSTM. High accuracy is not required at this stage since the purpose is to use this approximate one-dimensional space to identify a low-dimensional latent space via an autoencoder. Ultimately, adaptive Kriging will refine the estimated failure probability using the detected latent variables $\mathbf{Z}$. The loss function for training rLSTM can be defined by:

$$L(\boldsymbol{\lambda}) = \frac{1}{N}\sum_{i=1}^{N}\left\|y^i(t) - \hat{y}^i(\boldsymbol{\lambda}, t)\right\|_2^2 \tag{5-17}$$

where $\boldsymbol{\lambda}$ denotes trainable weights and biases of the rLSTM, which can be determined by $\hat{\boldsymbol{\lambda}} = \arg\min_{\boldsymbol{\lambda}} L(\boldsymbol{\lambda})$. N is the size of data and $\hat{y}(\boldsymbol{\lambda}, t)$ is the estimated response. Note that the normalized data by Eq. (5-9) is utilized when training deep neural networks.

The second step in the proposed rLSTM-AE approach is to detect a low-dimensional latent space $\mathbf{Z}$ to decompose the one-dimensional extreme value space using an autoencoder. The autoencoder in the rLSTM-AE network differs from its conventional use. Typically, an autoencoder is an unsupervised learning method, and its loss function can be defined as follows:

$$L(\boldsymbol{\varphi}, \boldsymbol{\theta}) = \frac{1}{N} \sum_{i=1}^{N} \left\| \mathbf{x}^i - D_{\boldsymbol{\theta}} \left(E_{\boldsymbol{\varphi}} \left(\mathbf{x}^i \right) \right) \right\|_2^2 \tag{5-18}$$

where $\{\boldsymbol{\varphi}, \boldsymbol{\theta}\}$ denotes the trainable weights and biases of the autoencoder, which can be determined by $\{\boldsymbol{\varphi}, \boldsymbol{\theta}\} = \arg\min_{\boldsymbol{\varphi}, \boldsymbol{\theta}} L(\boldsymbol{\varphi}, \boldsymbol{\theta})$. While for the autoencoder in rLSTM-AE network, the loss function gives:

$$L(\boldsymbol{\varphi}, \boldsymbol{\theta}) = \frac{1}{N} \sum_{i=1}^{N} \left\| y_{\text{ev}}^i - D_{\boldsymbol{\theta}} \left(E_{\boldsymbol{\varphi}} \left(y_{\text{ev}}^i \right) \right) \right\|_2^2 \tag{5-19}$$

The encoding and decoding functions can be defined by $E_{\boldsymbol{\varphi}} : Y_{\text{ev}} \to \mathbf{Z}$ and $D_{\boldsymbol{\theta}} : \mathbf{Z} \to Y_{\text{ev}}$, respectively. Obviously, autoencoder here is adopted as a supervised learning tool. When training the autoencoder, the actual extreme responses are used since they are available in the training dataset. However, for unobserved data, the real extreme responses are not available. Therefore, the approximate extreme responses

generated by rLSTM, i.e., $Y_{\text{ev}}^{\text{rLSTM}}$, are employed to detect the latent space $\mathbf{Z}$ for unobserved data. The dimension flow in this step can be expressed by:

$$Y_{\text{ev}}^{\text{rLSTM}} \in \mathbb{R}^1 \xrightarrow{\text{Autoencoder}} \mathbf{Z} \in \mathbb{R}^{d_z} \tag{5-20}$$

where d_z is the dimension of the latent variable $\mathbf{Z}$ and $d_z \geq 2$. The autoencoder here is to represent a 1-dimensional space by a d_z-dimensional latent space, which constitutes a dimension-expansion step.

A crucial step is to determine an appropriate dimension for the potential latent space. The latent variable is employed to construct a Kriging model so the dimension of $\mathbf{Z}$ is restricted within the interval [2, 20] to ensure the feasibility and efficiency of the active learning-based Kriging. The fundamental goal in determining the dimension d_z is to ensure the accuracy of the reconstructed Kriging model. Hence, in the proposed paradigm, the dimension of the latent variables d_z is adaptively determined by minimizing the following Kriging construction error:

$$L^K\left(d_z\right) = \frac{1}{N}\sum_{i=1}^{N}\left\| y_{\text{ev}}^i - K\left(\mathbf{z}^i\right)\right\|_2^2, \mathbf{z} \in \mathbb{R}^{N\times d_z} \tag{5-21}$$

where $\mathbf{z}^i$ is the latent space corresponding to the observed data y_{ev}^i, i.e., $\mathbf{z}^i = E_{\boldsymbol{\varphi}}\left(y_{\text{ev}}^i\right)$. The notation $K(\cdot)$ denotes a Kriging model. Then, the optimal dimension can be selected as:

$$d_z = \underset{2\leq d_z \leq 20}{\arg\min}\, L^K\left(d_z\right) \tag{5-22}$$

Therefore, Eq. (5-21) can assist in selecting the optimal latent space, enabling Kriging to reconstruct the extreme value space using the latent variable **Z**.

There are three main steps for the proposed rLSTM-AE approach:

Step 1: The trained rLSTM can provide an approximate one-dimensional extreme value space for unobserved data:

$$Y_{\mathrm{ev}}^{\mathrm{rLSTM}} = \max\left(\mathrm{abs}\left(\hat{Y}\left(t\right)\right)\right), \hat{Y}\left(t\right) = \mathrm{rLSTM}\left(\left(a\left(t\right), \mathbf{X}_S\left(t\right)\right)\right) \tag{5-23}$$

Step 2: The one-dimensional approximate extreme value space can be decomposed by a trained autoencoder into the low-dimensional latent variables **Z**:

$$\mathbf{Z} = E_{\varphi}\left(Y_{\mathrm{ev}}^{\mathrm{rLSTM}}\right) \tag{5-24}$$

Step 3: The detected latent variables can be employed to construct a Kriging model, which can be used for the active learning-based reliability analysis.

$$Y_{\mathrm{ev}}^{K} = K\left(\mathbf{Z}\right) \tag{5-25}$$

rLSTM-AE enables Kriging to predict extreme responses with an accuracy comparable to that of rLSTM. This will be demonstrated in the following illustrative examples. Although this accuracy may not meet the requirements for reliability analysis, Kriging can be combined with an active learning strategy to enhance the accuracy of failure probability estimation, which rLSTM alone cannot achieve. The proposed rLSTM-AE offers three advantages based on the previously discussed reasons 1 to 3 regarding the limitations of using autoencoders directly:

Advantage 1: instead of the original high-dimensional input space **X**, the pertinent feature, i.e., stochastic excitation $a(t)$, is concatenated with the sequential random structural parameters $\mathbf{X}_S(t)$ for latent variables detection with the aid of the rLSTM.

Advantage 2: it is easy for the autoencoder to represent a one-dimensional space by several to dozens of latent variables.

Advantage 3: the time-dependent property in the sequence-to-sequence data (time-dependent complex dynamics) is accounted for by the rLSTM network during the dimension reduction process.

Moreover, the proposed rLSTM-AE is not restricted by the way of generating stochastic excitation, as the excitation is directly employed as the input feature. The observed dataset $\mathcal{D}$ generated by the Latin hypercube sampling is divided into two parts to obtain the best rLSTM-AE model. Training set with N_{train} samples aims to fit the parameters of the network. Validation set with N_{valid} samples here is to select a best model during the learning process. Test set with N_{test} unobserved data generated by MCS is to assess the performance of the rLSTM-AE. Denote the dimension of input features as I_{dim}, the dimension of the output feature as O_{dim} and the size of hidden state as h_s. The detailed pseudo code for rLSTM-AE is indicated in algorithm 3.

5.3.3 rLSTM-AE for the active learning-based reliability analysis: rLSTM-AE-AK

Once the latent variables are identified by the proposed rLSTM-AE, they can be employed to construct a Kriging model. The active learning strategy is available for reliability analysis of high-dimensional stochastic dynamic systems. The core steps for the active learning approach expressed by Eqs. (5-12) and (5-13) can be reformulated as:

$$\mathbf{z}^* = \min_{\mathbf{z}\in\Omega_{\mathbf{Z}}} U\left(\mathbf{z}\right) \tag{5-26}$$

and

$$\min\left(U\left(\mathbf{z}\right)\right) \geq 2, \forall \mathbf{z} \in \Omega_{\mathbf{Z}} \tag{5-27}$$

where $\Omega_{\mathbf{Z}} \subseteq \mathbb{R}^{d_z}$ is the latent candidate pool detected by rLSTM-AE from the original candidate pool $\Omega \subseteq \mathbb{R}^{d_1+d_2}$. Denote Kriging combined with the rLSTM-AE and the active learning strategy as rLSTM-AE-AK. The pseudo code of rLSTM-AE-AK is indicated in algorithm 4.

The contributions of the proposed paradigm are listed as the follows:

1. The rLSTM network utilizes stochastic excitation as a relevant input feature, bypassing the need to handle high-dimensional random phases for generating excitation. This ensures that the rLSTM is applicable regardless of the method used to generate the stochastic process.

2. The rLSTM simultaneously accounts for both time-variant stochastic excitation and time-invariant random structural parameters, enabling the direct construction of metamodels for high-dimensional stochastic dynamic systems.

3. To address the insufficient accuracy of the rLSTM network (due to limited observations) for dynamic reliability analysis, the autoencoder is utilized to decompose the approximate one-dimensional extreme response with the aid of rLSTM, which brings insights for latent variables extraction from the perspective of output space decomposition.

4. The rLSTM-AE network for low-dimensional latent space detection considers the complex time-dependent dynamics of stochastic systems by the rLSTM while conventional dimension-reduction techniques ignore this issue.

5. The proposed method makes the active learning-based reliability analysis method available for the high-dimensional dynamic reliability analysis.

Table 5-1 rLSTM-AE for the low-dimensional latent space detection

Algorithm 3: rLSTM-AE for the low-dimensional latent space detection

Input: Random structural parameters $\mathbf{x}_S$, the stochastic excitation $a(t)$ and observed responses $y(t)$.

Output: rLSTM-AE model and latent variable **Z**.

..1. **Data normalization and concatenation:**

..2. $\left\{\left(\tilde{a}(t),\tilde{\mathbf{x}}_S(t)\right),\tilde{y}(t)\right\} \xleftarrow{\text{Eqs.(5.8) and (5.9)}} \left\{a(t),\mathbf{x}_S,y(t)\right\}$.

..3. $\left\{\tilde{\mathbf{x}}_{\text{train}}\right\} \leftarrow \left\{\left(\tilde{a}^i(t),\tilde{\mathbf{x}}_S^i(t)\right)\right\},\left\{\tilde{y}_{\text{train}}\right\} \leftarrow \left\{\tilde{y}^i(t)\right\}, i=1,2,...,N_{\text{train}}$.

..4. $\left\{\tilde{\mathbf{x}}_{\text{valid}}\right\} \leftarrow \left\{\left(\tilde{a}^i(t),\tilde{\mathbf{x}}_S^i(t)\right)\right\},\left\{\tilde{y}_{\text{valid}}\right\} \leftarrow \left\{\tilde{y}^i(t)\right\}, i=N_{\text{train}}+1,N_{\text{train}}+2,...,N_{\text{train}}+N_{\text{valid}}$.

..5. **rLSTM training:**

..6. Specify rLSTM structure: $I_{\text{dim}}=d_2+1$, $O_{\text{dim}}=1$, $l=2$, $h_s=50$ and dropout value 0.5.

..7. **for** *m* =1:epoch (epoch=500) **do**

..8. **for** *n*=1:batch (samples in each batch $N_{\text{batch}}=100$) **do**

..9. $\left\{\tilde{\mathbf{x}}_{\text{batch}}\right\}_n \subseteq \left\{\tilde{\mathbf{x}}_{\text{train}}\right\},\left\{\tilde{y}_{\text{batch}}\right\}_n \subseteq \left\{\tilde{y}_{\text{train}}\right\};\left\{\tilde{\mathbf{x}}_{\text{batch}}\right\}_i \cap \left\{\tilde{\mathbf{x}}_{\text{batch}}\right\}_j = \varnothing, i \neq j$.

10. $\left\{\hat{y}_{\text{batch}}\right\}_n = \text{rLSTM}\left(\left\{\tilde{\mathbf{x}}_{\text{batch}}\right\}_n\right)$.

Table 5-1 (continued) rLSTM-AE for the low-dimensional latent space detection

Algorithm 3: rLSTM-AE for the low-dimensional latent space detection

11. $L_{\text{train}}\left(\boldsymbol{\lambda}\right)=\dfrac{1}{N_{\text{batch}}}\left\|\left\{\tilde{y}_{\text{batch}}\right\}_n-\left\{\hat{y}_{\text{batch}}\right\}_n\right\|_2^2$.

12. Backward $L_{\text{train}}\left(\boldsymbol{\lambda}\right)$ and optimize $\boldsymbol{\lambda}$ with the optimizer "Adam" with a learning rate 0.01.

13. **end for**

14. $\left\{\hat{y}_{\text{valid}}\right\}=\text{rLSTM}\left(\left\{\tilde{\mathbf{x}}_{\text{valid}}\right\}\right)$.

15. $L_{\text{valid}}\left(m\right)=\dfrac{1}{N_{\text{valid}}}\left\|\left\{\tilde{y}_{\text{valid}}\right\}-\left\{\hat{y}_{\text{valid}}\right\}\right\|_2^2$.

16. **end for**

17. Find the minimum validation loss L_{valid} and save the best rLSTM model.

18. **Autoencoder training:**

19. $\left\{\tilde{y}_{\text{ev,train}}\right\}=\left\{\tilde{y}_{\text{ev}}^i=\max\left(\text{abs}\left(\tilde{y}^i\left(t\right)\right)\right)\right\},i=1,2,...,N_{\text{train}}$.

20. $\left\{\tilde{y}_{\text{ev,valid}}\right\}=\left\{\tilde{y}_{\text{ev}}^i=\max\left(\text{abs}\left(\tilde{y}^i\left(t\right)\right)\right)\right\},i=N_{\text{train}}+1,N_{\text{train}}+2,...,N_{\text{train}}+N_{\text{valid}}$.

21. **for** d_z=2:20 **do**

22. Specify the autoencoder structure: $I_{\text{dim}}=1$, $O_{\text{dim}}=1$ and number of nodes in each layer, i.e., $(4d_z,2d_z,d_z)$ for $E_{\boldsymbol{\varphi}}$ and $(2d_z,4d_z,O_{\text{dim}})$ for $D_{\boldsymbol{\theta}}$.

23. **for** q =1:epoch (epoch=500) **do**

24. **for** k =1:batch ($N_{\text{batch}}=100$) **do**

25. $\left\{\tilde{y}_{\text{ev,batch}}\right\}_k\subseteq\left\{\tilde{y}_{\text{ev,train}}\right\},\left\{\tilde{y}_{\text{ev,batch}}\right\}_i\cap\left\{\tilde{y}_{\text{ev,batch}}\right\}_j=\varnothing,i\neq j$.

26. $\left\{\hat{y}_{\text{ev,batch}}\right\}_k=D_{\boldsymbol{\theta}}\left(E_{\boldsymbol{\varphi}}\left(\left\{\tilde{y}_{\text{ev,batch}}\right\}_k\right)\right)$.

27. $L_{\text{train}}^{\text{AE}}\left(\boldsymbol{\varphi},\boldsymbol{\theta}\right)=\dfrac{1}{N_{\text{batch}}}\left\|\left\{\tilde{y}_{\text{ev,batch}}\right\}_k-\left\{\hat{y}_{\text{ev,batch}}\right\}_k\right\|_2^2$.

28. Backward $L_{\text{train}}^{\text{AE}}\left(\boldsymbol{\varphi},\boldsymbol{\theta}\right)$ and optimize $\left(\boldsymbol{\varphi},\boldsymbol{\theta}\right)$ with the optimizer "Adam" and a learning rate 0.01.

29. **end for**

30. $\left\{\hat{y}_{\text{ev,valid}}\right\}=D_{\boldsymbol{\theta}}\left(E_{\boldsymbol{\varphi}}\left(\left\{\tilde{y}_{\text{ev,valid}}\right\}\right)\right)$.

31. $L_{\text{valid}}^{\text{AE}}\left(q\right)=\dfrac{1}{N_{\text{batch}}}\left\|\left\{\tilde{y}_{\text{ev,valid}}\right\}-\left\{\hat{y}_{\text{ev,valid}}\right\}\right\|_2^2$.

32. **end for**

33. Find the minimum validation loss and save the best autoencoder as $M\left(d_z\right)$.

34. Obtain latent variables for training Kriging: $\mathbf{z}_{\text{train}}\in R^{N_K\times d_z}\leftarrow\mathbf{z}_{\mathbf{0}}^{1:N_K},\mathbf{z}_{\mathbf{0}}=E_{\boldsymbol{\varphi}}\left(\left\{\tilde{y}_{\text{ev}}\right\}\right)$.

35. Obtain the original extreme responses for training Kriging:

$$y_{\text{ev,train}}\leftarrow y_{\text{ev}}^{1:N_K},y_{\text{ev}}=\max\left(\text{abs}\left(y\left(t\right)\right)\right).$$

36. Train Kriging and compute error: $L^K\left(d_z\right)=\dfrac{1}{N}\sum_{i=1}^{N}\left\|y_{\text{ev}}^i-K\left(\mathbf{z}_0^i\right)\right\|_2^2,N=N_{\text{train}}+N_{\text{valid}}$.

37. **end for**

38. Obtain the best d_z and save the best AE model among $M\left(d_z\right)$ by finding the minimum error $L^K\left(d_z\right)$.

39. **Latent variables detection by the trained rLSTM-AE given unobserved data $a_{\text{new}}\left(t\right)$ and $\mathbf{x}_{S,\text{new}}$:**

Table 5-1 (continued) rLSTM-AE for the low-dimensional latent space detection

Algorithm 3: rLSTM-AE for the low-dimensional latent space detection

40. $\left\{\left(\tilde{a}_{\text{new}}(t), \tilde{\mathbf{x}}_{S,\text{new}}(t)\right)\right\} \xleftarrow{\text{Eqs.(5-8)and(5-9)}} \left\{a_{\text{new}}(t), \mathbf{x}_{S,\text{new}}\right\}$.

41. $\hat{y}_{\text{new}}(t) = \text{rLSTM}\left(\left\{\left(\tilde{a}_{\text{new}}(t), \tilde{\mathbf{x}}_{S,\text{new}}(t)\right)\right\}\right), y_{\text{ev}}^{\text{rLSTM}} = \max\left(\text{abs}\left(\hat{y}_{\text{new}}(t)\right)\right)$.

42. $\mathbf{z} = E_{\varphi}\left(y_{\text{ev}}^{\text{rLSTM}}\right)$.

43. Output the rLSTM-AE model and the latent variable $\mathbf{Z}$.

Table 5-2 rLSTM-AE with the active learning-based Kriging: rLSTM-AE-AK

Algorithm 4: rLSTM-AE with the active learning-based Kriging: rLSTM-AE-AK

Input: Information of random variables, the response function *H* and performance function *G*

Output: Failure probability $\hat{P}_f$.

..1. Initiate a candidate pool $\Omega : \mathbf{x}_{\text{CP}}$ with the sample size ΔN and the target CoV of $\hat{P}_f$, e.g. $\text{CoV}_{\text{tol}} = 5\%$.

..2. Draw $N_{\text{train}} + N_{\text{valid}}$ samples from $f_{\mathbf{X}}(\mathbf{x})$ by Latin hypercube sampling, denoted as $\mathbf{x} = (\mathbf{x}_E, \mathbf{x}_S)$

..3. Generate the stochastic excitation $a(t)$ by $\mathbf{x}_E$ and Eq. (5-2).

..4. Calculate the corresponding responses $y(t) = H(a(t), \mathbf{x}_S)$ and $y_{\text{ev}} = \max\left(\text{abs}\left(y(t)\right)\right)$.

..5. Generate the observed dataset $\left\{a(t), \mathbf{x}_S, y(t)\right\}$ and train rLSTM-AE via the algorithm 3.

..6. Randomly select N_K samples from the observed dataset as the initial training set of Kriging, i.e., $\left\{\mathbf{x}^{1:N_K}, G\left(\mathbf{x}^{1:N_K}\right)\right\}$.

..7. Transform the initial training set into latent space by the trained rLSTM-AE:

$$\{\mathcal{Z}, \mathcal{W}\} \leftarrow \left\{\mathbf{z}^{1:N_K}, G\left(\mathbf{x}^{1:N_K}\right)\right\} \leftarrow \left\{\mathbf{x}^{1:N_K}, G\left(\mathbf{x}^{1:N_K}\right)\right\}$$

..8. **while** $\text{CoV}\left(\hat{P}_f\right) > \text{CoV}_{\text{tol}}$ **do**

..9. Transform the candidate pool into the latent space: $\Omega_{\mathbf{Z}} : \mathbf{z}_{\text{CP}} \leftarrow \Omega : \mathbf{x}_{\text{CP}}$

10. **while** $\min\left(U\left(\mathbf{z}_{\text{CP}}\right)\right) < 2$ **do**

11. Build Kriging via training set $\{\mathcal{Z}, \mathcal{W}\}$ and evaluate $\mathbf{z}_{\text{CP}}$ on Kriging.

12. Calculate $U(\mathbf{z}_{\text{CP}}) = \mu_G(\mathbf{z}_{\text{CP}}) / \sigma_G(\mathbf{z}_{\text{CP}})$.

13. Enrich $\{\mathcal{Z}, \mathcal{W}\}$ by U learning function with the point corresponding to:

$$\mathbf{z}^* = \min\left(U\left(\mathbf{z}_{\text{CP}}\right)\right)$$

where the corresponding output is calculated in the original space, i.e., $G\left(\mathbf{x}^*\right)$.

14. **end while**

15. Calculate $\hat{P}_f$ and $\text{CoV}\left(\hat{P}_f\right)$ by Eqs. (2-4) and (2-5), respectively.

16. Enrich the candidate pool Ω by adding ΔN samples.

17. **end while**

18. Output the failure probability $\hat{P}_f$.

5.4 Illustrative Examples

A single-degree-of-freedom system (SDOF) and a 3D reinforced concrete frame structure subjected to the stochastic excitation are investigated in this section. The structures of the rLSTM and autoencoder are constructed by PyTorch. The structure of rLSTM-AE network is specified as follows. The number of LSTM layers for rLSTM network is specified as $l = 2$, one fully connected neural network layer is used and the size of hidden state is set as $h_s = 50$. The encoding function E_{φ} is a fully connected neural network with three layers, containing $4d_z$, $2d_z$ and d_z nodes, respectively. The corresponding decoding function D_{θ} is also a three-layer fully connected neural network, with layers containing $2d_z$, $4d_z$ and 1 nodes, respectively. The activation function is adopted as ReLU. In this thesis, 1000 observed data generated by Latin hypercube sampling are employed, among which $N_{\text{train}} = 800$ are used for training and $N_{\text{valid}} = 200$ for validation. Additionally, 10000 unobserved data generated by MCS is employed for testing the rLSTM-AE model.

Regarding the reliability analysis problem of the high-dimensional stochastic systems investigated in this chapter, MCS is adopted as the reference method. To the best of the authors' knowledge, there is no existing surrogate model that can directly handle this high-dimensional stochastic system due to the curse of dimensionality. Conventional metamodels, such as polynomial chaos expansion, support vector regression, and Kriging, are all unsuitable. The moment-based methods can be employed for comparisons since the extreme responses are of interest. Herein, the popular maximum entropy method (MEM) and a mixture distribution approach by

combining inverse Gaussian and lognormal distribution termed MIGLD (Dang & Xu, 2020) are employed for the failure probability estimation of the stochastic dynamic system. The failure probabilities by the proposed metamodel (rLSTM), Kriging with the detected latent variables by rLSTM-AE (termed rLSTM-AE-K) and the adaptive Kriging with the identified latent variables (called rLSTM-AE-AK) are provided.

5.4.1 Example 1: a SDOF system subjected to stochastic excitation

A single-degree-of-freedom system modeled by the Bouc-Wen hypothesis shown in Figure 5-5 is investigated (Zhang, Dong, & Feng, 2023). The restoring force F of this system can be expressed by:

$$F(u,r)=k\left[qu+(1-q)r\right] \tag{5-28}$$

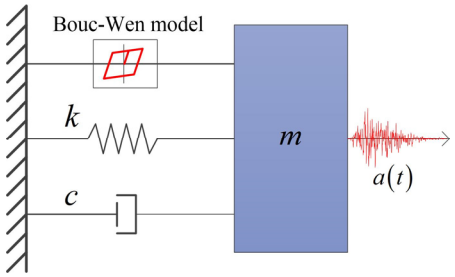

Figure 5-5 A SDOF system

where k is the stiffness and r is the hysteretic displacement following the Bouc-Wen hypothesis:

$$\dot{r}=A\dot{u}-B\left|\dot{u}\right|\left|r\right|^{e-1}r-C\dot{u}\left|r\right|^{e} \tag{5-29}$$

where the parameters are set as follows: $q=0.2$, A=1, $B=C=5\times10^{5}$ and e=3. Three random variables of the SDOF, i.e., the lumped mass m, the stiffness k and the viscous damping c are of concern. The mass m follows a normal distribution with a mean of

41000 kg and a CoV of 0.1. The stiffness k follows a lognormal distribution with a mean of 1.5×10^{6} N/m and a CoV of 0.2. The damping c is a lognormal distribution with a mean of 4.35×10^{4} N·s/m and a CoV of 0.2.

The detail of spectral representation method for generating the stochastic ground motions is provided in section 5.2.1. This system has three random structural parameters and 1001 random phases for generating the stochastic excitation, making it a high-dimensional problem with 1004 input random variables. The mean and standard deviation of the fully non-stationary stochastic excitation, simulated by 1000 Latin hypercube samples, are shown in Figure 5-6 (a) and (b), respectively. The simulated values are in good accordance with the target ones, indicating that the 1000 samples generated by Latin hypercube sampling effectively simulate the stochastic excitation. The time history displacement of the SDOF is of interest.

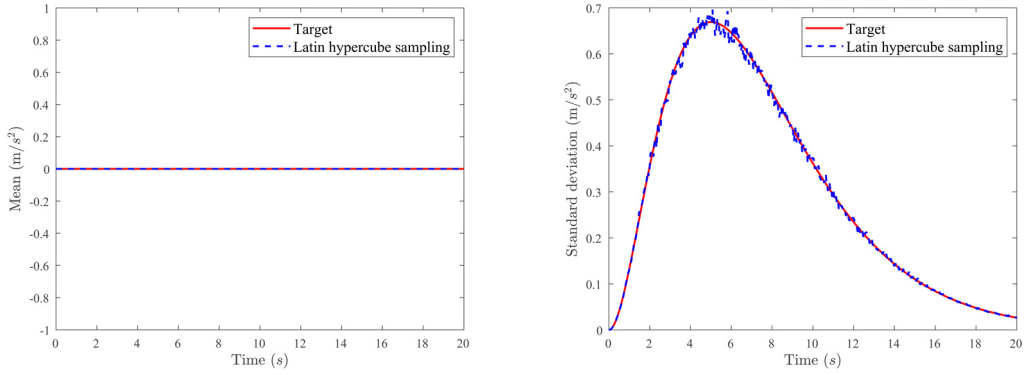

(a) Mean (b) Standard deviation

Figure 5-6 Mean and standard deviation of the fully non-stationary stochastic ground motions

These 1000 observations are used to train the rLSTM-AE network. The training and validation losses for both LSTM-GM and rLSTM are shown in Figure 5-7, where the notation "LSTM-GM" represents that only the stochastic ground

motions serve as input features for training. It is evident that there is a significant gap between the losses of LSTM-GM and rLSTM. This gap arises because LSTM-GM ignores the time-invariant random structural parameters, highlighting that the uncertainties of structural parameters also play an important role in the stochastic system. The proposed rLSTM provides a direct way for metamodeling of the high-dimensional stochastic systems considering both time-variant excitations and time-invariant random variables. Four representative time history responses predicted by the rLSTM and LSTM-GM are depicted in Figure 5-8. The red dashed line, predicted by rLSTM, aligns well with the ground truth (the black line). In contrast, the blue line, predicted by LSTM-GM, shows significantly different time history responses compared to the true values, underscoring the importance of accounting for time-invariant random structural parameters.

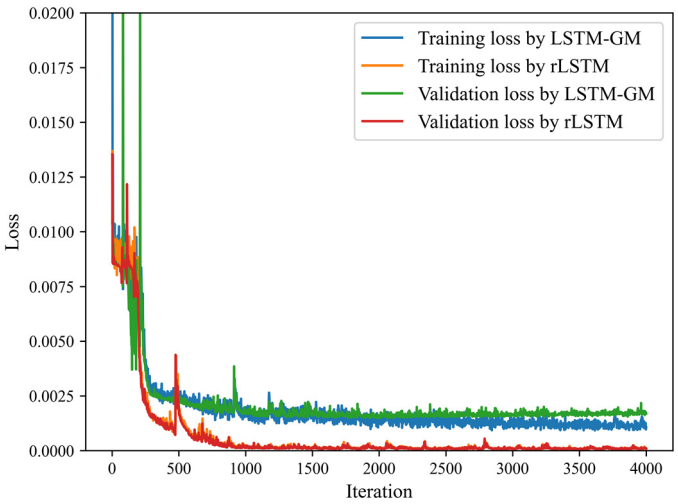

Figure 5-7 Training and validation losses for the SDOF system

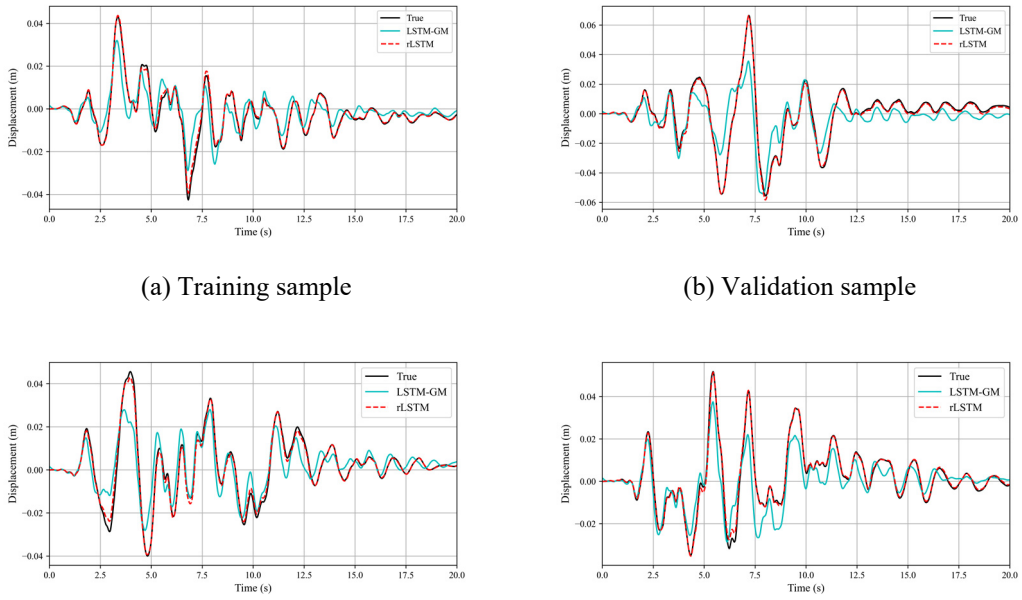

(a) Training sample

(b) Validation sample

(c) Test sample 1

(d) Test sample 2

Figure 5-8 Representative samples predicted by rLSTM for the SDOF system

The extreme responses are of interest, Figure 5-9 (a) depicts predictions of training and validation datasets and (b) shows predictions of 10000 test samples. The green and black dashed lines represent relative errors of 10% and 20% compared to the ground truth, respectively. The determination coefficient R^2 by the rLSTM network is also provided in the figure. It can be observed that the trained rLSTM network accurately fits both the 1000 observed data points and the 10000 unobserved test data. The relative errors of predictions on the test set fall mainly within the 10% bound and the R^2 is close to 1, i.e., 0.9745. The results demonstrate that the proposed rLSTM network can effectively construct a metamodel for the stochastic system with 1004 input random variables. Additionally, K-fold cross-validation (using 5 folds) is employed to assess the generalization ability of the rLSTM. The determination coefficients are 0.9710, 0.9753, 0.9769, 0.9410, and 0.9687, all of which are close to 1. The average determination coefficient is 0.9666, indicating the strong

generalization ability of the proposed rLSTM. Figure 5-10 displays the PDF of the extreme responses and the curve of the probability of exceedance (POE) in logarithmic scale by the proposed rLSTM, based on predictions from 10^5 unobserved samples. The reference results are by 10^5 MCS. It is evident that while the rLSTM captures the main body of the distribution well, its accuracy in the tail regions is limited. This limitation arises because achieving high accuracy across the entire domain of a high-dimensional stochastic dynamic system with limited observations is challenging. Therefore, to improve failure probability estimation, it is necessary to identify a low-dimensional latent space and construct an adaptive Kriging model with the aid of the rLSTM.

The extreme responses from the 1000 observed data are also employed to train the autoencoder. In algorithm 3, $N_{\text{train}} = 800$, $N_{\text{valid}} = 200$ and the size of the training set for Kriging is $N_K = 100$. To determine the optimal dimension of the latent space, we initially specify dimensions ranging from 2 to 20, and the autoencoder's structure is adjusted accordingly. The autoencoder is trained using the observed data, and the best autoencoder model, along with the Kriging construction error for each dimension d_z is saved. After training the autoencoder with dimensions from 2 to 20, the dimension that results in the minimum Kriging construction error is selected as the best latent space dimension.

The error of the Kriging construction with respect to the dimension d_z is plotted in Figure 5-11 (a). The red point denotes the minimum error so the optimal dimension of the latent space is $d_z = 11$ in this example. Figure 5-11 illustrates the

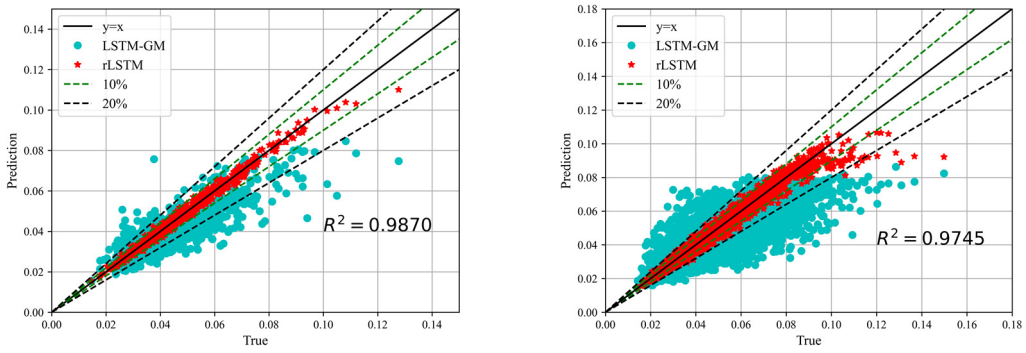

(a) Training and validation (1000 samples) (b) Test (10000 samples)

Figure 5-9 Predictions on extreme responses for the SDOF system

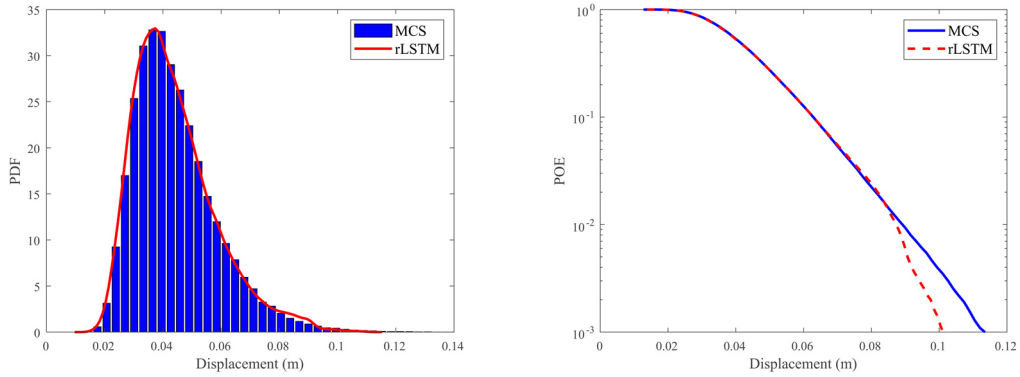

(a) PDF (b) POE

Figure 5-10 PDF and POE of the extreme responses predicted by rLSTM for the SDOF system

accuracy of the autoencoder and Kriging in reconstructing the approximate extreme value space (extreme responses obtained from rLSTM). The accuracy is validated using 10000 test samples. The horizontal axis represents the extreme responses estimated by rLSTM and the vertical axis denotes predictions by the trained autoencoder or Kriging with the low-dimensional latent variables obtained from the trained autoencoder. It can be found the trained autoencoder (rLSTM-AE) can accurately reconstruct the extreme space approximated by rLSTM, which means that the detected latent variables well capture the features of the extreme space by rLSTM.

This accuracy is primarily due to the autoencoder's ability to efficiently detect d_z features for a one-dimensional space.

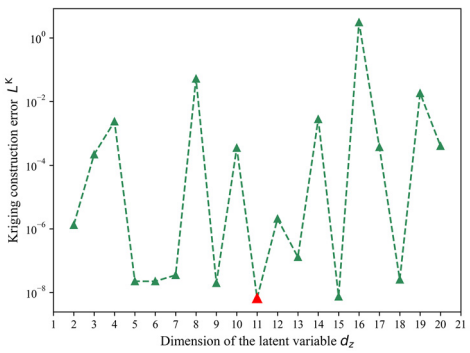

(a) Kriging construction error

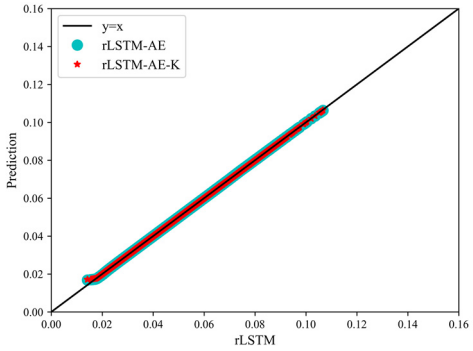

(b) Compared to the rLSTM

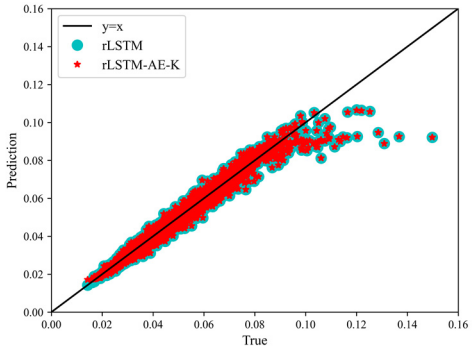

(c) Compared to the ground truth

Figure 5-11 Performance of rLSTM-AE and rLSTM-AE-K for the SDOF system

Therefore, Kriging using the latent variables detected by rLSTM-AE, referred to as rLSTM-AE-K, can also accurately reconstruct the approximate extreme value space. This capability allows Kriging to achieve accuracy in predicting extreme responses comparable to that of the rLSTM network. This conclusion is further supported by Figure 5-11 (c), which compares the extreme responses predicted by rLSTM and rLSTM-AE-K with the ground truth. The accuracy of Kriging is nearly equivalent to that of rLSTM in estimating extreme responses. Although this accuracy

may be insufficient for reliability analysis, rLSTM-AE-K can utilize active learning strategies to enhance failure probability estimation, a capability that rLSTM alone does not possess.

Two cases corresponding to the thresholds of 80 mm and 95 mm are of concern. The initial training set size for Kriging is set to $N_K = 100$. The active learning processes are shown in Figure 5-12 (a) and (b), respectively. It can be observed that the estimated failure probability converges to the reference value as the training set is enriched. The results by different methods are listed in Table 5-3, where N_{call} represents the number of calls to the stochastic system and the notation "R.E." denotes the relative error of the estimated failure probability. In Case 1, the failure probabilities estimated by MEM and MIGLD are less accurate compared to the proposed rLSTM-based methods. Both rLSTM and rLSTM-AE-K achieve the same level of accuracy, as Kriging constructed with the detected latent variables has equivalent predictive capability for extreme responses as rLSTM, which is consistent with the results shown in Figure 5-11 (c). However, as previously noted, the accuracy of the rLSTM network alone is insufficient for reliability analysis due to the limited observations available for constructing a metamodel across the entire domain. In Case 1, the relative errors for both rLSTM and rLSTM-AE-K are 8.40%. By employing an active learning strategy, rLSTM-AE-AK provides a more accurate failure probability estimate, with a relative error of 4.62%. Note that 1000 observed samples are used for training the rLSTM-AE network, and 258 training samples are identified through the learning function, resulting in a total of 1258 calls for rLSTM-AE-AK.

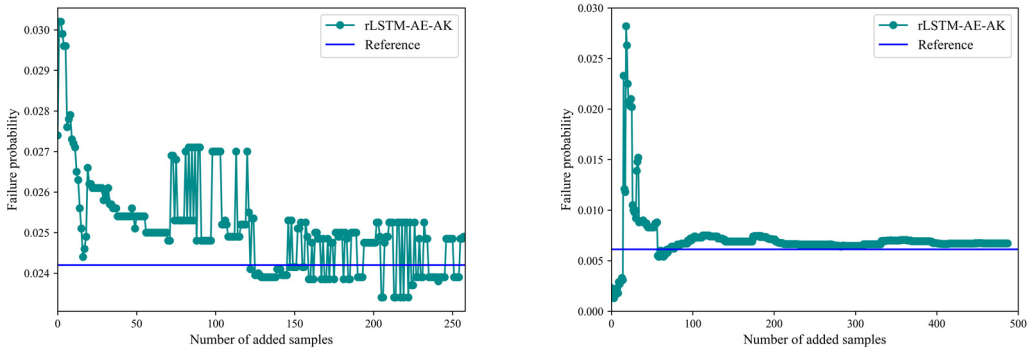

(a) Case 1 (b) Case 2

Figure 5-12 Failure probabilities estimation for the SDOF system

Table 5-3 Results obtained by different methods for the SDOF system

	Method	N_{call}	P_f	CoV(%)	R.E. (%)
Case 1	MCS	10^5	2.38×10^{-2}	2.03	-
	MEM	1000	2.94×10^{-2}	-	23.53
	MIGLD	1000	2.70×10^{-2}	-	13.58
	rLSTM	1000	2.58×10^{-2}	4.35	8.4.
	rLSTM-AE-K	1000	2.58×10^{-2}	4.35	8.40
	rLSTM-AE-AK	1258	2.49×10^{-2}	4.42	4.62
Case 2	MCS	10^5	6.41×10^{-3}	3.94	-
	MEM	1000	9.23×10^{-3}	-	43.96
	MIGLD	1000	7.13×10^{-3}	-	11.25
	rLSTM	1000	2.88×10^{-3}	5.88	55.07
	rLSTM-AE-K	1000	2.88×10^{-3}	5.88	55.07
	rLSTM-AE-AK	1487	6.72×10^{-3}	4.96	4.78

When considering a small failure probability in case 2, i.e., 6.41×10^{-3} by 10^5 MCS, the MEM, MIGLD, rLSTM, rLSTM-AE-K yield unsatisfactory results. The relative errors for both rLSTM and rLSTM-AE-K are as high as 55.07%. However, with the assistance of the active learning approach, rLSTM-AE-AK achieves significantly improved accuracy, reducing the relative error from 55.07% to 4.78% by adaptively adding 487 samples. Additionally, for a smaller failure probability corresponding to a threshold of 120 mm, where 10^6 MCS simulations result in a failure probability of 6.10×10^{-4}. The failure probabilities by rLSTM and rLSTM-AE-K are both 0. In contrast, rLSTM-AE-AK estimates a failure probability of 2.10×10^{-4}.

Although the accuracy of the failure probability by the proposed method is not yet sufficient, the active learning strategy can improve the accuracy for small failure probability estimation. Indeed, Monte Carlo Simulation (MCS) is not ideal for generating a candidate pool for estimating small failure probabilities or for active learning-based reliability analysis, as it requires a substantial number of samples to ensure reliable estimates (Echard et al., 2013; Huang et al., 2016). Consequently, more advanced sampling techniques are needed to complement active learning for accurate small failure probability estimation. This challenge is compounded in the context of stochastic dynamics, where generating stochastic excitation is also time-consuming. Therefore, further investigation into combining advanced sampling approaches with the proposed high-dimensional active learning strategy is essential for improving small failure probability estimation.

5.4.2 Example 2: a 3D reinforced concrete frame

To validate the proposed method for the practical engineering applications, a 3D reinforced concrete frame structure subjected to the fully non-stationary stochastic seismic excitation is investigated. The structural configuration and reinforcement information are shown in Figure 5-13. The finite element model is constructed using OpenSees, with the Concrete01 and Steel01 constitutive laws applied. Seven random structural variables, listed in Table 3-1 are considered, resulting in a total of 1008 input random variables for this example. The time history displacement at point A in the Figure 5-13 is of interest.

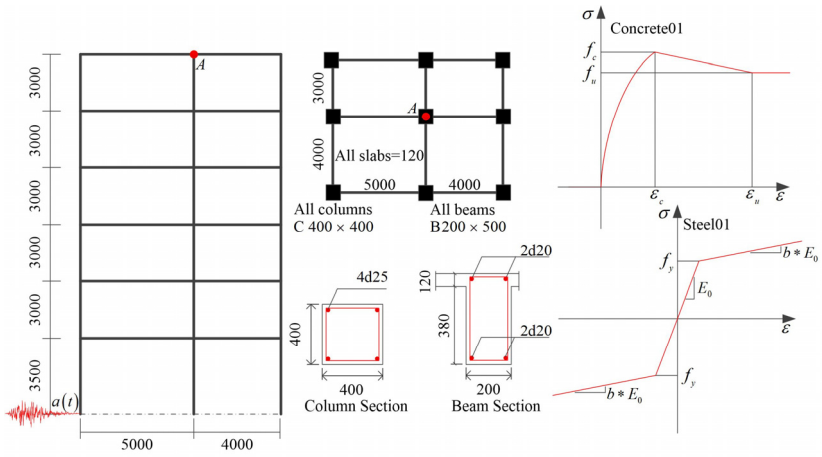

Figure 5-13 A 3D reinforced concrete frame structure

Table 5-4 Random variables for the 3D concrete frame structure

Variable	Description	Distribution	Mean	CoV
f_c	Concrete compressive strength	Lognormal	26.8 MPa	0.20
ε_c	Concrete strain at maximum strength	Lognormal	0.0015	0.05
f_u	Concrete crushing strength	Lognormal	10 MPa	0.20
ε_u	Concrete strain at crushing strength	Lognormal	0.0033	0.05
f_y	Yield strength of rebar	Lognormal	400 MPa	0.20
E_0	Initial elastic modulus of rebar	Lognormal	206 GPa	0.20
b	Strain-hardening ratio of rebar	Lognormal	0.01	0.05

Similarly, 1000 observed data are employed to train rLSTM-AE network. The training and validation losses for both the rLSTM and LSTM-GM models are presented in Figure 5-14. Throughout the training process, a consistent gap between LSTM-GM and rLSTM is observed, highlighting the importance of considering uncertainties in structural parameters for the response of interest. This underscores the necessity of incorporating both time-variant and time-invariant input features in the rLSTM for metamodel construction in stochastic dynamic systems. Figure 5-15 showcases four representative samples, further demonstrating that rLSTM outperforms LSTM-GM. Figure 5-16 (a) illustrates the accuracy of extreme response predictions by rLSTM and LSTM-GM on the training and validation datasets. Figure

5-16 (b) displays the accuracy of these predictions on 10000 test samples. It is evident that the relative errors in the rLSTM predictions are predominantly below 20%, whereas the accuracy of the LSTM-GM predictions, indicated by the blue samples, is unsatisfactory. The determination coefficient calculated by rLSTM on the 10000 test samples is close to 1, indicating a high level of accuracy. To further assess the generalization ability of the proposed rLSTM, K-fold cross-validation is performed, yielding determination coefficients of 0.9414, 0.9369, 0.9445, 0.8831 and 0.9141, respectively. The mean R^2 is 0.9240, which is close to 1, thus further validating the generalization capability of rLSTM. Moreover, the PDF and POE in logarithmic scale by 10^5 MCS are depicted in Figure 5-17, demonstrating that rLSTM effectively captures the main body of the extreme response distribution. However, rLSTM shows some loss of accuracy in the distribution tail, as constructing a metamodel for a stochastic dynamic system across the entire domain with limited observations is challenging.

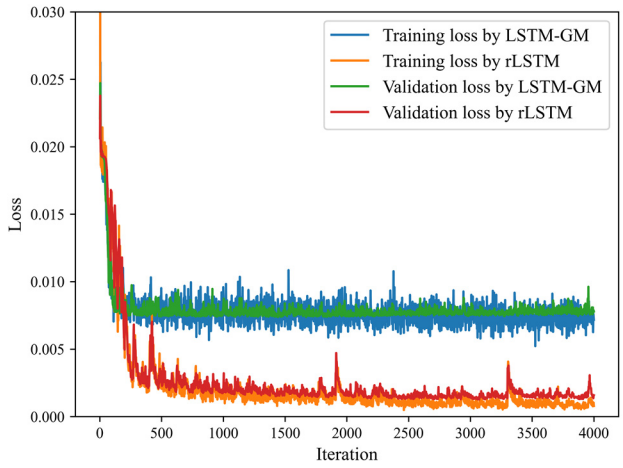

Figure 5-14 Training and validation losses for the 3D concrete frame structure

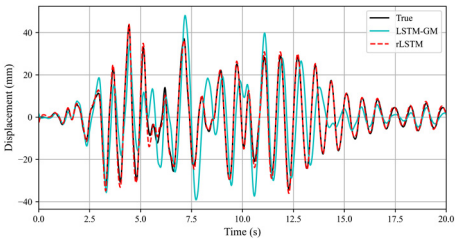

(a) Training sample

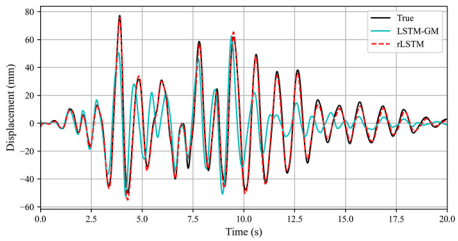

(b) Validation sample

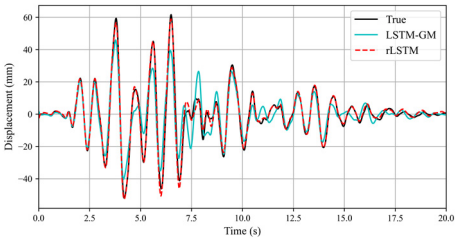

(c) Test sample 1

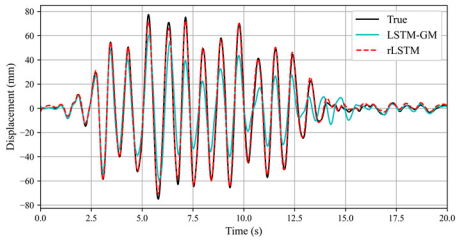

(d) Test sample 2

Figure 5-15 Representative samples predicted by rLSTM for the 3D concrete frame structure

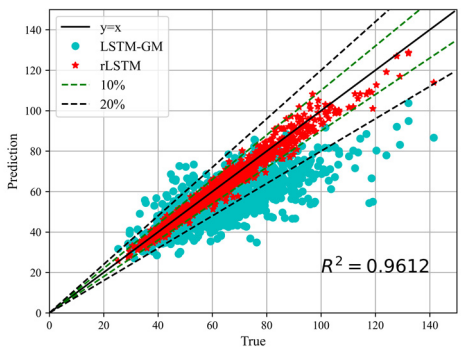

(a) Training and validation (1000 samples)

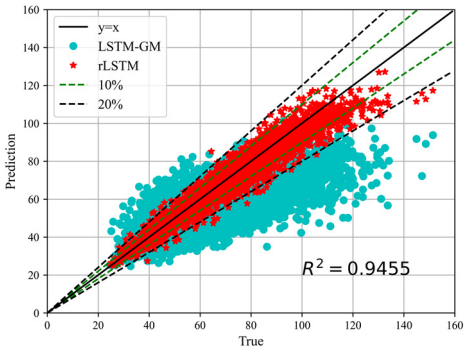

(b) Test (10000 samples)

Figure 5-16 Predictions on extreme responses for the 3D concrete frame structure

Regarding the reliability analysis of this 1008-dimensional stochastic dynamic system, the low-dimensional latent variables are required to be identified as the accuracy of rLSTM remains insufficient for failure probability estimation given the current limited observations. To enhance the reliability analysis, an active learning-based Kriging metamodel can then be constructed.

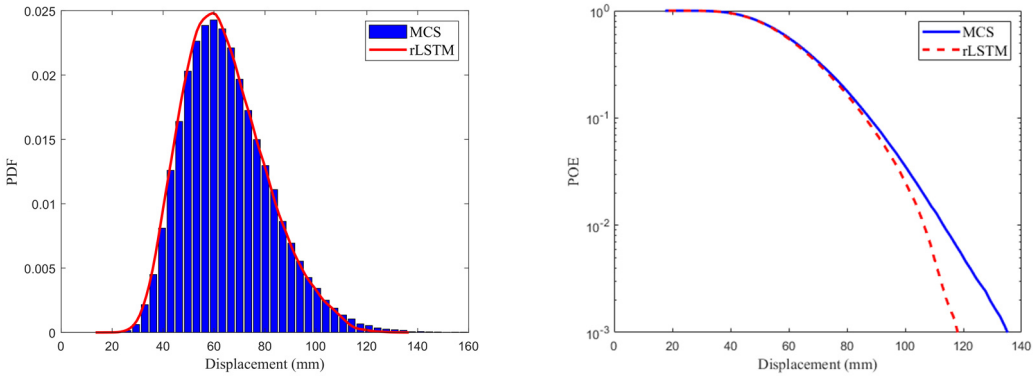

(a) PDF (b) POE

Figure 5-17 PDF and POE of the extreme responses predicted by rLSTM for the 3D concrete frame structure

Figure 5-18 (a) depicts the Kriging construction error with respect to the dimension of the latent variables d_z. It can be found that $d_z = 2$ is the best dimension for constructing a Kriging metamodel in this example. Figure 5-18 (b) demonstrates the performance of the trained autoencoder and rLSTM-AE-K in reconstructing the extreme responses predicted by rLSTM. Both methods achieve high accuracy, indicating that Kriging, using the latent variables identified by rLSTM-AE, can accurately reconstruct the extreme value space predicted by rLSTM. Figure 5-18 (c) showcases that the rLSTM-AE-K is equivalent to the rLSTM regarding the extreme responses estimation. Then, rLSTM-AE-K can combine the active learning strategy for the failure probability estimation. In this example, two cases corresponding to the thresholds of 100 mm and 119 mm are of concern. Figure 5-19 shows the active learning process for failure probabilities estimation. With the aid of the active learning, the accuracy of the estimated failure probability increases with the enrichment of training set and the final failure probability converges to the benchmark by MCS.

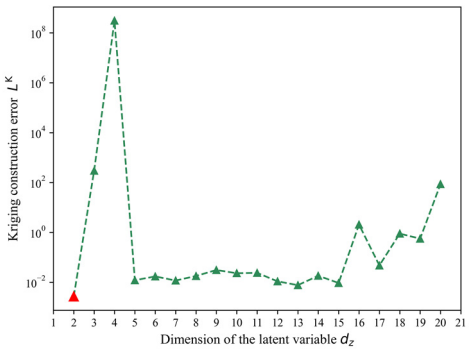

(a) Kriging construction error

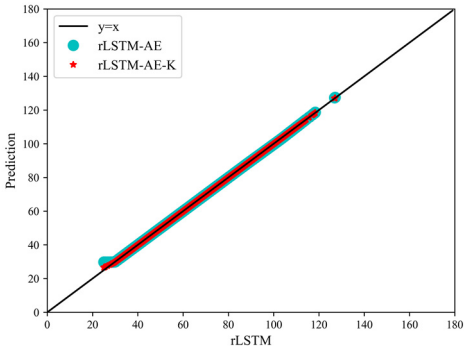

(b) Compared to the rLSTM

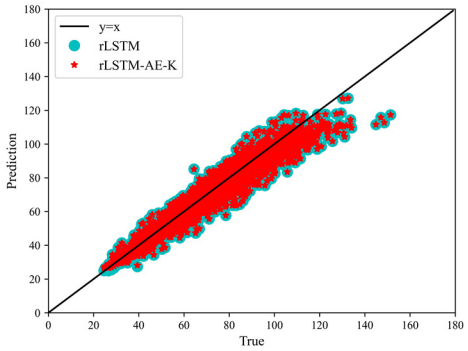

(c) Compared to the ground truth

Figure 5-18 Performance of rLSTM-AE and rLSTM-AE-K for the 3D concrete frame structure

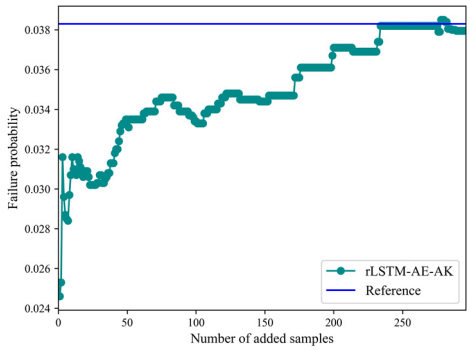

(a) Case 1

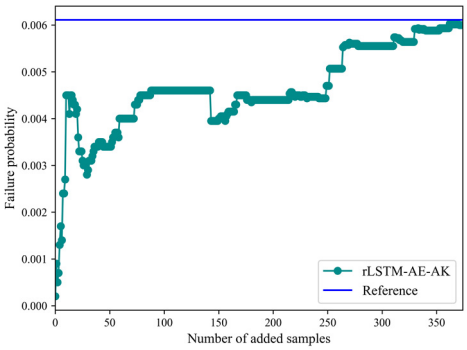

(b) Case 2

Figure 5-19 Failure probabilitties estimation for the 3D concrete frame structure

Moreover, the failure probabilities by different methods are listed in Table 5-5. For case 1, the relative errors by MEM and MIGLD are larger than 5%. rLSTM and rLSTM-AE-K do not produce satisfactory results and the relative errors of the failure probability are as large as 33.12%, which results from the insufficient accuracy of the rLSTM for reliability analysis under limited observations. rLSTM-AE-AK produces an accurate failure probability by adaptively adding 295 samples and the relative error is as small as 0.86%. Regarding case 2, the reference failure probability i.e., 6.11×10^{-3} is produced by 10^5 MCS. MIGLD obtains more accurate result than MEM by consuming the same number of function calls. Again, the accuracy of the rLSTM and rLSTM-AE-K is not sufficient for reliability analysis and the relative errors are both over 80%. By leveraging the active learning, the training set for Kriging construction is enriched by 374 samples and the accuracy of the estimated failure probability is significantly improved. The relative error is reduced to 1.8% from 84.62% compared to the rLSTM.

Table 5-5 Results obtained by different methods for the 3D concrete frame structure

	Method	N_{call}	P_f	CoV(%)	R.E. (%)
Case 1	MCS	10^5	3.83×10^{-2}	1.59	-
	MEM	1000	3.43×10^{-2}	-	10.28
	MIGLD	1000	3.52×10^{-2}	-	8.01
	rLSTM	1000	2.56×10^{-2}	4.36	33.12
	rLSTM-AE-K	1000	2.56×10^{-2}	4.36	33.12
	rLSTM-AE-AK	1295	3.80×10^{-2}	3.56	0.86
Case 2	MCS	10^5	6.11×10^{-3}	4.03	-
	MEM	1000	6.49×10^{-3}	-	6.13
	MIGLD	1000	6.35×10^{-3}	-	3.85
	rLSTM	1000	9.40×10^{-4}	10.31	84.62
	rLSTM-AE-K	1000	9.30×10^{-4}	10.36	84.62
	rLSTM-AE-AK	1374	6.00×10^{-3}	4.86	1.80

5.5 Summary

In this chapter, a rLSTM network considering both time-variant and time-invariant input features for metamodeling of the high-dimensional stochastic dynamic systems is developed. The stochastic excitation is employed as the pertinent input but not the random phases for simulating the excitation. The proposed rLSTM is capable of capturing the main body of the extreme response distribution of a high-dimensional stochastic dynamic system by consuming the limited observations. Regarding the reliability analysis, it is usually hard to build a high-accuracy metamodel across the whole domain under the limited training samples. To surmount the insufficient accuracy of reliability analysis induced by the limited observations, the rLSTM is combined with the autoencoder to detect a low-dimensional latent space for the approximate extreme value space. The best latent variables for reconstructing the approximate extreme value space is selected by minimizing the error between the Kriging predictions and the ground truth. Finally, the active learning-based Kriging is combined with the identified latent variables to improve the accuracy of failure probabilities estimation. The results of a 1004-dimensional SDOF system and a 1008-dimensional reinforced concrete frame structure subjected to the stochastic excitation validate that the proposed method is capable of building metamodel and accurately approximating the failure probability for the high-dimensional stochastic dynamic systems. The proposed rLSTM provides a way of metamodeling for a stochastic dynamic system with more than 1000 input features. The rLSTM-AE brings insights for the low-dimensional features extraction from the perspective of the approximate output space, which makes the active learning-based reliability analysis available for the high-dimensional stochastic dynamic systems. The future study will focus on

combining the more advanced sampling techniques with the proposed high-dimensional active learning strategy for the small failure probabilities estimation.

CHAPTER 6 PHYSICS-INFORMED RLSTM FOR METAMODELING OF STOCHASTIC DYNAMIC SYSTEMS GOVERNED BY THE UNCERTAIN DIFFERENTIAL EQUATION

6.1 Introduction

In this chapter, a physics-informed long short-term memory (PhyrLSTM) model is introduced for modeling of stochastic dynamic systems. This model integrates physical laws into the loss function, enhancing the training process by incorporating fundamental principles of dynamics. Conventional deep learning models rely solely on observed data and often overlook physical laws, such as the governing equations of a dynamic system. As a result, purely data-driven models may struggle with strongly nonlinear systems or limited data. By embedding physical laws into the training loss, the PhyrLSTM can capture the underlying principles of the system, leading to more reliable and robust predictions. Furthermore, this chapter addresses uncertainties in structural parameters, which results in uncertain governing equations. The physics-informed rLSTM is designed to learn the uncertain governing equation during the training process. The effectiveness of the proposed PhyrLSTM is demonstrated through a case study of a highway bridge subjected to the stochastic seismic excitation. The results show that the physics-informed rLSTM significantly outperforms the traditional rLSTM model.

6.2 Physics-informed rLSTM for metamodeling of stochastic dynamic systems

Generally, the stochastic dynamic systems can be governed by the following equation:

$$\mathbf{M}\left(\mathbf{X}_S\right)\ddot{\mathbf{u}}+\mathbf{C}\left(\mathbf{X}_S\right)\dot{\mathbf{u}}+\mathbf{K}\left(\mathbf{X}_S\right)\mathbf{u}+\mathbf{F}\left(\mathbf{r}\right)=-\mathbf{M}\left(\mathbf{X}_S\right)\mathbf{I}a\left(\mathbf{X}_E,t\right) \tag{6-1}$$

where $\mathbf{M}$, $\mathbf{C}$ and $\mathbf{K}$ are the mass, damping and stiffness matrix, respectively; $\ddot{\mathbf{u}}$, $\dot{\mathbf{u}}$ and $\mathbf{u}$ are acceleration, velocity and displacement vector, respectively; $\mathbf{F}$ denotes the restoring force vector and the notation $\mathbf{r}$ is the hysteretic parameter; $\mathbf{I}$ is the force distribution factor; $a\left(\mathbf{X}_E,t\right)$ represents the non-stationary stochastic seismic ground motions. $\mathbf{X}_E=\left(X_{E1},X_{E2},...,X_{Ed_1}\right)$ includes d_1 random variables accounting for uncertainties in seismic ground motions. $\mathbf{X}_S=\left(X_{S1},X_{S2},...,X_{Sd_2}\right)$ is a random vector containing d_2 structural random variables.

Eq. (6-1) can be reformulated as:

$$\mathbf{M}\left(\mathbf{X}_S\right)\ddot{\mathbf{u}}+\mathbf{H}\left(\mathbf{X}_S\right)=-\mathbf{M}\left(\mathbf{X}_S\right)\mathbf{I}a\left(\mathbf{X}_E,t\right) \tag{6-2}$$

where $\mathbf{H}\left(\mathbf{X}_S\right)$=$\mathbf{C}\left(\mathbf{X}_S\right)\dot{\mathbf{u}}+\mathbf{K}\left(\mathbf{X}_S\right)\mathbf{u}+\mathbf{F}$. By normalizing Eq. (6-2) with mass matrix, we can get:

$$\ddot{\mathbf{u}}+\mathbf{g}\left(\mathbf{X}_S\right)=-\mathbf{I}a\left(\mathbf{X}_E,t\right) \tag{6-3}$$

where $\mathbf{g}\left(\mathbf{X}_S\right)=\mathbf{M}^{-1}\left(\mathbf{X}_S\right)\mathbf{H}\left(\mathbf{X}_S\right)$ is called the mass-normalized restoring force (R. Zhang et al., 2020b). The mass-normalized restoring force is an unknown latent

function of state variables $\mathbf{P} = \{\mathbf{u}, \dot{\mathbf{u}}, \mathbf{r}\}^{\mathrm{T}}$ and random structural parameters $\mathbf{X}_S$. Purely data-driven surrogate models may struggle to capture the underlying complex physics, particularly when uncertainties are involved.

Surrogate models can enable rapid prediction of state variables. In the context of engineering structures subjected to stochastic seismic excitation, LSTM networks are powerful tools for time-series data prediction. The rLSTM network discussed in chapter 5 can be utilized for predicting state variables, especially given the concern for time-invariant random structural parameters. However, challenges arise in obtaining all state variables, such as time-series velocity and hysteretic parameters, with the latter often being non-observable. These state variables are determined by the normalized governing equation. i.e., Eq. (6-3). Thus, the governing equation can serve as a constraint in developing a physics-informed rLSTM network (R. Zhang et al., 2020b). R. Zhang et al. (2020b) proposed a physics-informed multi-LSTM network, focusing on the deterministic governing equation and assuming that two state variables, i.e., the displacement and the velocity, are known. In contrast to their study, we assume that only the displacement is known and incorporate random structural parameters as additional inputs to the network.

The three state variables ($\mathbf{u}$, $\dot{\mathbf{u}}$ and **r)** are first predicted by an rLSTM network. Then, these state variables can be considered the input of the second rLSTM network, which is utilized to predict the mass-normalized force $\mathbf{g}(\mathbf{X}_S)$. Additionally, the relationships between state variables, where the first derivative of displacement is velocity and the first derivative of velocity is acceleration, are embedded into the physics-informed network using a central finite difference filter-based numerical

differentiator (R. Zhang et al., 2020b). The framework of physics-informed rLSTM network is shown in Figure 6-1.

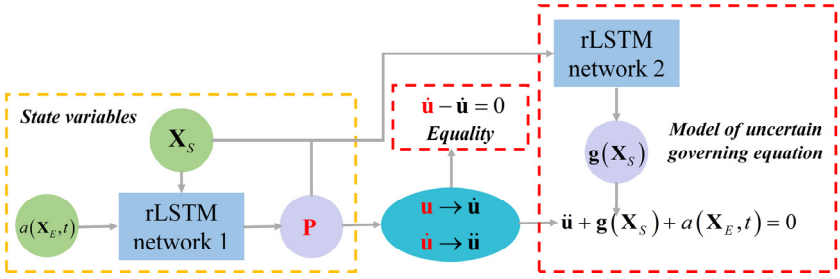

Figure 6-1 PhyrLSTM network

The PhyrLSTM network comprises two rLSTM networks and a filter to generate derivatives. The first rLSTM network constructs a nonlinear mapping from stochastic ground motions and time-invariant random structural parameters to structural responses ($\mathbf{u}$, $\dot{\mathbf{u}}$ and $\mathbf{r}$). The input dimension of this network is 1+d_2 and the output dimension is 3. Denote the first rLSTM network as rLSTM^1, then we have:

$$\mathbf{P}=\left\{\mathbf{P}_1,\mathbf{P}_2,\mathbf{P}_3\right\}^{\mathrm{T}}=\mathrm{rLSTM}^1\left(a\left(\mathbf{X}_E,t\right),\mathbf{X}_S\,|\,\boldsymbol{\theta}_1\right) \tag{6-4}$$

where $\boldsymbol{\theta}_1$ is the trainable weights and biases of rLSTM^1; $\mathbf{P}_1=\mathbf{u}$, $\mathbf{P}_2=\dot{\mathbf{u}}$ and $\mathbf{P}_3=\mathbf{r}$. Note that the concatenation of input features (ground motions and random structural parameters) and data preprocessing follow the same procedures as described in chapter 5. The available training data for this step consists of displacement measurements $\mathbf{u}_d$. The data loss function can be defined as:

$$L_d\left(\boldsymbol{\theta}_1\right)=\sum_{i=1}^{N_d}\left\|\mathbf{p}_1^i\left(\boldsymbol{\theta}_1\right)-\mathbf{u}_d^i\right\|_2^2 \tag{6-5}$$

where N_d is the number of training samples. The derivatives of state variables can be obtained by the finite difference-based filtering. Denote the derivatives of state variables as $\dot{\mathbf{P}} = \left\{\dot{\mathbf{P}}_1, \dot{\mathbf{P}}_2, \dot{\mathbf{P}}_3\right\}^{\mathrm{T}}$, i.e., $\left\{\dot{\mathbf{u}}, \ddot{\mathbf{u}}, \dot{\mathbf{r}}\right\}^{\mathrm{T}}$. The first derivative of the displacement is the velocity, which can be expressed by $\dot{\mathbf{P}}_1 - \mathbf{P}_2 = 0$. Thus, we can get the so-called equality loss:

$$L_e\left(\boldsymbol{\theta}_1\right) = \sum_{i=1}^{N_c} \left\| \dot{\mathbf{p}}_1^i\left(\boldsymbol{\theta}_1\right) - \mathbf{p}_2^i\left(\boldsymbol{\theta}_1\right) \right\|_2^2 \tag{6-6}$$

where N_c is the number of collocation points. Another rLSTM network is utilized to predict the mass-normalized restoring force $\mathbf{g}\left(\mathbf{X}_S\right)$, which can be denoted as:

$$g\left(\mathbf{X}_S\right) = \mathrm{rSLTM}^2\left(\mathbf{P}\left(\boldsymbol{\theta}_1\right), \mathbf{X}_S \mid \boldsymbol{\theta}_2\right) \tag{6-7}$$

where $\boldsymbol{\theta}_2$ is the trainable weights and biases of the second rLSTM network. Consider the uncertain governing equation, we have the following governing loss function:

$$L_g\left(\boldsymbol{\theta}_1, \boldsymbol{\theta}_2\right) = \sum_{i=1}^{N_c} \left\| \dot{\mathbf{p}}_2^i\left(\boldsymbol{\theta}_1\right) + \mathbf{g}^i\left(\boldsymbol{\theta}_1, \boldsymbol{\theta}_2\right) + \mathbf{I} a_g \right\|_2^2 \tag{6-8}$$

The total loss can be given by:

$$L\left(\boldsymbol{\theta}_1, \boldsymbol{\theta}_2\right) = \omega_1 L_d\left(\boldsymbol{\theta}_1\right) + \omega_2 L_e\left(\boldsymbol{\theta}_2\right) + \omega_3 L_g\left(\boldsymbol{\theta}_1, \boldsymbol{\theta}_2\right) \tag{6-9}$$

where ω_1, ω_2 and ω_3 are user-defined weights for convergence control. The parameters $\boldsymbol{\theta}_1, \boldsymbol{\theta}_2$ can be found by solving the following optimization problem:

$$\{\boldsymbol{\theta}_1, \boldsymbol{\theta}_2\} = \arg\min_{\boldsymbol{\theta}_1, \boldsymbol{\theta}_2} L(\boldsymbol{\theta}_1, \boldsymbol{\theta}_2) \tag{6-10}$$

Besides, the structure of the rLSTM network is shown in Figure 6-2:

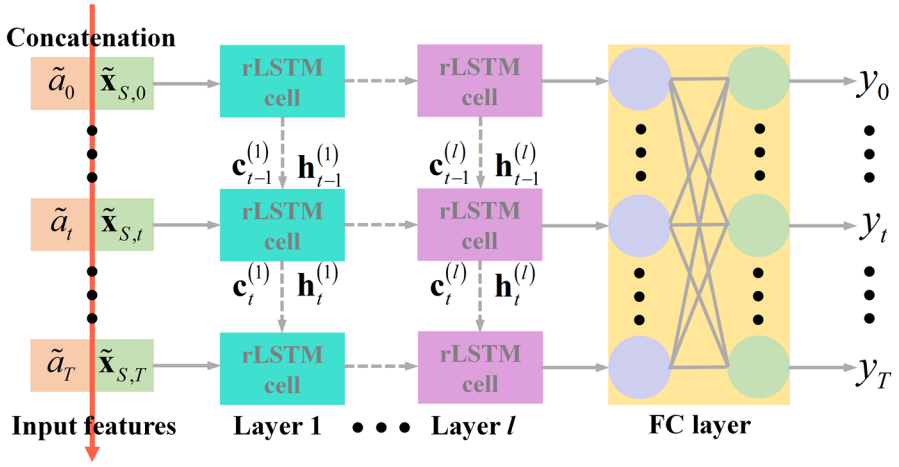

Figure 6-2 The structure of the rLSTM network in chapter 6

where two fully-connected layers are employed in this chapter and the notations $\tilde{a}_t$, $\tilde{\mathbf{x}}_t$ are seismic ground motions and random structural parameters, respectively, which are preprocessed by the normalization process stated in chapter 5. y_t represents the output of the rLSTM network.

6.3 PhyrLSTM for metamodeling of a highway bridge

6.3.1 The stochastic highway bridge model

A three-span continuous concrete highway bridge subjected to the stochastic seismic excitations is investigated. The geometric configuration of the bridge is described in Figure 6-3. The length of this highway bridge is 30×4=120 m and the deck utilizes a box-girder with 8.5 m width and 1.9 m depth. Double circular cross-section columns with a diameter of 1.2 m are adopted to support the deck ends and the diameter of the

interior columns is 1.6 m. Each column is 10 m in height and is erected on a pile-group foundation consisting of double piles with a diameter of 1.5 m. The decks and the footings are constructed by using the Chinese grade concrete C50 and C35, respectively. The columns employ the concrete C40 and HRB400 reinforcement.

The numerical finite element model is built by the OpenSees platform (McKenna, 2011), the simulation model details are shown in Figure 6-4. The deck is modeled by the elastic beam-column elements. The bearing is simulated by the zero-length element and the horizontal stiffness of the bearing can be calculated as $K_b = \mu F_v / d_y$, in which the friction coefficient μ is equal to 0.02, the yield displacement is adopted as d_y=0.003 m and F_v is the vertical reaction force. The yield force of the bearing can be given by $F_y = K_b d_y$. The spherical steel bearings are modeled by elastic-perfectly plastic material shown in Figure 6-4 (a). The soil-structure interaction is modeled by a 6-degree-of-freedom linear soil spring shown in Figure 6-4 (b) and the stiffness refers to Mangalathu's study (Mangalathu et al., 2018). Non-linear beam-column fiber elements described in Figure 6-4 (c) are adopted to simulate the columns, where “Concrete04” and “Steel02” materials are employed to describe the constitutive laws of the concrete and reinforcement fibers, receptively. Rayleigh damping with appropriate coefficients $\alpha_m = 0.344$ and $\beta_k = 0.002$ are adopted, where α_m and β_k are mass and stiffness proportional coefficients, respectively. The random structural parameters of this highway bridge refer to peers' studies (Mangalathu et al., 2018; X. Wang et al., 2022), and are listed in Table 6-1. These uncertainties affect the mass, damping and stiffness matrices, leading to an uncertain governing equation.

Table 6-1 Random variables for the highway bridge

Variable	Description	Distribution	Mean	CoV
Pier				
ρ_l	Longitudinal reinforcement ratio	Uniform	0.02	0.29
ρ_s	Transverse reinforcement ratio	Uniform	0.009	0.33
f_c (MPa)	Concrete compressive strength	Lognormal	40	0.12
f_y (MPa)	Rebar yield strength	Lognormal	448	0.08
Translational stiffness				
K_{ts} (kN/m)	Single-column bent	Lognormal	350300	0.001
K_{td} (kN/m)	Double-column bent	Lognormal	175100	0.003
Rotational stiffness				
K_{rs}	Single-column bent	Lognormal	9040000	0.031
K_{rd}	Double-column bent	Lognormal	1360000	0.206

The pier drift is of concern, and the maximum pier drift is expressed by:

$$D_{\max} = \max_{1 \le i \le 7} \left(\Delta_i^{\text{Pier top}} \right) \tag{6-11}$$

where $\Delta_i^{\text{Pier top}}$ represents the top displacement of the *i*-th pier.

The stochastic seismic can be simulated by the spectrum representation method (Liu et al., 2016):

$$a(t) = \sqrt{2} \sum_{k=0}^{d_1 - 1} \sqrt{2 S_A(w_k, t) \Delta w} \left[w_k t + \phi_k \right] \tag{6-12}$$

in which $S_A(w,t)$ is the double-sided evolutionary power spectral density function of time *t* and frequency *w*:

$$S_A(w,t) = \left| A(w,t) \right|^2 S(w) \tag{6-13}$$

where $A(w,t)$ is a modulating function defined as:

$$A(w,t)=\exp\left(-\eta_0\frac{wt}{w_a t_a}\right)\cdot\left[\frac{t}{c}\exp\left(1-\frac{t}{c}\right)\right]^2 \tag{6-14}$$

and $S(w)$ is the one-sided power spectral density function given as:

$$S(w)=\frac{w_g^4+4\zeta_g^2 w_g^2 w^2}{\left(w^2-w_g^2\right)^2+4\zeta_g^2 w_g^2 w^2}\cdot\frac{w^4}{\left(w^2-w_f^2\right)^2+4\zeta_f^2 w_f^2 w^2}S_0 \tag{6-15}$$

The phase angle ϕ_k s follow independent uniform distributions with support on the interval $[0,2\pi]$. In this paper, the dimension of the random variables involved in the stochastic seismic excitations are 1001, i.e., $n_1=1001$. The other parameters involved in the stochastic process can be specified by the follows: $\Delta t=0.02$ s and $T=$ 30 s; $\eta_0=0.15$, $w_a=5\pi$ rad/s, $t_a=30$ s and $c=9$; $w_g=w_a$, $w_f=0.1w_g$, $\zeta_g=\zeta_f=0.60$ and $S_0=48.9332$ cm^2/s. The representative seismic excitations are shown in Figure 6-5.

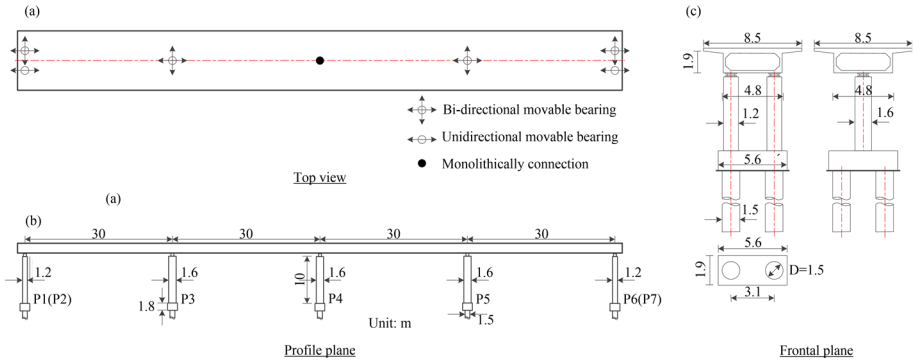

Figure 6-3 A highway bridge

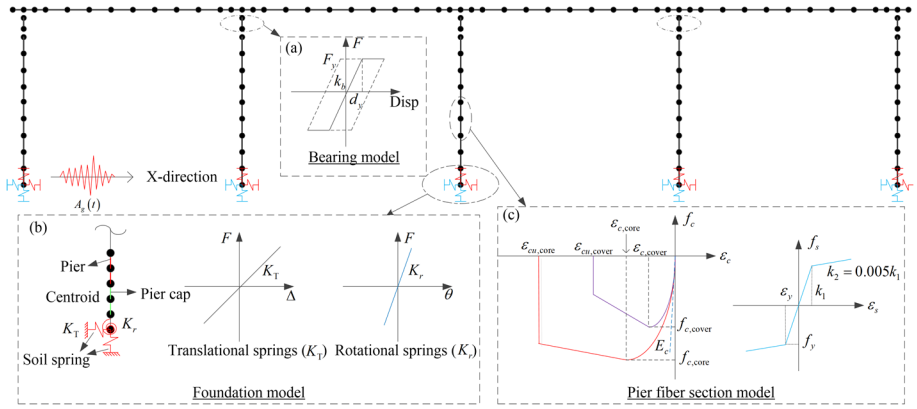

Figure 6-4 Finite element model of the highway bridge

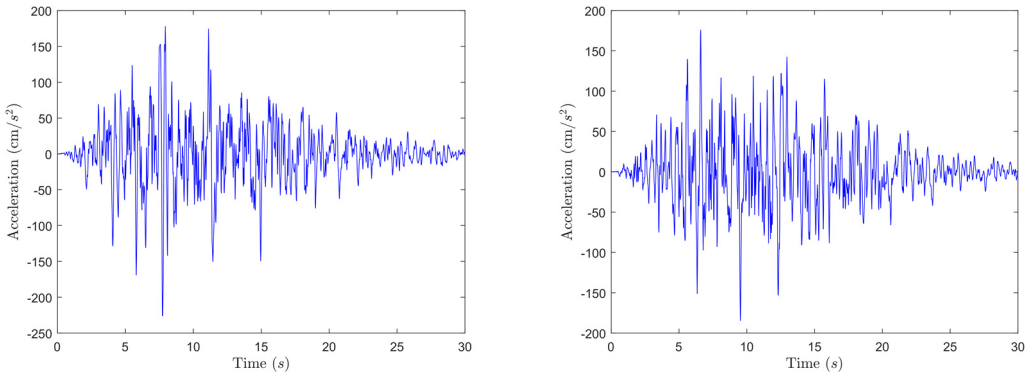

(a) Sample 1 (b) Sample 2

Figure 6-5 Representative samples of the stochastic seismic excitation

6.3.2 PhyrLSTM for metamodeling of the highway bridge

The structures of rLSTM network 1 and network 2 are specified as follows: both networks have 2 LSTM layers, two fully-connected neural network layers, and a hidden state size of 50. The input feature size for rLSTM network 1 is 30 (comprising 29 random structural parameters and 1 dimension for the seismic excitation), and its output dimension is 3. The input dimension for rLSTM network 2 is 32 (comprising 29 random structural parameters and the 3 predicted outputs from rLSTM network 1). The output feature size for rLSTM network 2 is 1. A learning rate of 0.01 and the

Adam optimizer are adopted. The user-defined weights for data, equality, and governing equation losses are 1, 0.1, and 0.1, respectively. The normal rLSTM network used for comparisons has the same structure as rLSTM network 1. A total of 10000 test samples are employed to validate the performance of the proposed PhyrLSTM network.

First, 200 observed samples are used to train both the normal rLSTM and PhyrLSTM networks, with 160 samples for training and 40 for validation. The batch size is set to 80, and the number of epochs is specified as 2000. The samples are generated using the Latin hypercube sampling technique. During the training process, the best neural network, i.e., the one with the smallest validation loss, is saved. To account for variability due to the random seed, we train the rLSTM and PhyrLSTM networks 20 times. Figure 6-6 illustrates three representative training and validation loss curves, highlighting the varying accuracy of the rLSTM models. The determination coefficients (R^2) on 200 observed samples for rLSTM, as shown in Figure 6-6 (a), (b), and (c), are -1.70, 0.44, and 0.85, respectively. In contrast, the PhyrLSTM model consistently achieves higher R^2 values of 0.93, 0.92, and 0.93, respectively. As seen in the figures, the training loss for the normal rLSTM is nearly identical to that of PhyrLSTM. However, the validation loss for the normal rLSTM network is significantly larger than that for the PhyrLSTM. Thus, embedding physical knowledge into the neural network can significantly improve its generalization ability. To validate that PhyrLSTM can learn the underlying physics, the equality loss and governing equation loss are depicted in Figure 6-7. Both losses approach zero as the training progresses.

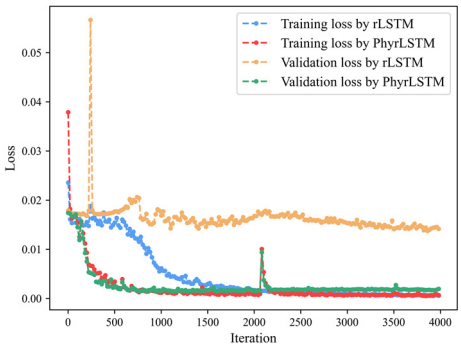

(a) Random Seed 1

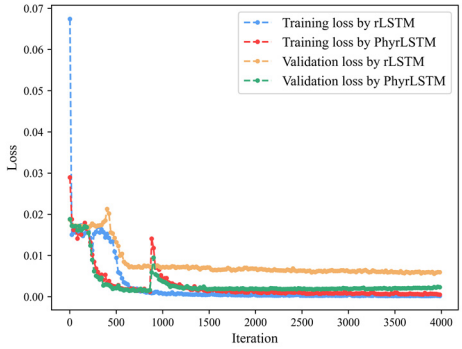

(b) Random Seed 2

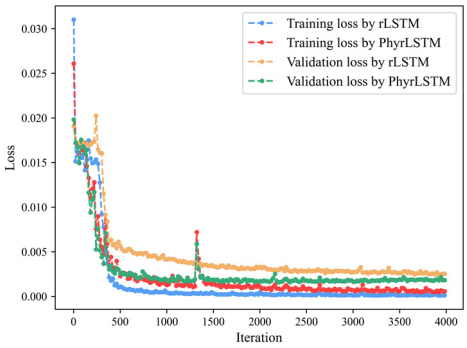

(c) Random Seed 3

Figure 6-6 Training and validation losses (trained by 200 samples)

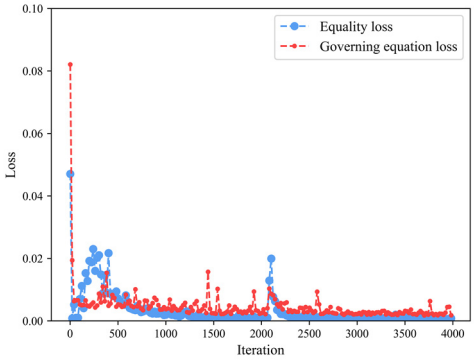

(a) Random Seed 1

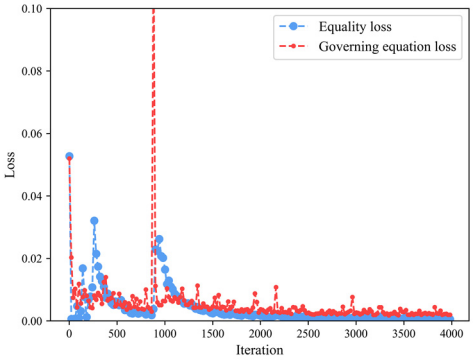

(b) Random Seed 2

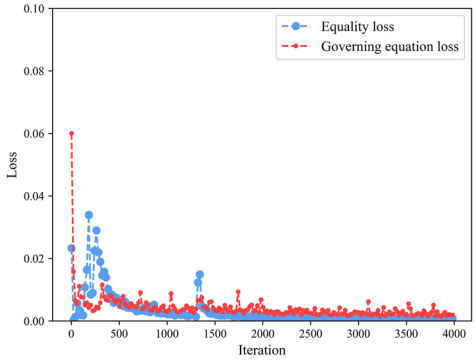

(c) Random Seed 3

Figure 6-7 Physical loss (trained by 200 samples)

Figure 6-8 presents representative training, validation, and test samples. The time history displacement curves predicted by the PhyrLSTM model align more closely with the reference results. As shown Figure 6-8 (c) and (d), the PhyrLSTM significantly outperforms the rLSTM. Figure 6-9 compares the extreme responses predicted by the three typical rLSTM and PhyrLSTM models for the training and test samples. The determination coefficients (R^2) are provided in the figure. The PhyrLSTM consistently achieves higher R^2 values on both the training and test sets compared to the rLSTM. A negative R^2 value indicates that the rLSTM is not suitable for modeling the test data.

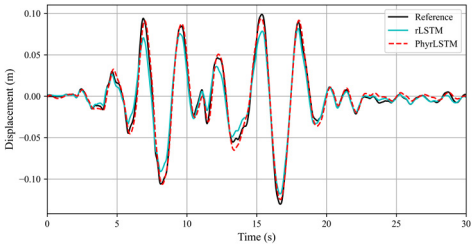

(a) Training sample

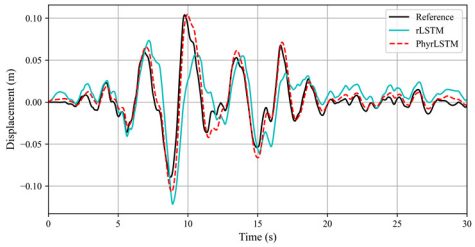

(b) Validation sample

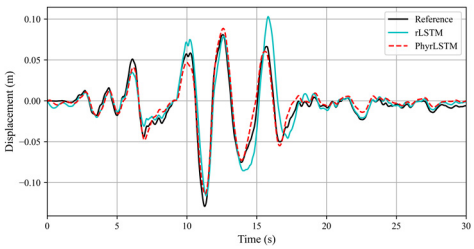

(c) Test sample 1

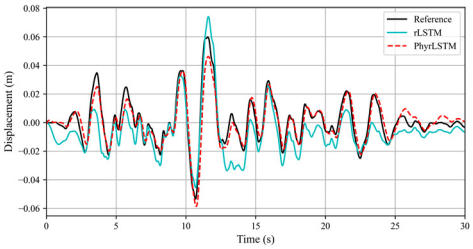

(d) Test sample 2

Figure 6-8 Time history responses by rLSTM and PhyrLSTM (trained by 200 samples)

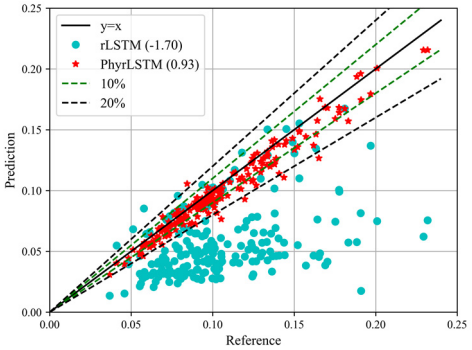

(a) Random Seed 1 (Training)

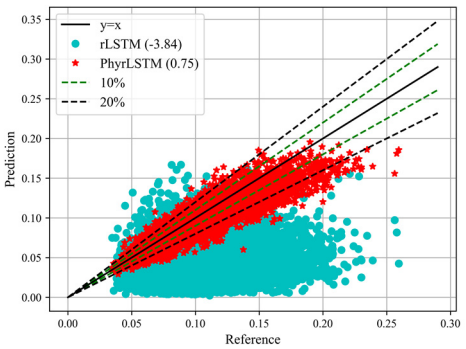

(b) Random Seed 1 (Test)

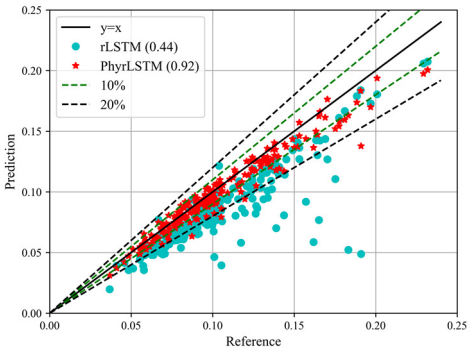

(c) Random Seed 2 (Training)

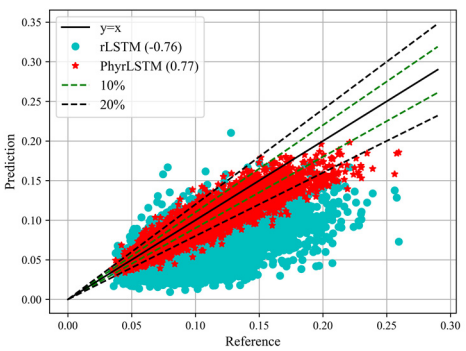

(d) Random Seed 2 (Test)

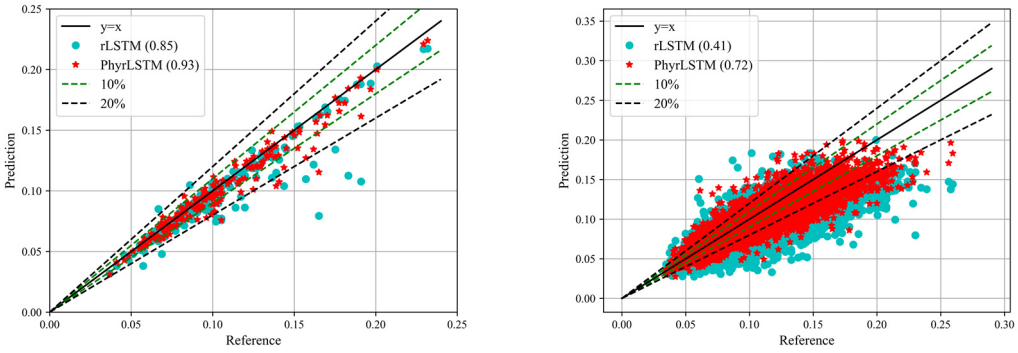

(e) Random Seed 3 (Training)

(f) Random Seed 3 (Test)

Figure 6-9 The extreme responses by rLSTM and PhyrLSTM (trained by 200 samples)

Three commonly used metrics, i.e., mean absolute error (MAE), root mean squared error (RMSE) and the determination coefficient (R^2), are utilized to assess the performance of rLSTM and PhyrLSTM. The boxplots of these metrics across 20 rounds of training are shown in Figure 6-10. The notation "MAE-r" refers to the MAE obtained from rLSTM, while "MAE-P" corresponds to the MAE from PhyrLSTM, and similar notation applies to the other metrics. To clearly display boxplots of different metrics, each metric is normalized by its maximum absolute value. The normalized metrics are represented by red points in the figure. Note that R^2 calculated by rLSTM contains negative values, so the normalization for R^2 is handled separately for positive and negative values. The values of three metrics from 200 observed samples and 10000 test samples are listed in Table 6-2 and Table 6-3, respectively. According to the boxplots, PhyrLSTM demonstrates greater stability compared to rLSTM. The variation in MAE, RMSE and R^2 for PhyrLSTM is minimal, whereas these metrics for rLSTM exhibit a wide range of scatter. Additionally, the normalized MAE, RMSE and R^2 values are closely concentrated near 0, 0, and 1, respectively, indicating that PhyrLSTM offers greater accuracy compared to the standard rLSTM.

Note that R^2 values for rLSTM include several negative values, suggesting that the trained rLSTM model is not well-suited for representing the observed samples. Based on the results in Table 6-2 and Table 6-3, R^2 values by PhyrLSTM are consistently around 0.9 with 200 samples and around 0.7 with 10000 test samples. In most cases, R^2 values by rLSTM are smaller than those for PhyrLSTM.

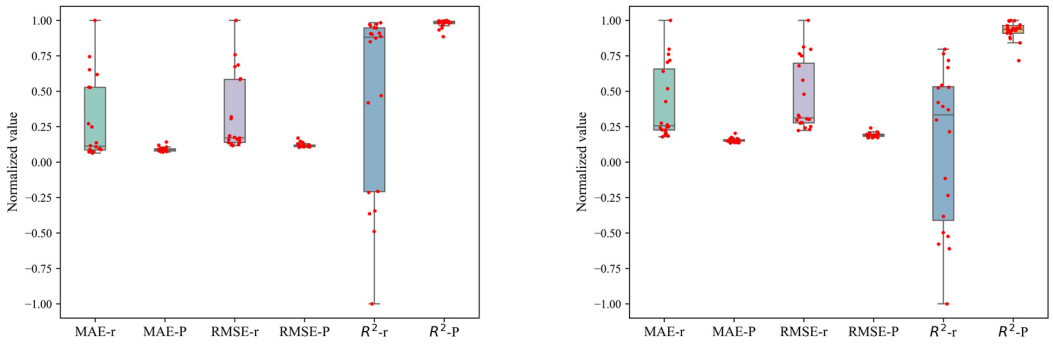

(a) Training and validation sets

(b) Test set

Figure 6-10 Performance of rLSTM and PyrLSTM (trained by 200 samples)

Table 6-2 The accuracy of rLSTM and PhyrLSTM on training and validation sets (trained by 200 samples)

No.	MAE-r	MAE-P	RMSE-r	RMSE-P	R^2-r	R^2-P
1	0.0077	0.0058	0.0144	0.0098	0.8430	0.9279
2	0.0076	0.0061	0.0142	0.0093	0.8476	0.9345
3	0.0810	0.0061	0.0889	0.0098	-4.9515	0.9282
4	0.0528	0.0070	0.0610	0.0096	-1.8022	0.9308
5	0.0059	0.0086	0.0124	0.0124	0.8846	0.8848
6	0.0501	0.0073	0.0599	0.0098	-1.7038	0.9274
7	0.0111	0.0077	0.0165	0.0104	0.7941	0.9182
8	0.0202	0.0072	0.0273	0.0102	0.4391	0.9211
9	0.0059	0.0067	0.0111	0.0105	0.9074	0.9164
10	0.0072	0.0075	0.0141	0.0104	0.8509	0.9180
11	0.0062	0.0116	0.0110	0.0151	0.9085	0.8275
12	0.0061	0.0064	0.0116	0.0095	0.8985	0.9322
13	0.0429	0.0081	0.0518	0.0116	-1.0181	0.8987
14	0.0220	0.0068	0.0284	0.0097	0.3913	0.9299
15	0.0072	0.0060	0.0123	0.0096	0.8862	0.9304
16	0.0603	0.0073	0.0674	0.0099	-2.4191	0.9265
17	0.0095	0.0064	0.0156	0.0103	0.8176	0.9197
18	0.0427	0.0070	0.0523	0.0104	-1.0604	0.9186

Table 6-2 (continued) The accuracy of rLSTM and PhyrLSTM on training and validation sets (trained by 200 samples)

No.	MAE-r	MAE-P	RMSE-r	RMSE-P	R^2-r	R^2-P
19	0.0052	0.0096	0.0104	0.0131	0.9191	0.8717
20	0.0088	0.0074	0.0151	0.0111	0.8288	0.9064

Table 6-3 The accuracy of rLSTM and PhyrLSTM on test set (trained by 200 samples)

No.	MAE-r	MAE-P	RMSE-r	RMSE-P	R^2-r	R^2-P
1	0.0193	0.0125	0.0253	0.0168	0.3263	0.7025
2	0.0181	0.0122	0.0237	0.0164	0.4094	0.7192
3	0.0793	0.0126	0.0853	0.0168	-6.6394	0.7046
4	0.0509	0.0109	0.0580	0.0148	-2.5369	0.7700
5	0.0198	0.0131	0.0261	0.0174	0.2861	0.6819
6	0.0604	0.0117	0.0679	0.0154	-3.8375	0.7500
7	0.0218	0.0122	0.0282	0.0163	0.1660	0.7198
8	0.0339	0.0110	0.0409	0.0147	-0.7589	0.7745
9	0.0154	0.0139	0.0206	0.0182	0.5556	0.6521
10	0.0181	0.0119	0.0238	0.0159	0.4057	0.7345
11	0.0162	0.0161	0.0215	0.0206	0.5166	0.5548
12	0.0142	0.0110	0.0191	0.0147	0.6176	0.7723
13	0.0570	0.0118	0.0653	0.0156	-3.4782	0.7452
14	0.0411	0.0120	0.0494	0.0160	-1.5615	0.7329
15	0.0178	0.0108	0.0235	0.0147	0.4210	0.7734
16	0.0632	0.0120	0.0694	0.0160	-4.0522	0.7320
17	0.0200	0.0123	0.0257	0.0163	0.3044	0.7195
18	0.0559	0.0122	0.0640	0.0165	-3.2964	0.7157
19	0.0147	0.0134	0.0197	0.0176	0.5924	0.6747
20	0.0209	0.0119	0.0271	0.0160	0.2304	0.7320

Then, 1000 observed time history responses are employed for training the rLSTM and PhyrLSTM, among which 800 samples are allocated to training set and 200 samples to validation set. Similarly, the rLSTM and PhyrLSTM models are each trained 20 times to account for variability. Three representative results are presented in Figure 6-11. The R^2 values on 1000 training and validation samples for rLSTM, as indicated in Figure 6-11 (a), (b) and (c), are -4.00, 0.71 and 0.94, respectively, while those for PhyrLSTM are 0.95, 0.95 and 0.96, respectively. Due to the influence of random seeds, the training process of the rLSTM is less stable than that of the PhyrLSTM, even when 1000 observed samples are used for training. As shown in

Figure 6-12, the reduction in physical loss demonstrates that the PhyrLSTM effectively captures the underlying physics. The extreme responses by training and test samples are shown in Figure 6-13. The determination coefficients for rLSTM on both training set and test set are lower than those by the PhyrLSTM, indicating the higher accuracy of the PhyrLSTM. Additionally, the relative errors for the PhyrLSTM predominantly fall within the 20% error bounds, whereas those for the rLSTM are more unstable.

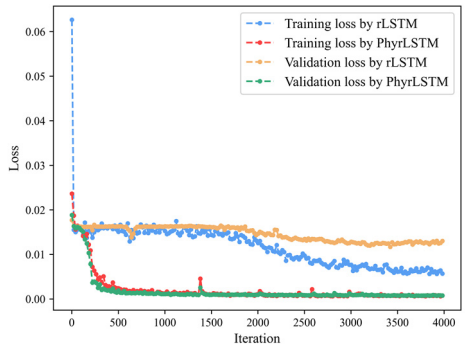

(a) Random Seed 1

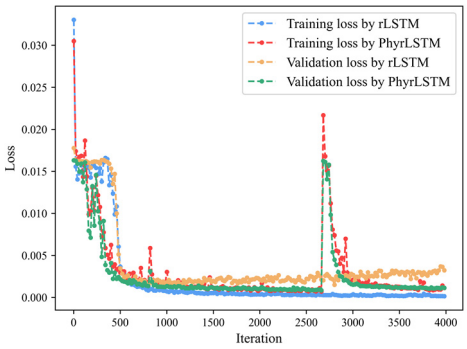

(b) Random Seed 2

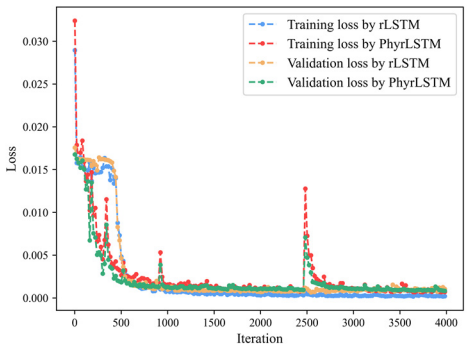

(c) Random Seed 3

Figure 6-11 Training and validation losses (trained by 1000 samples)

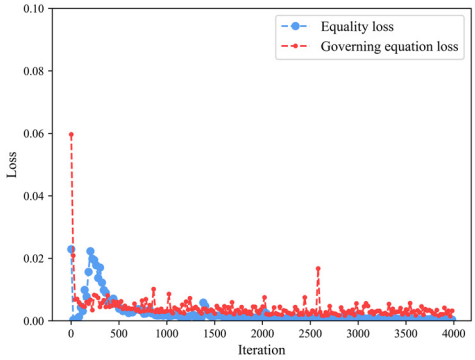

(a) Random Seed 1

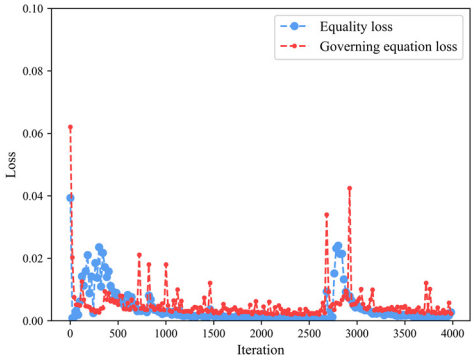

(b) Random Seed 2

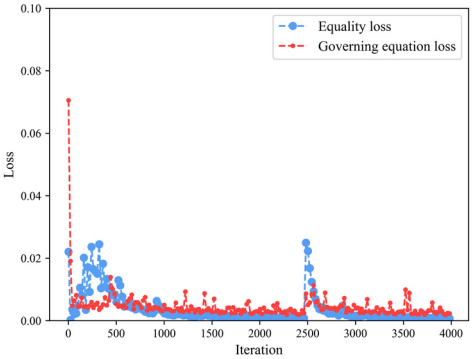

(c) Random Seed 3

Figure 6-12 Physical loss (trained by 1000 samples)

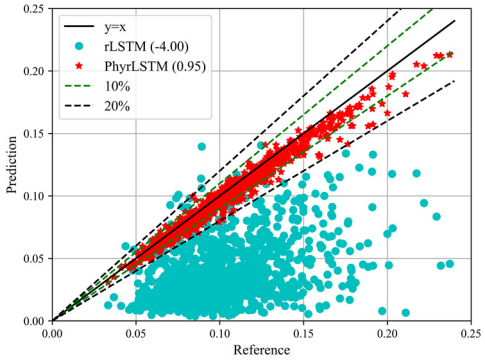

(a) Random Seed 1 (Training)

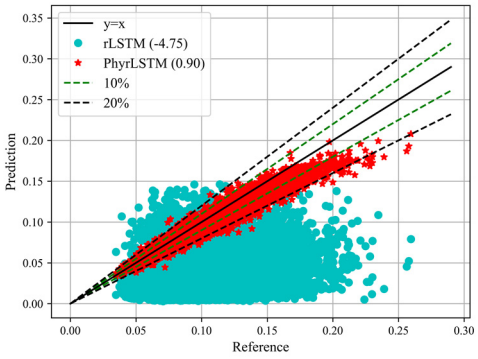

(b) Random Seed 1 (Test)

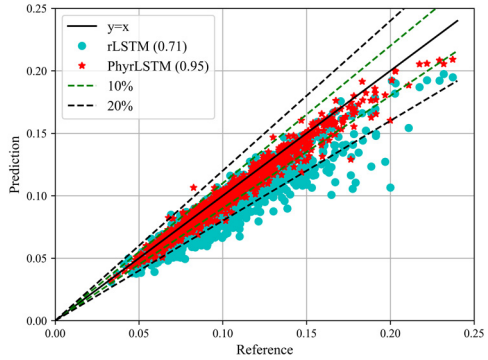

(c) Random Seed 2 (Training)

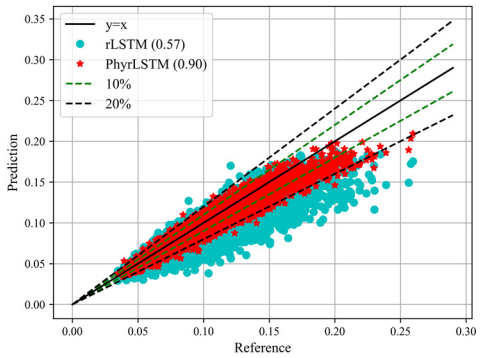

(d) Random Seed 2 (Test)

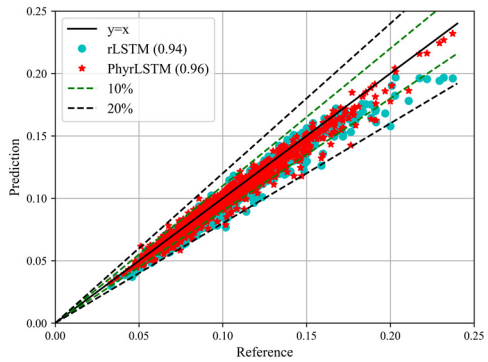

(e) Random Seed 3 (Training)

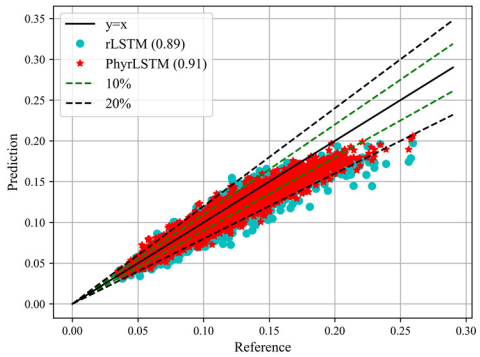

(f) Random Seed 3 (Test)

Figure 6-13 The extreme responses by rLSTM and PhyrLSTM (trained by 1000 samples)

The boxplots of three metrics are depicted in Figure 6-14. The normalized MAE and RMSE values produced by PhyrLSTM are tightly clustered near 0, and the normalized R^2 values are concentrated near 1. In contrast, the normalized values produced by rLSTM exhibit significant variability. Moreover, the values of the three metrics on training and test sets are listed in Table 6-4 and Table 6-5, respectively. The accuracy has significantly improved compared to models trained with only 200 observed samples. The R^2 values obtained from PhyrLSTM consistently exceed 0.9, indicating a high level of accuracy in predicting time history responses. However, rLSTM does not achieve the same level of accuracy or stability in its predictions. It

can be found in Table 6-4 that 8 rLSTM models produce negative R^2 values, which means unacceptable errors are generated by these rLSTM models. Consequently, the results demonstrate that even with 1000 observed samples, neural networks lacking physical knowledge still do not perform as well as the PhyrLSTM for metamodeling of the highway bridge.

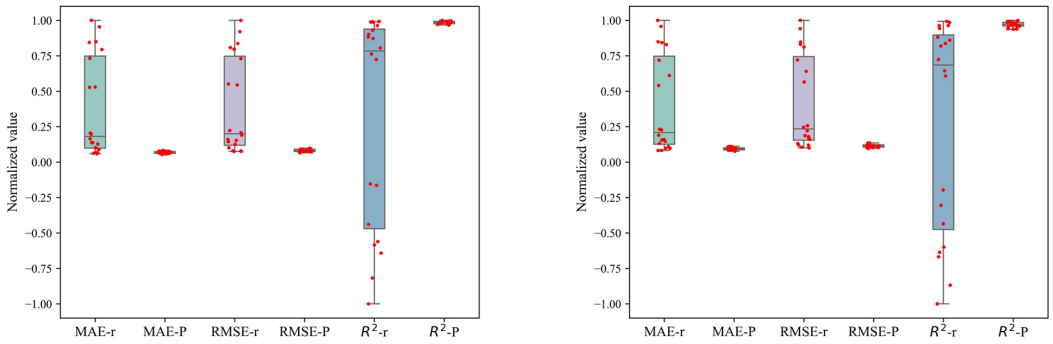

(a) Training and validation sets

(b) Test set

Figure 6-14 Performance of rLSTM and PyrLSTM (trained by 1000 samples)

Table 6-4 The accuracy of rLSTM and PhyrLSTM on training and validation sets (trained by 1000 samples)

No.	MAE-r	MAE-P	RMSE-r	RMSE-P	R^2-r	R^2-P
1	0.0358	0.0056	0.0430	0.0077	-0.8002	0.9424
2	0.0060	0.0047	0.0079	0.0063	0.9391	0.9609
3	0.0094	0.0044	0.0124	0.0061	0.8494	0.9639
4	0.0112	0.0041	0.0149	0.0058	0.7853	0.9669
5	0.0093	0.0042	0.0120	0.0062	0.8609	0.9622
6	0.0572	0.0047	0.0630	0.0064	-2.8600	0.9600
7	0.0044	0.0044	0.0062	0.0060	0.9625	0.9654
8	0.0647	0.0052	0.0717	0.0071	-4.0029	0.9509
9	0.0538	0.0037	0.0620	0.0052	-2.7454	0.9741
10	0.0041	0.0042	0.0060	0.0058	0.9655	0.9677
11	0.0134	0.0053	0.0174	0.0071	0.7060	0.9511
12	0.0576	0.0045	0.0653	0.0062	-3.1425	0.9630
13	0.0045	0.0039	0.0062	0.0054	0.9632	0.9711
14	0.0677	0.0041	0.0779	0.0058	-4.8978	0.9676
15	0.0496	0.0040	0.0569	0.0057	-2.1513	0.9686
16	0.0359	0.0052	0.0424	0.0071	-0.7506	0.9516
17	0.0139	0.0052	0.0162	0.0074	0.7432	0.9467
18	0.0069	0.0045	0.0098	0.0063	0.9069	0.9619
19	0.0043	0.0050	0.0059	0.0073	0.9665	0.9481
20	0.0087	0.0049	0.0112	0.0067	0.8776	0.9568

Table 6-5 The accuracy of rLSTM and PhyrLSTM on test set (trained by 1000 samples)

No.	MAE-r	MAE-P	RMSE-r	RMSE-P	R^2-r	R^2-P
1	0.0422	0.0077	0.0504	0.0106	-1.6638	0.8815
2	0.0075	0.0068	0.0104	0.0093	0.8868	0.9083
3	0.0111	0.0063	0.0148	0.0086	0.7708	0.9221
4	0.0131	0.0064	0.0174	0.0091	0.6810	0.9135
5	0.0108	0.0065	0.0142	0.0090	0.7877	0.9143
6	0.0573	0.0068	0.0638	0.0096	-3.2776	0.9032
7	0.0067	0.0059	0.0095	0.0082	0.9055	0.9288
8	0.0661	0.0071	0.0740	0.0097	-4.7486	0.9009
9	0.0587	0.0053	0.0666	0.0076	-3.6531	0.9400
10	0.0067	0.0058	0.0095	0.0081	0.9062	0.9316
11	0.0157	0.0069	0.0202	0.0094	0.5716	0.9073
12	0.0582	0.0060	0.0653	0.0084	-3.4785	0.9262
13	0.0057	0.0058	0.0079	0.0081	0.9342	0.9311
14	0.0690	0.0060	0.0785	0.0084	-5.4751	0.9252
15	0.0497	0.0058	0.0567	0.0083	-2.3755	0.9282
16	0.0374	0.0072	0.0444	0.0099	-1.0717	0.8980
17	0.0161	0.0077	0.0194	0.0105	0.6059	0.8834
18	0.0091	0.0064	0.0128	0.0090	0.8290	0.9152
19	0.0058	0.0074	0.0083	0.0105	0.9273	0.8845
20	0.0102	0.0066	0.0135	0.0091	0.8093	0.9136

6.3.3 Adaptive Kriging incorporated with PhyrLSTM for dynamic reliability analysis of the highway bridge

It is known that the reliability analysis requires a highly accurate surrogate model for failure probability estimation while the observed data is usually insufficient for training such a model. Active learning strategy can select the samples in the vicinity of the limit state surface so that we can build an adaptive Kriging model. Once the surrogate model for the limit state surface is constructed, the signs of samples in failure or safe region can be identified. Hence, a surrogate model across the entire region is not necessary by leveraging the adaptive Kriging model, as the exact values of samples far away from the limit state surface are not important as long as the signs of them are correctly identified.

Similarly, extreme responses, i.e., the maximum pier drift, are of interest. First, we need to reconstruct extreme responses using a Kriging model. As introduced in chapter 5, a low-dimensional latent space can be detected using the rLSTM-AE network. Herein, the rLSTM-AE is replaced by the PhyrLSTM-AE. The autoencoder's structure remains the same as in the rLSTM-AE. Denote the dimension of the detected latent variables as d_z. The encoding function of AE is a fully connected neural network with three layers, containing $4d_z$, $2d_z$ and d_z nodes, respectively. The corresponding decoding function is also a three-layer fully connected neural network and each layer contains $2d_z$, $4d_z$ and 1 nodes, respectively. The activation function is adopted as ReLU. For details on implementation, please refer to Algorithm 3 in chapter 5.

Herein, a PhyrLSTM network with a R^2 of 0.97 on 1000 observed samples is selected. Figure 6-15 illustrates the accuracy of the selected PhyrLSTM on both training and test sets. Figure 6-15 (b) reveals that the relative errors of the predicted extreme responses are mostly within 20%. First, the low dimensional latent variables need to be identified. During the training of the autoencoder, exact extreme values from the 1000 observed samples can be used. For unobserved samples, approximate extreme values predicted by the PhyrLSTM can be employed to identify an approximate latent space.

Figure 6-16 shows Kriging reconstruction error defined by Eq. (5-21), which calculated by 1000 observed samples. The dimension of the latent variables is specified from 2 to 20 when training the autoencoder. 100 training samples are

adopted for constructing the Kriging model. The red point denotes the minimum value of the construction error, with the optimal latent variable dimension being 6.

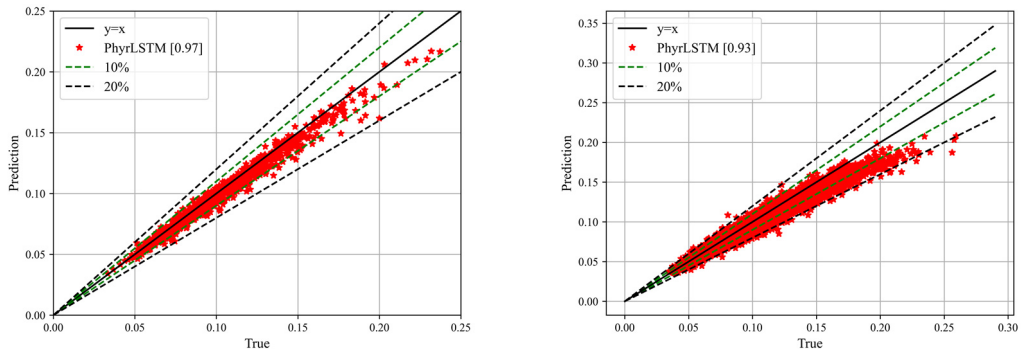

(a) Training and validation (1000 samples) (b) Test (10000 samples)

Figure 6-15 The performance of the selected PhyrLSTM network

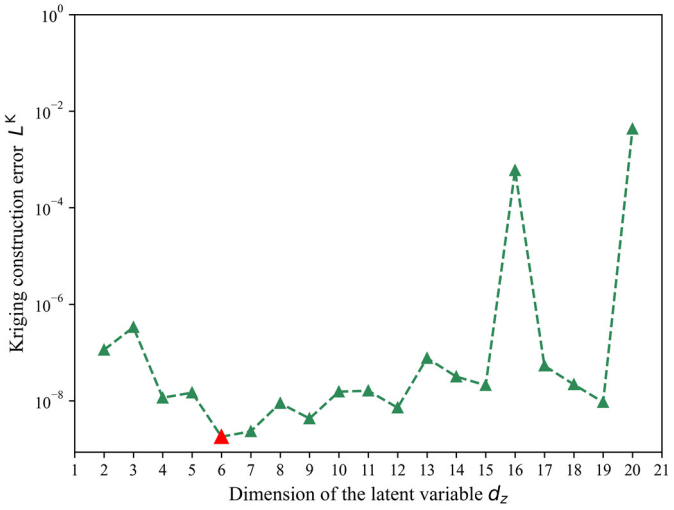

Figure 6-16 Kriging construction error

The performance of the trained autoencoder and the constructed Kriging are plotted in Figure 6-17. The notation AE-K denotes that Kriging is built on the basis of detected latent variables by AE. PhyrLSTM-AE-K refers to Kriging constructed using latent variables detected from the approximate extreme value space by the PhyrLSTM.

Figure 6-17 (a) shows the accuracy of the trained autoencoder and constructed Kriging based on the detected latent variables from the observed extreme values (1000 observed samples). It can be observed that both the trained autoencoder and Kriging well describe the observed extreme value space. Figure 6-17 (b) reflects the performance of the trained autoencoder and the Kriging in reconstructing 10000 approximate extreme values by PhyrLSTM. Both the extreme values predicted by the trained autoencoder and the constructed Kriging align well with those predicted by the PhyrLSTM, demonstrating that Kriging with the detected latent variables effectively reconstructs the approximate extreme value space. Compared to the true test extreme values, the Kriging model achieves nearly the same accuracy as the PhyrLSTM, indicating that Kriging can serve as a substitute for the PhyrLSTM in extreme response prediction. This capability enhances the applicability of the active learning strategy for dynamic reliability analysis of stochastic systems.

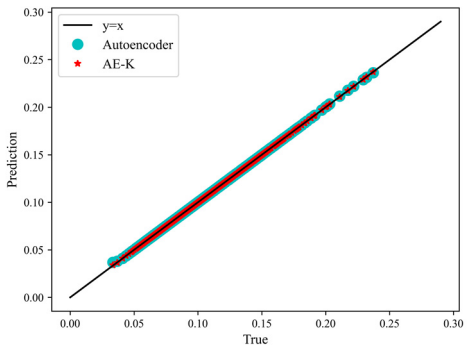

(a) Compared to true training samples

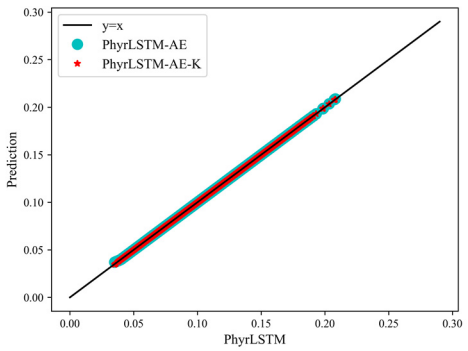

(b) Compared to PhyrLSTM (test samples)

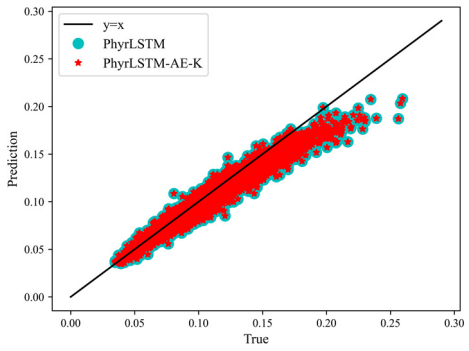

(c) Compared to true test samples

Figure 6-17 The accuracy of the PhyrLSTM and PhyrLSTM-AE-K

Once the latent variables are obtained, the active learning strategy can be employed to build an adaptive Kriging model. The threshold of the maximum pier drift is set to 0.15 m in case 1 and the failure probability by 2×10^4 MCS is 7.07×10^{-2}. The candidate pool for the active learning-based Kriging is also set to 2×10^4, allowing for comparison with the reference results provided by MCS. An initial Design of Experiments (DoE) for the Kriging model consists of 100 training samples. The U learning function and U stopping criterion defined in chapter 5 are used to enrich the DoE. The proposed method, which integrates PhyrLSTM with the autoencoder and the adaptive Kriging, is denoted as PhyrLSTM-AE-AK. The convergence curve for case 1 is plotted in Figure 6-18 (a). It can be observed that the failure probability converges to the reference line as the sample size increase. The enrichment process stops after adding 324 samples. The estimated failure probability is 7.07×10^{-2} with a relative error of 6.85%. Besides, two moments methods, MIGLD (Dang & Xu, 2020) and MEM (Li & Zhang, 2011), are adopted to estimate the failure probability for comparisons. Both methods consume 1000 calls to the finite element model and produce relative errors of 17.35% and 13.68%, respectively. PhyrLSTM

and PhyrLSTM-AE-K are also employed for failure probability estimation, however, the relative errors by them exceed 40%. The proposed PhyrLSTM-AE-AK, requiring 1324 finite element model evaluations, achieves significantly improved accuracy with a relative error of 6.85%.

Case 2 investigates a failure probability of 6.15×10^{-3} by 2×10^{4} MCS. The convergency curve shown in Figure 6-18 (b) reveals that the accuracy is continuously improved by the active learning strategy. The results are listed in Table 6-6. The active learning process terminates when 224 samples are added into the DoE. PhyrLSTM-AE-AK estimates the failure probability at 5.37×10^{-3} with a relative error of 12.74%. Both MEM and MIGLD yield unsatisfactory results, with relative errors of 48.58% and 46.07%, respectively. The PhyrLSTM model, trained with 1000 samples, is insufficient for reliability analysis, exhibiting a relative error of 95.12%. The Kriging model based on the detected latent variables performs nearly identically to PhyrLSTM in predicting extreme responses, resulting in the same relative error for PhyrLSTM-AE-K as for PhyrLSTM.

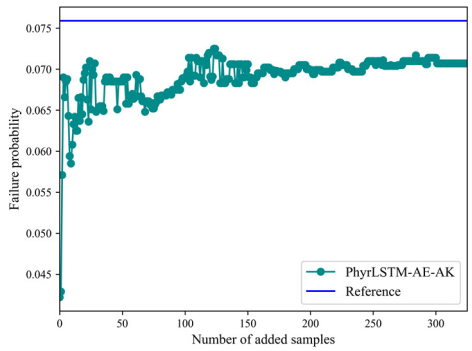

(a) Case 1

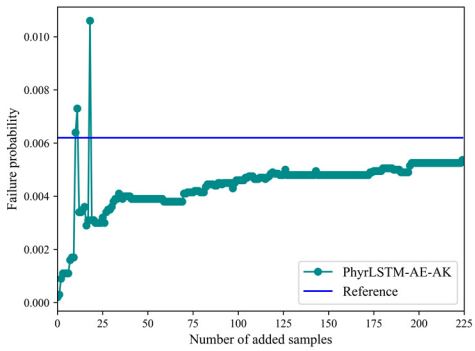

(b) Case 2

Figure 6-18 Failure probabilities estimation for the highway bridge

Table 6-6 Results by different methods for the highway bridge

	Method	N_{call}	P_f	CoV(%)	R.E. (%)
Case 1	MCS	2×10^4	7.59×10^{-2}	2.47	–
	MEM	1000	8.91×10^{-2}	–	17.35
	MIGLD	1000	8.63×10^{-2}	–	13.68
	PhyrLSTM	1000	4.28×10^{-2}	3.44	43.61
	PhyrLSTM-AE-K	1000	4.30×10^{-2}	3.34	43.41
	PhyrLSTM-AE-AK	1324	7.07×10^{-2}	4.42	6.85
Case 2	MCS	2×10^4	6.15×10^{-3}	8.99	–
	MEM	1000	9.14×10^{-3}	–	48.58
	MIGLD	1000	8.98×10^{-3}	–	46.07
	PhyrLSTM	1000	3.00×10^{-4}	40.82	95.12
	PhyrLSTM-AE-K	1000	3.00×10^{-4}	40.82	95.12
	PhyrLSTM-AE-AK	1224	5.37×10^{-3}	9.73	12.74

6.4 Summary

The metamodeling of a stochastic highway bridge system is investigated in this chapter. The stochastic seismic excitation is generated by the spectrum representation method, leading to a high-dimensional stochastic system. To build the surrogate model for this system, rLSTM network is utilized. However, conventional rLSTM networks rely solely on observed data, neglecting the underlying physical knowledge. To address this, a physics-informed rLSTM (PhyrLSTM) is proposed to incorporate the governing dynamics equations. Additionally, the PhyrLSTM can embed uncertain structural parameters into the network, allowing it to model an uncertain governing equation. When only 200 observed data points are utilized, the rLSTM, which lacks physical knowledge, exhibits reduced accuracy on the validation and test sets and the results are unstable. In contrast, the PhyrLSTM demonstrates superior predictive performance on the unobserved data. Even with an increase to 1000 observed data points, the rLSTM still lacks training reliability and, in most cases, is not as accurate as the PhyrLSTM. Consequently, PhyrLSTM provides a more

reliable and accurate surrogate model for the highway bridge. However, this accuracy is still insufficient for dynamic reliability analysis. To address this, an autoencoder is used to detect a latent space for the approximate extreme value space by PhyrLSTM. Subsequently, an adaptive Kriging model is constructed using the active learning strategy. The results demonstrate that the accuracy of failure probability estimation is significantly improved with PhyrLSTM-AE-AK.

CHAPTER 7 AN ERROR-BASED OFFLINE LEARNING STRATEGY FOR DYNAMIC RELIABILITY ANALYSIS INCORPORATED WITH RLSTM

7.1 Introduction

Adaptive Kriging model has been widely used in structural reliability analysis since it can significantly reduce the computational effort by leveraging the active learning strategy. Typically, the design of experiments is enriched incrementally, requiring the computational model to provide labels for newly added points. This iterative process can become extremely time-consuming. Although multi-point enrichment strategies have been proposed, the updating process of the surrogate model cannot be completed in a single step, continuously requiring new information from the computational model, which can be regarded as an online learning strategy. This approach, however, impedes parallel computing and significantly increases computational effort. In this chapter, a so-called offline learning strategy is introduced. Kriging model can be updated in a single step based on the accuracy of a trained rLSTM network. First, this strategy is validated by a highway bridge model subjected to the stochastic seismic excitation. Then, metamodeling of a practical transmission tower subjected to stochastic wind loads is investigated. Kriging model incorporated with the rLSTM and the offline learning strategy is employed for the dynamic reliability analysis of a transmission tower subjected to stochastic wind loads.

7.2 A prediction error-based offline learning strategy

7.2.1 Conventional online active leaning strategy for adaptive Kriging model

The conventional active learning strategy aims to continuously enrich the DoE through learning functions until the stopping criterion is satisfied. For example, the U learning function reflects the risk of a point crossing the limit sate surface or the probability of the wrong classification:

$$U\left(\mathbf{x}\right)=\frac{\left|\mu_K\left(\mathbf{x}\right)\right|}{\sigma_K\left(\mathbf{x}\right)} \tag{7-1}$$

where $\mu_K\left(\mathbf{x}\right)$ and $\sigma_K^2\left(\mathbf{x}\right)$ are mean and variance predicted by Kriging model, respectively. The probability of wrong classification can be calculated by:

$$P_{\mathrm{w}}\left(\mathbf{x}\right)=\Phi\left(-\frac{\left|\mu_K\left(\mathbf{x}\right)\right|}{\sigma_K\left(\mathbf{x}\right)}\right) \tag{7-2}$$

where Φ is the cumulative distribution function of the standard normal distribution. For example, $U\left(\mathbf{x}\right)=2$ represents that a probability of wrong classification is equal to 2.3%. The next best point is selected by the following:

$$\mathbf{x}^*=\arg\min_{\mathbf{x}\in\Omega}U\left(\mathbf{x}\right) \tag{7-3}$$

meaning the point with the maximum probability of incorrect classification in the entire candidate domain Ω is selected as the best point. Once the best point is selected, the response can be obtained by running the performance function *G:*

$$w = G\left(\mathbf{x}^*\right) \tag{7-4}$$

The U stopping criterion is defined as:

$$\min\left(U\left(\mathbf{x}\right)\right) \geq 2 \tag{7-5}$$

when the stopping criterion is satisfied, the probability of wrong classification on points in the candidate domain is small than 2.3%.

It can be seen that this strategy selects one best point in each step, and then the computational model is called to obtain the corresponding response. The DoE can be updated as:

$$\{\mathcal{X}, \mathcal{W}\} \leftarrow \left\{\left(\mathcal{X}, \mathbf{x}^*\right), \left(\mathcal{W}, G\left(\mathbf{x}^*\right)\right)\right\} \tag{7-6}$$

This learning process continues until the stopping criterion is satisfied, requiring the computational model to continuously provide new information (one point at a time) to update the Kriging model. This strategy does not support parallel computing, making the learning process time-consuming. Although some researchers have proposed multi-point learning strategies to allow parallel computing, such as a selection strategy based on the bounds of the limit state surface that considers the uncertainty of the Kriging model (Schöbi et al., 2017). Kriging model is still hard to be refined in one step and the computational model is still required for the updating process. Moreover, the convergence issue of complex finite element models built by commercial software sometimes makes the active learning process much more complicated. For instance, if one finite element model corresponding to the best point fails to converge, the whole learning process fails.

7.2.2 An offline learning strategy for adaptive Kriging model

It is known that the learning process of AKMCS starts with an initial DoE and the size of the DoE is usually very small, e.g., 12 initial training samples are usually recommended (Echard et al., 2011). Therefore, the Kriging model iteratively obtains information from the computational model to refine itself, particularly focusing on samples near the limit state surface. For the reliability analysis of stochastic dynamic systems, an rLSTM network is first built to approximate the extreme space, which is then used to construct a latent space for the Kriging model. Denote the trained rLSTM model as $\mathcal{M}$, the time history response can be obtained by:

$$\hat{Y}(t) = \mathcal{M}\left(\mathbf{X}_S(t), a(t)\right) \tag{7-7}$$

The extreme response can be obtained by:

$$\hat{Y}_{\text{ev}} = \max\left(\left|\hat{Y}(t)\right|\right) \tag{7-8}$$

where the notation $\mathbf{X}_S(t)$ represents expanded random structural parameters and $a(t)$ denotes external stochastic loads. The latent space for building Kriging model can be found by the autoencoder:

$$\mathbf{Z} = E_{\boldsymbol{\varphi}}\left(\hat{Y}_{\text{ev}}\right) \tag{7-9}$$

where $E_{\boldsymbol{\varphi}}(\cdot)$ is the encoder function of autoencoder and $\boldsymbol{\varphi}$ is the trainable weights and biases of autoencoder. The details of training the rLSTM and autoencoder networks are the same as those in chapter 5.

In addition to providing the approximate extreme value space, the relative errors of the observed data can also be obtained.:

$$\delta_i = \left| \frac{\hat{y}_{\text{ev}}^i - y_{\text{ev}}^i}{y_{\text{ev}}^i} \right| \times 100\% \tag{7-10}$$

where y_{ev}^i is the *i*-th observed data. The core idea of AKMCS is to construct an adaptive Kriging model for the limit state surface with added samples typically located near this surface. However, the process of selecting these "best" points is time-consuming and does not support parallel computing. The limit state surface depends on a given threshold *b*. The relative error of the observed data can help identify samples near the limit state surface. Due to prediction errors, the bounds of the threshold can be defined by:

$$b^- \le \hat{b} \le b^+ \tag{7-11}$$

where $b^- = b(1-\delta)$, $b^+ = b(1+\delta)$. The choice of δ depends on the relative errors of predictions predominantly being within specified error bounds, typically set at 10% or 20%. If the prediction error is too large, the trained rLSTM network may be not suitable for metamodeling of observed data and for latent variables detection. As the Kriging model with latent variables $\mathbf{Z}$ is ultimately employed for extreme responses prediction, the extreme response predicted by Kriging model is utilized to identity samples within threshold bounds. Denote the trained Kriging model as $\mathcal{M}_K$:

$$\hat{Y}_{\text{ev},K} = \mathcal{M}_K(\mathbf{Z}) \tag{7-12}$$

The training of the Kriging model follows the same procedure as described in chapter 5, with an initial DoE size of 100.

Assume a MC candidate pool Ω_{MC} with N_{MC} samples, the latent space $\Omega_{\mathbf{Z}}$ can be determined by Eqs. (7-7), (7-8) and (7-9). Denote samples within the threshold bounds as:

$$\left\{\mathbf{z}_b^j \,|\, b^- \le \hat{y}_{\text{ev},K}^j \le b^+\right\}, j = 1, 2, ..., N_b \tag{7-13}$$

where $\mathbf{z}_b$ is the latent variables identified from the approximate extreme value $\hat{Y}_{\text{ev}}$ and $\mathbf{z}_b \in \Omega_{\mathbf{Z}}$. $\hat{y}_{\text{ev,K}}^j$ is the j-th extreme response predicted by the initial Kriging model. The notation N_b is the number of samples within the threshold bounds. Although the U learning function can select samples near the limit state surface, it is not very efficient and relies on information from the computational model. In contrast, while some samples far from the limit state surface may be chosen, Eq. (7-13) can select samples in a single step and only requires information from the surrogate model. The number of samples within the bounds depends on the number of candidate samples, i.e., N_{MC}. To achieve a target $\text{CoV}\left[\hat{P}_f\right] = 0.1$ given a failure probability $\hat{P}_f$, the number of MCS samples should satisfy:

$$N_{\text{MC}} \ge \frac{1}{\hat{P}_f\left(\text{CoV}\left[\hat{P}_f\right]\right)^2} = \frac{100}{\hat{P}_f} \tag{7-14}$$

The number of failure points can be calculated by:

$$\hat{N}_f = N_{\text{MC}}\hat{P}_f \ge 100 \tag{7-15}$$

The online learning strategy primarily selects samples near the limit sate surface so it may require fewer calls to the computational model. The threshold bounds rely on the prediction error by the trained rLSTM network and the selected samples may include additional samples in both the safe and failure domains. If the bounds encompass the failure domain, the number of samples should be at least 100. To make a reliable estimation of failure probability, it is suggested that $N_b = 100k$ and k can be 1, 2, and etc. Note that k should not be too large since these samples will be embedded into the initial DoE for training Kriging model. N_b can determine the number of required candidate samples, and the candidate pool $\Omega_{\mathbf{Z}}$ is enriched with ΔN samples at each step. Therefore, a threshold of N_b, i.e., $\overline{N}_b = 100k$, is set to determine the candidate pool.

Then, the computational model is called to obtain true responses of the selected samples:

$$y_{\text{ev}}^j = H\left(\mathbf{x}_b^j\right), j = 1, 2, ..., N_b \tag{7-16}$$

where $\mathbf{x}_b^j$ is a sample corresponding to the latent variable $\mathbf{z}_b^j$. $H\left(\cdot\right)$ is the response function defined in chapter 5. Once the selected samples and their corresponding responses are obtained, the Kriging model can be trained in a single step and no longer requires the computational model. This makes it an offline learning strategy and enables the construction of an adaptive Kriging model in one step. Denote the final Kriging model as $\mathcal{M}_K^1$, the extreme responses on the candidate pool $\Omega_{\mathbf{Z}}$ can be calculated as:

$$\hat{y}_{\text{ev},K}^{i} = \mathcal{M}_{K}^{1}\left(\mathbf{z}^{i}\right), i = 1,2,...,N_{\text{MC}} \tag{7-17}$$

Table 7-1 Offline learning strategy for dynamic reliability analysis

Algorithm 5: offline learning strategy for dynamic reliability analysis
Input: b, $\bar{N}_b$, $\delta_{\max}$, $N_b = 0$, and ΔN
Output: the estimated failure probability $\hat{P}_f$
1. **While** $N_b \le \bar{N}_b$
2. Enrich the candidate pool Ω_{MC} with ΔN samples.
3. Generate the corresponding ΔN stochastic loads $a(t)$ and structural random variable $\mathbf{X}_S$.
4. Calculate the extreme response $\hat{y}_{\text{ev}}^{i}, i = 1,2,...,\Delta N$ by Eqs. (7-7) and (7-8).
5. Determine the latent variables $\mathbf{z}^{i} = E_{\boldsymbol{\varphi}}\left(\hat{y}_{\text{ev}}^{i}\right)$ and put them into $\Omega_{\mathbf{Z}}$
6. Calculate the extreme response by an initial Kriging $\hat{y}_{\text{ev},K}^{k} = \mathcal{M}_{K}\left(\mathbf{z}^{k}\right)$
7. Determine the samples within the bounds $\left\{\mathbf{z}_b \mid b^{-} \le \hat{y}_{\text{ev},K} \le b^{+}\right\}$ and denote the size as N_z
8. $N_b = N_b + N_z$
9. **End While**
10. Enrich the initial DoE o by adding $\left\{\mathbf{z}_b, H\left(\mathbf{x}_b\right)\right\}$ and train Kriging model
11. Calculate the failure probability $\hat{P}_f$ by Eq. (7-18)

The failure probability can be readily estimated by:

$$\hat{P}_f = \frac{1}{N_{\text{MC}}} \sum_{i=1}^{N_{\text{MC}}} I\left(y_{\text{ev},K}^{i}\right) \tag{7-18}$$

in which $I(\cdot)$ is an indicator function such that $I = 1$ for $y_{\text{ev},K} \ge b$ and $I = 0$ otherwise.

The algorithm 5 for the proposed offline learning strategy is indicated in Table 7-1.

7.3 Validation of the proposed offline strategy on a stochastic highway bridge model

The proposed offline strategy for adaptive Kriging model construction is first validated on the highway bridge model investigated in chapter 6. An expanded latent space is introduced to facilitate the training of the offline adaptive Kriging model. Subsequently, samples within the threshold bounds are selected based on the prediction error of the PhyrLSTM model established in chapter 6, which helps determine the number of candidate samples. The computational model is evaluated on these selected samples, allowing the Kriging model to be refined in one step. The failure probability can then be readily calculated.

7.3.1 Expanded latent variables for Kriging model

In chapter 5, the latent variables $\mathbf{Z}$ are determined by the rLSTM-AE network, and are based solely on the approximate extreme value space provided by the rLSTM, as described in Eq. (7-9). However, if two different extreme responses predicted by the rLSTM are close to each other due to prediction errors, the latent variables derived from them will also be similar. Therefore, it is beneficial to expand the latent variables using additional prior knowledge. For example, incorporating structural parameters and peak ground motion into the latent space can create a more flexible representation. Note that the latent variables constructed in chapter 5 are derived from normalized extreme responses. Therefore, the expanded latent variable $\mathbf{Z}_E$ can be defined as:

$$\mathbf{Z}_E = \left\{ \mathbf{Z}, \tilde{\mathbf{X}}_S, \tilde{\mathbf{F}} \right\} \tag{7-19}$$

where $\tilde{\mathbf{X}}_S$ and $\tilde{\mathbf{F}}$ are the normalized random structural parameters and the normalized extreme loads, respectively. The performance of the expanded latent variables needs to be validated first. In chapter 5, it was shown that the Kriging model constructed using the latent variables $\mathbf{Z}$ can achieve accuracy comparable to that of the rLSTM. The input variables, consisting of structural parameters and extreme external loads, i.e., $\mathbf{Z}_0 = \left\{\tilde{\mathbf{X}}_S, \tilde{\mathbf{F}}\right\}$, are also investigated. As stated in chapter 5, the optimal dimension for the latent space based on the approximate extreme response space is 6. 29 random structural parameters are of interest for the highway bridge model so the dimensions of $\mathbf{Z}_0$ and $\mathbf{Z}_E$ are 30 and 36, respectively. To validate the accuracy of the expanded latent variables for Kriging reconstruction, 10000 extreme responses predicted by the PhyrLSTM are employed for comparison. Figure 7-1 shows the performance of different latent variables. Kriging models based solely on structural parameters and extreme external loads cannot accurately reconstruct the extreme responses predicted by the PhyrLSTM. Both $\mathbf{Z}$ and $\mathbf{Z}_E$ are capable of accurately reconstructing these extreme responses. As $\mathbf{Z}_E$ contains more features, it will be adopted for Kriging construction.

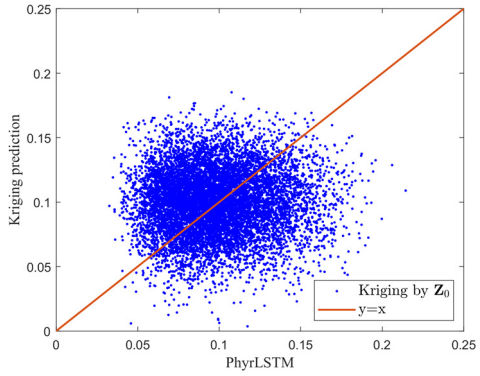

(a) $\mathbf{Z}_0$

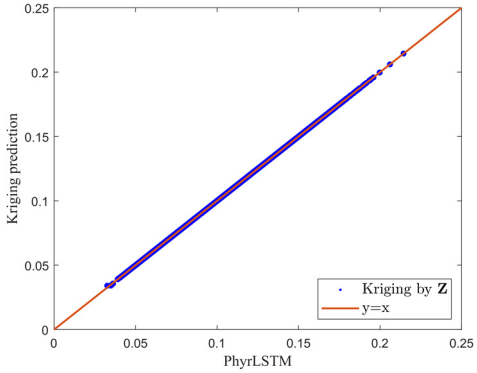

(b) $\mathbf{Z}$

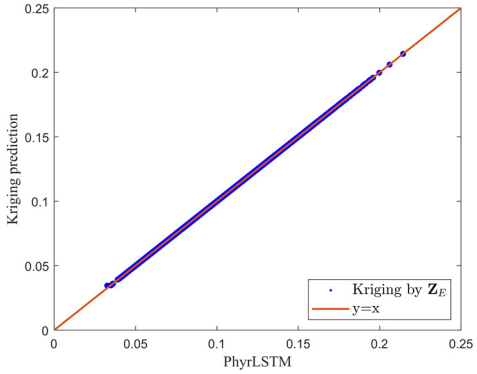

(c) $\mathbf{Z}_E$

Figure 7-1 The performance of different latent variables for the bridge

7.3.2 The proposed offline strategy for dynamic reliability analysis

The trained PhyrLSTM network from chapter 6 is used, and the relative errors are within 20% bounds. Consequently, a 20% prediction error is adopted for selecting samples within the threshold bounds. In algorithm 5, $\bar{N}_b = 300$ and ΔN is specified as 1000.

Case 1 considers a threshold of 0.15. The size of candidate pool is determined as 1000 and 207 samples are identified within the threshold bounds by algorithm 5. The initial Kriging is constructed by 100 training samples from the observed data with

the expanded latent variables $\mathbf{Z}_E$, referred to as Kriging-$\mathbf{Z}_E$. Figure 7-2 (a) displays the results of the initial Kriging model, showing that most points are within the 20% bounds. The red samples in Figure 7-2 (b) are samples within the threshold bounds. It can be observed that these points cover almost the whole failure domain and the vicinity of limit state surface, making them crucial for failure probability estimation. Therefore, they are incorporated into the training samples to construct the one-step offline adaptive Kriging model. The results of the failure probability estimation are summarized in Table 7-2. The notation PhyrLSTM-AE-OAK refers to the offline adaptive Kriging model integrated with PhyrLSTM-AE. The initial Kriging model produces an inaccurate result, with a relative error of 47.30%. Both PhyrLSTM-AE-AK and PhyrLSTM-AE-OAK yield similar results, however, PhyrLSTM-AE-AK requires 324 iterations to obtain the failure probability while OAK only needs one iteration. The CoV by OAK is approximately 10%, which is consistent with Eq. (7-14).

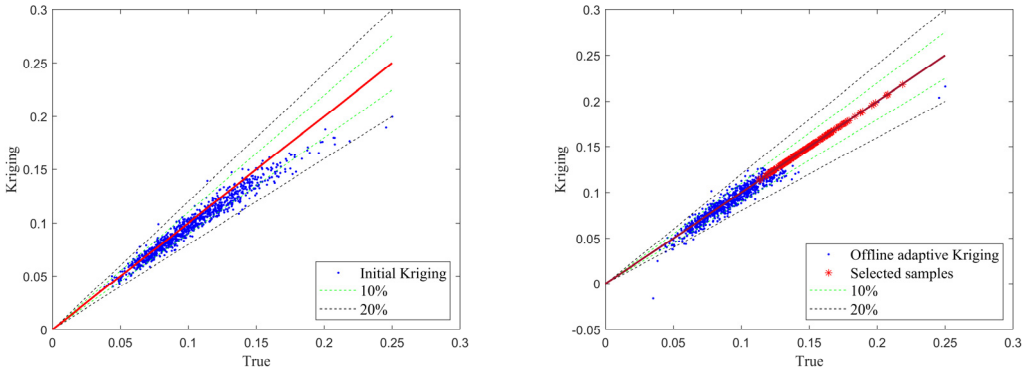

(a) Initial Kriging (b) Offline adaptive Kriging

Figure 7-2 Initial and offline adaptive Kriging given $b = 0.15$

Table 7-2 Failure probability estimation by different methods for the highway bridge

	Method	N_{call}	P_f	CoV(%)	R.E. (%)
Case 1	MCS	20000	7.59×10^{-2}	2.47	–
	MEM	1000	8.91×10^{-2}	–	17.35
	MIGLD	1000	8.63×10^{-2}	–	13.68
	Kriging- $\mathbf{Z}_E$	1000	4.00×10^{-2}	15.49	47.30
	PhyrLSTM-AE-AK	1324	7.07×10^{-2}	4.42	6.85
	PhyrLSTM-AE-OAK	1299	7.20×10^{-2}	11.35	5.14
Case 2	MCS	20000	6.15×10^{-3}	8.99	–
	MEM	1000	9.14×10^{-3}	–	48.58
	MIGLD	1000	8.98×10^{-3}	–	46.07
	Kriging- $\mathbf{Z}_E$	1000	2.14×10^{-4}	57.73	96.52
	PhyrLSTM-AE-AK	1224	5.37×10^{-3}	9.73	12.74
	PhyrLSTM-AE-OAK	1299	6.21×10^{-3}	10.69	1.05
Case 3	MCS	20000	3.50×10^{-4}	37.79	–
	MEM	1000	6.09×10^{-5}	–	–
	MIGLD	1000	7.24×10^{-4}	–	–
	Kriging- $\mathbf{Z}_E$	1000	0	–	–
	PhyrLSTM-AE-AK	1004	1.26×10^{-5}	30.15	–
	PhyrLSTM-AE-OAK	1300	1.51×10^{-4}	8.70	–

Case 2 investigate a threshold of 0.2. The candidate pool size is determined as 14000, with 299 samples falling within the threshold bounds. Figure 7-3 illustrates the performance of both the initial Kriging model and OAK in comparison to the ground truth. The added samples in Figure 7-3 (b) encompass the whole failure domain and parts of the safety domain. Consequently, OAK, incorporating these added samples, achieves an accurate failure probability estimation, with a relative error as low as 1.05%, as listed in Table 7-2. Although OAK produces some negative predictions within the safety domain, these values are always below the threshold *b* and thus do not impact the failure probability estimation. PhyrLSTM-AE-AK requires 224 iterations and has a relative error in failure probability of 12.74%, which is larger than that of PhyrLSTM-AE-OAK. The initial Kriging model uses 1000 observed data points but produces an extremely large relative error of 96.52%. OAK refines the

initial Kriging model in one step, significantly improving the accuracy and efficiency of the reliability analysis.

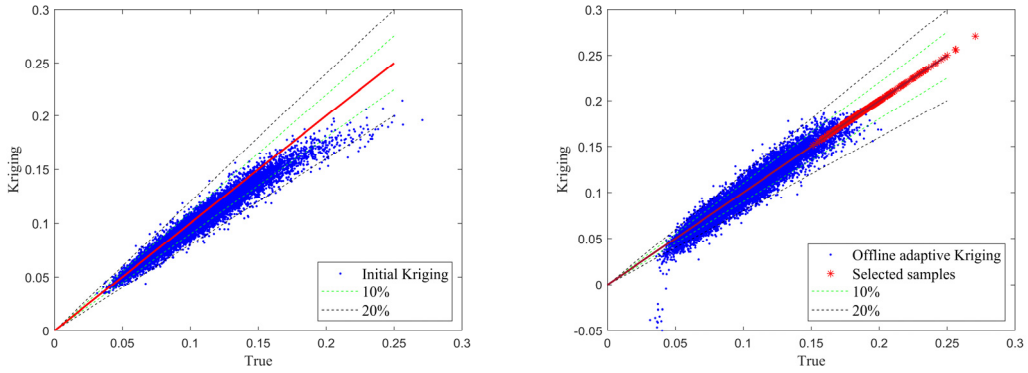

(a) Initial Kriging (b) Offline adaptive Kriging

Figure 7-3 Initial and offline adaptive Kriging given $b = 0.20$

A small failure probability is of concern in case 3 and the threshold is set to 0.25. The failure probability by 2×10^4 MCS is 3.50×10^{-4} with a CoV of 37.79%. Hence, 2×10^4 MCS cannot provide a reliable estimation of the small failure probability. To estimate a failure probability of 10^{-4}, 10^6 MCS is required, which is not feasible for the highway bridge model. PhyrLSTM-AE-OAK determines 867000 candidate samples for reliability estimation and the size of selected samples is 300. The distribution of selected samples is shown in Figure 7-4. It can be observed that most of the selected samples fall within the bounds [0.23, 0.27], which are close to the threshold $b = 0.25$. PhyrLSTM-AE-AK employs the same candidate pool as OAK. As seen from Table 7-2, the relative errors of failure probability are not provided since there is no reliable reference result. However, it can be inferred that the level of the failure probability should be around 10^{-4} based on 2×10^4 MCS. PhyrLSTM-AE-AK appears to fail in estimating the failure probability in this case. PhyrLSTM-AE-OAK selects samples in the vicinity of limit state surface and incorporates them into the

DoE, allowing for accurate predictions in this area. Therefore, OAK can provide a reliable estimation of the failure probability, i.e., 1.51×10^{-4}.

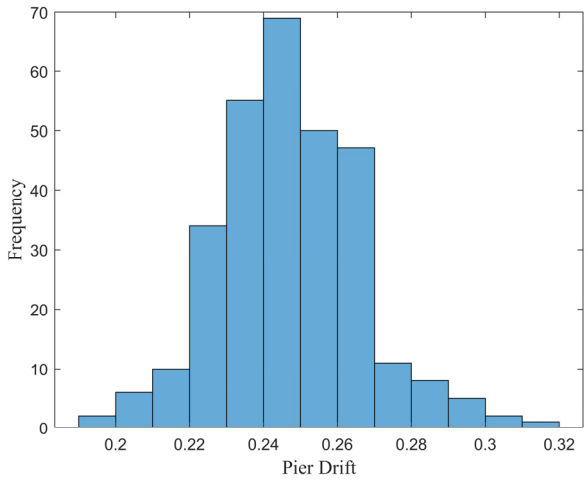

Figure 7-4 The distribution of the selected samples given $b = 0.25$

Additionally, when threshold $b = 0.25$ m, the responses of 74 samples within the threshold bounds exceed 0.26 m, indicating that these 74 samples are in the failure domain given $b = 0.26$ m. Therefore, the OAK trained by $b = 0.25$ m can be also employed for the failure probability estimation given b=0.26 m, with a corresponding failure probability of 8.45×10^{-5} and a CoV of 11.62%. Note that the failure probability by 2×10^4 MCS is 1.50×10^{-4} with a CoV of 57.73%. Obviously, 2×10^4 MCS cannot obtain a reliable estimation for this small failure probability. If $b = 0.26$ m is adopted for training the OAK, 3191000 candidate samples are determined and 300 samples are within the threshold bounds. The distribution of these selected samples is shown in Figure 7-5. The failure probability estimated by PhyrLSTM-AE-OAK is 9.28×10^{-5} with a CoV of 5.81%. Moreover, 109 samples are in the failure domain given $b = 0.27$ m. This OAK model can also be used for reliability analysis

with b = 0.27, eliminating the need for a new OAK model. Accordingly, the failure probability given b = 0.27 m is 3.85×10^{-5} with a CoV of 9.02%.

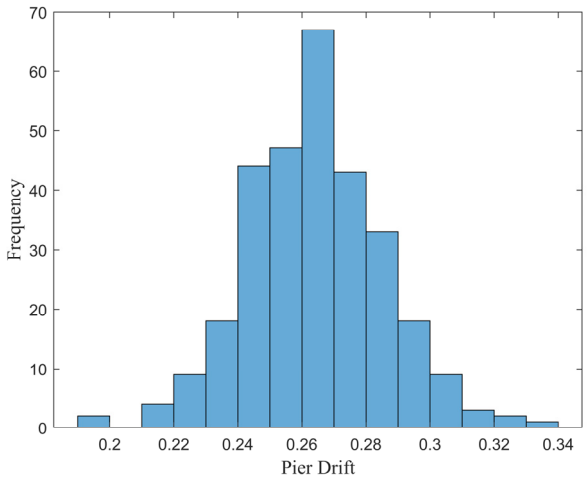

Figure 7-5 The distribution of the selected samples given b = 0.26

7.4 Application to the dynamic reliability analysis of a transmission tower subjected to stochastic wind loads

7.4.1 Structural modeling and uncertainties

A practical 1000 kV latticed transmission tower with a height of 102 m and a square base of 17.99×17.99 m is investigated in this section. The geometric configuration of the tower is depicted in Figure 7-6. The main and diagonal members are composed of Q345 and Q420 steel pipes, and the detailed design is also illustrated in Figure 7-6. The whole tower is divided into 7 segments. The finite element model, constructed using ABAQUS, is shown in Figure 7-7. Beam elements (B31) are utilized to model tower members. The definition of wind attack angle is shown in Figure 7-7. In this analysis, stochastic wind loads are applied perpendicular to the transmission lines, resulting in an attack angle of 0 degree. We consider three uncertain material

parameters: the Young's modulus with a mean of 206 GPa and a CoV of 0.03, the yield strength of Q345 with a mean of 345 MPa and a CoV of 0.08, and the yield strength of Q420 with a mean of 420 MPa and a CoV of 0.08.

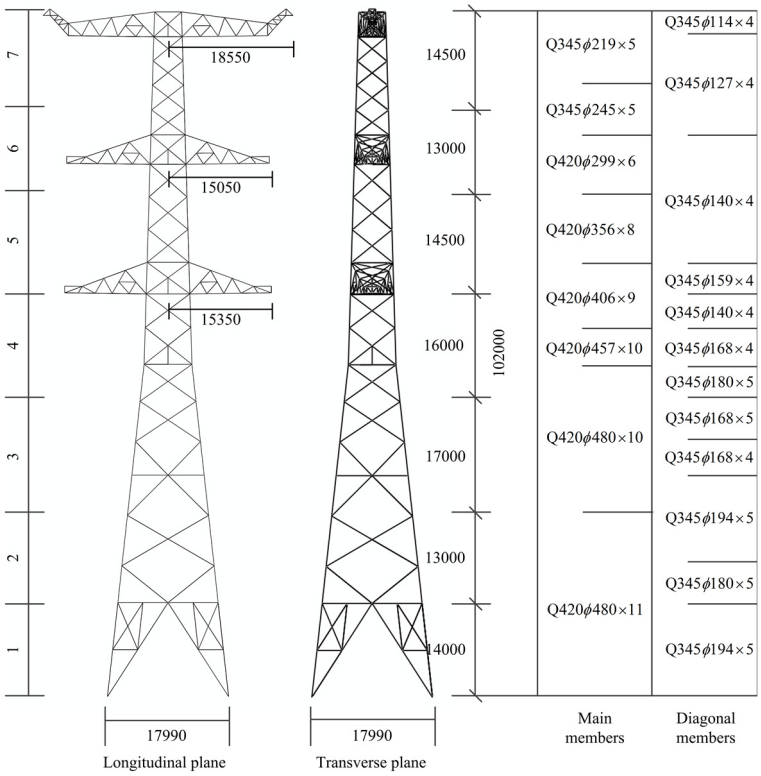

Figure 7-6 The geometric configuration of the transmission tower (unit: mm)

The performance of the transmission tower under stochastic wind loads is of interest. Wind speed is simulated as a stationary stochastic process including mean and fluctuating components. The mean wind speed can be simulated by a modified logarithmic wind profile (Bi et al., 2023):

$$\overline{v} = \begin{cases} \dfrac{1}{k}u^* \ln\left(\dfrac{h}{h_0}\right) & h < 30m \\ \dfrac{1}{k}u^* \left(\ln\left(\dfrac{h}{h_0}\right) + 34.5ezu^*\right) & 30m \le h < 300m \end{cases} \tag{7-20}$$

where k is the Kalman constant, u^* is the friction velocity and e is the Coriolis parameter. The fluctuating wind speed can be simulated as a stationary Gaussian process. The Kaimal spectrum (Deodatis, 1996) and Davenport's coherence function (Davenport, 1967) are adopted, with the linear filter method employed to simulate the time-series wind speed. Wind loads are calculated according to IEC standards. For simplicity, wind loads induced by transmission lines are also calculated and applied to the relevant nodes of the tower. The simulation points are indicated by red points in Figure 7-7. The design wind speed is 30 m/s, and the wind speed at 1st, 4th and 7th simulation points are shown in Figure 7-8.

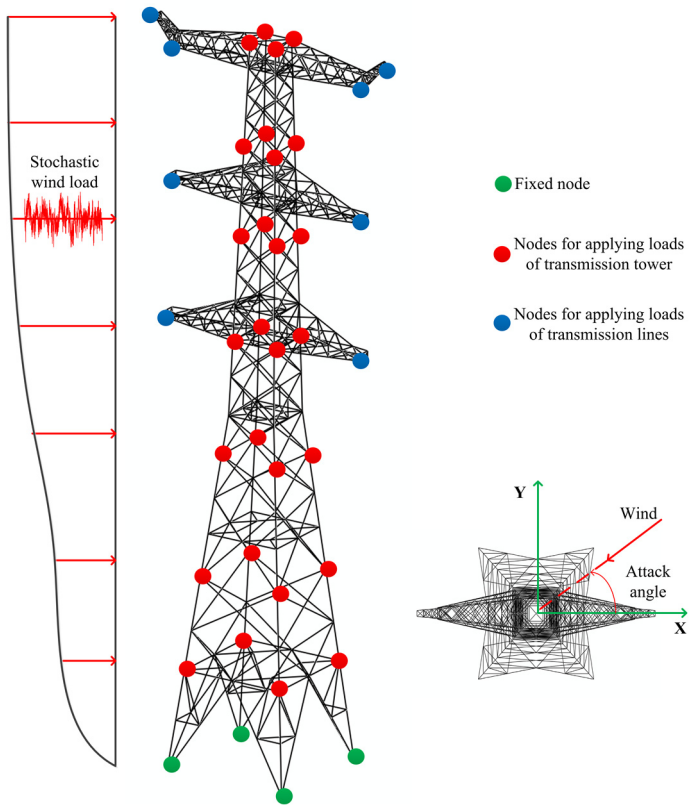

Figure 7-7 The stochastic FE model of the transmission tower

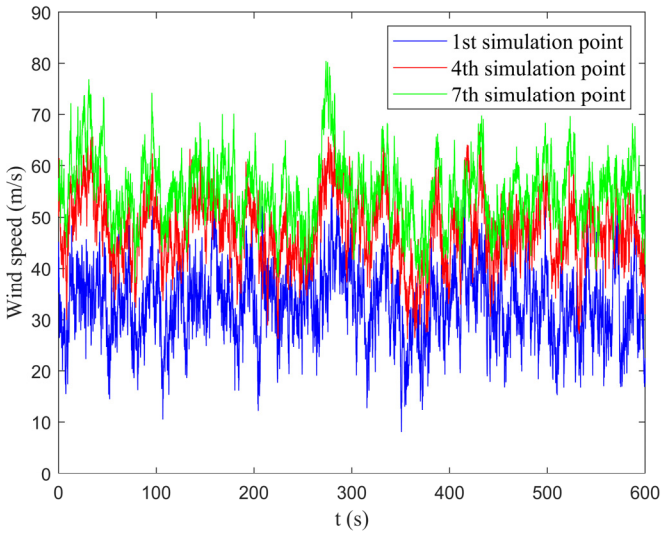

Figure 7-8 Simulated wind speed at different points

7.4.2 rLSTM for metamodeling of a transmission tower subjected to stochastic wind loads

The top displacement of the transmission tower subjected to stochastic wind loads is of concern. Time series wind loads simulated at eleven nodes and three random structural parameters are used as input features, resulting in a total of 14 input features. The rLSTM network architecture consists of three LSTM layers and two fully connected layers. The "tanh" activation function is used, with the hidden state dimension set to 50 and a learning rate of 0.01. Considering the complexity of FEM, only 200 observed time series of top displacements are collected, with 160 samples used for training and 40 samples used for validation.

Representative training and validation samples are presented in Figure 7-9 and Figure 7-10, respectively. It can be observed that the trained rlSTM can effectively capture the 10-minute time series top displacements. The performance of the trained rLSTM on a test sample is shown in Figure 7-11. It can be seen that the maximal top

displacement is close to 1.4 m and this sample is actually far away from observed samples (the extreme response of observed samples is around 1.2 m). Consequently, the rLSTM prediction shows a slight deviation. Additionally, the extreme responses predicted by rLSTM for the observed data are depicted in Figure 7-12 and the determination coefficient is 0.96. The maximum relative error in predicting extreme responses is smaller than 10%, indicating that the trained rLSTM achieves high accuracy. However, as shown in Figure 7-11, the accuracy of the trained rLSTM is still not sufficient for some samples far away from the observed region, which contribute a lot to reliability analysis. It is of vital importance to build an adaptive Kriging model for extreme responses prediction and improve the accuracy of samples in the vicinity of failure domains.

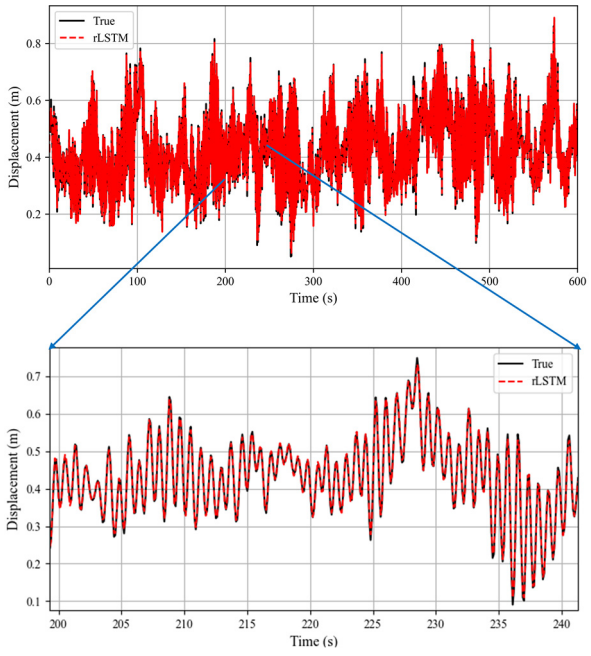

Figure 7-9 A representative training sample

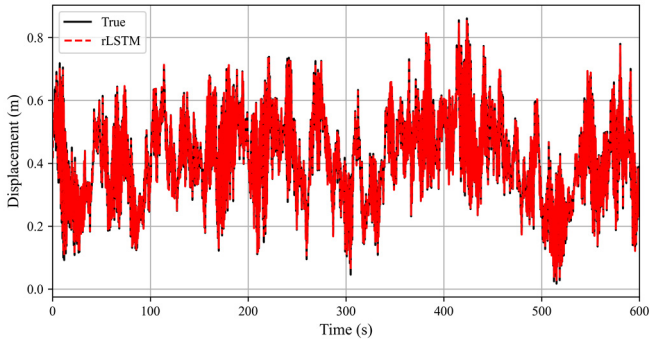

Figure 7-10 A representative validation sample

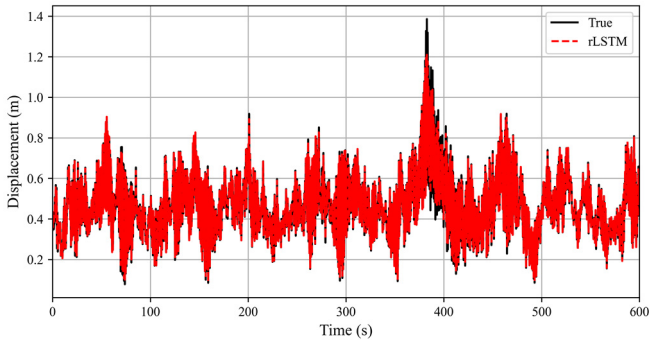

Figure 7-11 A representative test sample

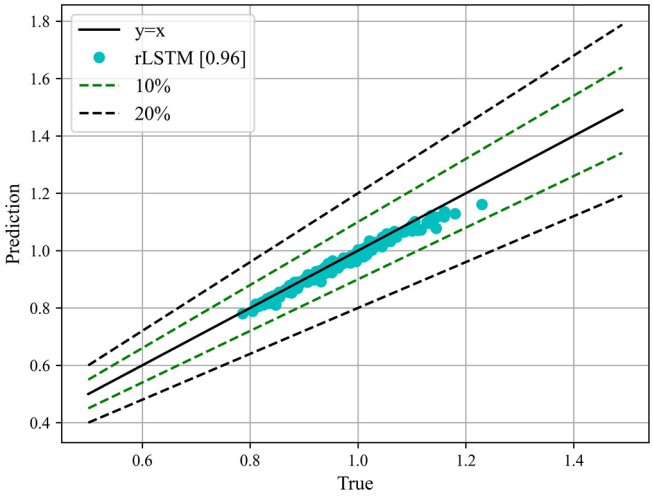

Figure 7-12 Extreme responses of observed samples

7.4.3 Dynamic reliability analysis by an offline adaptive Kriging model

To build Kriging model for the stochastic transmission tower system, it is first necessary to identify the latent space. The rLSTM-AE network is used to extract latent variables from the predicted extreme top displacements. The autoencoder structure is the same as that used in previous sections. A total of 160 training samples are used to train the autoencoder, while the remaining 40 samples from the validation set for model selection. The dimension of latent variables ranges from 2 to 20, and the Kriging construction error is shown in Figure 7-13.

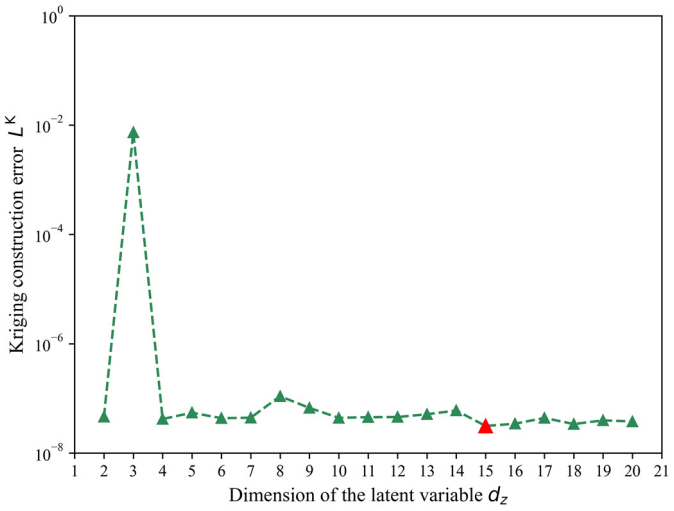

Figure 7-13 Kriging construction error for the transmission tower

Therefore, the optimal dimension for the latent variables is determined to be 15. The expanded latent space $\mathbf{Z}_{\mathrm{E}}$ includes latent variables detected form the extreme responses space, along with three structural parameters and extreme wind loads. To ensure that the Kriging model matches the rLSTM's performance in predicting extreme responses, the performance of Kriging model with three types of input

features are shown in Figure 7-14. It can be seen that Kriging with $\mathbf{Z}_0$, which only includes structural parameters and extreme wind loads, cannot accurately reconstruct the extreme response space generated by the rLSTM. Kriging with $\mathbf{Z}$ and $\mathbf{Z}_E$ achieve similar accuracy. Although both of them loss some accuracy when the extreme top displacement is smaller than 0.8 m, it does not affect the results of reliability analysis results under the design wind speed.

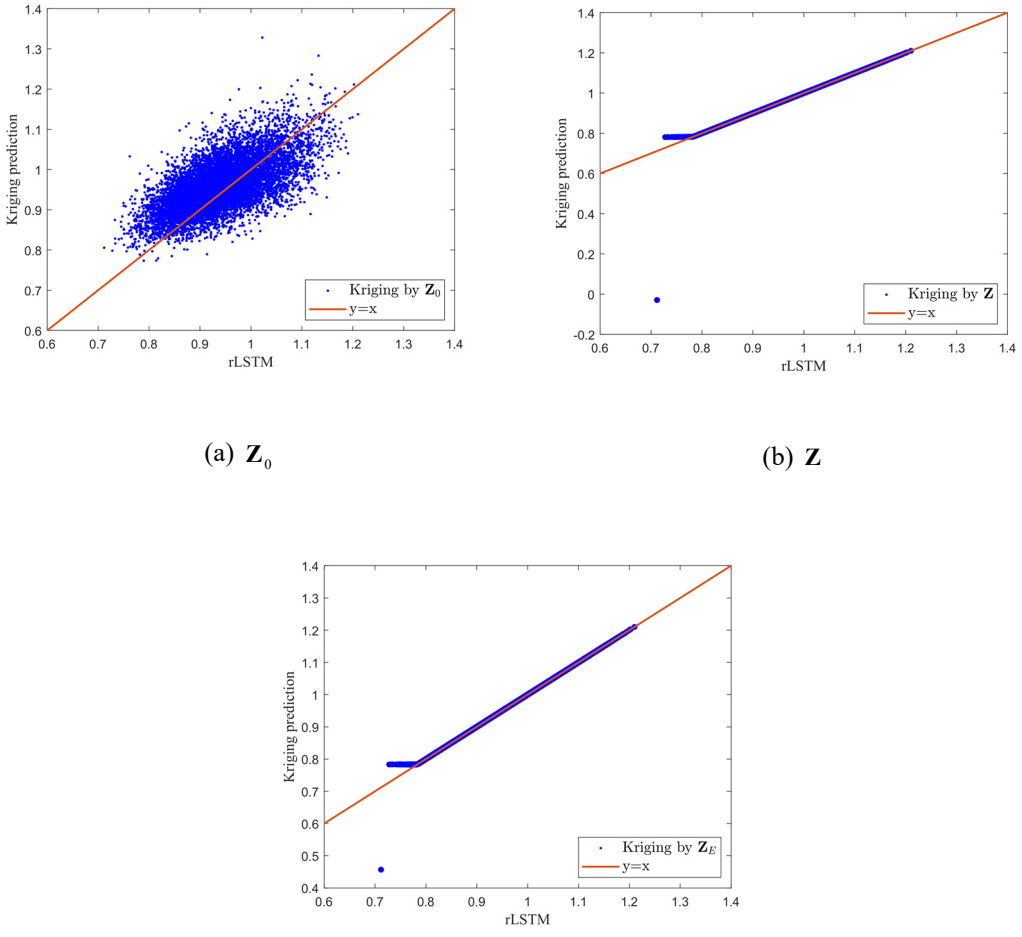

(a) $\mathbf{Z}_0$ (b) $\mathbf{Z}$

(c) $\mathbf{Z}_E$

Figure 7-14 The performance of different latent variables for the transmission tower

The relative errors of the extreme top displacement are within 10% bounds, and 10% is used to determine the size of candidate pool and samples for updating Kriging model. First, a threshold of 1.3 m is of concern. A total of 122000 candidate samples are identified, from which 300 samples are selected to refine the Kriging model using Algorithm 5. The distribution of the extreme top displacements of the selected 300 samples is pictured in Figure 7-15. The selected samples encompass the safety and failure domains, as well as the limit state surface, which will significantly enhance the accuracy of the Kriging model for reliability analysis. MEM and MIGLD are also employed for comparisons and the results are listed in Table 7-3. MCS is not available since evaluating this transmission tower is time-consuming. Both MIGLD and the proposed method estimate failure probabilities at a level of 10^{-4}, whereas MEM appears to underestimate the risk. The Kriging model with the expanded latent variables fails to produce a reasonable result, yielding a failure probability of 0. This outcome also indicates that the accuracy of rLSTM is not sufficient for reliability analysis.

To improve the accuracy of rLSTM for the region distant from the original training set, the selected 300 samples near the failure domain defined by b=1.3 m are added into the training set. Thus, a total of 500 observed samples are utilized for training. Representative training, validation and test samples are presented in Figures 7-16~18, illustrating the improved performance of the enhanced rLSTM. Notably, Figure 7-18 shows the same test sample as Figure 7-11, with the extreme response approaching 1.4 m. The enhanced rLSTM model closely aligns with the reference time history response.

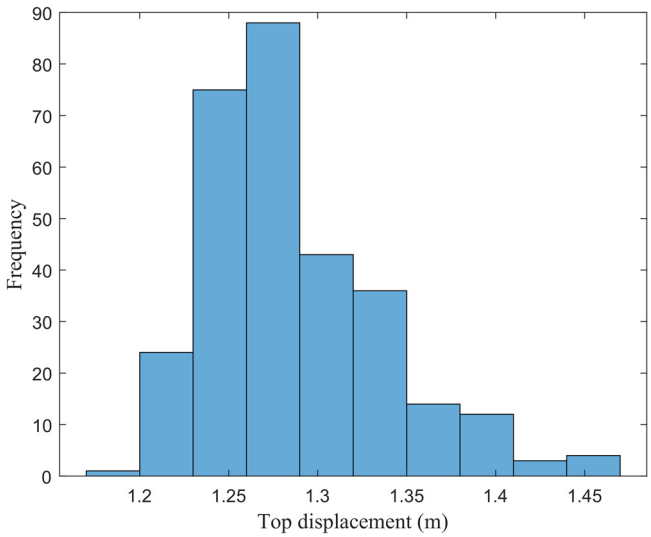

Figure 7-15 The distribution of the selected samples given b = 1.3 m

Figure 7-19 demonstrates the enhanced rLSTM in predicting extreme top displacements. The determination coefficient is 0.94 and the relative errors fall mostly within 10% error bounds. The enhanced rSLTM is then utilized for latent variables identification and the Kriging model construction error is presented in Figure 7-20. Clearly, the optimal dimension for the latent space is still 15. Figure 7-21 illustrates the performance of Kriging in reconstructing the approximate extreme value space using the rLSTM with three different sets of latent variables. It is evident that Kriging with peak loads and structural parameters is not suitable for constructing the approximate extreme responses. In contrast, Kriging with $\mathbf{Z}$ and $\mathbf{Z}_E$ perform well in constructing the extreme value space, leading to the adoption of the expanded latent variables $\mathbf{Z}_E$.

Given a threshold of 1.45 m, 300 samples near the failure domain are selected, and the candidate pool size is determined to be 1779000 by algorithm 5. The distribution of selected samples is shown in Figure 7-22, where responses ranging

from 1.3 to 1.65 meters are captured, crossing both the safety and failure domains. Thus, enriching the DoE for Kriging with the selected samples can remarkably improve the accuracy of reliability analysis. The estimated failure probabilities are listed in Table 7-3. The proposed method estimates a failure probability of 2.33×10^{-5} with a CoV of 15.43%, and a corresponding reliability index of 4.07. However, Kriging with the expanded latent variables does not provide a reliable estimation, as it reflects the accuracy of the rLSTM network, which is insufficient for reliability analysis. Both MEM and MIGLD tend to underestimate the failure probabilities. In addition, the pushover analysis, as shown in Figure 7-23, indicates that the tower collapses when the top displacement reaches approximately 1.6 meters. The failure probability estimated by OAK is as small as 1.67×10^{-6} with a CoV of 57.73%. Therefore, at least 10^8 candidate samples are required for failure probability estimation. However, due to the time-consuming process of wind field simulations, generating such a large number of candidate samples is not feasible. It is noteworthy that a high level of reliability is achieved with a threshold of 1.45 meters, corresponding to a reliability index of 4.07. Therefore, the safety of the transmission tower is significantly ensured under a design wind speed of 30 m/s.

Table 7-3 Failure probability estimation by different methods for the transmission tower

	Method	N_{call}	P_f	CoV(%)
Case 1	MEM	200	1.27×10^{-5}	–
	MIGLD	200	4.50×10^{-5}	–
	Kriging- $\mathbf{Z}_E$	200	0	–
	rLSTM-AE-OAK	500	7.34×10^{-4}	10.54
Case 2	MEM	200	7.40×10^{-16}	–
	MIGLD	200	3.00×10^{-6}	–
	Kriging- $\mathbf{Z}_E$	500	1.67×10^{-6}	57.73
	rLSTM-AE-OAK	800	2.33×10^{-5}	15.43

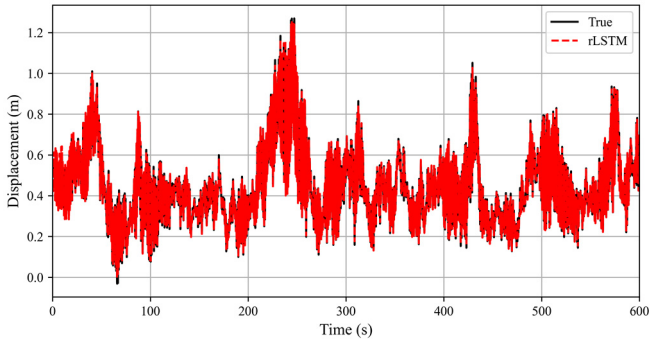

Figure 7-16 A representative training sample with the enhanced rLSTM

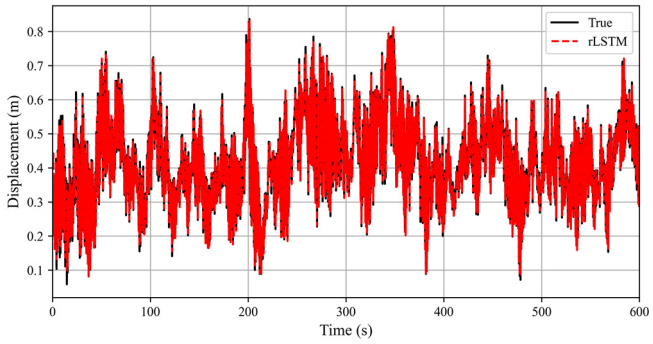

Figure 7-17 A representative validation sample with the enhanced rLSTM

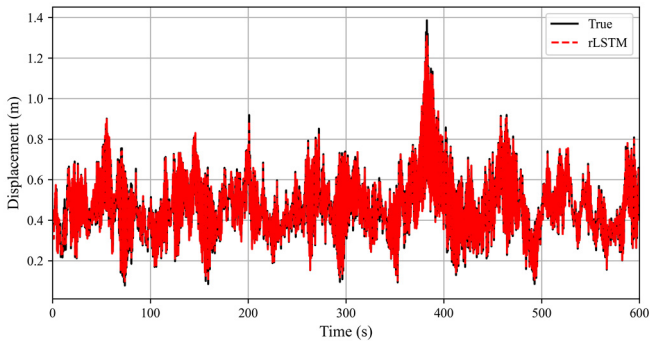

Figure 7-18 A representative test sample with the enhanced rLSTM

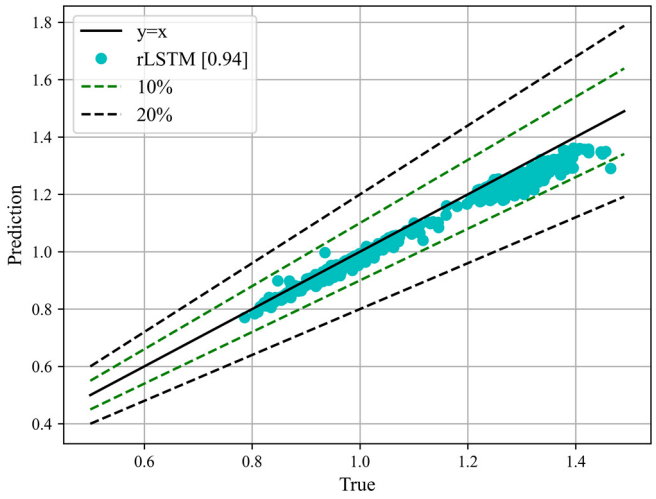

Figure 7-19 Extreme responses of observed samples with the enhanced rLSTM

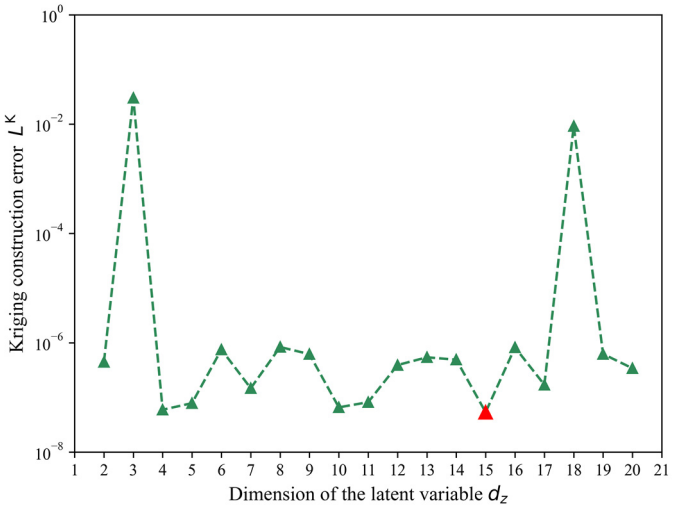

Figure 7-20 Kriging construction error with the enhanced rLSTM

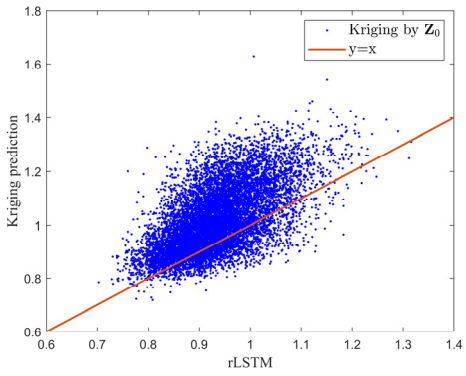

(a) $\mathbf{Z}_0$

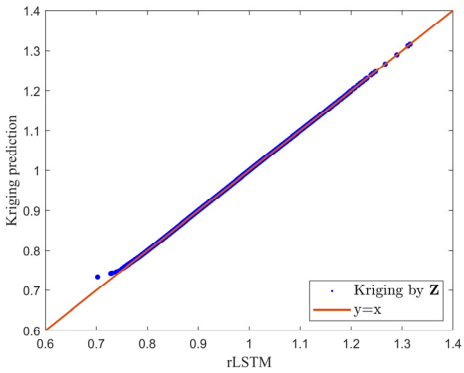

(b) $\mathbf{Z}$

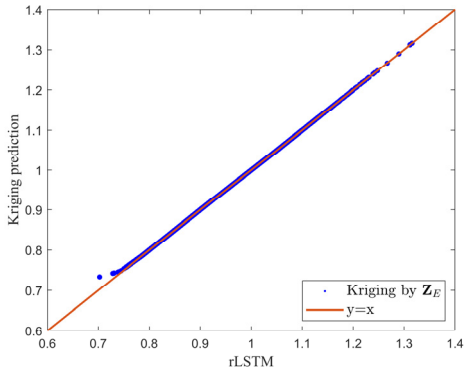

(c) $\mathbf{Z}_E$

Figure 7-21 The performance of different latent variables with the enhanced rLSTM

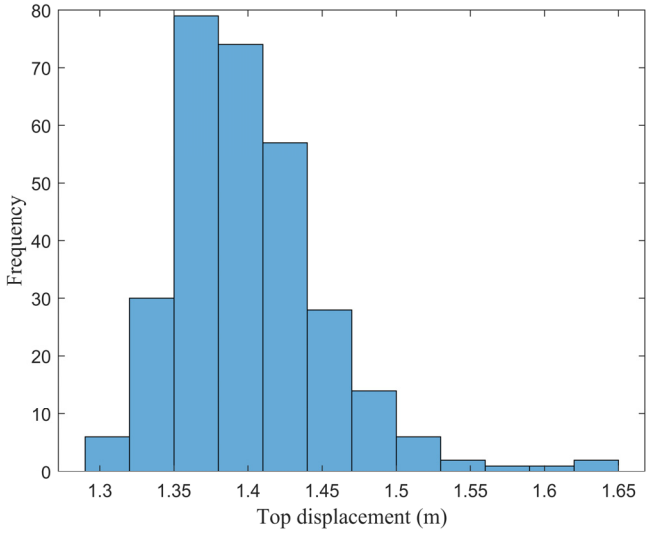

Figure 7-22 The distribution of the selected samples given b = 1.45 m

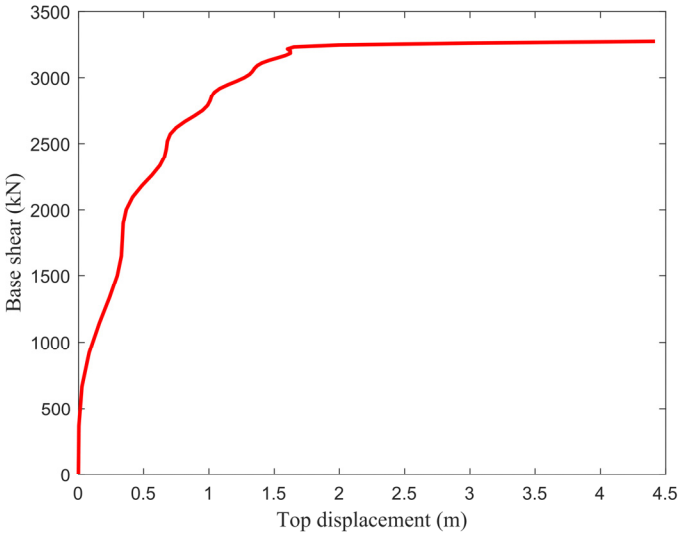

Figure 7-23 Pushover analysis

7.5 Summary

In this chapter, an offline learning strategy is proposed to refine adaptive Kriging in a single step. The error bounds of the constructed rLSTM for stochastic dynamic systems are used to identify samples that cover the limit state surface. These samples are then added to the DoE to refine the Kriging model. Since the samples are selected in a single step, parallel computing can be utilized, avoiding the need for continuous updates to the Kriging model. To enhance the flexibility of the latent variables, peak loads and random structural parameters are combined with the latent variables identified by the rLSTM-AE for Kriging construction. A highway bridge under stochastic seismic excitation is first investigated to validate the performance of the proposed offline learning strategy. The results show that the offline adaptive Kriging model can effectively estimate the failure probabilities. Furthermore, a practical transmission tower subjected to stochastic wind loads is studied. It is demonstrated that the proposed rLSTM can also capture the time history responses induced by stochastic wind loads. By utilizing the error bounds provided by rLSTM, the adaptive Kriging model can be refined in a single step, efficiently offering a more reliable estimation of failure probability.

CHAPTER 8 CONCLUSIONS AND FUTURE WORK

8.1 Main conclusions

Efficient structural reliability analysis methods have been extensively studied in recent years, yet estimating failure probabilities for practical engineering structures remains challenging. Recently, surrogate modeling techniques, particularly the Kriging model, have gained significant attention due to the development of adaptive Kriging models, which can iteratively enrich the DoE via an active learning strategy. However, adaptive Kriging model encounters disadvantages for reliability analysis of practical engineering models such as estimating small failure probabilities, performing dynamic reliability analysis, and supporting parallel computing. This thesis focuses on addressing these challenges by improving adaptive Kriging models for rare failure probabilities estimation and dynamic reliability analysis. The major contributions of this work are as follows:

1) Adaptive Kriging model with the crude MCS is not efficient for rare events estimation since a large MC population is involved. The proposed distance-based subdomain can detect candidate samples in the vicinity of limit state surface on the basis of a location point. During the active learning process, Kriging model is refined within each detected distance-based subdomain rather than across the entire candidate pool. This refinement process reduces the number of samples requiring Kriging predictions, thereby significantly accelerating the active learning process, particularly for estimating small failure probabilities.

2) It is known that the conventional U stopping criterion is conservative for failure probability estimation since it focuses too much on the accuracy of Kriging model. An error-based stopping criterion is particularly designed for reliability analysis. The effect of the candidate points with high probabilities of misclassification on failure probability estimation is theoretically analyzed and the expected upper bound of the relative error of failure probability is formulated. A new stopping criterion is accordingly developed based on the expected upper bound of relative error of failure probability. Additionally, a suitable target threshold for this criterion is proposed, based on the impact of the threshold on failure probability estimation. The proposed stopping criterion enables the active learning process to be terminated at an appropriate stage, thereby balancing accuracy and efficiency in reliability analysis.

3) Regarding very rare events estimation, e.g., the failure probability is smaller than 10^{-6}, a spherical decomposition-based MCS is employed to generate the candidate pool for training adaptive Kriging model. SDMCS has proven to be much more efficient than the crude Monte Carlo simulation. However, SDMCS may produce more samples near the limit state surface, which can complicate the termination of the adaptive Kriging model's refinement process. The error-based stopping criterion tailored for AKMCS is reformulated for AKSDMCS. It is observed that the number of incorrectly classified points in each SDMCS subregion follows a binomial distribution, allowing for the formulation of the expected upper bound of the relative error in failure probability estimation. The new stopping criterion significantly reduces the computational burden associated with expensive model evaluations, compared to other criteria that do not consider the relative error in failure probability estimation.

4) Constructing surrogate models for engineering structures subjected to the stochastic excitation is still an open question due to the highly nonlinear structural behaviors and implicit input features. Long short-term memory is a powerful machine learning tool for modeling sequence-to-sequence data. In this work, a novel rLSTM network is developed for metamodeling of stochastic dynamic systems. The rLSTM network simultaneously accounts for time-series stochastic excitation and random structural parameters, effectively avoiding non-essential input features such as random phases used in generating stochastic excitation. Although the accuracy of rLSTM may be insufficient for reliability analysis due to limited observations, it proves valuable for detecting latent variables, which can then be used to construct an adaptive Kriging model.

5) Generally, extreme responses are of primary interest, and failure probabilities can be estimated from the perspective of extreme value theory. The rLSTM network approximates the extreme value space, which can be further decomposed by an autoencoder with a dimension ranging from 2 to 20. The proposed rLSTM-AE network effectively identifies latent variables for constructing a Kriging model, achieving accuracy in extreme response predictions comparable to that of rLSTM. The rLSTM-AE approach facilitates the development of Kriging models for stochastic dynamic systems, enabling the use of adaptive Kriging models for reliability analysis of engineering structures subjected to stochastic excitations.

6) Data-driven rLSTM may encounter instability and inaccuracy since underlying physical laws of a physical system are ignored when constructing the network. To address this, a physics-informed rLSTM network, termed PhyrLSTM, is

developed by incorporating the uncertain governing equation of stochastic dynamic systems. The PhyrLSTM network consists of two rLSTM components: one for predicting state variables such as displacement and velocity, and the other for predicting the mass-normalized restoring force. Compared to standard rLSTM models, PhyrLSTM offers greater stability and accuracy. Nevertheless, the accuracy of PhyrLSTM is not sufficient for reliability analysis. Adaptive Kriging model is constructed with the aid of PhyrLSRM-AE networks and the accuracy of failure probability estimation is remarkably improved compared to PhyrLSTM.

7) Adaptive Kriging model continuously requires information from the computationally expensive performance functions and the parallel computing is unavailable, and the lack of parallel computing capabilities significantly hinders its application in the reliability analysis of practical engineering structures. Additionally, the convergence issues of FEM pose a challenge to active learning strategies. Besides providing an approximate extreme response space for latent variables identification, the prediction error by rLSTM is also adopted to determine candidate pool and samples near the limit sate surface. These selected samples, which are anticipated to be close to the limit state surface, are incorporated into the DoE for training the Kriging model. This approach, regarded as an offline learning strategy, avoids the requirement for iterative training and allows for parallel computing. The offline adaptive Kriging model thus offers a more efficient alternative by circumventing iterative training processes and leveraging parallel computing capabilities.

8.2 Suggestions for future work

Some recommendations for future work are listed as follows:

1) The current study primarily addresses improvements in candidate pool generation and stopping criteria for adaptive Kriging models. It employs the U learning function but does not explore the efficiency of various learning functions. The U learning function focuses on regions near the limit state surface or the accuracy of the Kriging model in those areas. For more effective reliability analysis, future work should explore the development of learning functions that take into account both the accuracy of failure probability estimation and the information from input random variables.

2) Constructing surrogate models for engineering structures subjected to stochastic excitation is of paramount importance for the subsequent construction of adaptive Kriging model. Currently, long short-term memory is employed to model sequency-to-sequency data. To improve the accuracy of LSTM network, the attention mechanism can be added into the structure and the performance of attention-based LSTM should be explored for metamodeling of stochastic dynamic systems.

3) In this thesis, rLSTM is incorporated with the autoencoder to identify the latent variables for Kriging model construction. The latent variables detection relies on the decomposition of the approximate extreme value space generated by rLSTM. The direct identification of latent variables from the original input space should be further explored in the future work.

4) This thesis explores rLSTM-based surrogate models for structures subjected to earthquake and wind loads. Beyond individual structures, this technique can be extended to construct surrogate models for infrastructural networks in the context of

climate change, enabling real-time prediction and risk assessment of infrastructural networks.

REFERENCES

Afshari, S. S., Enayatollahi, F., Xu, X., & Liang, X. (2022). Machine learning-based methods in structural reliability analysis: A review. *Reliability Engineering & System Safety*, *219*, 108223.

Alibrandi, U., Alani, A. M., & Ricciardi, G. (2015). A new sampling strategy for SVM-based response surface for structural reliability analysis. *Probabilistic Engineering Mechanics*, *41*, 1-12.

Alpsten, G. (1972). Variations in mechanical and cross-sectional properties of steel, State of the Art Report. Proceedings of the International Conference on the Planning and Design of Tall Buildings, ASCE-IABSE, Lehigh University,

Ang, G. L., Ang, A. H.-S., & Tang, W. H. (1992). Optimal importance-sampling density estimator. *Journal of Engineering Mechanics*, *118*(6), 1146-1163.

Au, S.-K., & Beck, J. L. (1999). A new adaptive importance sampling scheme for reliability calculations. *Structural Safety*, *21*(2), 135-158.

Au, S.-K., & Beck, J. L. (2001). Estimation of small failure probabilities in high dimensions by subset simulation. *Probabilistic Engineering Mechanics*, *16*(4), 263-277.

Barlow, R. E., & Proschan, F. (1996). *Mathematical theory of reliability*. SIAM.

Berveiller, M., Sudret, B., & Lemaire, M. (2006). Stochastic finite element: a non intrusive approach by regression. *European Journal of Computational Mechanics/Revue Européenne de Mécanique Numérique*, *15*(1-3), 81-92.

Bhattacharyya, B. (2021). Structural reliability analysis by a Bayesian sparse polynomial chaos expansion. *Structural Safety*, *90*, 102074.

Bi, W., Tian, L., Li, C., & Ma, Z. (2023). A Kriging-based probabilistic framework for multi-hazard performance assessment of transmission tower-line systems under coupled wind and rain loads. *Reliability Engineering & System Safety*, *240*, 109615.

Bichon, B. J., Eldred, M. S., Swiler, L. P., Mahadevan, S., & McFarland, J. M. (2008). Efficient global reliability analysis for nonlinear implicit performance functions. *AIAA journal*, *46*(10), 2459-2468.

Blatman, G., & Sudret, B. (2010a). An adaptive algorithm to build up sparse polynomial chaos expansions for stochastic finite element analysis. *Probabilistic Engineering Mechanics*, *25*(2), 183-197.

Blatman, G., & Sudret, B. (2010b). Efficient computation of global sensitivity indices using sparse polynomial chaos expansions. *Reliability Engineering & System Safety*, *95*(11), 1216-1229.

Blatman, G., & Sudret, B. (2011). Adaptive sparse polynomial chaos expansion based on least angle regression. *Journal of Computational Physics*, *230*(6), 2345-2367.

Bourinet, J.-M. (2016). Rare-event probability estimation with adaptive support vector regression surrogates. *Reliability Engineering & System Safety*, *150*, 210-221.

Bourinet, J.-M., Deheeger, F., & Lemaire, M. (2011). Assessing small failure probabilities by combined subset simulation and support vector machines. *Structural Safety*, *33*(6), 343-353.

Cadini, F., Santos, F., & Zio, E. (2014). An improved adaptive kriging-based importance technique for sampling multiple failure regions of low probability. *Reliability Engineering & System Safety*, *131*, 109-117.

Cardoso, J. B., de Almeida, J. R., Dias, J. M., & Coelho, P. G. (2008). Structural reliability analysis using Monte Carlo simulation and neural networks. *Advances in Engineering Software*, *39*(6), 505-513.

Celik, O. C., & Ellingwood, B. R. (2010). Seismic fragilities for non-ductile reinforced concrete frames–Role of aleatoric and epistemic uncertainties. *Structural Safety*, *32*(1), 1-12.

Chen, J.-B., & Li, J. (2007). The extreme value distribution and dynamic reliability analysis of nonlinear structures with uncertain parameters. *Structural Safety*, *29*(2), 77-93.

Chen, J., Kong, F., & Peng, Y. (2017). A stochastic harmonic function representation for non-stationary stochastic processes. *Mechanical Systems and Signal Processing*, *96*, 31-44.

Chen, J., & Li, J. (2005). Extreme value distribution and reliability of nonlinear stochastic structures. *Earthquake Engineering and Engineering Vibration*, *4*(2), 275-286.

Chen, W., Xu, C., Shi, Y., Ma, J., & Lu, S. (2019). A hybrid Kriging-based reliability method for small failure probabilities. *Reliability Engineering & System Safety*, *189*, 31-41.

Choi, S.-K., Grandhi, R. V., Canfield, R. A., & Pettit, C. L. (2004). Polynomial chaos expansion with latin hypercube sampling for estimating response variability. *AIAA journal*, *42*(6), 1191-1198.

Culver, C. (1976). Survey Results for Fire Loads and Live Loads in Office Buildings, Nat. Bur. Stand.(US)'. *Bldg. Sci. Ser*, *85*, 157.

Dai, H., Zhang, B., & Wang, W. (2015). A multiwavelet support vector regression method for efficient reliability assessment. *Reliability Engineering & System Safety*, *136*, 132-139.

Dang, C., Valdebenito, M. A., Faes, M. G., Song, J., Wei, P., & Beer, M. (2023). Structural reliability analysis by line sampling: A Bayesian active learning treatment. *Structural Safety*, *104*, 102351.

Dang, C., Valdebenito, M. A., Song, J., Wei, P., & Beer, M. (2023). Estimation of small failure probabilities by partially Bayesian active learning line sampling: Theory and algorithm. *Computer methods in applied mechanics and engineering*, *412*, 116068.

Dang, C., Wei, P., & Beer, M. (2021). An approach to evaluation of EVD and small failure probabilities of uncertain nonlinear structures under stochastic seismic excitations. *Mechanical Systems and Signal Processing*, *152*, 107468.

Dang, C., Wei, P., Faes, M. G., Valdebenito, M. A., & Beer, M. (2022). Parallel adaptive Bayesian quadrature for rare event estimation. *Reliability Engineering & System Safety*, *225*, 108621.

Dang, C., & Xu, J. (2020). A mixture distribution with fractional moments for efficient seismic reliability analysis of nonlinear structures. *Engineering Structures*, *208*, 109912.

das Chagas Moura, M., Zio, E., Lins, I. D., & Droguett, E. (2011). Failure and reliability prediction by support vector machines regression of time series data. *Reliability Engineering & System Safety*, *96*(11), 1527-1534.

Davenport, A. (1967). The dependence of wind loads on meteorological parameters.

Deodatis, G. (1996). Simulation of ergodic multivariate stochastic processes. *Journal of Engineering Mechanics*, *122*(8), 778-787.

Ding, C., & Xu, J. (2021). An improved adaptive bivariate dimension-reduction method for efficient statistical moment and reliability evaluations. *Mechanical Systems and Signal Processing*, *149*, 107309.

Echard, B., Gayton, N., & Lemaire, M. (2011). AK-MCS: an active learning reliability method combining Kriging and Monte Carlo simulation. *Structural Safety*, *33*(2), 145-154.

Echard, B., Gayton, N., Lemaire, M., & Relun, N. (2013). A combined importance sampling and Kriging reliability method for small failure probabilities with time-demanding numerical models. *Reliability Engineering & System Safety*, *111*, 232-240.

Engelund, S., & Rackwitz, R. (1993). A benchmark study on importance sampling techniques in structural reliability. *Structural Safety*, *12*(4), 255-276.

Fauriat, W., & Gayton, N. (2014). AK-SYS: an adaptation of the AK-MCS method for system reliability. *Reliability Engineering & System Safety*, *123*, 137-144.

Feng, K., Lu, Z., Yang, Y., Ling, C., He, P., & Dai, Y. (2023). Novel Kriging based learning function for system reliability analysis with correlated failure modes. *Reliability Engineering & System Safety*, *239*, 109529.

Gaspar, B., Teixeira, A. P., & Soares, C. G. (2017). Adaptive surrogate model with active refinement combining Kriging and a trust region method. *Reliability Engineering & System Safety*, *165*, 277-291.

Goh, A. T., & Kulhawy, F. H. (2003). Neural network approach to model the limit state surface for reliability analysis. *Canadian Geotechnical Journal*, *40*(6), 1235-1244.

Grigoriu, M., & Samorodnitsky, G. (2014). Reliability of dynamic systems in random environment by extreme value theory. *Probabilistic Engineering Mechanics*, *38*, 54-69.

Guo, Q., Liu, Y., Chen, B., & Zhao, Y. (2020). An active learning Kriging model combined with directional importance sampling method for efficient reliability analysis. *Probabilistic Engineering Mechanics*, *60*, 103054.

Harris, R. (1996). Gumbel re-visited-a new look at extreme value statistics applied to wind speeds. *Journal of Wind Engineering and Industrial Aerodynamics*, *59*(1), 1-22.

Hasofer, A. M., & Lind, N. C. (1974). Exact and invariant second-moment code format. *Journal of the Engineering Mechanics*, *100*(1), 111-121.

He, W., Zeng, Y., & Li, G. (2020). An adaptive polynomial chaos expansion for high-dimensional reliability analysis. *Structural and Multidisciplinary Optimization*, *62*, 2051-2067.

Hinton, G. E., & Salakhutdinov, R. R. (2006). Reducing the dimensionality of data with neural networks. *science*, *313*(5786), 504-507.

Hu, C., & Youn, B. D. (2011). Adaptive-sparse polynomial chaos expansion for reliability analysis and design of complex engineering systems. *Structural and Multidisciplinary Optimization*, *43*, 419-442.

Hu, Z., & Du, X. (2013). Time-dependent reliability analysis with joint upcrossing rates. *Structural and Multidisciplinary Optimization*, *48*, 893-907.

Huang, X., Chen, J., & Zhu, H. (2016). Assessing small failure probabilities by AK–SS: An active learning method combining Kriging and Subset Simulation. *Structural Safety*, *59*, 86-95.

Jaynes, E. T. (1957). Information theory and statistical mechanics. *Physical Review*, *106*(4), 620.

Jia, D.-W., & Wu, Z.-Y. (2024). An improved adaptive Kriging model for importance sampling reliability and reliability global sensitivity analysis. *Structural Safety*, *107*, 102427.

Jiang, C., Qiu, H., Yang, Z., Chen, L., Gao, L., & Li, P. (2019). A general failure-pursuing sampling framework for surrogate-based reliability analysis. *Reliability Engineering & System Safety*, *183*, 47-59.

Johnson, N. L., Kotz, S., & Balakrishnan, N. (1995). *Continuous univariate distributions, volume 2* (Vol. 289). John wiley & sons.

Jones, D. R., Schonlau, M., & Welch, W. J. (1998). Efficient global optimization of expensive black-box functions. *Journal of Global optimization*, *13*, 455-492.

Kaymaz, I. (2005). Application of kriging method to structural reliability problems. *Structural Safety*, *27*(2), 133-151.

Kingston, G. B., Rajabalinejad, M., Gouldby, B. P., & Van Gelder, P. H. (2011). Computational intelligence methods for the efficient reliability analysis of complex flood defence structures. *Structural Safety*, *33*(1), 64-73.

Koutsourelakis, P.-S. (2004). Reliability of structures in high dimensions. Part II. Theoretical validation. *Probabilistic Engineering Mechanics*, *19*(4), 419-423.

Koutsourelakis, P.-S., Pradlwarter, H. J., & Schueller, G. I. (2004). Reliability of structures in high dimensions, part I: algorithms and applications. *Probabilistic Engineering Mechanics*, *19*(4), 409-417.

Kurtz, N., & Song, J. (2013). Cross-entropy-based adaptive importance sampling using Gaussian mixture. *Structural Safety*, *42*, 35-44.

Le Maıtre, O. P., Reagan, M. T., Najm, H. N., Ghanem, R. G., & Knio, O. M. (2002). A stochastic projection method for fluid flow: II. Random process. *Journal of Computational Physics*, *181*(1), 9-44.

Lelièvre, N., Beaurepaire, P., Mattrand, C., & Gayton, N. (2018). AK-MCSi: A Kriging-based method to deal with small failure probabilities and time-consuming models. *Structural Safety*, *73*, 1-11.

Li, G., & Zhang, K. (2011). A combined reliability analysis approach with dimension reduction method and maximum entropy method. *Structural and Multidisciplinary Optimization*, *43*(1), 121-134.

Lim, H., & Manuel, L. (2021). Distribution-free polynomial chaos expansion surrogate models for efficient structural reliability analysis. *Reliability Engineering & System Safety*, *205*, 107256.

Ling, C., Lu, Z., Feng, K., & Zhang, X. (2019). A coupled subset simulation and active learning kriging reliability analysis method for rare failure events. *Structural and Multidisciplinary Optimization*, *60*, 2325-2341.

Liu, Z., Liu, W., & Peng, Y. (2016). Random function based spectral representation of stationary and non-stationary stochastic processes. *Probabilistic Engineering Mechanics*, *45*, 115-126.

Low, Y. M. (2013). A new distribution for fitting four moments and its applications to reliability analysis. *Structural Safety*, *42*, 12-25.

Lu, C., Feng, Y.-W., Liem, R. P., & Fei, C.-W. (2018). Improved Kriging with extremum response surface method for structural dynamic reliability and sensitivity analyses. *Aerospace Science and Technology*, *76*, 164-175.

Lucor, D., & Karniadakis, G. E. (2004). Adaptive generalized polynomial chaos for nonlinear random oscillators. *SIAM Journal on Scientific Computing*, *26*(2), 720-735.

Lutes, L. D., & Sarkani, S. (2004). *Random vibrations: analysis of structural and mechanical systems*. Butterworth-Heinemann.

Lv, Z., Lu, Z., & Wang, P. (2015). A new learning function for Kriging and its applications to solve reliability problems in engineering. *Computers & Mathematics with Applications*, *70*(5), 1182-1197.

Mangalathu, S., Heo, G., & Jeon, J.-S. (2018). Artificial neural network based multi-dimensional fragility development of skewed concrete bridge classes. *Engineering Structures*, *162*, 166-176.

Matheron, G. (1973). The intrinsic random functions and their applications. *Advances in applied probability*, *5*(3), 439-468.

McKenna, F. (2011). OpenSees: a framework for earthquake engineering simulation. *Computing in Science & Engineering*, *13*(4), 58-66.

Melchers, R. (1989). Importance sampling in structural systems. *Structural Safety*, *6*(1), 3-10.

Melchers, R. E., & Beck, A. T. (2018). *Structural Reliability Analysis and Prediction*. John wiley & sons.

Moustapha, M., Marelli, S., & Sudret, B. (2022). UQLab user manual–Active learning reliability. *Report UQLab-V2, in Chair of Risk, Safety and Uncertainty Quantification, ETH Zurich*, 0-117.

Næss, A., & Gaidai, O. (2009). Estimation of extreme values from sampled time series. *Structural Safety*, *31*(4), 325-334.

Naess, A., & Gaidai, O. (2008). Monte Carlo methods for estimating the extreme response of dynamical systems. *Journal of Engineering Mechanics*, *134*(8), 628-636.

Pan, Q., & Dias, D. (2017). An efficient reliability method combining adaptive support vector machine and Monte Carlo simulation. *Structural Safety*, *67*, 85-95.

Papadopoulos, V., Giovanis, D. G., Lagaros, N. D., & Papadrakakis, M. (2012). Accelerated subset simulation with neural networks for reliability analysis. *Computer methods in applied mechanics and engineering*, *223*, 70-80.

Papadrakakis, M., Papadopoulos, V., & Lagaros, N. D. (1996). Structural reliability analyis of elastic-plastic structures using neural networks and Monte Carlo simulation. *Computer methods in applied mechanics and engineering*, *136*(1-2), 145-163.

Papaioannou, I., Ehre, M., & Straub, D. (2019). PLS-based adaptation for efficient PCE representation in high dimensions. *Journal of Computational Physics*, *387*, 186-204.

Phoon, K.-K., Huang, H., & Quek, S. T. (2005). Simulation of strongly non-Gaussian processes using Karhunen–Loeve expansion. *Probabilistic Engineering Mechanics*, *20*(2), 188-198.

Rackwitz, R. (2001). Reliability analysis—a review and some perspectives. *Structural Safety*, *23*(4), 365-395.

Rahman, S., & Xu, H. (2004). A univariate dimension-reduction method for multi-dimensional integration in stochastic mechanics. *Probabilistic Engineering Mechanics*, *19*(4), 393-408.

Rice, S. O. (2013). Mathematical analysis of random noise. *Bell System Technical Journal*.

Richard, B., Cremona, C., & Adelaide, L. (2012). A response surface method based on support vector machines trained with an adaptive experimental design. *Structural Safety*, *39*, 14-21.

Roberts, J., & Spanos, P. (1986). Stochastic averaging: an approximate method of solving random vibration problems. *International Journal of Non-Linear Mechanics*, *21*(2), 111-134.

Roy, A., & Chakraborty, S. (2023). Support vector machine in structural reliability analysis: A review. *Reliability Engineering & System Safety*, *233*, 109126.

Schöbi, R., & Sudret, B. (2017). Uncertainty propagation of p-boxes using sparse polynomial chaos expansions. *Journal of Computational Physics*, *339*, 307-327.

Schöbi, R., Sudret, B., & Marelli, S. (2017). Rare event estimation using polynomial-chaos Kriging. *ASCE-ASME Journal of Risk and Uncertainty in Engineering Systems, Part A: Civil Engineering*, *3*(2), D4016002.

Schueremans, L., & Van Gemert, D. (2005). Benefit of splines and neural networks in simulation based structural reliability analysis. *Structural Safety*, *27*(3), 246-261.

Shields, M. D., & Zhang, J. (2016). The generalization of Latin hypercube sampling. *Reliability Engineering & System Safety*, *148*, 96-108.

Shinozuka, M., & Deodatis, G. (1991). Simulation of stochastic processes by spectral representation.

Simiu, E., Bietry, J., & Filliben, J. J. (1978). Sampling errors in estimation of extreme winds. *Journal of the Structural Division*, *104*(3), 491-501.

Song, J., Valdebenito, M., Wei, P., Beer, M., & Lu, Z. (2020). Non-intrusive imprecise stochastic simulation by line sampling. *Structural Safety*, *84*, 101936.

Su, M., Xue, G., Wang, D., Zhang, Y., & Zhu, Y. (2020). A novel active learning reliability method combining adaptive Kriging and spherical decomposition-MCS (AK-SDMCS) for small failure probabilities. *Structural and Multidisciplinary Optimization*, *62*, 3165-3187.

Sudret, B. (2008a). Analytical derivation of the outcrossing rate in time-variant reliability problems. *Structure and Infrastructure Engineering*, *4*(5), 353-362.

Sudret, B. (2008b). Global sensitivity analysis using polynomial chaos expansions. *Reliability Engineering & System Safety*, *93*(7), 964-979.

Sun, Z., Wang, J., Li, R., & Tong, C. (2017). LIF: A new Kriging based learning function and its application to structural reliability analysis. *Reliability Engineering & System Safety*, *157*, 152-165.

Tabandeh, A., Jia, G., & Gardoni, P. (2022). A review and assessment of importance sampling methods for reliability analysis. *Structural Safety*, *97*, 102216.

Wang, J., Lu, Z., & Wang, L. (2023). An efficient method for estimating failure probability bounds under random‐interval mixed uncertainties by combining line sampling with adaptive Kriging. *International Journal for Numerical Methods in Engineering*, *124*(2), 308-333.

Wang, J., Xu, G., Li, Y., & Kareem, A. (2022). AKSE: A novel adaptive Kriging method combining sampling region scheme and error-based stopping criterion for structural reliability analysis. *Reliability Engineering & System Safety*, *219*, 108214.

Wang, X., Yuan, X., Feng, R., & Dong, Y. (2022). Data‐driven probabilistic curvature capacity modeling of circular RC columns facilitating seismic fragility analyses of highway bridges. *Earthquake Engineering and Resilience*, *1*(2), 211-224.

Wang, Z., & Shafieezadeh, A. (2019). ESC: an efficient error-based stopping criterion for kriging-based reliability analysis methods. *Structural and Multidisciplinary Optimization*, *59*, 1621-1637.

Wang, Z., & Wang, P. (2015). A double-loop adaptive sampling approach for sensitivity-free dynamic reliability analysis. *Reliability Engineering & System Safety*, *142*, 346-356.

Wiener, N. (1938). The homogeneous chaos. *American Journal of Mathematics*, *60*(4), 897-936.

Win t′ erstein, S. R. (1988). Nonlinear vibration models for extremes and fatigue. *Journal of Engineering Mechanics*, *114*(10), 1772-1790.

Xiang, Z., Chen, J., Bao, Y., & Li, H. (2020). An active learning method combining deep neural network and weighted sampling for structural reliability analysis. *Mechanical Systems and Signal Processing*, *140*, 106684.

Xiao, N.-C., Yuan, K., & Zhan, H. (2022). System reliability analysis based on dependent Kriging predictions and parallel learning strategy. *Reliability Engineering & System Safety*, *218*, 108083.

Xiao, S., Oladyshkin, S., & Nowak, W. (2020). Reliability analysis with stratified importance sampling based on adaptive Kriging. *Reliability Engineering & System Safety*, *197*, 106852.

Xiong, Y., & Sampath, S. (2021). A fast-convergence algorithm for reliability analysis based on the AK-MCS. *Reliability Engineering & System Safety*, *213*, 107693.

Xiu, D., & Karniadakis, G. E. (2002). The Wiener--Askey polynomial chaos for stochastic differential equations. *SIAM Journal on Scientific Computing*, *24*(2), 619-644.

Xu, H., & Rahman, S. (2004). A generalized dimension‐reduction method for multidimensional integration in stochastic mechanics. *International Journal for Numerical Methods in Engineering*, *61*(12), 1992-2019.

Xu, J., & Dang, C. (2019). A novel fractional moments-based maximum entropy method for high-dimensional reliability analysis. *Applied Mathematical Modelling*, *75*, 749-768.

Xu, J., & Kong, F. (2018). An adaptive cubature formula for efficient reliability assessment of nonlinear structural dynamic systems. *Mechanical Systems and Signal Processing*, *104*, 449-464.

Xu, J., Wang, J., & Wang, D. (2020). Evaluation of the probability distribution of the extreme value of the response of nonlinear structures subjected to fully nonstationary stochastic seismic excitations. *Journal of Engineering Mechanics*, *146*(2), 06019006.

Xu, J., Zhang, Y., & Dang, C. (2020). A novel hybrid cubature formula with Pearson system for efficient moment-based uncertainty propagation analysis. *Mechanical Systems and Signal Processing*, *140*, 106661.

Yue, X., Zhang, J., Gong, W., Luo, M., & Duan, L. (2021). An adaptive PCE-HDMR metamodeling approach for high-dimensional problems. *Structural and Multidisciplinary Optimization*, *64*, 141-162.

Yun, W., Lu, Z., & Jiang, X. (2018). An efficient reliability analysis method combining adaptive Kriging and modified importance sampling for small failure probability. *Structural and Multidisciplinary Optimization*, *58*, 1383-1393.

Yun, W., Lu, Z., Jiang, X., Zhang, L., & He, P. (2020). AK-ARBIS: an improved AK-MCS based on the adaptive radial-based importance sampling for small failure probability. *Structural Safety*, *82*, 101891.

Zhang, C., Wang, Z., & Shafieezadeh, A. (2021). Error quantification and control for adaptive kriging-based reliability updating with equality information. *Reliability Engineering & System Safety*, *207*, 107323.

Zhang, D., Shen, S., Jiang, C., Han, X., & Li, Q. (2022). An advanced mixed-degree cubature formula for reliability analysis. *Computer methods in applied mechanics and engineering*, *400*, 115521.

Zhang, J., Gong, W., Yue, X., Shi, M., & Chen, L. (2022). Efficient reliability analysis using prediction-oriented active sparse polynomial chaos expansion. *Reliability Engineering & System Safety*, *228*, 108749.

Zhang, J., Xiao, M., & Gao, L. (2019). An active learning reliability method combining Kriging constructed with exploration and exploitation of failure region and subset simulation. *Reliability Engineering & System Safety*, *188*, 90-102.

Zhang, R., Chen, Z., Chen, S., Zheng, J., Büyüköztürk, O., & Sun, H. (2019). Deep long short-term memory networks for nonlinear structural seismic response prediction. *Computers & Structures*, *220*, 55-68.

Zhang, R., Liu, Y., & Sun, H. (2020a). Physics-guided convolutional neural network (PhyCNN) for data-driven seismic response modeling. *Engineering Structures*, *215*, 110704.

Zhang, R., Liu, Y., & Sun, H. (2020b). Physics-informed multi-LSTM networks for metamodeling of nonlinear structures. *Computer methods in applied mechanics and engineering*, *369*, 113226.

Zhang, X., & Pandey, M. D. (2013). Structural reliability analysis based on the concepts of entropy, fractional moment and dimensional reduction method. *Structural Safety*, *43*, 28-40.

Zhang, X., & Quek, S. T. (2022). Efficient subset simulation with active learning Kriging model for low failure probability prediction. *Probabilistic Engineering Mechanics*, *68*, 103256.

Zhang, X., Wang, L., & Sørensen, J. D. (2019). REIF: a novel active-learning function toward adaptive Kriging surrogate models for structural reliability analysis. *Reliability Engineering & System Safety*, *185*, 440-454.

Zhang, X., Wang, L., & Sørensen, J. D. (2020). AKOIS: an adaptive Kriging oriented importance sampling method for structural system reliability analysis. *Structural Safety*, *82*, 101876.

Zhang, Y., Dong, Y., & Feng, R. (2023). Bayes-informed mixture distribution for the EVD estimation and dynamic reliability analysis. *Mechanical Systems and Signal Processing*, *197*, 110352.

Zhang, Y., Dong, Y., & Xu, J. (2023). An accelerated active learning Kriging model with the distance-based subdomain and a new stopping criterion for reliability analysis. *Reliability Engineering & System Safety*, *231*, 109034.

Zhang, Y., & Xu, J. (2021). Efficient reliability analysis with a CDA-based dimension-reduction model and polynomial chaos expansion. *Computer methods in applied mechanics and engineering*, *373*, 113467.

Zhao, H., Li, S., & Ru, Z. (2017). Adaptive reliability analysis based on a support vector machine and its application to rock engineering. *Applied Mathematical Modelling*, *44*, 508-522.

Zhao, Y.-G., & Ono, T. (2001). Moment methods for structural reliability. *Structural Safety*, *23*(1), 47-75.

Zhou, T., & Peng, Y. (2022). Efficient reliability analysis based on deep learning-enhanced surrogate modelling and probability density evolution method. *Mechanical Systems and Signal Processing*, *162*, 108064.

Zhu, X., Lu, Z., & Yun, W. (2020). An efficient method for estimating failure probability of the structure with multiple implicit failure domains by combining Meta-IS with IS-AK. *Reliability Engineering & System Safety*, *193*, 106644.